AN INVESTIGATION INTO THE BONDING OF COPPER(I) MACROCYCLES TO FIFTH LIGANDS

Thesis by

Judith Lee Allison

In Partial Fulfillment of the Requirements

for the Degree of

Doctor of Philosophy

California Institute of Technology

Pasadena, California

1979

(Submitted November 27, 1978)

To Malcolm:

Love is not all: it is not meat nor drink
Nor slumber nor a roof against the rain;
Nor yet a floating spar to men that sink
And rise and sink and rise and sink again;
Love can not fill the thickened lung with breath,
Nor clean the blood, nor set the fractured bone;
Yet many a man is making friends with death
Even as I speak, for lack of love alone.
It well may be that in a difficult hour,
Pinned down by pain and moaning for release,
Or nagged by want past resolution's power,
I might be driven to sell your love for peace,
Or trade the memory of this night for food.
It well may be. I do not think I would.

-Edna St. Vincent Millay
from "Fatal Interview"

ACKNOWLEDGMENTS

The enthusiasm I have for chemistry stems largely from my association with Professor John Burmeister, who has an unswerving belief in people and in science. My ability to do research in chemistry at Caltech was aided tremendously by my friends, and by my husband, Malcolm. Discovery of the Los Angeles Wheelmen led to Fred and Kala (and eventually Bill!) and innumerable feats of excess. I only wish for many more!

My advisor, Bob Gagné, and his indefatigable group, have encouraged my scientific and personal development. May the next female chemist in the group survive the experience.

When I needed someone to talk to, I could always find a sympathetic listener in Sue, Charlotte, Roger or Jan. Advice and help of all types came from Carl, Ace, Cliff and Mike. The men of the glass shop, stockroom, and electronics shop have been unerringly helpful. Pat and Beth put up with a lot, but were always ready to do more to help. These people have kept me going.

All types of support were provided unselfishly by Nina and Austen and Janie for Malcolm and me and our sunny southern California adventures. My parents have also continuously supported our endeavors. I thank them for rearing me to think for myself and to do whatever I chose to do well. That they never hinted that a woman's future had any more limitations than a man's is a grand tribute to them. Dad, thanks for sodium chloride and chemistry (you may keep the physics). Mom, thank you for music, rhodendendrons, and happiness.

I am grateful that I have been helped by so many people.

ABSTRACT

The properties and reactivities of an unusual copper(I) macrocyclic complex have been investigated. The complex, $Cu(LBF_2)$ ([1,1-difluoro-4,5,11,12-tetramethyl-1-bora-3,6,10,13-tetraaza-2,14-dioxo-cyclotetradeca-3,5,10,12-tetraenato]copper(I)), reacts with carbon monoxide to form an isolable complex, $Cu(LBF_2)CO$. The crystal structure of $Cu(LBF_2)CO$, which was previously determined, shows a square-pyramidal geometry around copper(I) with an apical carbon monoxide and four basal nitrogens.

The crystal and molecular structure of the four-coordinate complex, $Cu(LBF_2)$, was determined. The copper binds to the four nitrogens of the macrocycle in a distorted square-planar array. The nitrogens are twisted toward a tetrahedron with resulting dihedral angles of 23 and 27° between the two sets of planes defined by copper and two adjacent nitrogens. The amount of the tetrahedral distortion is limited by the macrocycle's steric limitations.

The complex, $Cu(LBF_2)$, has an unusual geometry for copper(I). It also has unusual reactivities. The five-coordinate complex, $Cu(LBF_2)CO$, is the result of the binding of carbon monoxide to $Cu(LBF_2)$. Other neutral molecules bind to $Cu(LBF_2)$. Study of the binding of various ligands to $Cu(LBF_2)$ was undertaken to delve into the driving forces for the formation of five-coordinate complexes of copper(I). The binding constants for a range of π-acceptor and

σ-base ligands were determined. The π-acceptors bind more strongly to $Cu(LBF_2)$ than the σ-bases.

Copper(I) complexes with macrocycles related to LBF_2 were synthesized. These derivatized complexes bind carbon monoxide to varying degrees depending on both the electronic and steric requirements of the macrocycle. Complexes with macrocycles not directly related to LBF_2 also bind carbon monoxide.

The binding of fifth ligands to four-coordinate copper(I) complexes is not limited to $Cu(LBF_2)$ or even to closely related complexes. However, not all four-coordinate copper(I) complexes bind carbon monoxide. Again the electronic and steric requirements of the ligand are important.

A simple, qualitative description of the bonding of carbon monoxide to $Cu(LBF_2)$ is presented. When $Cu(LBF_2)$ coordinates to carbon monoxide, the copper-nitrogen bonds lengthen significantly. The resulting geometry of the five-coordinate $Cu(LBF_2)CO$ is an abnormal square pyramid. The bonding is better described as a linear array of the carbon monoxide and the macrocycle about copper(I).

TABLE OF CONTENTS

INTRODUCTION

Solid state structures have been crystallographically analyzed for a wealth of copper(I) complexes (1-4). For monomeric complexes the usual stoichiometries are three or four ligands for each copper(I) center. The resultant geometries about the copper are trigonal planar and tetrahedral for coordination numbers three and four. The four-coordinate tetrahedral geometry is most frequently encountered. Examples of three- and four-coordinate copper(I) complexes with nitrogen ligands are the trigonal planar tris(2-picoline)copper(I) perchlorate (5) and the tetrahedral tetraacetonitrilecopper(I) perchlorate (6).

The discovery of the reaction of [1,1-difluoro-4,5,11,12-tetramethyl-1-bora-3,6,10,13-tetraaza-2,14-dioxo-cyclotetradeca-3,5,10,12-tetraenato]copper(I), $Cu(LBF_2)$, 1, and carbon monoxide to form an isolable adduct, $Cu(LBF_2)CO$, 2 (Figure 1), led to speculation of a new geometry for copper(I) (7). The stoichiometry indicated a five-coordinate copper(I). The solid state crystal structure of $Cu(LBF_2)CO$, 2, shows a square-pyramidal geometry about copper(I) (8). The four macrocyclic nitrogens are in the basal plane and the carbon monoxide occupies the apical position of the square pyramid.

Prior to the analysis of the structure of $Cu(LBF_2)CO$, 2, there were no monomeric copper(I) complexes with a coordination number greater than four. The copper centers in cluster complexes bind

Figure 1

The five-coordinate complex, $Cu(LBF_2)CO$, 2, is the product of the reaction of $Cu(LBF_2)$, 1, and carbon monoxide.

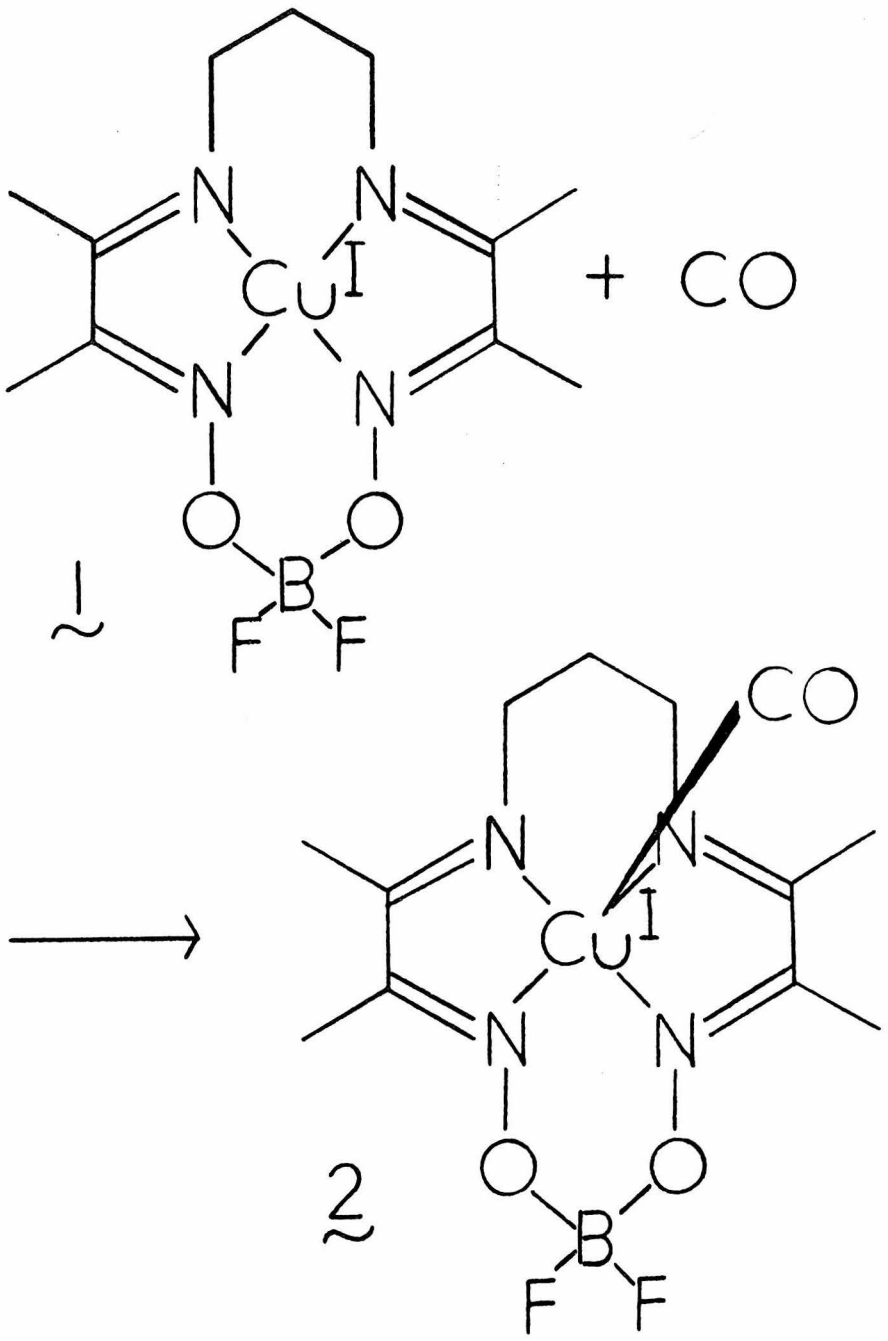

Figure 1

two, three, or four ligands, but have formal coordination numbers of two through seven. Coordination numbers greater than the number of ligands result from the inclusion of copper-copper interactions. Formally five-, six-, and seven-coordinate structures are found in tetrameric and hexameric clusters with copper-copper distances 2.40 to 2.95 Å (9). Distances shorter than copper metal's copper-copper length of 2.56 Å indicate attractive interactions, but the meaning of longer distances is obscure. Lively literature discussion addresses the question of what constitutes d^{10}-d^{10} bonding. Mehrotra and Hoffmann (10) have examined the metal-metal interactions of copper clusters with two to four copper centers by extended Hückel calculations. Weak copper-copper atractive interactions exist, even with the complications of the stereochemical demands of bridging ligands. Structural evidence for metal-metal attractive interactions in three $Cu_8S_{12}^{4-}$ clusters with copper-copper distances of about 2.8 Å has been presented (11). On the other hand, a molecular orbital study of a core $Cu_8S_{12}^{4-}$ cluster by Avdeef and Fackler (12) finds no net copper-copper bonding. The authors attribute the cluster's stability to ligand stereochemical restraints.

The coordination possibilities of copper(I) in clusters are diverse when metal-metal bonding is introduced. However, the nature of copper(I)-copper(I) interactions is difficult to delineate. The complex, $Cu(LBF_2)CO$, 2, illustrates the ability of copper(I) to bind ligands in a complex manner even in monomers.

The binding of five ligands to d^{10} metals is not unknown. Five-coordination is common for zinc(II) complexes, which form square-pyramidal (13) and trigonal-bipyramidal (14) structures. However, it is unusual for carbon monoxide to bind to a metal that already has a noble gas configuration, irrespective of the number of ligands coordinating to the metal.

The discovery of a new geometry for a first row transition metal is rare. The four-coordinate precursor of $Cu(LBF_2)CO$, 2, evolved from a series of macrocyclic copper(I) complexes used for oxygen binding studies. Because macrocycles do not easily dissociate from bonded metals (15), they provide a constant ligand environment about labile copper(II) and copper(I) centers. By fixing the basic coordination sphere about the metal, a simplification of characterization work is realized. In general, extrapolation from solid state crystal structures to solution properties is difficult to support unequivocably. However, with a stable macrocyclic structure, solution properties can be compared directly to the predictions of solid state structural work.

Because copper(I) has a filled d shell, its ligand geometry cannot be explained by ligand field stabilization. Copper(I) should require a simple symmetric array of ligand electron density. Indeed, symmetric ligand coordination is often found. If the electron density about copper(I) in $Cu(LBF_2)CO$, 2, approximates a sphere more closely than that in $Cu(LBF_2)$, 1, there is a predictable

driving force for adduct formation. An investigation into the occurrence of the unprecedented binding of carbon monoxide to an eighteen-electron metal center has been carried out. This thesis presents the results and conclusions of the general study of the binding of fifth ligands to copper(I).

SECTION A

Early Copper(I) Macrocyclic Work

This investigation into the binding of fifth ligands to copper(I) macrocyclic complexes began with the study of the interaction of oxygen with copper(I). Two basic requirements directed the choice of macrocycles. They had to stabilize copper(I) against disproportionation and bind effectively to copper(II).

There are two synthetic routes to copper(I) complexes. The first is direct incorporation of copper(I) in the macrocycle, which is synthesized separately. An indirect approach involves the use of a ligand-forming template reaction about copper(II) with subsequent one-electron reduction to the copper(I) complex. The second route is possible only when the copper(II) complex is stable. To have an isolable complex of both copper(II) and copper(I), the tetraaza macrocyclic configuration was selected.

The syntheses of the copper(II) and copper(I) adducts of the first macrocycle studied, 5,7,7,12,14,14-hexamethyl-1,4,8,11-tetraazacyclotetradeca-4,11-diene, trans-diene (Figure 2A) are found in the literature (16). The copper(II) complex, Cu(trans-diene)$(ClO_4)_2$, 3, was reduced by constant potential electrolysis (CPE) to Cu(trans-diene)ClO_4, 4, in a discrete one-electron step. The yellow copper(I) solution is highly air-sensitive and reacts with 1.9 moles of oxygen

Figure 2

Skeletal representations of two tetraaza macrocycles, A. trans-diene and B. TAAB, and one macrocycle precursor, C. LH_2.

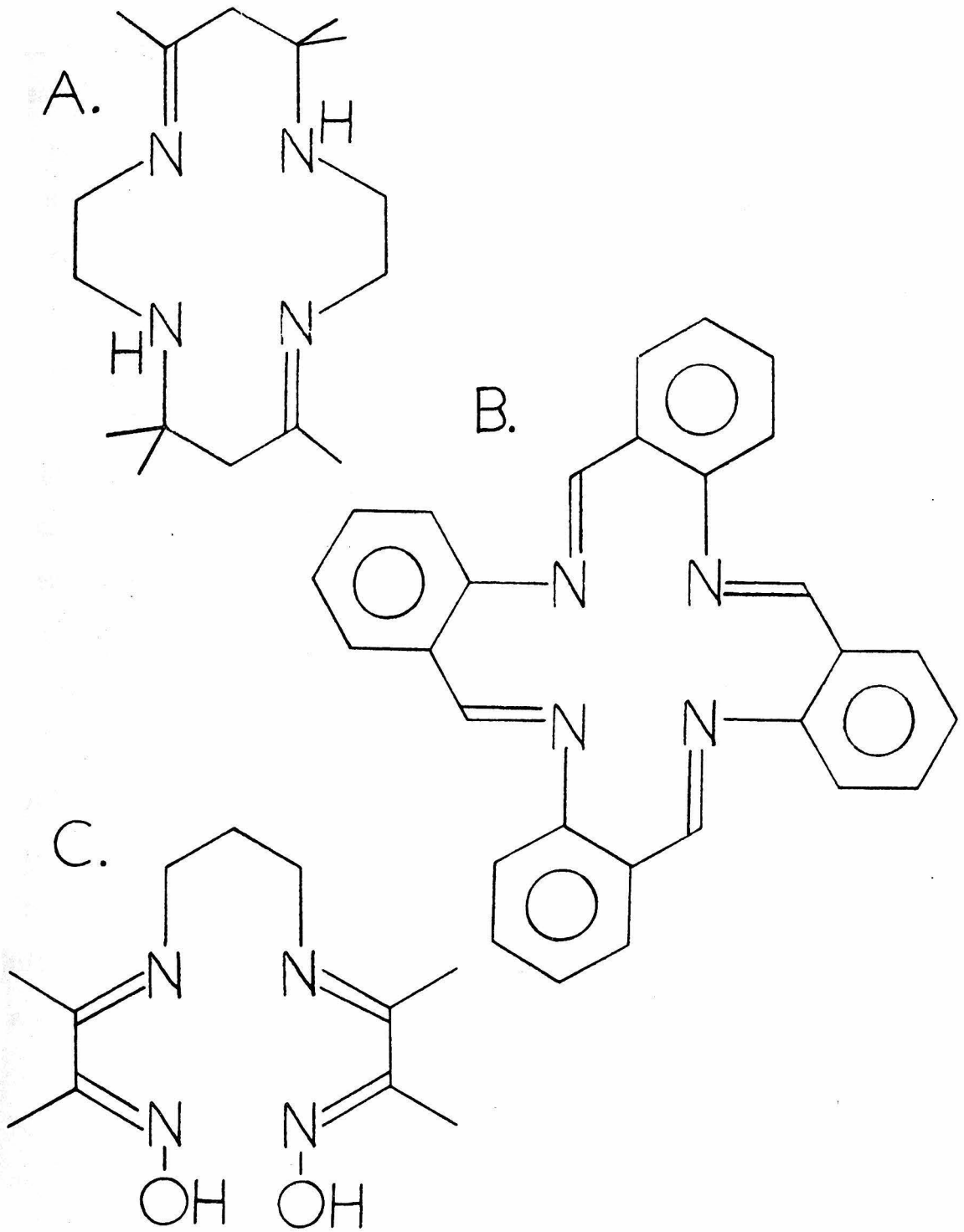

Figure 2

per mole of copper(I). The oxygen to copper stoichiometry can be explained if ligand oxidative dehydrogenation, such as in the reaction of [Fe(trans-diene)$(CH_3CN)_2$]$(ClO_4)_2$, 5, with oxygen (17), is postulated. A ligand-oxygen reaction was not of interest and further oxygen chemistry with Cu(trans-diene)ClO_4, 4, has not been pursued. However, the reactivity of this copper macrocyclic complex with other fifth ligands has been examined and the results are presented in Section F.

A new macrocycle was needed to exclude the complications of ligand participation in the copper-oxygen reaction. In the mechanism of oxidative dehydrogenation proposed for [Fe(trans-diene)$(CH_3CN)_2$]$(ClO_4)_2$, 5, a proton bound to a nitrogen is initially lost (17). A decision to eliminate the hydrogens on the ligating nitrogens was made to simplify the oxygen reaction. Two approaches to removing these hydrogens are available. The trans-diene macrocycle can be directly modified by removal of the hydrogens as protons. The new macrocycle is dianionic. Alternatively, a completely new macrocycle can be synthesized which has increased nitrogen unsaturation. This second approach was utilized to avoid a dianionic macrocycle.

The macrocycle, tetrabenzo[b,f,j,n][1,5,9,13]tetraazacyclohexadecine, TAAB (Figure 2B), does not have hydrogens bound to any ligating nitrogen. The copper(II) complex, Cu(TAAB)$(NO_3)_2$, 6 (18), was reduced chemically by copper(0) or electrochemically by one-electron to Cu(TAAB)NO_3, 7 (19,20). The blue copper(I) complex is

not air-sensitive in solution or in the solid state. It has been suggested, but never conclusively shown, that the reduction occurs at the highly conjugated ligand (19,20). No further work on the copper-TAAB system has been done, except to investigate the complexes' propensities to bind fifth ligands. These results are presented in Section F.

The reduction of a copper(II) macrocyclic complex to copper(I) can occur unambiguously when the macrocycle reduces at a more negative potential than the metal. The potential of the reduction of a macrocycle can be decreased by limiting its conjugation. Choice of a macrocycle now depended on two factors: the elimination of protons on ligating nitrogens and a change in conjugation of the ligand. A macrocycle precursor that met these requirements is 4,8-diaza-3,9-dimethylundeca-3,8-diene-2,10-dione dioxime, LH_2 (Figure 2C). This polydentate ligand binds to a metal by four imine nitrogens to form metal complexes of the formula $[M^{+n}(LH)]^{n-1}$ (M^{+n}=Ni(II) (21), Co(III) (22), and Rh(I), Rh(III) (23)). The syntheses and properties of the copper complexes of a macrocyclic form of the LH_2 ligand are described in Section B.

SECTION B

The Reaction of $Cu(LBF_2)$, 1, with Carbon Monoxide and 1-Methylimidazole

The ligand precursor, 4,8-diaza-3,9-dimethylundeca-3,8-diene-2,10-dione dioxime, LH_2, reacted with $Cu(ClO_4)_2 \cdot 6H_2O$ to form the complex $Cu(LH)ClO_4 \cdot H_2O$, 8 (Figure 3). This polydentate copper complex was converted into a macrocyclic complex by reaction with BF_3 to form $[Cu(LBF_2)]_2(ClO_4)_2 \cdot C_4H_8O_2$, 9 (Figure 3). The blue copper(I) complex, $Cu(LBF_2)$, 1, was synthesized by the one-electron reduction of $Cu(LBF_2)ClO_4$, 9, by CPE. Dissolved in various solvents, e.g. acetonitrile and acetone, the complex reacts with oxygen. No oxygen reaction occurs in the solid state. When carbon monoxide was bubbled through an acetone solution of $Cu(LBF_2)$, 1, the blue solution turned yellow. The adduct, $Cu(LBF_2)CO$, 2, was isolated by slow evaporation of acetone.

The crystal structure of $Cu(LBF_2)CO$, 2, was done by Dr. R. S. Gall, a postdoctoral member of the Gagné group (8). The crystallographic data have been published, the paper is presented in Appendix 2. The five-coordinate copper(I) in $Cu(LBF_2)CO$, 2, is bound by four macrocyclic nitrogens in the basal plane of a square pyramid and an apical carbon monoxide (Figure 4). There are two distinct sets of copper-nitrogen bond lengths which average 2.164 and 2.104 Å.

Figure 3

The ligand precursor, LH_2, reacts with $Cu(ClO_4)_2 \cdot 6H_2O$ in acetone, 1, to form the polydentate complex, $Cu(LH)ClO_4 \cdot H_2O$, 8. This copper(II) complex reacts with BF_3 in dioxane, 2, to give the macrocyclic complex, $[Cu(LBF_2)]_2(ClO_4)_2 \cdot C_4H_8O_2$, 9.

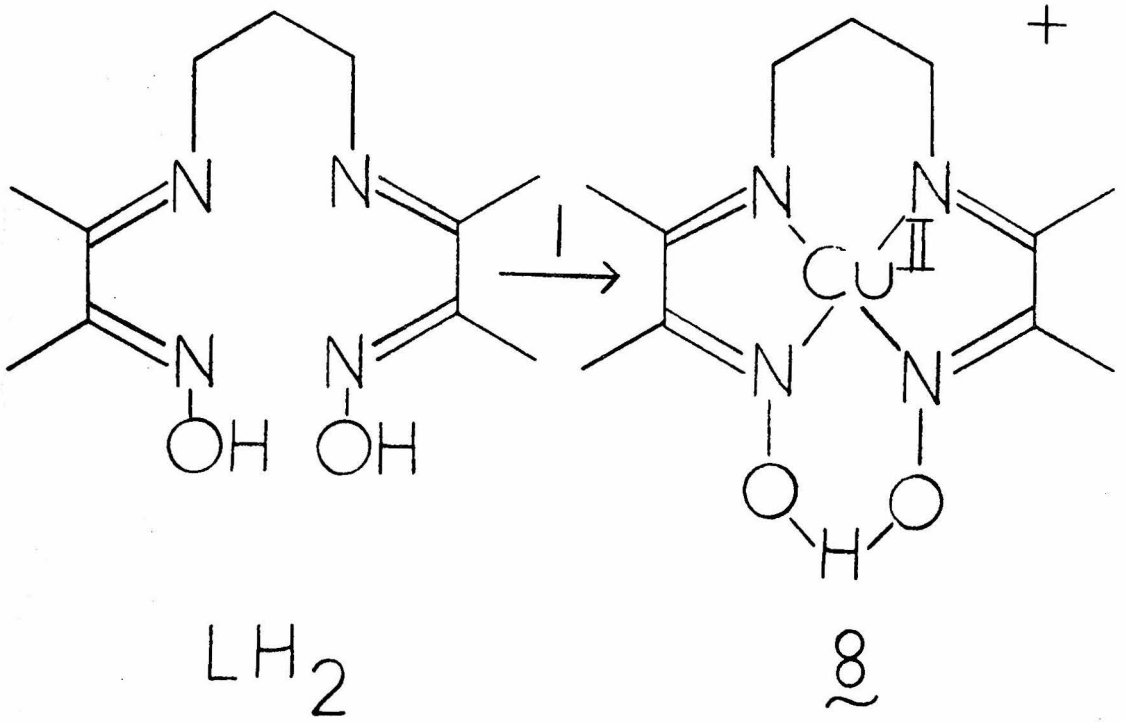

LH_2 8

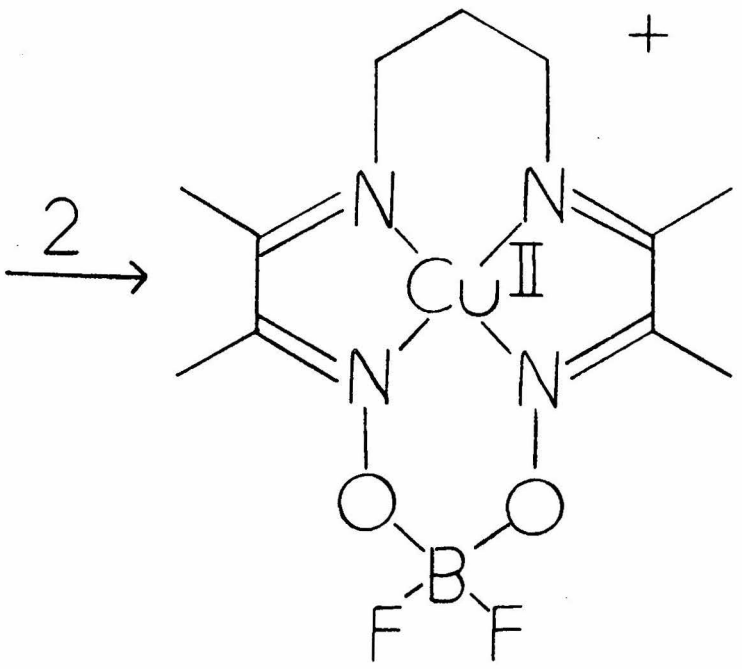

9

Figure 3

Figure 4

An ORTEP drawing of the complex, $Cu(LBF_2)CO$, 2, with the four copper-nitrogen bonds labeled. Thermal ellipsoids are at the 50% probability level. Hydrogen atoms are omitted.

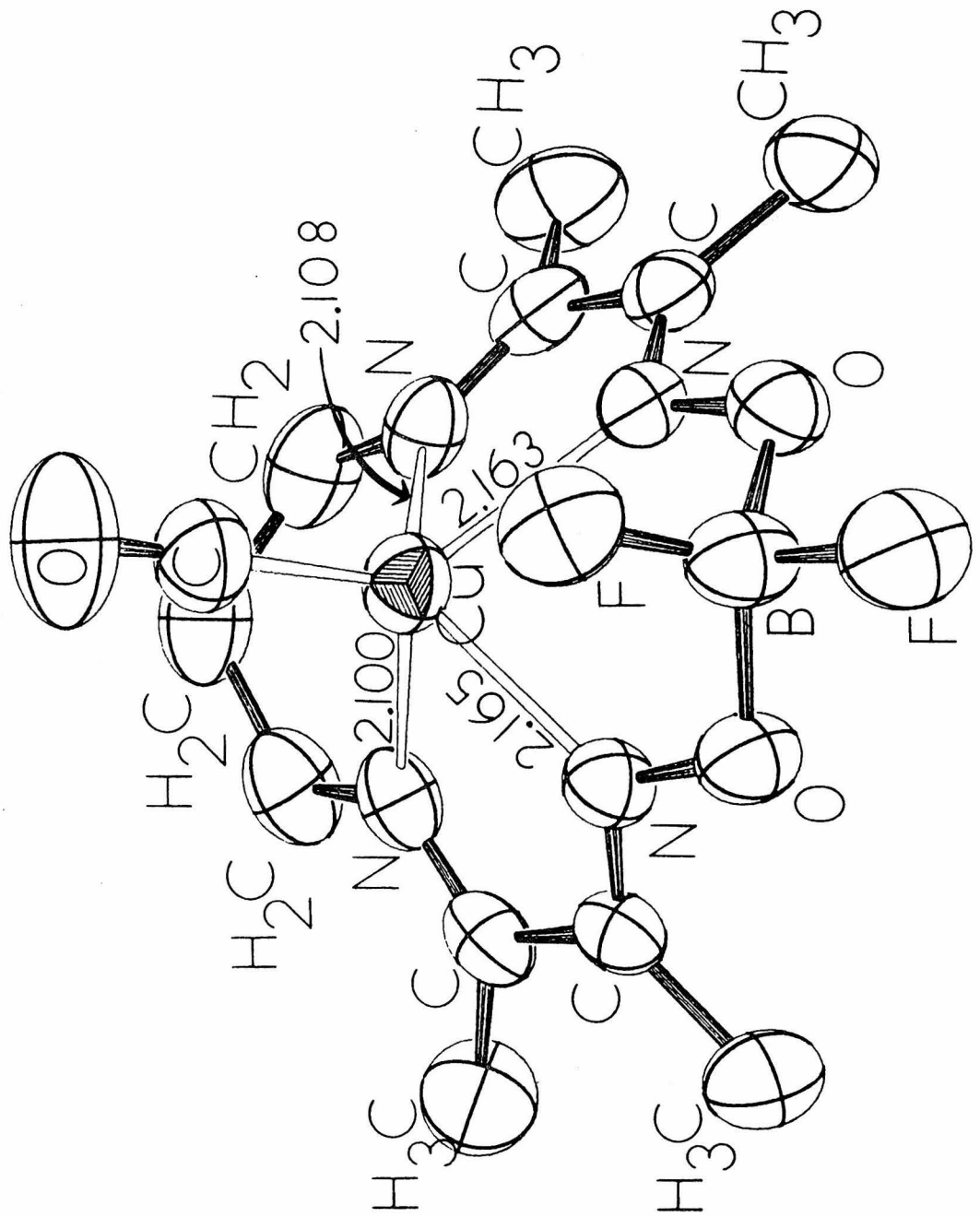
2.108
2.163
2.100
2.165
O
C
CH2
N
U
F
B
F
O
N
C
CH3
C
CH3
H2C
H2C
N
C
C
H3C
H3C

Figure 4

The structure of $Cu(LBF_2)CO$, 2, is unusual in several ways. The copper(I) has a coordination number of five and a monomeric square-pyramidal geometry. This type of coordination is unprecedented for copper(I). The other copper-carbon monoxide complexes that have been crystallographically analyzed have the expected tetrahedral geometry about copper(I). Two monomeric complexes, carbonyl[hydrotris(1-pyrazolyl)borato]copper(I), $Cu[HB(pz)_3]CO$, 10 (24), and carbonyl(diethylenetriamine)copper(I) tetraphenylborate, $[Cu(dien)CO]BPh_4$, 11 (25), and one dimeric complex, $[Cu_2(Hm)_3(CO)_2](BPh_4)_2$, 12 (26) (Hm = two tautomeric forms of histamine, 4-(2-aminoethyl)imidazole and 5-(2-aminoethyl)imidazole) have been studied. Table I compares relevant copper-carbon monoxide data for the five different copper centers. Despite the two distinct geometries found for these complexes, the carbon monoxide binds similarly in all five instances.

The square pyramid about copper(I) in $Cu(LBF_2)CO$, 2, is unusual. In normal square-pyramidal complexes, the angle α (Figure 5) is 100° (27). In $Cu(LBF_2)CO$, 2, the angle ranges from 114.9(1)° to 120.3(1)°. The increase in this angle α is the consequence of the large displacement, 0.96 Å, of the copper(I) out of the four macrocycle plane (Figure 5). Other cases of large metal displacements out of basal planes are known. The extremes are found for Tl(III): 0.74 Å in chloro-5,10,15,20-tetraphenylporphinatothallium(III) and 0.98 Å in methyl-5,10,15,20-tetraphenylporphinatothallium(III) (28). The displacement of copper(II) from the four-nitrogen plane in

Table I. Copper-Carbon Monoxide Crystallographic Data.

Complex	Cu-C distance, Å	C-O distance, Å	Cu-C-O angle, °
$Cu(LBF_2)CO$, 2 (8)	1.780(3)	1.112(4)	177.5(3)
$Cu[HB(pz)_3]CO$, 10[a] (24)	1.755(11),1.775(5)	1.120(13),1.120(6)	180.0,176.6(5)
$[Cu(dien)CO]BPh_4$, 11 (25)	1.776(5)	1.123(6)	176.57(54)
$[Cu_2(Hm)_3(CO)_2](BPh_4)_2$,	1.80(2)	1.12(3)	169(2)
12 (26)	1.79(2)	1.13(3)	172(2)

[a] Two sets of data are given because there are two crystallographically distinct molecules of $Cu[HB(pz)_3]CO$, 10, in the unit cell.

Figure 5

Schematic drawing of $Cu(LBF_2)CO$, 2, to illustrate the definition of angle, α, and the large copper out-of-plane displacement. The copper-carbon and carbon-oxygen bond lengths are labeled.

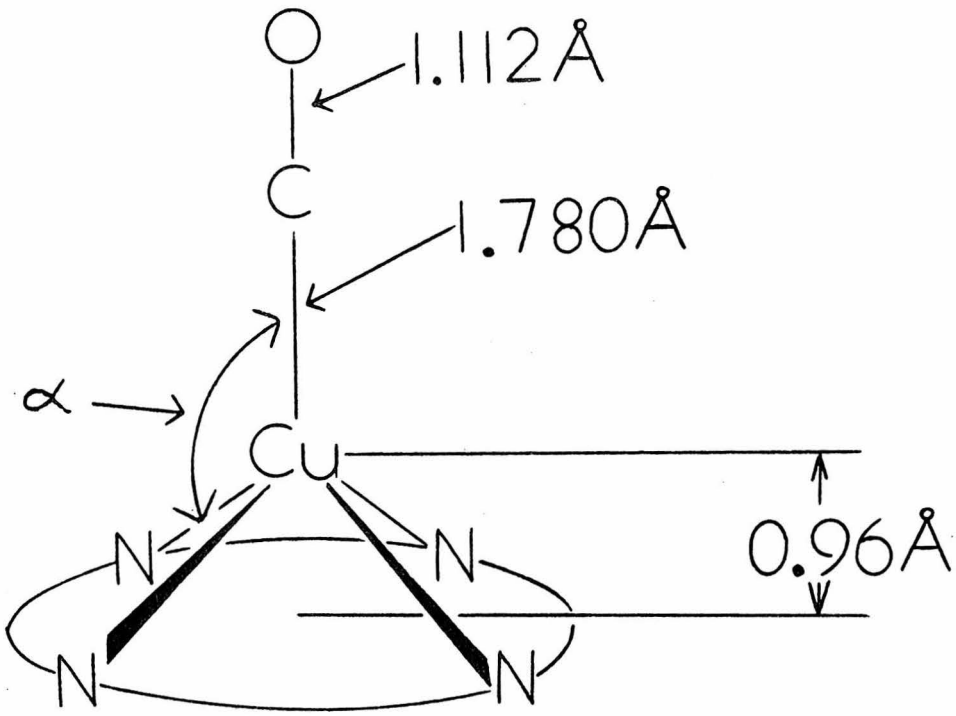

Figure 5

$Cu(LBF_2)NCO$, 13 (29), is 0.58 Å; usual copper(II) displacements are less than 0.4 Å (30). The large out-of-plane displacement and α angles for $Cu(LBF_2)CO$, 2, make this complex unusual for any other metal as well as for copper(I).

Why does $Cu(LBF_2)$, 1, bind carbon monoxide to form a twenty-electron complex, an electron count unprecedented for coordinated carbon monoxide? Initial insight into the coordinative bonding of $Cu(LBF_2)CO$, 2, comes from the crystal structure analysis. The copper-carbon bond length of 1.780(3) Å is normal for the copper(I)-carbon monoxide bonds known (Table I). All of these bonds are short when compared to other copper(I)-carbon bonds which range from 1.87(2) to 2.01(1) Å for many tetrahedral and trigonal copper(I) complexes (31-36). Bridging carbon-copper bond lengths are even longer (9e,37), but a precise description of the coordination geometry about copper(I) for comparative purposes is difficult. Because the copper(I)-carbon bonds in copper-CO complexes are short, their covalent character is substantial. The possibility of some π-bonding from copper to carbon monoxide (to be addressed below) also exists.

The two sets of copper-nitrogen bond lengths in $Cu(LBF_2)CO$, 2, average 2.104 and 2.164 Å. Copper(I)-nitrogen bond lengths are found over the broad range 1.90(2) to 2.28(2) Å (6,9e,24-26,32,34,38-43). However, the majority of the bond lengths for copper-unsaturated nitrogen bonds are 1.95 to 2.09 Å. For example, in tetrapyridine-copper(I) perchlorate the bond length is 2.05(1) Å (41). The longer copper-nitrogen bonds in $Cu(LBF_2)CO$, 2, indicate weaker bonding than

expected for copper(I) bonding to unsaturated nitrogens. Viewed crystallographically, the bonding of $Cu(LBF_2)CO$, 2, includes a strong copper-carbon and four weak copper-nitrogen interactions.

To chemically delve into the nature of the bonding of $Cu(LBF_2)$, 1, and fifth ligands, binding studies were done. The formation of five-coordinate complexes, $Cu(LBF_2)B$, where B is a potential ligand, was investigated by visible spectroscopic studies. The binding of B to $Cu(LBF_2)$, 1, was assumed to obey equation 1 with a concentration equilibrium constant, K_C, equal to the ratio of product to reactant concentrations (equation 2).

$$Cu(LBF_2) + B \rightleftharpoons Cu(LBF_2)B \tag{1}$$

$$K_C = \frac{[Cu(LBF_2)B]}{[Cu(LBF_2)][B]} \tag{2}$$

The visible spectrum of $Cu(LBF_2)$, 1, is distinctive. There is a strong absorption at 677 nm that has a molar absorptivity of $1.03 \times 10^4\ M^{-1}\ cm^{-1}$ in acetone at 25° C. On addition of a sufficient excess of carbon monoxide and 1-methylimidazole, 1-MeIm, the band at 677 nm disappeared. The disappearance of the 677 nm absorption was monitored with incremental amounts of B. The equilibrium concentration of $Cu(LBF_2)$, 1, was based on the solution's absorbance at 677 nm. The equilibrium concentrations of B and $Cu(LBF_2)B$ were calculated from the decrease in the absorbance of a $Cu(LBF_2)$, 1, solution from the theoretical zero B concentration level.

A new band appeared in the visible region (420 nm) on the addition of 1-MeIm to $Cu(LBF_2)$, 1. Figure 6 shows typical visible spectral changes observed with increasing 1-MeIm concentrations. Because of slight variations in pathlengths, isosbestic behavior was approximate. With the assumption of the formation of only a 1:1 adduct of $Cu(LBF_2)$, 1, and B, K_c for 1-MeIm was calculated. A value of 16(3) M^{-1} was obtained.

For carbon monoxide, similar isosbestic behavior was observed with varying CO concentrations. The initially calculated pressure equilibrium constant, K_p (equation 3), was 500 atm^{-1} (P(CO) = pressure of CO).

$$K_p = \frac{[Cu(LBF_2)CO]}{[Cu(LBF_2)]P(CO)} \qquad (3)$$

Conversion of P(CO) to concentration of carbon monoxide in acetone completed the calculation of the binding constant, K_c, with carbon monoxide, 4.7(2) x 10^4 M^{-1}.

These spectroscopic binding studies of $Cu(LBF_2)$, 1, indicate much stronger binding with carbon monoxide (K_c = 4.7 x 10^4 M^{-1}) than with 1-methylimidazole (K_c = 16 M^{-1}). Carbon monoxide is a much better π-acceptor and a worse σ-base than 1-MeIm. If the copper(I) of $Cu(LBF_2)$, 1, binds a fifth ligand to delocalize its π-electron density, a strong bond between $Cu(LBF_2)$, 1, and a π-acceptor is predicted. Similarly, a weak interaction is predicted for the

Figure 6

Visible spectral changes observed on addition of 1-methylimidazole to a solution of $Cu(LBF_2)$, 1, in acetone.

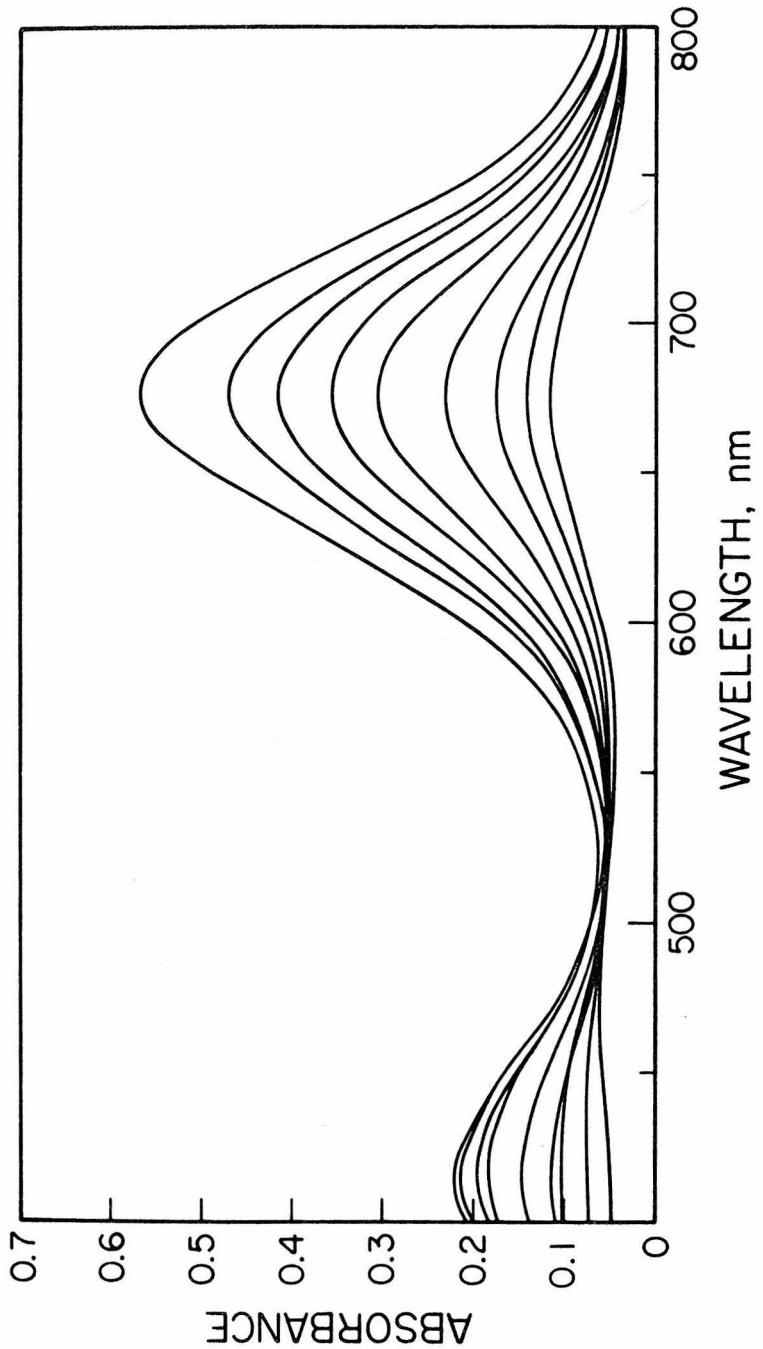

Figure 6

binding of an electron-rich metal and σ-base. Because of the strong CO binding constant, the copper(I) in the four-coordinate complex is electron rich and delocalizes electron density onto carbon monoxide.

The CO stretching frequency of $Cu(LBF_2)CO$, 2, is 2068 cm^{-1} (nujol) and 2080 cm^{-1} (CH_2Cl_2 solution). The other copper(I)-carbon monoxide complexes crystallographically analyzed have CO stretching frequencies from 2083 cm^{-1} ($Cu[HB(pz)_3]CO$, 10, nujol (44)) to 2066 and 2055 cm^{-1} ($[Cu_2(Hm)_3(CO)_2](BPh_4)_2$, 12, nujol (26)). Similar frequencies are found for other copper(I)-carbon monoxide complexes (45). The stretching frequencies are reduced from the free CO value, ν_{CO} = 2143 cm^{-1}. If carbon monoxide binds solely by its carbon σ-lone pair, it is theoretically predicted (46) and experimentally confirmed that the carbon-oxygen bond strength increases. The complex, H_3B-CO, has a CO stretching frequency of 2164 cm^{-1} (47). Therefore, further evidence of a π-interaction between copper(I) and carbon in copper-CO complexes is provided by the reduction in ν_{CO}.

From the similarities in the CO stretching frequencies of copper(I)-carbon monoxide complexes, no substantial electronic differences appear to exist in the copper-carbon bonds. However, there is no correlation between $Cu(LBF_2)CO$, 2, and the other copper-CO complexes in either geometry or effective atomic number. Some difference must exist either in the overall electronic make-up of the complex or in the geometry of the complex due to the macrocycle.

The geometries available to copper(I) when coordinated to the macrocycle, LBF_2, may be unusual or severely strained. To probe a steric explanation for the existence of the complex, $Cu(LBF_2)CO$, 2, the crystal structure of the precursor $Cu(LBF_2)$, 1, was determined. In Sections C and H the results are reported.

SECTION C

Crystal and Molecular Structure of $Cu(LBF_2)$, 1

An inquiry into the coordination geometry of copper(I) in $Cu(LBF_2)$, 1, is necessary to the understanding of $Cu(LBF_2)CO$, 2. With the knowledge of the structure of the five-coordinate complex, possible structures for the precursor were postulated. If the metal was simply too large for the LBF_2 macrocycle, the structure might show solid state oligomerization or, fantastically, the copper may sit out of the four-nitrogen plane bare. Another structure, not predicted by analytical results, has a solvent molecule as a fifth ligand. The molecular structure found for $Cu(LBF_2)$, 1, is summarized in this section and Section H, a copy of a paper accepted for publication in Inorganic Chemistry, December, 1978.

The copper in $Cu(LBF_2)$, 1, is four-coordinate. The metal sits essentially within the macrocycle, equidistant from the four nitrogens. Copper-nitrogen bond lengths range from 1.937(2) to 1.943(2) Å (Figure 7). The geometry about copper(I) is best described as a distorted square plane. Cis N-Cu-N bond angles, 90° in a perfect square, range from 82.3(1) to 103.3(1)° (Figure 8A). The trans N-Cu-N angles, theoretically 180°, are 161.5(1) and 162.9(1)°.

The four nitrogens of the macrocycle twist around the copper, distorting the square plane. Dihedral angles of 23° and 27° are

Figure 7

An ORTEP drawing of the four-coordinate complex, $Cu(LBF_2)$, 1, with the copper-nitrogen bond lengths labeled. Thermal ellipsoids are at the 50% probability level. Hydrogen atoms are omitted.

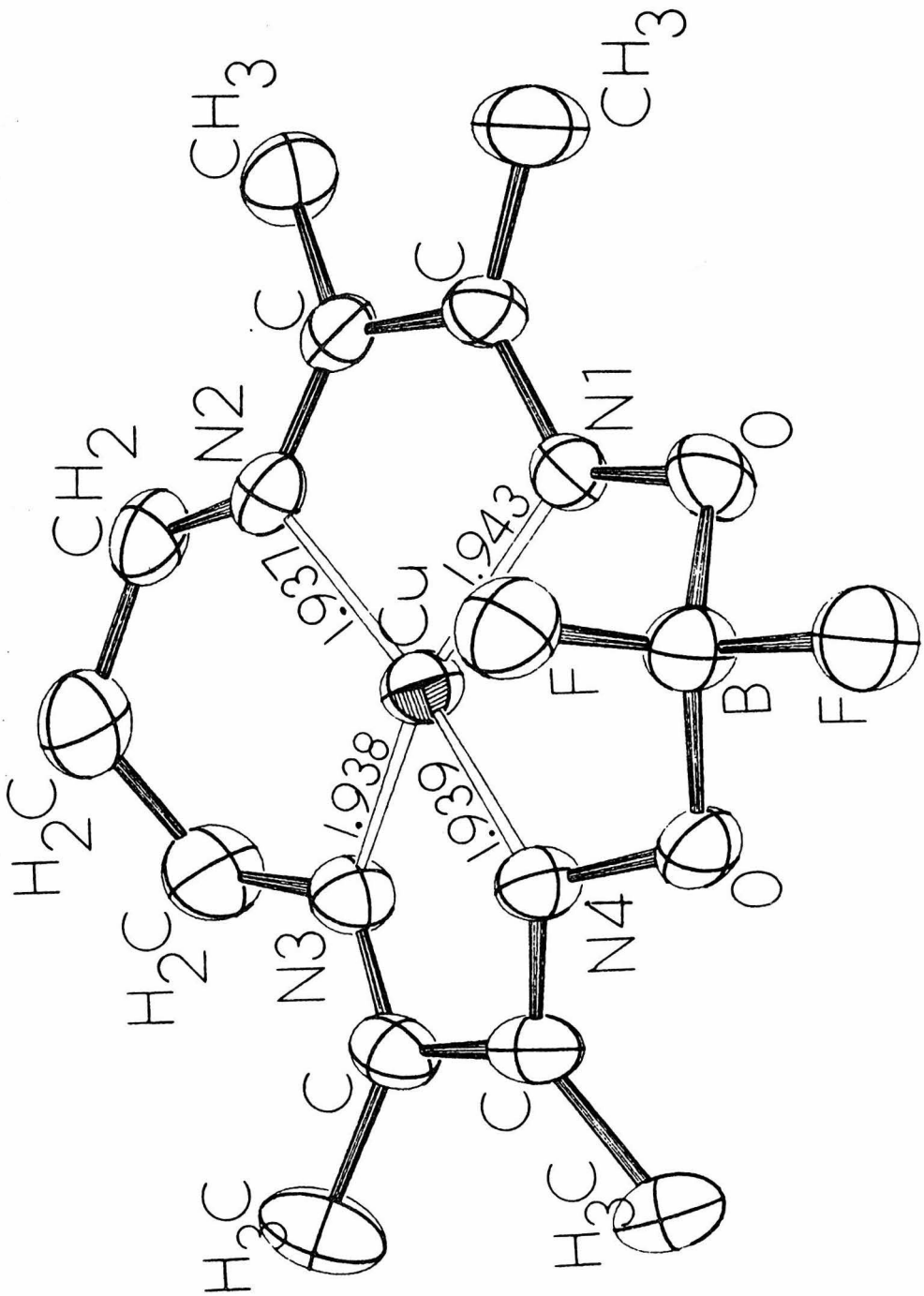
CH3
CH3
C
C
N2
N1
CH2
O
1.937
1.943
Cu
F
B
F
H2C
1.938
1.939
O
H2C
N3
N4
C
C
H3C
H3C

Figure 7

Figure 8

A. The four cis N-Cu-N angles are presented with a nitrogen labeling scheme identical to that in Figure 7. B. One dihedral angle, between the N2-Cu-N3 and N1-Cu-N4 planes, is illustrated.

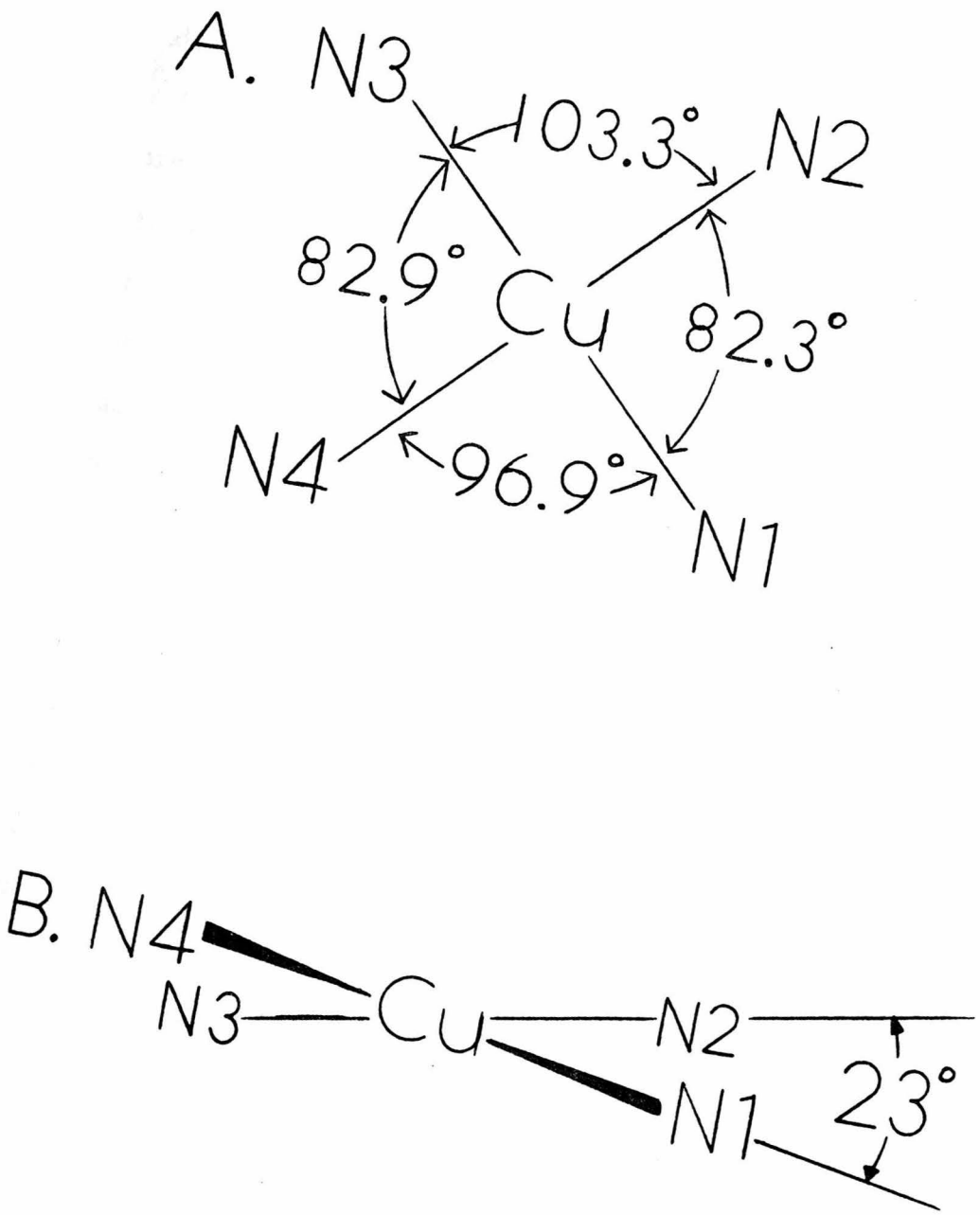

Figure 8

found between opposing copper, two nitrogen planes (Figure 8B). For a square plane there is no dihedral angle; for a tetrahedron dihedral angles equal 90°.

Characterization of a four-coordinate copper(I) complex as a square plane vs. a tetrahedron is unusual. A distorted square-planar geometry is found for copper(I) in copper(I) acetate (48,49). Each metal center binds three oxygen atoms and is 2.556(2) Å from another copper. The copper coordination is precisely planar (trans angles equal 180°), but cis angles range from 80.4(2)° to 110.5(3)°. No other square-planar complexes are known for copper(I).

Other than $Cu(LBF_2)CO$, 2, and $Cu(LBF_2)$, 1, there is apparently only one other copper(I) macrocyclic complex that has been crystallographically analyzed. The complex is 1,4,8,11-tetrathiacyclotetradecanecopper(I) perchlorate, $Cu(14\text{-ane-}S_4)ClO_4$, 14 (50). The copper in $Cu(14\text{-ane-}S_4)ClO_4$, 14, binds to three sulfurs of one macrocycle and one sulfur of a second macrocycle for a distorted tetrahedral geometry. The overall structure is a chain polymer with a three to one coordination pattern. The macrocycle, 14-ane-S_4, is not flexible enough to bind copper(I) in the preferred tetrahedral geometry, but it has a configuration capable of binding to two different metals tetrahedrally. The LBF_2 macrocycle does not seem to have the polymeric configuration available to it or solid state oligomerization would result. However, the basically square-planar macrocycle is capable of surprising distortion toward tetrahedrality.

In the complex, $Cu(LBF_2)$, 1, the four nitrogens of the macrocycle are alternately 0.3 Å above and below the best plane determined by the positions of the copper and four nitrogens. The copper is displaced only 0.01 Å from this plane. The macrocycle stabilizes the copper(I) by undergoing the maximum distortions of which it is capable.

The geometries of both $Cu(LBF_2)$, 1, and $Cu(LBF_2)CO$, 2, are unusual for copper(I) complexes. It has been suggested that the complexes might actually be copper(II) or (III) complexes with radical anion or dianion ligands. Evidence for the assignment of the copper(I) oxidation state for both complexes is found in Section D.

SECTION D

Oxidation State of Copper in $Cu(LBF_2)$, 1, and $Cu(LBF_2)CO$, 2

The basic structures of $Cu(LBF_2)$, 1, and $Cu(LBF_2)CO$, 2, square-planar and square-pyramidal, respectively, are unusual for d^{10} copper(I). However, for copper(II) centers, square-planar and square-pyramidal structures are relatively common. The formulation of the copper in $Cu(LBF_2)$, 1, and $Cu(LBF_2)CO$, 2, as copper(II), not copper(I) is superficially inviting because of coarse geometrical comparisons. Close examination of relevant experimental observations is necessary to unambiguously define the metal oxidation state.

The four-coordinate complex, $Cu(LBF_2)$, 1, was synthesized in acetone by a one-electron electrochemical reduction of the copper(II) complex, $Cu(LBF_2)ClO_4$, 9,(-0.7V, *vs.* normal hydrogen electrode, NHE) (8). The copper(II) complex was reduced reversibly at a half-wave potential of -0.456 V *vs.* NHE in dimethylformamide. Further reductions occurred below -1.5 V. To examine the reduction potential(s) of the macrocycle, either the ligand, isolated free of metal, or the analogous zinc(II) complex can be electrochemically studied. In both cases, the reduction process will occur on the ligand. The salt of the anionic ligand, LBF_2, has not been isolated. The zinc(II) complex, $[Zn(LBF_2)]_2(ClO_4)_2 \cdot CH_3OH$, 15, was synthesized and a sample was supplied by G. C. Lisensky. The zinc complex is electro-

chemically inactive in the region +0.20 to -0.95 V and has reduction waves below -0.95 V. Therefore, the site of reduction in $Cu(LBF_2)ClO_4$, 9, at -0.456 V, is the copper center; ligand reductions do not occur until a more negative potential is applied.

Both $Cu(LBF_2)$, 1, and $Cu(LBF_2)CO$, 2, are diamagnetic by magnetic susceptibility, and no EPR signals are observed for either complex. (EPR spectra were obtained by R. R. Gagné.) These points support a copper(I) oxidation state, a very closely coupled copper(II)-radical anion species, or a copper(III)-dianion complex.

There is no obvious structural evidence of macrocyclic ligand reduction in $Cu(LBF_2)$, 1, or $Cu(LBF_2)CO$, 2. (Detailed structural comparisons are made in Section H.) Furthermore, the LBF_2 ligand is distorted toward tetrahedrality in $Cu(LBF_2)$, 1. The four nitrogens are not in a square-planar array as would be expected for copper(II) or copper(III). No square-planar complex of LBF_2 has been crystallographically elucidated, but evidence of its ability to bind in a square plane is provided by the closely related macrocycle complex, $Rh(L'BF_2)(CH_3)I$, 16 (51). The crystal structure of this complex, where $L'BF_2$ is 1,1-difluoro-4,12-diethyl-5,11-dimethyl-1-bora-3,6,10,13-tetraaza-2,14-dioxo-cyclotetradeca-3,5,10,12-tetraenato ligand, has the four nitrogens of the macrocycle in a square plane around rhodium(III). The coarse geometrical argument for an oxidation state for $Cu(LBF_2)$, 1, other than copper(I) is totally invalid.

The four-coordinate $Cu(LBF_2)$, 1, binds both carbon monoxide, a good π-acceptor, and 1-methylimidazole, a good σ-base. Carbon

monoxide is bound more strongly (K_c = 4.7 x 10^4 M^{-1}in acetone) than 1-MeIm (K_c = 16 M^{-1}). That the complex, Cu(LBF_2), 1, binds a π- acceptor more strongly than a σ-base suggests an electron-rich copper atom. (Further ligand studies, described in Section E, support the finding that π-acceptors bind more strongly to Cu(LBF_2), 1, than σ-bases.)

The complex, Cu(LBF_2)CO, 2, is formed by rapid reaction of carbon monoxide and Cu(LBF_2), 1. No complexes characterized by spectral or physical properties to be copper(II) or copper(III) have been reported to bind CO. The copper in Cu(LBF_2), 1, reacts like copper(I).

Reduction potentials, magnetic properties, geometries, binding studies and reactivities provide evidence for a copper(I) oxidation state formalism for Cu(LBF_2), 1, and Cu(LBF_2)CO, 2. The x-ray photoelectron spectra of these complexes and other copper(II) and copper(I) complexes were measured by A. Mialki and R. A. Walton of Purdue University. By comparison of the copper binding energies of these complexes with the binding energies of known complexes, the oxidation states of the metal were assigned.

The results of the x-ray photoelectron spectroscopy (XPS) of copper macrocyclic complexes are given in Table II. The Cu $2p_{3/2}$ binding energies are in two sets. The range of binding energies of compounds 3, 6, and 9 is 935.2-935.4 eV. For Cu(LBF_2), 1, and Cu(LBF_2)B, where B is CO, 2, and 1-MeIm, 17, the binding energies

Table II. X-Ray Photoelectron Spectra of Copper Macrocyclic Complexes

Complex	Binding Energies, eV[a]				
	Cu $2p_{3/2}$	N 1s	C 1s	Cl $2p_{3/2}$	F 1s
Cu(trans-diene)$(ClO_4)_2$, 3	935.2(1.5)[b]	399.8(1.5)	285.1	207.5	
Cu(TAAB)$(NO_3)_2$, 6	935.4(2.0)[b]	400.2(1.3) 406.3(1.4)	285.1		
Cu$(LBF_2)ClO_4$, 9	935.4(1.7)[b]	399.7(1.4) 401.1(1.5)	285.4 286.4sh	207.5	686.1
Cu(LBF_2), 1	932.9(1.6)[c]	~399.9(3.0)	285.1		685.7
Cu(LBF_2)CO, 2	933.1(1.6)[c]	~400.0(4.0)	285.1		
Cu(LBF_2)(1-MeIm), 17[d]	932.9(1.8)[c]	400.0(3.3)	285.2		

[a] Full width half maximum values (fwhm) for the Cu $2p_{3/2}$ and N 1s peaks are given in parentheses. The Cu $2p_{1/2}$ component is located at 20.0 ± 0.2 eV above that of the $2p_{3/2}$ peak.

[b] Weak peak located at ~933.0 eV due to small amounts of Cu(I) produced by x-ray photoreduction. The intensity of this peak decreased further upon reduction of the x-ray power.

[c] A weak peak centered between 934.8 and 935.2 eV arises from trace amounts of surface oxidation to Cu(II). The oxidation occurs during sample preparation.

[d] Isolated by R. R. Gagné.

are lower and range from 932.9 to 933.1 eV. All six complexes have a basic four nitrogen coordination sphere. Binding energies for other copper complexes with nitrogen ligands are known and are presented in Table III with line drawings of three of the polydentate complexes in Figure 9.

The range of Cu $2p_{3/2}$ binding energies for the complexes in Table III is 934.0 to 935.3 eV. The compounds are characterized as copper(II) complexes. The macrocyclic complexes, Cu(trans-diene)$(ClO_4)_2$, 3, Cu(TAAB)$(NO_3)_2$, 6, and Cu$(LBF_2)ClO_4$, 9, have Cu $2p_{3/2}$ binding energies in the same range. Also, there are shake-up satellites to the high binding energy side of the primary $2p_{1/2,3/2}$ peaks for all these compounds. Shake-up satellites are found only for metals with unfilled d shells (56). The formulation of the macrocyclic complexes as copper(II) derivatives is supported, therefore, by both the similarity in Cu $2p_{3/2}$ binding energies with previously characterized Cu(II) compounds and the presence of shake-up satellites.

The Cu $2p_{3/2}$ binding energies of Cu(LBF_2), 1, Cu(LBF_2)CO, 2, and Cu(LBF_2)(1-MeIm), 17, are lower than those found for the copper(II) characterized complexes. There is a chemical shift of 2.5 eV in the Cu $2p_{3/2}$ binding energies between Cu$(LBF_2)ClO_4$, 9, and Cu(LBF_2), 1. This shift is indicative of a change in oxidation state from copper(II) to copper(I). Chemical shifts between related copper(II) and copper(I) compounds of 1.4 eV (CuO, Cu_2O) (56), 1.6 eV ($CuBr_2$, CuBr) (57), and 1.6-2.7 eV (Cu(II) and Cu(I) carboxylates) (58) are known. As a further indication of the copper(I) oxidation state, no shake-up

Table III. X-Ray Photoelectron Spectra of Copper Complexes with Nitrogen Ligands

Complex[b]	Binding Energy, eV[a] Cu $2p_{3/2}$
$[Cu(py)_2Cl_2]_n$ (52)	934.5
$Cu(py)_4(ClO_4)_2$ (53)	934.4
$[Cu(bipy)Cl_2]_n$ (54)	934.0
$Cu(terpy)Cl_2$ (54)	934.9
$[Cu(phen)Cl_2]_n$ (54)	934.3
$[Cu(en)_2](SCN)_2$ (52)	935.3
$Cu(trien)(ClO_4)_2 \cdot H_2O$ (54)	934.8
[Cu(tren)NCS]CNS (52)	935.0
$Cu(tren)Cl_2$ (52)	934.8
Cu(poly-1)[c] (55)	935.1
Cu(poly-2)[c] (55)	934.6
Cu(phthalocyanine)[c] (53)	934.1

[a]See X-Ray Photoelectron Spectroscopy in Experimental Section for explanation of binding energy standardization.

[b]Ligand abbreviations: py, pyridine; bipy, 2,2'-bipyridine; terpy, 2,2',2''-terpyridine; phen, 1,10-phenanthroline; en, ethylenediamine; trien, triethylene tetramine; tren, tris(2-aminoethyl)amine.

[c]See Figure 9 for ligand identification.

Figure 9

Skeletal representations of three copper(II) compounds with Cu $2p_{3/2}$ binding energies given in Table III. A. Cu(poly-1); B. Cu(poly-2); and C. Cu(phthalocyanine).

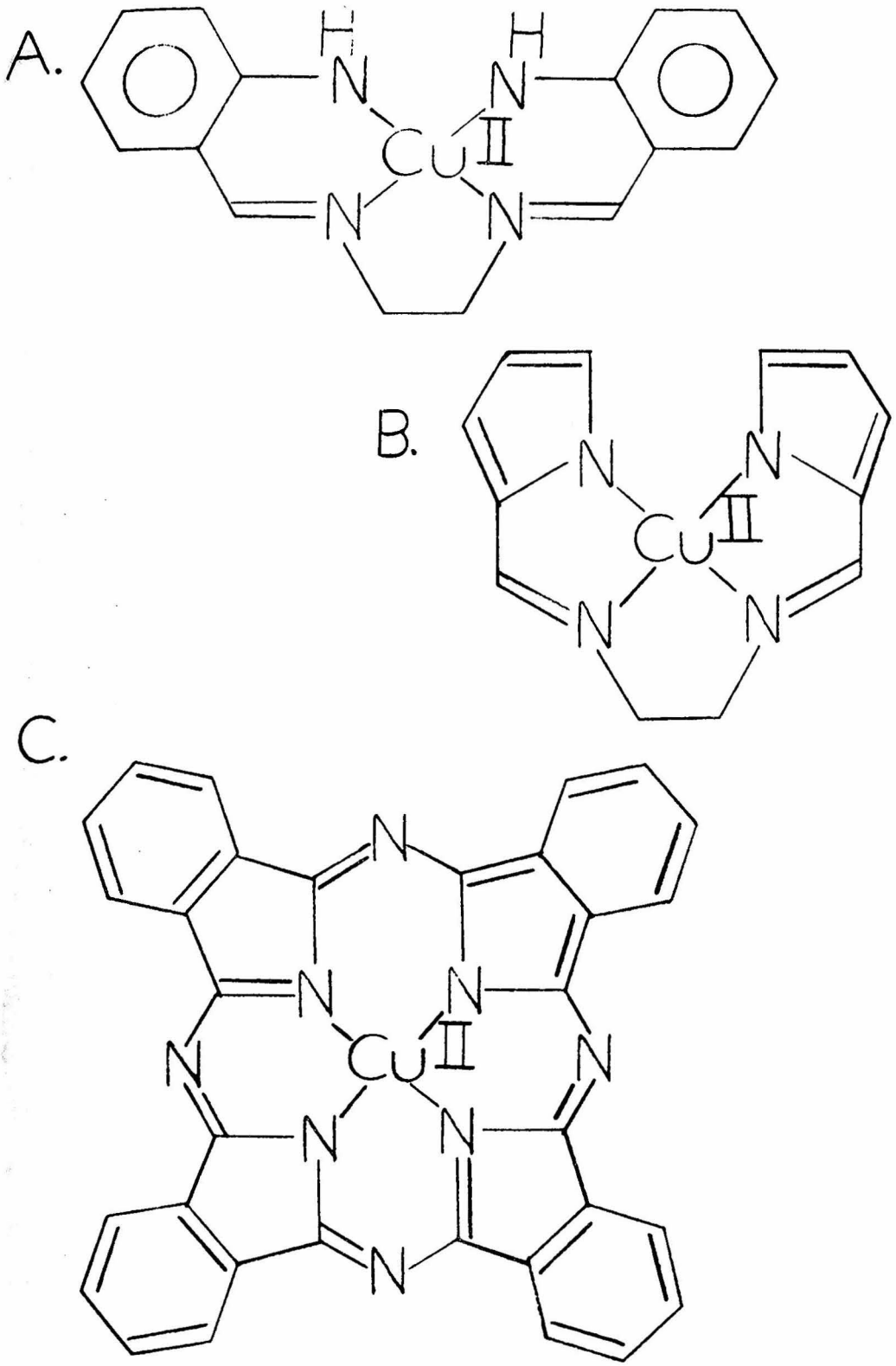

Figure 9

satellites were found for previously characterized copper(I) compounds (56-58) or for the copper macrocyclic complexes of this study, 1, 2, and 17. Formulation of these three complexes as copper(I) complexes is strongly supported by XPS.

A surface oxidation process, which is not a problem for bulk measurements, occurs for the three copper(I) complexes and causes the appearance of weak Cu 2p peaks at approximately 955 and 935 eV. These small peaks are found even though a nitrogen dri-lab is used in conjunction with the x-ray photoelectron spectrometer. With intentional exposure to air (up to thirty minutes), the weak 955 and 935 eV peaks increase in intensity until the intensity of the copper(II) peaks exceeds that of the copper(I) peaks. Solid state oxidation of $Cu(LBF_2)$, 1, $Cu(LBF_2)CO$, 2, and $Cu(LBF_2)$(1-MeIm), 17, is more consistent with the copper(I) oxidation state than the copper(II) formulation because few copper(II) compounds are oxidized to copper(III) by oxygen (59).

Through experimental observations the oxidation state of copper in $Cu(LBF_2)$, 1, and $Cu(LBF_2)CO$, 2, has been established to be +I. X-ray photoelectron spectroscopic data indicate the same oxidation state for $Cu(LBF_2)$(1-MeIm), 17. An investigation into the forces behind the binding of fifth ligands to $Cu(LBF_2)$, 1, proceeds on the foundation of these clearly characterized complexes. The following section presents the results of further ligand binding studies.

SECTION E

The Binding of Fifth Ligands to $Cu(LBF_2)$, 1, and $[Cu(LBF_2)]_2(ClO_4)_2 \cdot C_4H_8O_2$, 9

Binding constants for the coordination of carbon monoxide and 1-methylimidazole to $Cu(LBF_2)$, 1, were determined (Section B). The π- acceptor, carbon monoxide, binds more strongly (4.7×10^4 M^{-1}) than the σ-base, 1-MeIm (1.6×10^1 M^{-1}). To extend the binding constant studies to other ligands a new method was needed. The determination of binding constants by visible spectral measurements was tedious; the air-sensitive solutions had to be prepared in the helium dri-lab and large amounts of the electrochemically synthesized $Cu(LBF_2)$, 1, were consumed. To study a larger number of fifth ligands an approach with copper(II) as a starting material was used. This method is introduced in the following paragraphs.

From the Nernst equation (equation 4),

$$E = E^o + \frac{RT}{nF} \ln \frac{[M^{ox}]}{[M^{red}]} \qquad (4)$$

E = electrode potential.

E^o = the standard potential of the reduction of M^{ox}, oxidized species, to M^{red}, reduced species.

R = the gas constant.

T = temperature, ^oK.

n = equivalents of electrons per mole of electroactive species.

F = the Faraday.

an expression can be derived that relates reduction potentials and copper(II) and copper(I) binding constants. If only the two equilibria (equations 5 and 6) occur in solution,

$$Cu(II) + B \rightleftharpoons Cu(II)B \tag{5}$$

$$K^{II} \equiv \frac{[Cu(II)B]}{[Cu(II)][B]}$$

$$Cu(I) + B \rightleftharpoons Cu(I)B \tag{6}$$

$$K^{I} \equiv \frac{[Cu(I)B]}{[Cu(I)][B]}$$

the derived electrochemical equation (equation 7) is

$$E_{1/2}(B) = E_{1/2}(Ar) + \frac{RT}{nF} \ln \left[\frac{1+K^{I}[B]}{1+K^{II}[B]} \right] \tag{7}$$

$E_{1/2}(B)$ = potential with added ligand B.

$E_{1/2}(Ar)$= potential under argon.

Appendix 1 summarizes the derivation of equation 7.

Experimentally, half-wave potentials were determined for a copper(II) solution under argon and with various concentrations of ligand, B. The binding constants, K^{II} and K^{I}, were calculated using a form of equation 7, given in equation 8

$$\frac{1}{e^{\Delta E(nF/RT)}-1} = \frac{1}{K^{I}-K^{II}}\left(\frac{1}{[B]}\right) + \frac{K^{II}}{K^{I}-K^{II}} \qquad (8)$$

$$\Delta E \equiv E_{\frac{1}{2}}(B)-E_{\frac{1}{2}}(Ar).$$

This expression is used when $K^{I} > K^{II}$. (A slightly different form of equation 7 results when $K^{II} > K^{I}$.) A plot of the reciprocal of the exponential term, $e^{\Delta E(nF/RT)}-1$, vs. the reciprocal of [B] has a slope equal to $1/(K^{I}-K^{II})$ and a y-intercept equal to $K^{II}/(K^{I}-K^{II})$. The binding constants, K^{I} and K^{II}, are determined from the slope and intercept values.

A simpler expression can be used when either K^{II} or K^{I} is zero. If K^{II} is zero, equation 7 becomes

$$e^{\Delta E(nF/RT)}-1 = K^{I}[B] \qquad (9)$$

One potential shift due to a single B concentration allows calculation of K^{I}.

Half-wave potentials for the reduction of copper(II) to copper(I) were evaluated from sampled dc polarograms. Figure 10 shows polarograms for $Cu(LBF_2)ClO_4$, 9, in N,N-dimethylformamide (DMF) with

Figure 10

Sampled dc polarograms with curves smoothed of $Cu(LBF_2)ClO_4$, 9 (0.5 mM), in DMF with 1. carbon monoxide, $E_{1/2}$ = -.296 V, and 2. argon, $E_{1/2}$ = -.456 V.

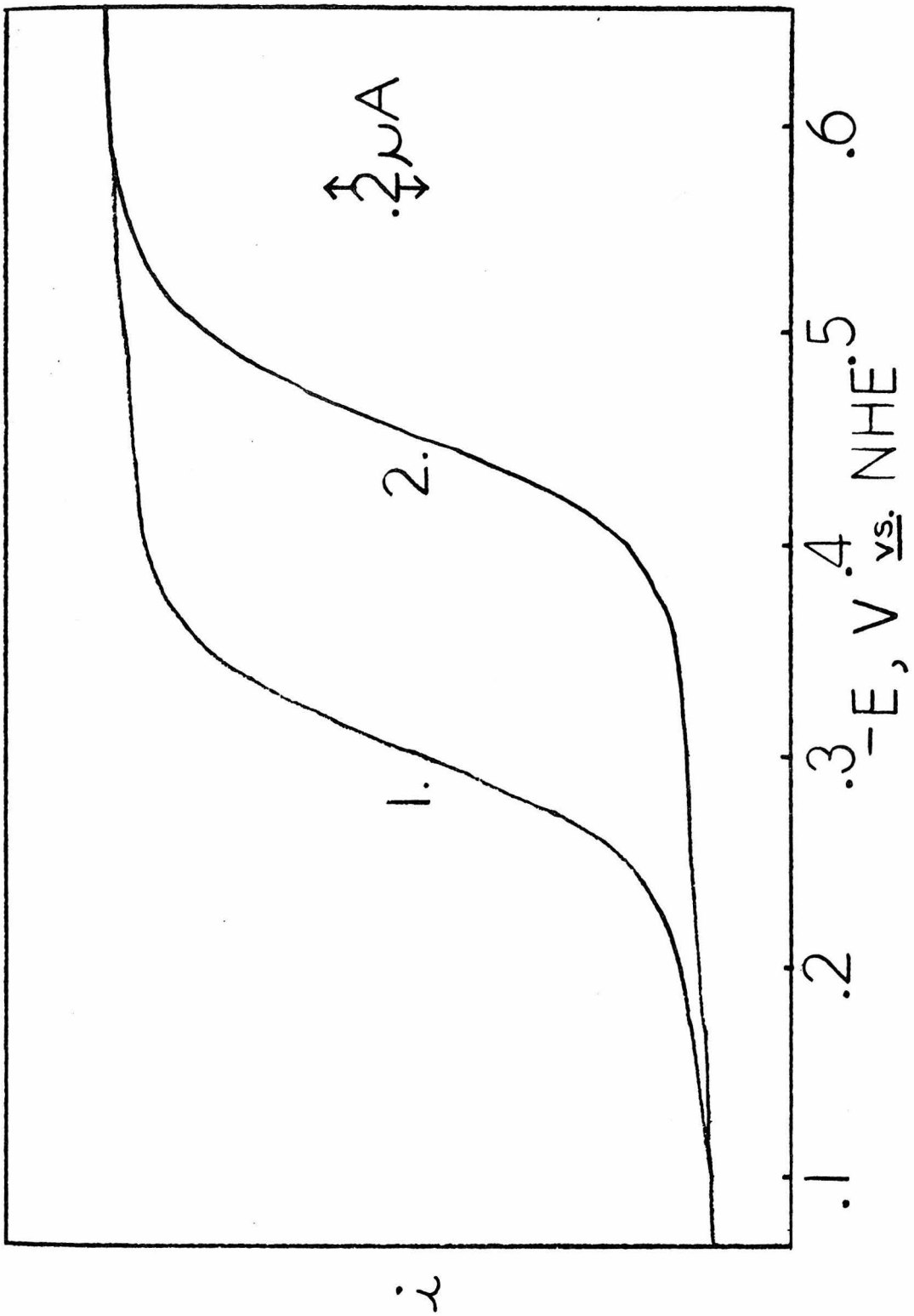

Figure 10

argon and carbon monoxide. The half-wave potential of a cathodic wave was evaluated using equation 10

$$E = E_{\frac{1}{2}} - \frac{RT}{nF} \ln \left[\frac{i}{i_d - i} \right] \qquad (10)$$

i = mean current.

i_d = mean diffusion current.

Figure 11 shows a polarogram with examples of i and i_d and the corresponding logarithmic analysis for $Cu(LBF_2)ClO_4$, 9. The first important value to be determined from the polarogram was the mean diffusion current, i_d. This current was used to calculate the diffusion current constant, I_d, which is characteristic of a compound in a particular solvent (equation 11).

$$I_d = \frac{i_d}{[C]m^{2/3}t^{1/6}} \qquad (11)$$

i_d = mean diffusion current, μA.

$[C]$ = bulk concentration of electroactive species, C, mM.

m = mercury flow rate per unit time, mg s^{-1}.

t = drop time, s.

The half-wave potential, $E_{\frac{1}{2}}$, is the intercept of the E *vs.* $\ln[i/(i_d-i)]$ plot (Figure 11). The slope of the plot equals -RT/nF, theoretically.

Figure 11

The upper drawing is the sampled dc polarogram of $Cu(LBF_2)ClO_4$, 9, (0.5 mM) in DMF with CO (Figure 10, 1.) with i and i_d labeled. The lower graph shows the logarithmic analysis of the polarogram. The y-intercept of the plot of E vs. $\ln[i/(i_d-i)]$ is the half-wave potential, $E_{\frac{1}{2}}$.

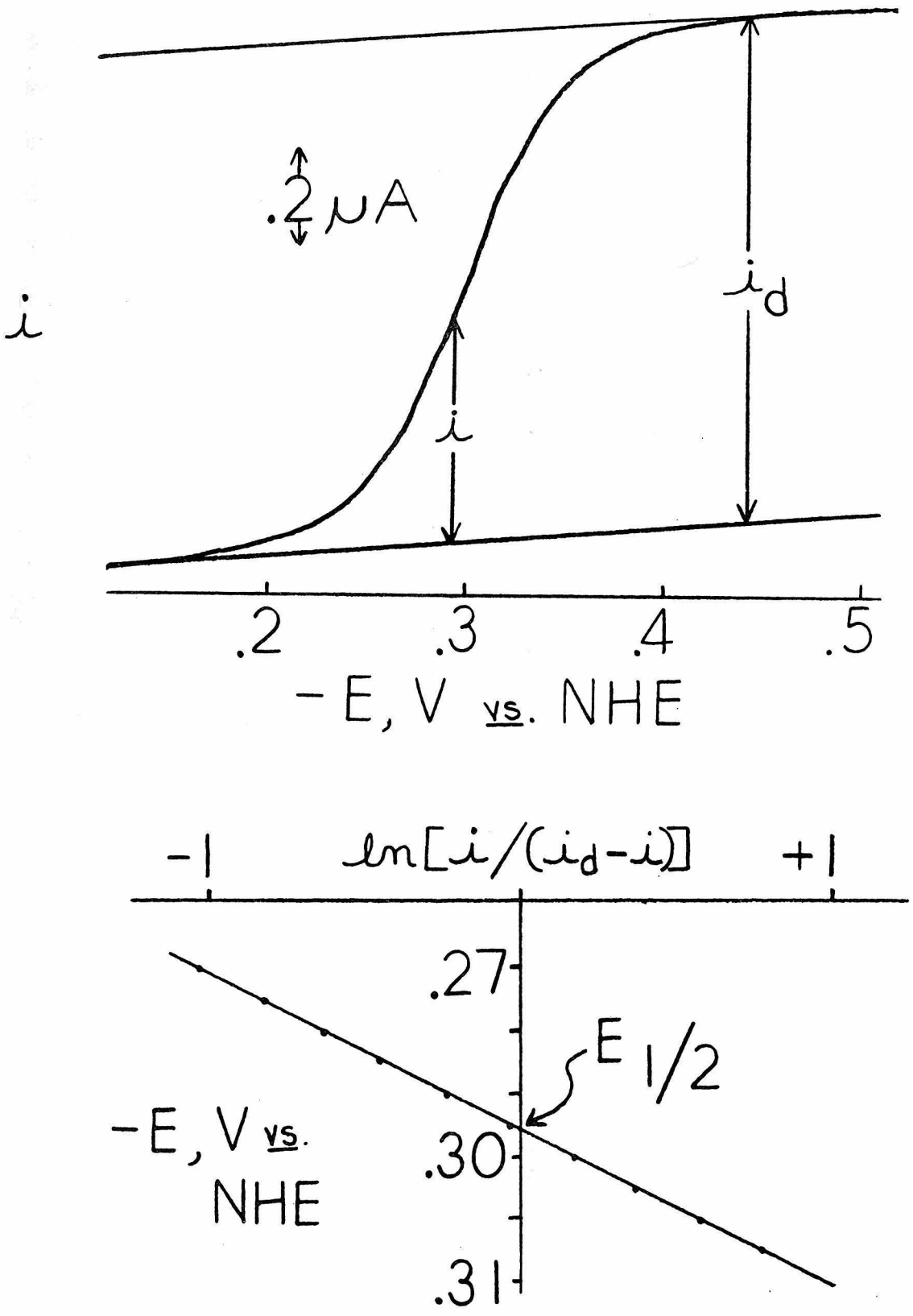

Figure 11

In practice the slope is used as a measure of the electrochemical reversibility of the redox couple; a reversible couple has a slope close to the theoretically predicted value. The logarithmic analyses of polarograms of $Cu(LBF_2)ClO_4$, 9, with added ligands at initial concentration, $[B]_i$, resulted in values for I_d, -slope, and $E_{\frac{1}{2}}(B)$, presented in Tables IV (solvent, DMF) and V (solvent, acetone). For some ligands other than $P(p\text{-}C_6H_4Cl)_3$ and pyridine a series of different ligand concentrations was examined, but the data presented are representative.

The mean diffusion coefficient, I_d, differs for $Cu(LBF_2)ClO_4$, 9, in DMF (1.70) and acetone (2.93) but is reasonably constant with added ligands, B, in a given solvent. The negative slope should be 58.6 mV at 22° C for n=1. For the reduction of copper(II) to copper(I) in the presence of ligand, B, the logarithmic analyses result in negative slopes varying from 54.8 to 81.5 mV. The majority of slopes are close to 58.6 mV and the reduction processes are electrochemically reversible. The glaring exceptions (in DMF) are $P(O\text{-}Bu)_3$ (-79.2 mV), $P(O\text{-}C_6H_{11})_3$ (-81.5 mV), and $P(p\text{-}C_6H_4Cl)_3$ at low $[B]_i$ (-67.2 to -72.1 mV). At low $[B]_i$ or at very high K^I a problem exists which is mirrored by the slope value. If the reduction process is reversible without B, on addition of B, a reversible process is found only if there is a sufficient excess of B to maintain the electrode surface concentration, $[B]_s$, at the initial level, $[B]_i$, throughout the polarographic run (60). If enough B is consumed

Table IV. Representative Sampled dc Polarographic Results for $Cu(LBF_2)ClO_4$, 9, and Fifth Ligands in N,N-dimethylformamide.[a]

Ligand, B	$[B]_i x10^3$, M	I_d[b]	-slope[c]	r^2[c]	$E_{1/2}(B)$, V[c]
no ligand[d]	0.0	1.70	56.8	.9993	-.456
p-NC(C_6H_4)NC	5.03	1.61	58.5	.9992	-.166
p-NO_2(C_6H_4)NC	5.08	1.69	64.5	.9996	-.168
P(O-C_6H_{11})$_3$	1.99	1.64	81.5	.9995	-.251
P(O-Bu)$_3$	2.06	1.65	79.2	.9995	-.270
P(O-p-C_6H_4Cl)$_3$	2.00	1.67	59.6	.9995	-.304
CO	4.64	1.70	57.3	.9997	-.296
P(O-p-$C_6H_4CH_3$)$_3$	1.03	1.60	67.0	.9999	-.349
P(O-o-$C_6H_4CH_3$)$_3$	2.41	1.53	58.7	.9998	-.337
P(p-C_6H_4Cl)$_3$	5.00	1.56	56.9	.9998	-.327
	2.00	1.71	62.9	.9998	-.352
	.960	1.69	67.2	.9998	-.375
	.800	1.64	68.2	.9993	-.380
	.640	1.70	72.1	.9997	-.389
P(p-$C_6H_4CH_3$)$_3$	2.00	1.56	64.0	.9989	-.360
P(C_6H_5)$_3$	2.00	1.71	62.6	.9999	-.363
P(o-$C_6H_4OCH_3$)$_3$	2.00	1.67	58.7	.9994	-.458
P(o-$C_6H_4CH_3$)$_3$	2.00	1.68	57.1	.9995	-.459

[a] [Cu(II)] = 5.00×10^{-4} M. Temperature, average value, 22° C. Drop time, t, 5 s.

[b] I_d, $\mu A\ s^{1/2}\ (mM)^{-1}\ (mg)^{-2/3}$.

[c] From linear regression fit of plot of E vs. $\ln[i/(i_d-i)]$: -slope, mV; r^2, coefficient of determination; $E_{1/2}(B)$, y-intercept.

[d] Average values.

Table V. Representative Sampled dc Polarographic Results for $Cu(LBF_2)ClO_4$, 9, and Fifth Ligands in Acetone.[a]

Ligand, B	$[B]_i x10^3$, M	I_d[b]	-slope[c]	r^2[c]	$E_{1/2}(B)$, V[c]
no ligand[d]	0.0	2.93	59.0	.9991	-.400
$P(O\text{-}Bu)_3$	2.05	2.70	59.9	.9987	-.168
$P(O\text{-}p\text{-}C_6H_4Cl)_3$	2.73	2.65	60.3	.9925	-.205
$P(C_6H_5)_3$	3.18	2.57	57.6	.9999	-.270
pyridine	100.4	2.78	57.3	.9994	-.462
	50.8	2.83	58.3	.9990	-.450
	33.5	2.81	58.0	.9995	-.440
	25.4	2.81	58.7	.9995	-.435
	20.3	2.80	58.0	.9993	-.431
	16.7	2.78	57.3	.9991	-.427
$4\text{-}(CH_3)_2N$pyridine	100.0	2.62	59.9	.9994	-.532
$(CH_3)_2N(C_6H_5)$	50.5	2.64	54.8	.9995	-.401
$4\text{-}CH_3OC(=O)$pyridine	116.9	2.60	56.9	.9997	-.434

[a] [Cu(II)] = 4.99×10^{-4} M. Temperature, average value, 22° C. Drop time, t, 5 seconds.

[b] I_d, $\mu A\ s^{1/2}\ (mM)^{-1}\ (mg)^{-2/3}$.

[c] From linear regression fit of plot of E vs. $\ln[i/(i_d-i)]$: -slope, mV; r^2, coefficient of determination; $E_{1/2}(B)$, y-intercept.

[d] Average values.

by its equilibrium with copper(I) (equation 6), $[B]_s$ decreases and $E_{1/2}$ changes to a more negative value during the reduction.

The strongly binding $P(O\text{-}Bu)_3$ and $P(O\text{-}C_6H_{11})_3$ have logarithmic plots with large negative slopes. A higher concentration of B is necessary to maintain $[B]_s$ throughout the reduction. Experimentally, plotting E vs. $\ln[i/(i_d\text{-}i)]$ is difficult for higher B concentrations due to background current problems (discussed below), so the polarograms at higher concentrations cannot be quantitatively analyzed. The data for $P(p\text{-}C_6H_4Cl)_3$ illustrate the gradual approach of the negative slope to 58.6 mV with increasing concentration.

Low concentrations of phosphine ligands were used due to background currents that increase with increasing ligand concentrations. Even with only 2 mM ligand, the polarogram of $P(p\text{-}C_6H_4CH_3)_3$ has non-parallel background and diffusion currents. The background current has a greater slope (i/E) initially due to the current from an oxidation wave of the ligand (61,62), which does not affect the more negative diffusion current of the copper(II) reduction. With increased ligand concentration, the very rapidly growing background current begins to overwhelm the slope of the copper(II) reduction, and accurate determination of the half-wave potential becomes difficult. Low concentrations of B were used to minimize the background current slope.

Problematically, however, low ligand B concentrations lead to variation in the slopes of the E vs. $\ln[i/(i_d\text{-}i)]$ plots from -58.6 mV, and also inaccuracy in $E_{1/2}$ determination. The value of $[B]_s$ at

equilibrium is not equal to the bulk or initial concentration of B, $[B]_i$, but is lowered by x, the concentration of Cu(I)B formed (equations 6 and 12).

$$Cu(I) + B \rightleftharpoons Cu(I)B \tag{6}$$

$$K^I = \frac{x}{([Cu(I)]_i - x)([B]_i - x)} \tag{12}$$

With $[B]_i$ and ΔE, an initial equilibrium constant, K_i^I, is calculated (equation 9). This constant, K_i^I, and $[B]_i$ are used to initiate an iterative calculation of x. The equilibrium or final concentration of B, $[B]_f$, is equal to $[B]_i$ minus the converged value of x. This value is used to determine K_f^I, the final equilibrium constant.

The calculated $[B]_f$ values for five concentrations of $P(p\text{-}C_6H_4Cl)_3$ are given in Table VI. Figure 12 graphically illustrates the difference between $[B]_i$ and $[B]_f$ in a plot of $e^{\Delta E(nF/RT)}-1$ *vs* [B] (see equation 9). The calculated y-intercepts of the two plots are -8.29, $[B]_i$, and -0.42, $[B]_f$. For any ligand at [B]=0, ΔE is zero and the plot should pass through the origin. The use of $[B]_f$ adjusted the y-intercept closer to zero, with minimal change in slope (3.33×10^4 to $3.34 \times 10^4\ M^{-1}$).

The other difficulty with low concentrations of ligand is ambiguity in the position of the half-wave potential. The $E_{\frac{1}{2}}$ values determined from E *vs*. $\ln[i/(i_d-i)]$ plots and $[B]_f$ values calculated

Table VI. Iterative Ligand Reduction Results for $Cu(LBF_2)ClO_4$, 2, and $P(p\text{-}C_6H_4Cl)_3$ in N,N-dimethylformamide.

$[B]_i x10^3$, M[a]	$(e^{\Delta E(nF/RT)}-1)$[b]	$K_i^I x10^{-4}$, M^{-1}[c]	$[B]_f x10^3$, M[a]	$K_f^I x10^{-4}$, M^{-1}[c]
5.00	158.3	3.17	4.74	3.33
2.00	58.63	2.93	1.75	3.34
0.960	23.15	2.41	0.720	3.21
0.800	18.84	2.35	0.563	3.35
0.640	12.93	2.02	0.408	3.17

[a] $[B]_i$, $[B]_f$ = initial and final B concentrations, respectively.

[b] $\Delta E \equiv E_{1/2}(B) - E_{1/2}(Ar)$.

[c] K_i^I, K_f^I = initial and final equilibrium constants, respectively. $K_{i,f}^I = (e^{\Delta E(nF/RT)}-1)/[B]_{i,f}$.

Figure 12

Graph of $e^{\Delta E(nF/RT)}-1$ *vs.* [B] for five concentrations of $P(p\text{-}C_6H_4Cl)_3$ in DMF with 0.5 mM $Cu(LBF_2)ClO_4$, 9. $\Delta E \equiv E_{\frac{1}{2}}[P(p\text{-}C_6H_4Cl)_3]-E_{\frac{1}{2}}(Ar)$. Line 1 is the plot using $[B]_f$, the corrected ligand concentration. The slope is 3.34×10^4 M^{-1}, the y-intercept is -0.42, and r^2 is 0.9999. Line 2 is the plot using $[B]_i$, the initial ligand concentration. The slope is 3.33×10^4 M^{-1}, the y-intercept is -8.29, and r^2 is 0.9999.

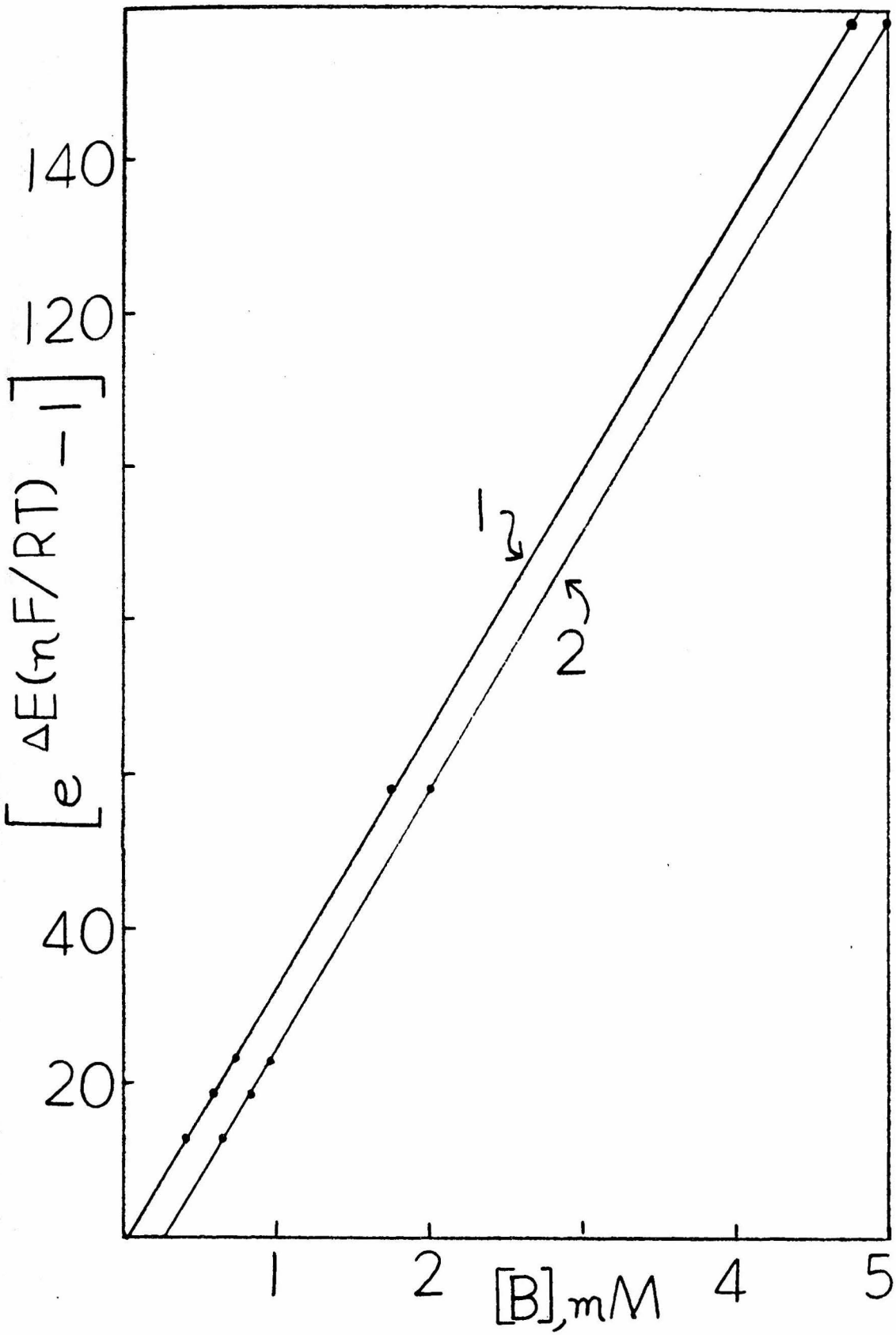

Figure 12

iteratively used to find K_f^I (equation 9). When several initial concentrations of B were examined, a plot of $e^{\Delta E(nF/RT)}-1$ *vs.* $[B]_f$ (as in Figure 12) was constructed and the slope, equal to K_f^I, determined. The coefficient of determination, r^2, is an indication of the linearity of the data pairs. Table VII condenses the results of both simple calculations of K_f^I from a single ΔE, $[B]_f$ pair and the linear regression calculations of slopes, intercepts and coefficients of determination for a series of ΔE, $[B]_f$ pairs. With the assumption that K_f^{II} is zero, K_f^I values are calculated and the r^2 values indicate a good data fit. Because of the correlation of high and low ligand concentration data, the determination of $E_{1/2}$ is concluded to be smaller than the theoretically predicted error, $\Delta E'$ (equation 13) (63).

$$\Delta E' \approx \frac{RT[Cu(II)]}{2nF[B]} \qquad (13)$$

The error, $\Delta E'$, is ±.0015 V with $[Cu(II)] = 5 \times 10^{-4}$ M and $[B] = 2 \times 10^{-3}$ M. An error of ±.0025 V in $E_{1/2}(B)$ is estimated, corresponding to $[B] = 1.25 \times 10^{-3}$ M or, as intended, large enough to include instrumental and technique errors at all B concentrations.

With an estimation of error in $E_{1/2}(B)$ the important question of binding constant values can be addressed. Binding constants were evaluated using the assumptions $K_f^{II}=0$ (Table VII) and $K_f^I=0$ (Table VIII). The equation used is

$$e^{\Delta E(nF/RT)}-1 = K_f^{I,II}[B]_f \qquad (14)$$

Table VII. Determination of Binding Constants, K_f^I, with Assumption, $K_f^{II}=0$.

Ligand, B	Solvent	Points[a]	r^2[b]	b[b]	K_f^I, M^{-1}[b]
p-NC(C_6H_4)NC	DMF	3	.9942	-2500.	1.9×10^7
p-NO_2(C_6H_4)NC	DMF	3	.9996	-620.	1.7×10^7
P(O-C_6H_{11})$_3$	DMF	2			1.8×10^6
P(O-Bu)$_3$	DMF	2			8.3×10^5
	acetone	2			5.1×10^6
P(O-p-C_6H_4Cl)$_3$	DMF	5	.9970	8.6	2.2×10^5
	acetone	2			8.6×10^5
CO	DMF	2			1.2×10^5
P(O-C_6H_5)$_3$	DMF	5	.9960	-2.6	1.1×10^5
P(O-p-$C_6H_4CH_3$)$_3$	DMF	4	.9946	0.74	8.7×10^4
P(O-o-$C_6H_4CH_3$)$_3$	DMF	2			4.9×10^4
P(p-C_6H_4Cl)$_3$	DMF	6	.9999	-0.60	3.3×10^4
P(p-$C_6H_4CH_3$)$_3$	DMF	5	.9986	-0.66	2.4×10^4
P(C_6H_5)$_3$	DMF	5	.9984	0.59	2.1×10^4
	acetone	2			5.6×10^4
P(o-$C_6H_4OCH_3$)$_3$	DMF	2			0.0
P(o-$C_6H_4CH_3$)$_3$	DMF	2			0.0

[a] Points = number of ΔE, $[B]_f$ points used to determine K_f^I. This number includes (0,0) which is used in each K_f^I calculation.

[b] Plot of $e^{\Delta E(nF/RT)}-1$ vs. $[B]_f$; $\Delta E = E_{\frac{1}{2}}(B)-E_{\frac{1}{2}}(Ar)$. Coefficient of determination = r^2, y-intercept = b, slope = K_f^I.

Table VIII. Determination of Binding Constants, K_f^{II}, with Assumption, $K_f^{I}=0$.

Ligand, B	Solvent	Points[a]	r^2[b]	b[b]	K_f^{II}, M^{-1}[b]
$P(o\text{-}C_6H_4OCH_3)_3$	DMF	2			4.1×10^1
$P(o\text{-}C_6H_4CH_3)_3$	DMF	2			6.4×10^1
pyridine	acetone	7	.9929	0.24	1.0×10^2
$4\text{-}(CH_3)_2N$pyridine	acetone	7	.9101	28.	1.6×10^3
$(CH_3)_2N(C_6H_5)$	acetone	2			7.9×10^{-1}
$4\text{-}CH_3OC(=O)$pyridine	acetone	6	.9926	-.09	2.7×10^1

[a] Points = number of ΔE, $[B]_f$ points used to determine K_f^{I}. This number includes (0,0) which is used in each K_f^{II} calculation.

[b] Plot of $e^{\Delta E(nF/RT)}-1$ vs. $[B]_f$; $\Delta E = E_{1/2}(Ar)-E_{1/2}(B)$. Coefficient of determination = r^2, y-intercept = b, slope = K_f^{II}.

where $\Delta E = |E_{1/2}(B) - E_{1/2}(Ar)|$ and either K_f^I or K_f^{II} is calculated. Each calculation includes the point (0,0) and the linearity of all the points is indicated by the coefficient of determination, r^2, and the closeness of the y-intercept to zero. The fit was good in most cases. In only two cases were the data better fit by removal of the assumption that K_f^I or K_f^{II} is equal to zero. These cases are given in Table IX with the binding constant values, calculated using equation 8 or a closely related expression. Finally, Table X summarizes the best fit K_f^I and K_f^{II} values with errors (error in $E_{1/2}(B) = \pm .0025$ V).

The binding constants for copper(I) and fifth ligands (Table X) include values both greater and less than $K_f^I(CO)$. A general π-acceptor series predicts an order: CO ~ RNC > $P(OR)_3$ > PR_3 (64). The para-substituted phenylisocyanides are better π-acceptors than CO with the electron-withdrawing $-NO_2$ and -CN groups. Their K_f^I values were the largest measured, 1.9(4) x 10^7 M^{-1} for p-$NC(C_6H_4)NC$ and 1.7(2) x 10^7 M^{-1} for p-$NO_2(C_6H_4)NC$. Bonding by the cyano group in p-$NC(C_6H_4)NC$ can be neglected because $NC(C_6H_5)$ at a concentration of 3 x 10^2 M did not shift the copper(II) reduction wave in DMF. Phosphites bind more strongly than phosphines to $Cu(LBF_2)$, 1, and generally follow a π-acceptor order (see below). Carbon monoxide does not bind as well as $P(O\text{-}p\text{-}C_6H_4Cl)_3$, but binds more strongly than $P(O\text{-}C_6H_5)_3$. It binds slightly more strongly in DMF (1.2 x 10^5 M^{-1}) than in acetone (6.7 x 10^5 M^{-1}) (8). Weak binding to copper(I) occurs with 1-MeIm (16 M^{-1}, spectroscopic technique) and 4-dimethyl-

Table IX. Determination of Binding Constants, K_f^I and K_f^{II}

Ligand, B	Solvent	Points[a]	r^2[b]	K_f^I, M^{-1}[b]	K_f^{II}, M^{-1}[b]
$P(O\text{-}p\text{-}C_6H_4Cl)_3$	DMF	4	.9977	2.5×10^5	2.2×10^1
$4\text{-}(CH_3)_2N$pyridine	acetone	6	.9815	1.5×10^1	4.3×10^3

[a]Points = number of ΔE, $[B]_f$ points used to determine $K_f^{I,II}$. The point (0,0) is not used in these calculations.

[b]Plot of $1/(e^{\Delta E(nF/RT)}-1)$ vs. $1/[B]_f$; $\Delta E = |E_{1/2}(B)-E_{1/2}(Ar)|$. For $K_f^I > K_f^{II}$, y-intercept = $K_f^{II}/(K_f^I-K_f^{II})$, slope = $1/(K_f^I-K_f^{II})$. For $K_f^{II} > K_f^I$, y-intercept = $K_f^I/(K_f^{II}-K_f^I)$, slope = $1/(K_f^{II}-K_f^I)$. Coefficient of determination = r^2.

Table X. Final Binding Constants of Ligands with $Cu(LBF_2)ClO_4$, 9.

Ligand, B	Solvent	K^I, M^{-1} [a]	K^{II}, M^{-1} [a]
p-NC(C_6H_4)NC	DMF	1.9(4) x 10^7	0
p-NO_2(C_6H_4)NC	DMF	1.7(2) x 10^7	0
P(O-C_6H_{11})$_3$	DMF	1.8(2) x 10^6	0
P(O-Bu)$_3$	DMF	8.3(8) x 10^5	0
	acetone	5.1(5) x 10^6	0
P(O-p-C_6H_4Cl)$_3$	DMF	2.5(3) x 10^5	2.2(3) x 10^1
	acetone	8.6(9) x 10^5	0
CO	DMF	1.2(2) x 10^5	0
P(O-C_6H_5)$_3$	DMF	1.1(2) x 10^5	0
P(O-p-$C_6H_4CH_3$)$_3$	DMF	8.7(10)x 10^4	0
P(O-o-$C_6H_4CH_3$)$_3$	DMF	4.9(5) x 10^4	0
P(p-C_6H_4Cl)$_3$	DMF	3.3(4) x 10^4	0
P(p-$C_6H_4CH_3$)$_3$	DMF	2.4(3) x 10^4	0
P(C_6H_5)$_3$	DMF	2.1(3) x 10^4	0
	acetone	5.6(6) x 10^4	0
P(o-$C_6H_4OCH_3$)$_3$	DMF	0	4(6) x 10^1
P(o-$C_6H_4CH_3$)$_3$	DMF	0	6(6) x 10^1
$(CH_3)_2N(C_6H_5)$	acetone	0	8(20) x 10^{-1}
pyridine	acetone	0	1.0(3) x 10^2
4-$(CH_3)_2$Npyridine	acetone	1.5(2) x 10^1	4.3(4) x 10^3
4-CH_3OC(=O)pyridine	acetone	0	2.7(8) x 10^1

[a] K^I, K^{II} = 0 indicates an equilibrium constant of ≤ 10.

aminopyridine (15 M^{-1}, polarographic technique). The other pyridines (pyridine and 4-$CH_3OC(=O)$pyridine) do not bind to copper(I) within experimental error.

The overall order of the ligands' copper(I) binding constants supports the hypothesis that $Cu(LBF_2)$, 1, binds better to π-acceptors than to σ-bases. Closer examination of the phosphite, phosphine data also leads to this conclusion. Two factors influence the binding of the phosphorus ligands to copper(I). There is both a steric factor, the ligand cone angle (65), and an electronic factor, the donor-acceptor parameter of the ligand (66). The phosphorus ligands with their respective ligand cone angles, donor-acceptor parameters, and copper(I) binding constants are listed in Table XI. A larger donor-acceptor parameter results either from decreased σ-basicity or increased π-acidity. The evidence for π-character of the copper-carbon bond in $Cu(LBF_2)CO$, 2, suggests the ligand's π-acidity, not σ-basicity, is important. Also, a higher binding constant reflects a stronger copper-ligand interaction, which is unlikely to result from the bonding of a poorer σ-base to copper(I). Therefore, Tolman's donor-acceptor parameter will be used as an indication of π-acceptor ability.

A ligand with a larger donor-acceptor parameter will lead to better copper(I) binding if steric effects can be ignored. Can steric effects be ignored? The two ligands, $P(O\text{-}C_6H_{11})_3$, cone angle = 133-156°, and $P(O\text{-}Bu)_3$, cone angle = 109-114°, have approximately equal donor-acceptor parameters. The tributylphosphite is expected to bind a little stronger to copper(I) on electronic

Table XI. Phosphine Binding Constants (DMF) Compared to Electronic Effects and Cone Angles.

Phosphorus Ligand	Ligand Cone Angle, deg[a]	Donor-Acceptor Parameter[b]	K_f^I, M^{-1}
$P(O\text{-}C_6H_{11})_3$	133-156[c]	15.9	1.8(2) x 10^6
$P(O\text{-}Bu)_3$	109-114[d]	19.5	8.3(8) x 10^5
$P(O\text{-}p\text{-}C_6H_4Cl)_3$	121±10[e]	33.3	2.5(3) x 10^5
$P(O\text{-}C_6H_5)_3$	121±10	29.1	1.1(2) x 10^5
$P(O\text{-}p\text{-}C_6H_4CH_3)_3$	121±10[e]	27.9	8.7(10)x 10^4
$P(O\text{-}o\text{-}C_6H_4CH_3)_3$	165±10	28.2	4.9(5) x 10^4
$P(p\text{-}C_6H_4Cl)_3$	145±2[e]	16.8	3.3(4) x 10^4
$P(p\text{-}C_6H_4CH_3)_3$	145±2[e]	10.5	2.4(3) x 10^4
$P(C_6H_5)_3$	145±2	12.9	2.1(3) x 10^4
$P(o\text{-}C_6H_4OCH_3)_3$	≥194±6[f]	2.7	0.0
$P(o\text{-}C_6H_4CH_3)_3$	194±6	10.5	0.0

[a]Ligand cone angle is a steric effect parameter defined in ref. 65.

[b]Donor-acceptor parameter of the ligand is a π-electronic factor defined in ref. 66.

[c]The cone angle for $P(O\text{-}C_6H_{11})_3$ is estimated to be in this range by comparison to $P(C_6H_{11})_3$, 179°, and other phosphite-phosphine couples.

[d]Cone angle of $P(O\text{-}Bu)_3$: less than cone angle of $P(O\text{-}i\text{-}C_3H_7)_3$, 114°, and greater than that of $P(O\text{-}CH_2CH_3)_3$, 109°.

[e]The para-substituted phenyl phosphites and phosphines have cone angles equal to triphenylphosphite, 121°, and triphenylphosphine, 145°.

[f]Cone angle of $P(o\text{-}C_6H_4OCH_3)_3$: greater than or equal to the cone angle of $P(o\text{-}C_6H_4CH_3)_3$.

grounds and a lot stronger to copper(I) if steric factors are important. Actually, $P(O\text{-}C_6H_{11})_3$ binds more strongly. The conclusion is reached that a cone angle in the range of 133-156° does not sterically inhibit binding.

Comparison of $P(O\text{-}\underline{p}\text{-}C_6H_4CH_3)_3$ and $P(O\text{-}\underline{o}\text{-}C_6H_4CH_3)_3$ is also instructive. The 43° difference in cone angles is reflected in K_f^I. The para-substituted ligand binds approximately twice as well as the ortho-substituted ligand. Therefore, a cone angle of 165°, $P(O\text{-}\underline{o}\text{-}C_6H_4CH_3)_3$, begins to inhibit binding to $Cu(LBF_2)$, 1. Ortho-substituted phosphine ligands, $P(\underline{o}\text{-}C_6H_4X)_3$ (X = $-OCH_3$ and $-CH_3$), have cone angles of at least 194° and do not bind copper(I) at all.

The cone angle difference between the phenyl phosphites and phenyl phosphines is 23° and the larger cone angle is only 145°. These angles are within the range in which there are no obvious steric effects, as illustrated by $P(O\text{-}C_6H_{11})_3$ and $P(O\text{-}Bu)_3$. The copper(I) binding constants of these six related phosphorus ligands can be examined solely from an electronic viewpoint.

The donor-acceptor parameters of the six phosphite and phosphine ligands range from 33.3 to 10.5. The ligand with the largest donor-acceptor parameter, $P(O\text{-}\underline{p}\text{-}C_6H_4Cl)_3$, binds most strongly to copper(I), $K_f^I = 2.5(3) \times 10^5\ M^{-1}$. The only pair of ligands with a reverse trend are $P(\underline{p}\text{-}C_6H_4CH_3)_3$ (donor-acceptor parameter = 10.5, $K_f^I = 2.4(3) \times 10^4\ M^{-1}$) and $P(C_6H_5)_3$ (12.9, $2.1(3) \times 10^4\ M^{-1}$). However, the two binding constants are equal within experimental error. A direct correlation exists between the π-acidity of these

six phosphorus ligands and the binding constant with $Cu(LBF_2)$, 1. The phosphite, $P(O\text{-}p\text{-}C_6H_4Cl)_3$, is even a better π-acceptor than CO, possibly because of its electron-withdrawing chlorine.

From consideration of Tolman's donor-acceptor parameter, the ligands, $P(O\text{-}C_6H_{11})_3$ and $P(O\text{-}Bu)_3$, bind copper(I) much too strongly. Values of K_f^I of about 3×10^4 M^{-1} are expected from the values found in Table XI. The small tributylphosphite might bind more strongly due to steric effects but the tricyclohexylphosphite (the same size or a little larger than the phenyl phosphines) should bind no better. Both the butyl and cyclohexyl phosphites are different from the other phosphorus ligands because of their saturated substituents. In acetone the binding constants of $P(O\text{-}Bu)_3$, $P(O\text{-}p\text{-}C_6H_4Cl)_3$, and $P(C_6H_5)_3$ all are larger than the DMF values. The increase in K_f^I is greatest for the butyl phosphite, 0.83-5.1 x 10^6 M^{-1}, and least for the phenyl phosphine, 2.1-5.6 x 10^4 M^{-1} (Table X). These results implicate solvation effects. In DMF the phenyl phosphite and phosphine ligands may be more highly solvated than the saturated phosphites, which therefore bind copper(I) more easily. In acetone all phosphorus ligands measured have higher binding constants and are possibly solvated to a lesser degree. The butyl phosphite continues to be solvated the least and to bind most strongly. Further solvent studies are necessary to investigate solvation effects.

The copper(II) binding constants (Table X) follow the expected σ-base order: $4\text{-}(CH_3)_2N$pyridine > pyridine > $4\text{-}CH_3OC(=O)$pyridine.

The binding of 4-$(CH_3)_2$Npyridine to copper(II) is strictly through the pyridine nitrogen. The potential ligand, $(CH_3)_2N(C_6H_5)$, did not shift the copper(II) reduction potential in acetone. The equilibrium constants correlate with para-Hammett constants, $\sigma p^{+,-}$, for $-N(CH_3)_2$, -H, and $-CO_2CH_3$ (67). The plot of $\log_{10}K_f^{II}$ vs. $\sigma p^{+,-}$ has a ρ factor of -0.932 and an $r^2 = 0.9991$. The negative ρ factor indicates a reaction in which electron-donating substituents increase the equilibrium constant. Weak binding to copper(II) is found for $P(O\text{-}p\text{-}C_6H_4Cl)_3$, $K_f^{II} = 2.2(3) \times 10^1\ M^{-1}$. This binding constant is insignificant relative to K_f^I ($2.5(3) \times 10^5\ M^{-1}$), so no conclusions are drawn from the 22 M^{-1} copper(II) binding constant.

The overall ligand binding trends indicate that copper(II) binds better to σ-bases than copper(I) and copper(I) binds better to π-acceptors. Furthermore, the copper(I) binding constants measured indicate that other ligands bind to $Cu(LBF_2)$, 1, as well as carbon monoxide. If the copper-carbon bond is a covalent bond with π-character, as suggested earlier, the copper-B bonds are similarly covalent.

The ordering of ligands for copper(I) binding consistent with decreasing π-acidity is:

$$XC_6H_5NC > P(O\text{-}p\text{-}C_6H_4Cl)_3 > CO >$$
$$P(O\text{-}C_6H_5)_3 > P(O\text{-}p\text{-}C_6H_4CH_3)_3 >$$
$$P(p\text{-}C_6H_4Cl)_3 > P(p\text{-}C_6H_4CH_3)_3 \sim$$
$$P(C_6H_5)_3 > 1\text{-MeIm}.$$

Literature cyclic voltammetric data indicate that CN^- binds copper(I) better than copper(II) in the LBF_2 ligand (68). The ligand CN^- can bind as a π-acceptor and qualitatively fits the trends discussed.

With the exceptions of $P(O\text{-}C_6H_{11})_3$ and $P(O\text{-}Bu)_3$, $Cu(LBF_2)$, 1, binds better to more electron-withdrawing ligands. With this knowledge, it is predicted that electronic changes in the macrocycle should change the bonding of the copper and fifth ligand. A complex with a macrocycle which makes the copper center more electron rich should bind CO more strongly. Work done to investigate this prediction is summarized in Section F.

SECTION F

The Binding of Fifth Ligands to Copper(I) Complexes

Carbon monoxide binds to $Cu(LBF_2)$, 1. The binding of fifth ligands to other four-coordinate copper(I) macrocyclic complexes was investigated initially to determine whether or not the LBF_2 macrocycle had unique properties. After it was found that other copper-macrocyclic complexes reacted with CO, a predicted correlation between copper-CO binding and the electron wealth of copper(I) due to macrocycle electronic changes was studied. Electrochemical measurements of carbon monoxide and p-$NO_2(C_6H_4)NC$ with various copper complexes were made. The results are presented in this section.

Binding constant data were collected and analyzed as described in Section E. Tables XII and XIII present sampled dc polarographic data for copper(II) complexes in DMF with CO and p-$NO_2(C_6H_4)NC$, respectively. The calculated K_f^I values are in Table XIV. The binding of the complexes, Cu(trans-diene)$(ClO_4)_2$, 3, and Cu(TAAB)$(NO_3)_2$, 6, with both ligands was studied. Carbon monoxide binding with three new complexes, $[Cu(dmgBF_2)_2]_3 \cdot 2C_4H_8O_2$, 18, $CuEt_2(LBF_2)ClO_4$, 19, and $[Cu(BuLBF_2)]_2(ClO_4)_2 \cdot C_4H_8O_2$, 20 (Figure 13) was also investigated. Table XV presents the p-$NO_2(C_6H_4)NC$ binding constants, K_f^I, with errors, Table XVI summarizes the results of the carbon monoxide binding studies of the six copper(II) macrocycles synthesized as part of the work of this thesis, and the results of similar studies

Table XII. Sampled dc Polarographic Results for Various Copper(II) Complexes with Carbon Monoxide in N,N-dimethylformamide.[a]

Copper Complex, [Cu(II)] x 10^4, M	Ligand, B	I_d[b]	-slope[c]	r^2[c]	$E_{1/2}(B)$, V[c]
$Cu(dmgBF_2)_2$, 18	no ligand	1.73	61.2	.9999	-.438
5.63	CO	1.46	53.9	.9997	-.228
$Cu(LBF_2)ClO_4$, 9[d]	no ligand	1.70	56.8	.9993	-.456
5.00	CO	1.70	57.3	.9997	-.296
$CuEt_2(LBF_2)ClO_4$, 19	no ligand	1.66	57.6	.9996	-.424
5.35	CO	1.62	56.9	.9999	-.299
$Cu(BuLBF_2)ClO_4$, 20	no ligand	1.74	58.7	.9997	-.270
4.96	CO	1.68	57.1	.9996	-.224
Cu(trans-diene)$(ClO_4)_2$, 3	no ligand	1.73	67.0	.9977	-.656
5.01	CO	1.73	65.2	.9998	-.651
$Cu(TAAB)(NO_3)_2$, 6	no ligand	1.71	63.8	.9991	-.010
4.73	CO	1.61	68.2	.9998	-.010

[a]Carbon monoxide, saturated solution in DMF, $[CO]_i = 4.64 \times 10^{-3}$ M. Temperature, average, 22° C. Drop time, t, 5 s.

[b]I_d, $\mu A\ s^{1/2}\ (mM)^{-1}\ (mg)^{-2/3}$.

[c]From linear regression fit of plot of E vs. $\ln[i/i_d-i)]$; -slope, mV; r^2, coefficient of determination; $E_{1/2}(B)$, y-intercept.

[d]Average values.

Table XIII. Sampled dc Polarographic Results for Various Copper(II) Complexes with p-$NO_2(C_6H_4)NC$ in N,N-dimethylformamide.[a]

Copper Complex, [Cu(II)] x 10^4, M	$[B]_i$ x 10^3, M	I_d[b]	-slope[c]	r^2[c]	$E_{1/2}(B)$, V[c]
$Cu(LBF_2)ClO_4$, 9	2.01	1.72	68.8	.9995	-.195
5.00	5.08	1.69	64.5	.9996	-.168
Cu(trans-diene)$(ClO_4)_2$, 3	5.05	1.65	55.7	.9996	-.555
5.02	10.1	1.50	55.3	.9999	-.533
$Cu(TAAB)(NO_3)_2$, 6	5.05	1.40	60.6	.9991	-.009
4.99					

[a]Temperature, average, 22° C. Drop time, t, 5 s.

[b]I_d, $\mu A\ s^{1/2}\ (mM)^{-1}\ (mg)^{-2/3}$.

[c]From linear regression fit of plot of E vs. $\ln[i/(i_d-i)]$; -slope, mV; r^2, coefficient of determination; $E_{1/2}(B)$, y-intercept.

Table XIV. Determination of Binding Constants, K_f^I, with Assumption $K_f^{II} = 0$.

Copper Complex	Ligand, B	Points[a]	r^2[b]	b[b]	K_f^I, M^{-1}[b]
$Cu(dmgBF_2)_2$, 18	CO	2			8.8×10^5
$Cu(LBF_2)ClO_4$, 9	CO	2			1.2×10^5
	p-$NO_2(C_6H_4)NC$	3	.9996	-620	1.7×10^7
$CuEt_2(LBF_2)ClO_4$, 19	CO	2			3.1×10^4
$Cu(BuLBF_2)ClO_4$, 20	CO	2			1.2×10^3
Cu(trans-diene)$(ClO_4)_2$, 3	CO	2			4.7×10^1
	p-$NO_2(C_6H_4)NC$	3	.9933	-3.0	1.3×10^4
$Cu(TAAB)(NO_3)_2$, 6	CO	2			0.0
	p-$NO_2(C_6H_4)NC$	2			8.0

[a]Points = number of ΔE, $[B]_f$ points used to determine K_f^I. This number includes (0,0) which is used in each K_f^I calculation.

[b]Plot of $e^{\Delta E(nF/RT)}-1$ vs. $[B]_f$; $\Delta E = E_{1/2}(B) - E_{1/2}(Ar)$. Coefficient of determination = r^2; y-intercept = b; slope = K_f^I.

Figure 13

Skeletal representations of three copper(II) macrocyclic complexes: A. $Cu(dmgBF_2)_2$, 18, B. $CuEt_2(LBF_2)ClO_4$, 19, and C. $Cu(BuLBF_2)ClO_4$, 20.

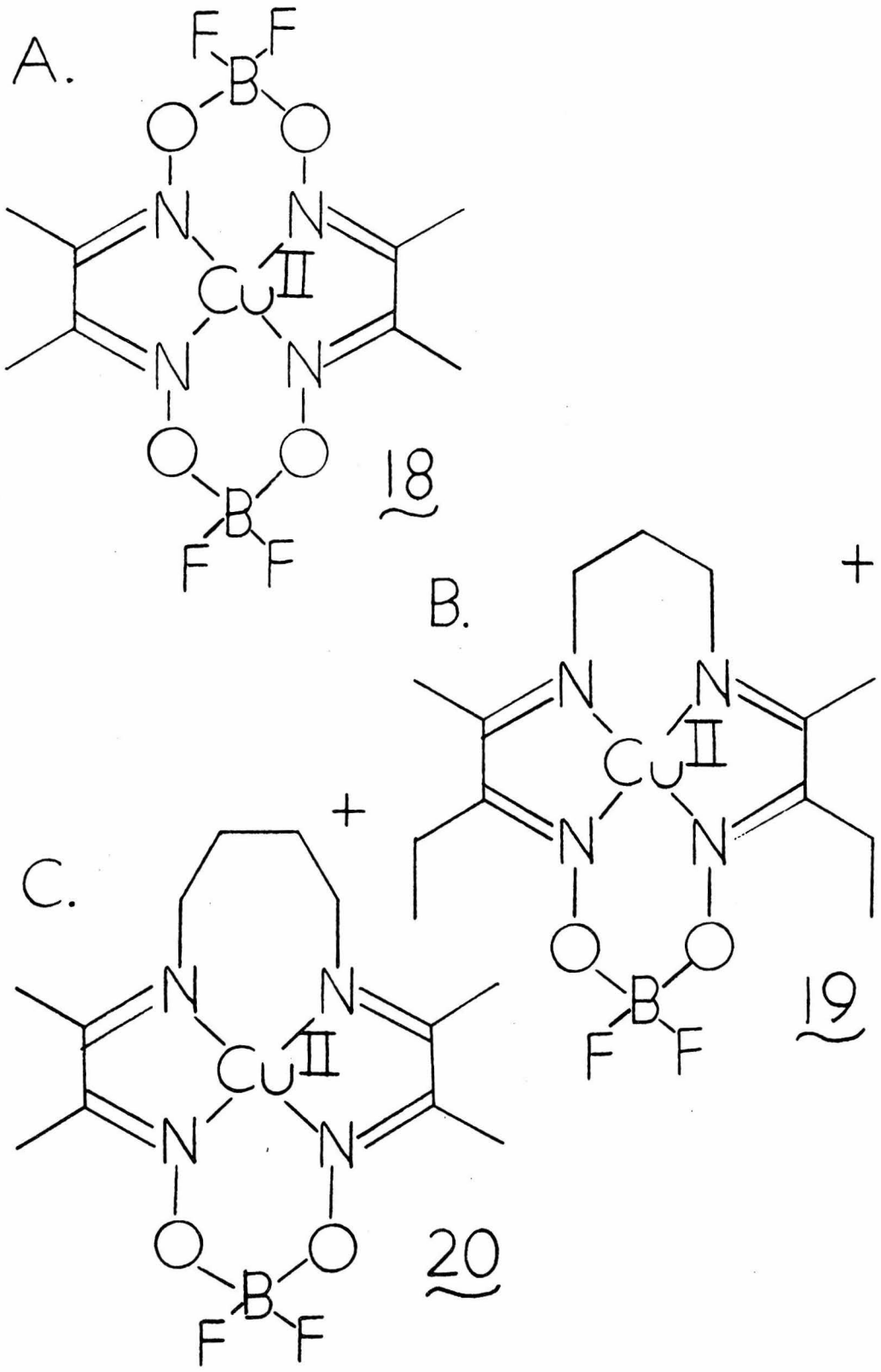
A.
F
B
F
O
O
N
N
Cu
II
N
N
O
O
B
F
F
18
B.
+
N
N
Cu
II
N
N
O
O
B
F
F
19
+
C.
N
N
Cu
II
N
N
O
O
B
F
F
20

Figure 13

Table XV. Final Binding Constants of Three Copper(II) Complexes with p-$NO_2(C_6H_4)NC$ in N,N-dimethylformamide.

Copper Complex	$E_{\frac{1}{2}}(Ar)$, V	K_f^I, M^{-1}[a]
Cu(trans-diene)$(ClO_4)_2$, 3	-.656	1.3(2) x 10^4
Cu$(LBF_2)ClO_4$, 9	-.456	1.7(2) x 10^7
Cu(TAAB)$(NO_3)_2$, 6	-.010	8(20)

[a]Errors are based on $E_{\frac{1}{2}}(B)$ error of ±.0025 V.

Table XVI. Final Binding Constants of Various Copper(II) Complexes with Carbon Monoxide in N,N-dimethylformamide.

Copper Complex	$E_{1/2}(Ar)$, V	K_f^I, M^{-1} [a]	Source
$Cu(sal)_2en$, 21	-1.303	2.6(3) x 10^3	b
$Cu(sal)_2$o-phen, 22	-1.191	4.7(30)x 10^1	b
$Cu(sal)_2pr$, 23	-1.099	2.1(3) x 10^3	b
Cu(trans-diene)$(ClO_4)_2$, 3	-.656	4.7(30)x 10^1	c
$Cu_2L(ClO_4)_2 \cdot 2H_2O$, 24[d]	-.517	3.1(3) x 10^4	b
$Cu(LBF_2)ClO_4$, 9	-.456	1.2(2) x 10^5	c
$Cu(dmgBF_2)_2$, 18	-.438	8.8(9) x 10^5	c
$CuEt_2(LBF_2)ClO_4$, 19	-.424	3.1(3) x 10^4	c
$Cu(BuLBF_2)ClO_4$, 20	-.270	1.2(2) x 10^3	c
$Cu(Bu'LBF_2)ClO_4$, 25	-.172	6.7(8) x 10^3	e
$CuMe_4(Bu'LBF_2)ClO_4$, 26	-.169	5.3(5) x 10^3	e
$Cu(TAAB)(NO_3)_2$, 6	-.010	0	c

[a]Errors are based on $E_{1/2}(B)$ error of ±.0025 V.

[b]C. A. Koval.

[c]This thesis.

[d]First reduction; see ref. 69.

[e]D. M. Ingle.

on complexes synthesized and studied by other members of the R. R. Gagné research group. Other copper(II) complexes studied with carbon monoxide are $Cu(sal)_2en$, 21, $Cu(sal)_2o$-phen, 22, and $Cu(sal)_2pr$, 23 (Figure 14), $Cu_2L(ClO_4)_2 \cdot 2H_2O$, 24 (Figure 15) (69), and $Cu(Bu'LBF_2)ClO_4$, 25, and $CuMe_4(Bu'LBF_2)ClO_4$, 26 (Figure 16).

Examination of the CO binding constants given in Table XVI shows that other copper(I) macrocycles bind a fifth ligand. Five-coordinate copper(I) is not restricted to $Cu(LBF_2)B$ complexes.

In Table XVI the copper(II) complexes are in the order of increasing $E_{\frac{1}{2}}(Ar)$. The range and order of these reduction potentials can be explained. Different factors influence the reduction of copper(II) chelates. Polarographic measurements in DMF by Patterson and Holm (70) showed that nonplanar bis(chelate) complexes are easier to reduce than their planar analogues. They also concluded that copper complexes with four ligating nitrogens are easier to reduce than those with two ligating nitrogens and two ligating oxygens. Busch, et al. (71), found that increased ligand unsaturation favors lower oxidation states. For this series of copper(II) complexes both steric and electronic factors are invoked.

The polydentate complexes, $Cu(sal)_2R$, have very negative reduction potentials because two negatively charged oxygen atoms bind to each copper center. The copper and four ligands are electron rich and addition of an electron to the complex is difficult. Within the three compound series both steric and electronic effects are seen. The compound, $Cu(sal)_2pr$, 23, has a more positive $E_{\frac{1}{2}}(Ar)$ than

Figure 14

Skeletal representations of three copper(II) polydentate complexes: A. $Cu(sal)_2en$, 21, R = $-CH_2CH_2-$, B. $Cu(sal)_2$o-phen, 22, R = o-phenylene, and C. $Cu(sal)_2pr$, 23, R = $-CH_2CH_2CH_2-$.

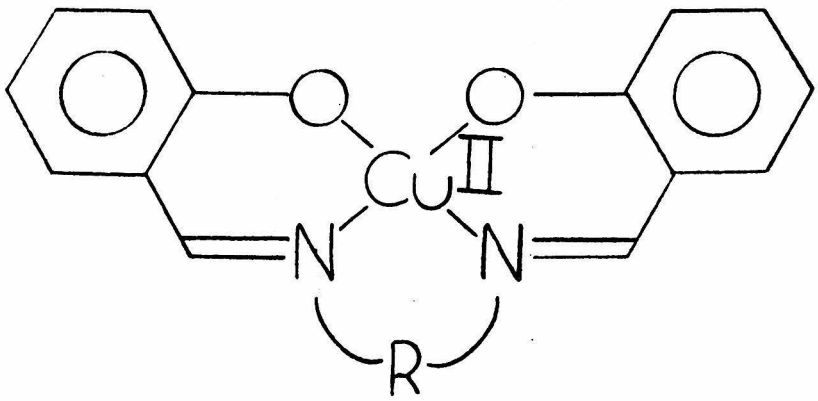

21 $R = -CH_2CH_2-$

22 R =

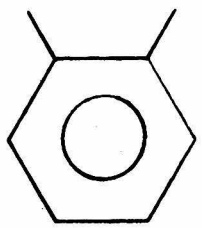

23 $R = -CH_2CH_2CH_2-$

Figure 14

Figure 15

Skeletal representation of copper(II) dimeric complex, $Cu_2L(ClO_4)_2 \cdot 2H_2O$, 24.

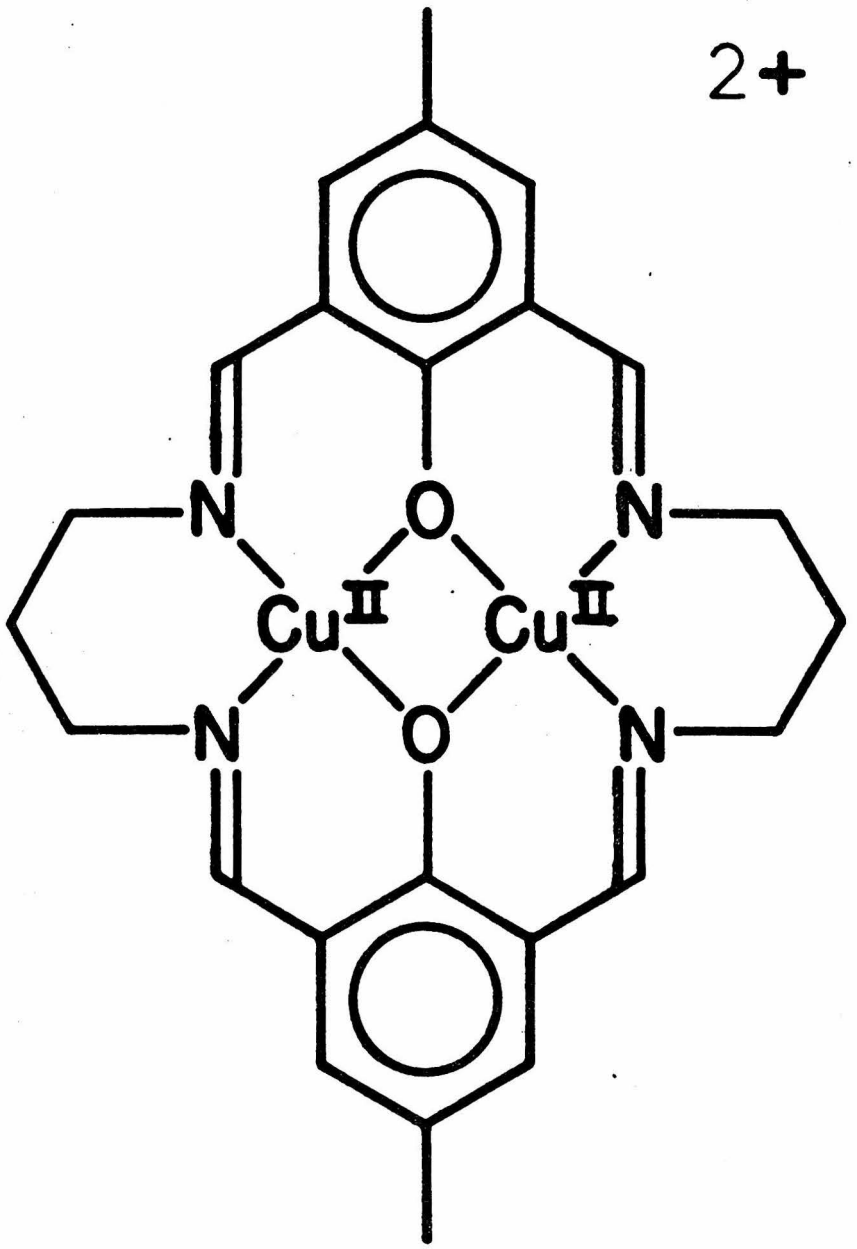

24

Figure 15

Figure 16

Skeletal representations of two copper(II) macrocyclic complexes: A. $Cu(Bu'LBF_2)ClO_4$, 25, and B. $CuMe_4(Bu'LBF_2)ClO_4$, 26.

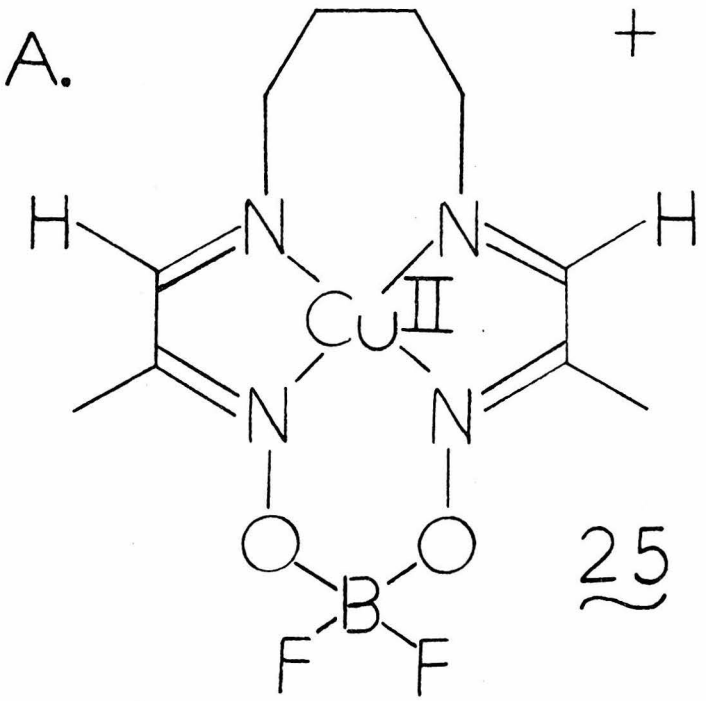

25

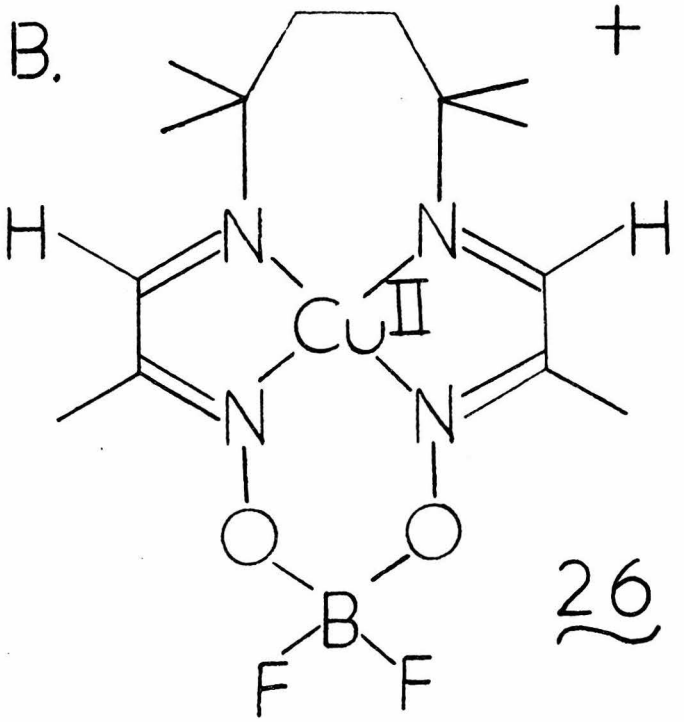

26

Figure 16

$Cu(sal)_2en$, 21, because the propyl bridge makes a tetrahedral twist easier. As a reminder, the d^{10} copper(I) center prefers a tetrahedral ligand geometry over a square-planar one. Comparison of the half-wave potentials of $Cu(sal)_2en$, 21, and $Cu(sal)_2$o-phen, 22, predicts that the ligand $(sal)_2$o-phen is either more flexible or more electronegative than $(sal)_2en$. Molecular models do not support the flexibility argument. Therefore, the o-phenylene bridge must withdraw more electron density from the ligating nitrogens than the ethylene bridge. The corresponding copper(II) complex is more easily reduced.

By overall charge a copper macrocyclic unit with a high positive charge should be reduced much more easily than a complex that is neutral or is negatively charged. Examination of the reduction potentials of the macrocycles in Table XVI does not show a correlation of overall charge and $E_{\frac{1}{2}}(Ar)$. The location of the macrocyclic ligand's charge coupled with the charge of individual ligating atoms is a more relevant factor.

The complex, $Cu(dmgBF_2)_2$, 18, has a more positive reduction potential than $Cu(LBF_2)ClO_4$, 9, although it is a neutral complex as the copper(II). The necessary conclusion is that the ligand's negative charges reside primarily on the $O\text{-}BF_2\text{-}O$ bridges. Two of the ligating nitrogens in $Cu(dmgBF_2)_2$, 18, have less electron density than in $Cu(LBF_2)ClO_4$, 9, due to the second oxime bridge. Therefore, the copper and four nitrogens are less electron rich and the complex is reduced at a more positive potential.

The series of LBF_2 related macrocycles is interesting. The more positive potential for $CuEt_2(LBF_2)ClO_4$, 19, is attributed to unfavorable ethyl steric interactions which favor a twisted geometry about the metal. The complex with a butylene bridge, $Cu(BuLBF_2)ClO_4$, 20, can flex into a tetrahedral geometry more easily than $Cu(LBF_2)ClO_4$, 9, and has a correspondingly more positive $E_{1/2}(Ar)$. The compounds with two hydrogen and two methyl substituents on the α-diimine part of the macrocycle, $Cu(Bu'LBF_2)ClO_4$, 25, and $CuMe_4(Bu'LBF_2)ClO_4$, 26, have more positive reductive potentials than $Cu(BuLBF_2)ClO_4$, 20. An electronic effect prevails with these complexes. Methyl groups are more electron donating than hydrogens. As a result, substitution of two hydrogens for two methyl groups makes the ligating nitrogens more positive and the complex more easily reduced.

The most positive reduction potential was found for $Cu(TAAB)(NO_3)_2$, 6. The highly conjugated, neutral ligand, TAAB, does not force excess electron density into copper(II). The metal can easily accept an electron to be reduced to copper(I).

The complex, Cu(trans-diene)$(ClO_4)_2$, 3, has a more negative reduction potential than $Cu(LBF_2)ClO_4$, 9. The ligating nitrogens of the two macrocycles have the same charge, because the negative charge of LBF_2 resides primarily on the -O-BF_2-O- bridge. The difference in $E_{1/2}(Ar)$ values results from the difference in the types of nitrogens. In Cu(trans-diene)$(ClO_4)_2$, 3, two saturated nitrogens destabilize the copper(I) oxidation state and the half-wave potential drops (71).

The reduction potential of $Cu_2L(ClO_4)_2 \cdot 2H_2O$, 24, is low because of the negatively charged oxygens binding to the copper.

In Section E the prediction was made that a more electron-rich copper would bind CO more strongly. The data presented in Table XVI allow an evaluation of this prediction.

With steric changes minimized, a more electron-rich copper should have a more negative half-wave potential. Increases in the electron density around copper, effected by electronic changes of the macrocycle, should be paralleled by increases in the CO binding constants. Therefore, a more negative half-wave potential predicts stronger copper-CO bonding. The data in Table XVI do not support this prediction. A possible explanation of binding constants which do not correlate may be based on steric factors. The evaluation of electronic vs. steric factors in the formation of five-coordinate copper(I) complexes follows.

The structure of the carbon monoxide adduct, $Cu(LBF_2)CO$, 2, is known (8). The copper(I) sits well out of the four-nitrogen plane toward CO. The α-diimine parts of the macrocycle dome down away from the copper-carbon linkage. An angle, β, is defined as the angle between the planes formed by two sets of atoms, N-Cu-N (Figure 17). For $Cu(LBF_2)CO$, 2, β is 120°. If electronic factors are equal, the ability of a macrocycle to dome might predict the strength of a copper-carbon bond. Comparison of the binding constants

Figure 17

The angle β between planes N1-Cu-N2 and N3-Cu-N4 is illustrated in the upper drawing. The corresponding numbering of the four nitrogens of the macrocycles: 1. LBF_2, and 2. $(dmgBF_2)_2$ is given below.

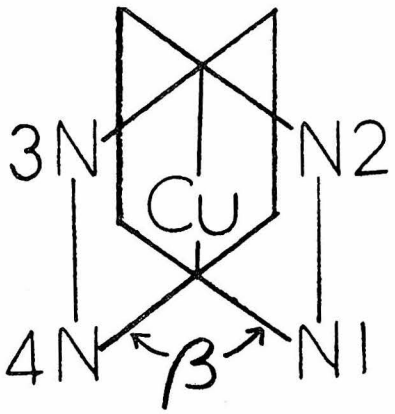

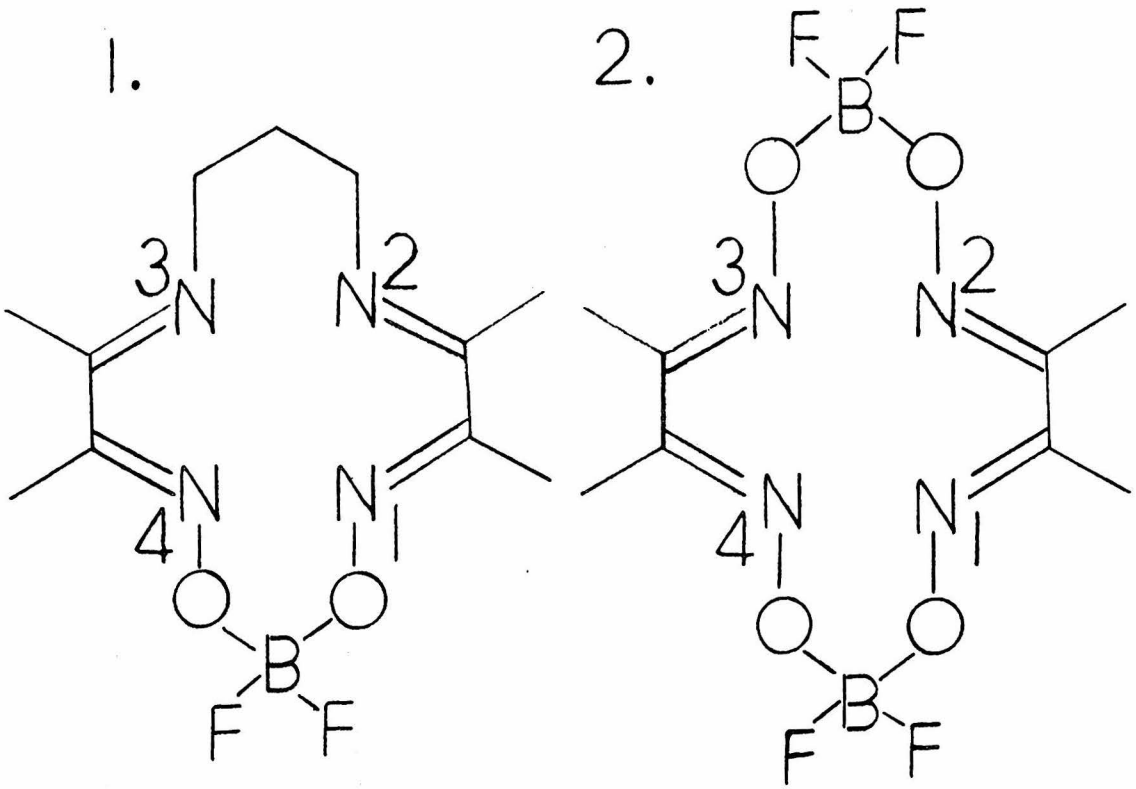

Figure 17

of complexes related to $Cu(LBF_2)ClO_4$, 9, to $K_f^I(CO)$ of $Cu(LBF_2)ClO_4$, 9, addresses this point.

The binding constant for carbon monoxide and $Cu(dmgBF_2)_2$, 18, is larger than expected. The ability of the dimethylglyoxime macrocycle to dome must be greater than that of the LBF_2 macrocycle. Preliminary data on the crystal structure of $Cu(dmgBF_2)_2CO$, 27, (crystallized by D. M. Ingle, crystallographic analysis by M. McCool), indicate a similar ligand conformation to that found in $Cu(LBF_2)CO$, 2. The dimethylgloxime ligand is in a boat conformation and is domed. The copper(I) is 1.03 Å out of the four nitrogen plane in $Cu(dmgBF_2)_2CO$, 27 (R factor $\cong$ 5%). This larger displacement suggests that the ligand will be domed more severely than in $Cu(LBF_2)CO$, 2. The severity of the dome can be quantitatively evaluated by examination of the angle, β (Figure 17). The angle β is 106° for $Cu(dmgBF_2)_2CO$, 27, and 120° for $Cu(LBF_2)CO$, 2. The dimethylglyoxime macrocycle is domed to a greater degree. The symmetry of the ligand may allow it to dome more effectively. There is no possibility of unfavorable C-H eclipsing interactions when the $-CH_2CH_2CH_2-$ bridge is replaced by the $-OBF_2O-$ bridge. Release of the strain in one bridge results in a stronger copper(I)-carbon monoxide interaction.

The ethyl-derivatized complex, $CuEt_2(LBF_2)ClO_4$, 19, has a binding constant in accord with the trend predicted. No steric rationale is required.

For the butyl-bridged complexes, $Cu(BuLBF_2)ClO_4$, 20, and $Cu(Bu'LBF_2)ClO_4$, 25, the binding constants increase with increasing

$E_{1/2}(Ar)$. If doming ability is important, the binding constant of the less bulky complex, $Cu(Bu'LBF_2)ClO_4$, 25, must be used as the norm. A change from four methyl substituents to two hydrogens and two methyl groups on the α-diimine part of the macrocycle is the only change in the two complexes. Molecular models indicate a small possibility of unfavorable alkyl bridge, $-CH_2CH_2CH_2CH_2-$, methyl group steric interactions in a domed configuration for the $BuLBF_2$ ligand. Replacement of the methyl groups by hydrogens removes the steric strain. The complex, $Cu(Bu'LBF_2)ClO_4$, 25, therefore, binds carbon monoxide more strongly than does $Cu(BuLBF_2)ClO_4$, 20.

The complex, $CuMe_4(Bu'LBF_2)ClO_4$, 26, binds almost as well as the complex without the four methyl groups. The methyl groups do not interfere sterically with axial coordination.

There are five complexes in Table XVI that have $E_{1/2}(Ar)$ values more negative than $Cu(LBF_2)ClO_4$, 9. These complexes have sterically different ligands from LBF_2. The values found for the binding constants of these complexes have obvious structural contributions. The trans-diene ligand has methyl groups and a hydrogen on nitrogen that can interfere with axial coordination (70). The ligand does have some ability to dome, but it cannot dome as well as LBF_2. Although it has a very small K_f^I for carbon monoxide, it binds well to the stronger π-acceptor, p-$NO_2(C_6H_4)NC$ (Table XV).

For the $Cu(sal)_2R$ compounds there is no way to definitively determine the coordination number in solution of copper(I) in the

presence of carbon monoxide. If an oxygen dissociates from copper, the resultant copper-CO structure is close to tetrahedral. The K_f^I values would correlate with the ability of the O-N-N ligand fragment to occupy three positions of a tetrahedron. This correlation is not seen. A solid state crystal structure of an adduct of carbon monoxide with $Cu(sal)_2en$, 21, or $Cu(sal)_2pr$, 23, is needed to establish the coordination geometry around copper(I). It must be noted, though, that a comparison with solution state properties, e.g. $K_f^I(CO)$, is ambiguous.

The binuclear complex, $Cu_2L(ClO_4)_2 \cdot 2H_2O$, 24, undergoes a first reduction at -.517 V. This mixed valence complex binds carbon monoxide well, $K_f^I = 3.1(3) \times 10^4\ M^{-1}$. The carbon monoxide binding of this complex illustrates that macrocycles, other than LBF_2, promote five coordination for copper(I).

The final complex, $Cu(TAAB)(NO_3)_2$, 6, has a very positive $E_{\frac{1}{2}}(Ar)$. It does not bind carbon monoxide nor does it bind strongly to p-$NO_2(C_6H_4)NC$. Molecular models show that TAAB has great difficulty doming. Steric control of fifth ligand binding to $Cu(TAAB)NO_3$, 7, is strongly implicated. However, similar weak bonding to π-acceptors is noted for five-coordinate iron(II)-TAAB complexes (72). These ferrous complexes do not bind carbon monoxide and benzyl isocyanide as well as other iron complexes including a bis(dimethylglyoximato)-ferrous complex. Because TAAB does not need to dome to form a six-coordinate Fe(TAAB)L(CO) complex, the electronic properties of TAAB must play an undetermined role in the binding of π-acceptors to metal-TAAB complexes.

The original prediction of an inverse relationship between $E_{1/2}(Ar)$ and $K_f^I(CO)$ for complexes with different macrocycles does not hold. Steric arguments have been introduced to explain the two major exceptions, $Cu(dmgBF_2)_2$, 18, and $Cu(BuLBF_2)ClO_4$, 20. The steric explanations become weaker on further inspection. Steric differences are used to explain binding constant discrepancies for the two pairs of complexes, $Cu(LBF_2)ClO_4$, 9, and $Cu(dmgBF_2)_2$, 18, and $Cu(Bu'LBF_2)ClO_4$, 25, and $Cu(BuLBF_2)ClO_4$, 20, that are sterically most similar to each other. The possibility exists that the correct trend is seen for $Cu(LBF_2)ClO_4$, 9, and $Cu(dmgBF_2)_2$, 18. Either a direct relationship between $E_{1/2}(Ar)$ and $K_f^I(CO)$ can be predicted or an alternate property of the copper complexes can be used to correlate with $K_f^I(CO)$.

The trend observed for the most sterically similar complexes, those based on the LBF_2 or $BuLBF_2$ macrocycles, is predicted by the concept of antisymbiosis (73) which is based on the classification of acids and bases as hard or soft (74-76). Antisymbiosis predicts a soft acid which binds to a soft base will prefer to coordinate a hard base in a trans-position. The complex, trans-LMB (where M is a soft acid and L is a hard base) is formed when B is a ligand capable of exerting a trans-influence (77). The greater the trans-influence of B, the harder base B can be for a complex of similar stability. (For hard acids, symbiosis which is the binding of like ligands is generally observed (78).)

The antisymbiotic relationship of the carbon monoxide binding constants is most easily seen if the copper(I)-CO bond is taken as the starting point and then the macrocycle is introduced trans to the CO. By antisymbiosis the harder the macrocycle, the more favorable the copper-CO bond. The hardness of the macrocycles follows an order based on the polarizability of substituents on the ligating nitrogens:

$$(dmgBF_2)_2 > LBF_2 > Et_2(LBF_2)$$
$$Bu'LBF_2 > Me_4(Bu'LBF_2) > BuLBF_2.$$

The complex with the hardest macrocycle, $Cu(dmgBF_2)_2$, 18, has the largest $K_f^I(CO)$. The binding constant of $Cu(Bu'LBF_2)ClO_4$, 25, is lower than that of the softest LBF_2 complex, $CuEt_2(LBF_2)ClO_4$, 19, because of steric problems. The 7-membered ring of $Cu(Bu'LBF_2)ClO_4$, 25, is not as stable as the 6-membered ring of $CuEt_2(LBF_2)ClO_4$, 19. The resulting $Cu(Bu'LBF_2)CO$ cannot have the boat configuration that $Cu(LBF_2)B$ (B = CO, 2, and NCO^-, 13) and $Cu(dmgBF_2)_2CO$, 27, adopt.

The order of $K_f^I(CO)$ values for the six complexes discussed is qualitatively predicted by antisymbiosis. The quantitative differences in $K_f^I(CO)$ are difficult to compare because the origin of the polarizability changes vary. By representation of a part of the macrocycle as R_1-N=C-R_2, it is seen that changes in both R_1 and R_2

occur. Only R_2 is changed for two pairs of complexes which are $Cu(LBF_2)ClO_4$, 9, and $CuEt_2(LBF_2)ClO_4$, 19, and $Cu(Bu'LBF_2)ClO_4$, 25, and $Cu(BuLBF_2)ClO_4$, 20. The difference in $K_f^I(CO)$ values for the first pair, 3.9, is smaller than that for the second pair, 5.6. Polarizability factors (67) predict a larger difference between H- and CH_3- than between CH_3- and CH_3CH_2-, as is found. To quantify these results further is impossible without a more extensive series of complexes.

The binding constants of the other copper complexes with CO and p-$NO_2(C_6H_4)NC$ are more difficult to evaluate because of the combination of steric and electronic effects. For Cu(trans-diene)$(ClO_4)_2$, 3, the electronic effects oppose the steric effects. The binding of two secondary nitrogens to copper should promote a stronger copper-CO bond, but the steric problems mentioned earlier hinder fifth ligand binding. However, the ligand, p-$NO_2(C_6H_4)NC$, is a strong enough trans-influencing ligand to overcome the steric restraints.

For Cu(TAAB)$(NO_3)_2$, 6, the effects of a highly polarizable and sterically restrained macrocycle work together to decrease the propensity of Cu(TAAB)NO_3, 7, to bind fifth ligands. Therefore, the very weak binding of p-$NO_2(C_6H_4)NC$ is predictable.

Antisymbiotic behavior is found for linear gold(I) complexes (79). An example of antisymbiosis for copper(I) might be the series of complexes, Cu(h^5-C_5H_5)B, (h^5-C_5H_5= pentahaptocyclopentadienyl) (80). The stability of complexes with ligand B is $P(C_6H_5)_3 > P(CH_2CH_3)_3 \cong P(C_4H_9)_3 > P(OCH_3)_3 >> CH_3NC > CO$. This order is predicted by

antisymbiosis because the cyclopentadienyl ligand is soft and the Cu($\underline{h}^5$-C_5H_5) unit will bind preferably to the B that exhibits the smallest trans-influence. The trans-directing influence of phosphorus ligands is ordered: P(O-phenyl)$_3$ > P(alkyl)$_3$ > P(phenyl)$_3$ (79). By analogy, an alkyl phosphite has a larger trans-influence than a phenyl phosphite. Therefore, Cu($\underline{h}^5$-C_5H_5) binds better to $P(C_6H_5)_3$ than to $P(O\text{-}CH_3)_3$.

The results of the binding of different ligands B to $Cu(LBF_2)ClO_4$, 9, (Section E) can be examined in terms of the predictions of antisymbiosis. The reverse order of Cu($\underline{h}^5$-C_5H_5)B is predicted because $\underline{h}^5$-C_5H_5 is a soft base and LBF_2 is a hard base. By the trans-influence criterion, carbon monoxide binds too weakly. However, the strong binding of $P(O\text{-}C_6H_{11})_3$ and P(O-Bu)$_3$ is now predicted.

The binding constants of $Cu(LBF_2)ClO_4$, 9, and fifth ligands, B, can be explained to a limited degree by either π-acceptor or trans-directing trends. For the binding of CO to copper complexes, trends are predicted by antisymbiosis without resort to subtle steric influences. Certainly, no explanation of either series results from invoking antisymbiosis. The concept has predictive value, but all that is concluded is that copper(I) is a soft acid which binds two ligands, one soft and one hard. Why $Cu(LBF_2)$, 1, binds carbon monoxide at the expense of weakening the copper-nitrogen bonds is still an unanswered question. Section G examines possible descriptions of the bonding in $Cu(LBF_2)CO$, 2, in the hope of understanding five-coordinate copper(I).

SECTION G

A Description of the Bonding of Carbon Monoxide to the Four-Coordinate $Cu(LBF_2)$, 1, Complex

A bonding description of $Cu(LBF_2)CO$, 2, the adduct formed on addition of carbon monoxide to $Cu(LBF_2)$, 1, is necessary for an understanding of the ability of copper(I) to bind multiple ligands in simple compounds and in clusters. Regretfully, the scope of this thesis allows only a qualitative picture of the bonding in $Cu(LBF_2)CO$, 2, to be drawn. A quantitative approach to the bonding of copper(I) in complexes like $Cu(LBF_2)B$ awaits the interest of theoretical chemists.

Carbon monoxide is not expected to bind to a transition metal center which formally has an inert gas configuration (18 valence electrons). The introduction of the two electrons of CO to $Cu(LBF_2)$, 1, an 18-electron species, to form $Cu(LBF_2)CO$, 2, a 20-electron species, initially raised the question of where the "extra" electrons resided. Attempts to formulate molecular orbital schemes to find the lowest unoccupied orbital in $Cu(LBF_2)$, 1, and the highest occupied orbital in $Cu(LBF_2)CO$, 2, can be made. However, without calculated knowledge of orbital energies and overlaps, molecular orbital schemes can be invented that put the "extra" electrons in almost any orbital desired. Such qualitative guesswork is unfulfilling.

An alternative approach to the enigma of the 20-electron species, $Cu(LBF_2)CO$, 2, is to question the validity of using a transition metal rule, i.e., the effective atomic number rule, for copper(I), a d^{10} metal. A transition metal is defined as a metal with a partially filled d shell. Copper(I) is not a transition metal by this definition. Does $Cu(LBF_2)CO$, 2, suddenly become a commonplace complex? The definition of a transition metal excludes copper(I), but examination of the usual properties of transition metals puts the problem into better perspective. Transition metals bind neutral molecules which are π-acceptors. Their d-orbitals interact with orbitals of proper symmetry and energy on the ligands. Copper(I) binds many π-acceptor ligands, but has d-orbitals that are contracted. These d-orbitals do not overlap with ligand orbitals as effectively as metals earlier in the transition series. Therefore, copper(I) has lost some ability to make use of its d-orbitals, while retaining an ability to bind π-acceptors. On the other hand, main group metals do not make use of filled d-orbitals for bonding nor do they bind π-acceptors well. Copper(I) has properties of both classes.

It is tempting to class d^{10} metals by themselves. A mixture of transition and main group metal properties is found in nickel(0), copper(I), and zinc(II) complexes. All three metals bind ligands which formally contribute ten electrons to a bonding scheme. Nickel(0) forms $Ni(\underline{h}^5\text{-}C_5H_5)_2$, 30 (81), copper(I) forms $Cu(LBF_2)CO$, 2 (8), and zinc(II) forms a variety of five-coordinate 20-electron complexes, including 2,3,7,8,12,13,17,18-octaethylporphinatopyridine-

zinc(II) (Zn(OEP)py, 31) (82). The number of ligands binding to these metals may depend less on formal electron count than on electron-pair repulsions, which are dictated to some extent by the steric restraints of the ligands. To reduce repulsions five-electron pairs arrange themselves about a metal center in either a trigonal bipyramid or a square pyramid. The complex, Zn(OEP)py, 31, is normal for known square-pyramidal complexes. The α-angle (see Figure 5) is approximately 100° and the metal is displaced 0.31 Å from the four-nitrogen best plane (82). Electron-pair repulsions seem to be minimized with these geometrical parameters.

The bonding of the square-pyramidal $Cu(LBF_2)CO$, 2, can be evaluated in a similar manner to that used for Zn(OEP)py, 31. The α angle is much larger, 115-120°, and the copper out of plane displacement is huge, 0.96 Å. Because of these extreme values, it cannot be concluded that the geometry of $Cu(LBF_2)CO$, 2, is simply the result of electron-pair repulsions.

A review of other salient features of the geometry of $Cu(LBF_2)CO$, 2, is worthwhile. The coordination of CO to $Cu(LBF_2)$, 1, results in a lengthening of the copper-nitrogen bonds from 1.94 Å to 2.10 and 2.16 Å with movement of the copper out of the four nitrogen plane. For comparative purposes there is only one other five-coordinate copper(I) complex known. The recently reported complex, [Cu(dien)-norbornene]BPh_4, 32, has a distorted trigonal-planar geometry around copper(I) (83). The two primary nitrogens of the dien ligand and

the double bond of the norbornene bind equatorially. The secondary nitrogen and a bridgehead hydrogen bind axially. The axial copper-nitrogen bond is longer and one equatorial copper-nitrogen bond is shorter than the corresponding bond lengths in the four coordinate [Cu(dien)CO]BPh_4, 11 (25). Since only the axial bond lengthens and an equatorial bond shortens in changing from the four-coordinate complex, 11, to the five-coordinate complex, 32, no parallel can be hypothesized between increasing coordination number and increasing copper-nitrogen bond length. The long copper-nitrogen bonds in $Cu(LBF_2)CO$, 2, are not indicative solely of the presence of the five ligands around copper(I). More likely, they are indicative of weakened interactions between copper and the macrocyclic nitrogens.

The unusual properties of the geometry of $Cu(LBF_2)CO$, 2, include a large metal out-of-plane displacement and long metal-nitrogen bonds, coupled with a normal metal-CO bond. These properties point toward the best bonding description of $Cu(LBF_2)CO$, 2, presently available. The ligands provide copper(I) with a symmetric electronic array, which is linear in nature. The single strong copper-carbon bond is balanced by four weak copper-nitrogen bonds. A linear, rather than square-pyramidal, description of $Cu(LBF_2)CO$, 2, is also supported by the changes in $K^I(CO)$ found for different macrocyclic-copper complexes (Section F). The influence of ligands on each other around a metal center is greatest if the ligands are oriented trans. Changes in the LBF_2 macrocycle cause significant changes in the

carbon monoxide binding constants. It is suggested that the size of the effects seen can only be explained by a geometry around copper(I) which is described as linear.

A d^{10}, filled-shell metal such as copper(I) requires spherical electron density around it. Forced into an unfavorable, distorted square-planar geometry, $Cu(LBF_2)$, 1, binds a fifth ligand to get closer to a spherical electronic array. $Cu(LBF_2)$, 1, binds π-acceptors better than σ-bases because the soft-soft interaction is more favorable. A copper-π-acceptor bond is strong enough to balance four copper-nitrogen interactions, which have become long and weaker along with the displacement of copper out of the four-nitrogen plane. Therefore, it is concluded that the electron density around copper(I) becomes spherical.

SECTION H

Unusual Structural and Reactivity Types for Copper: Structure of a Macrocyclic Ligand Complex Containing Copper(I) in a Distorted Square-Planar Coordination Geometry

Robert R. Gagné, Judith L. Allison, and George C. Lisensky

Contribution No. 5573 from the Division of Chemistry and Chemical Engineering, California Institute of Technology, Pasadena, California 91125

Accepted for publication in Inorganic Chemistry, 17, (12), 1978.

Abstract: The diamagnetic macrocyclic ligand complex [1,1-difluoro-4,5,11,12-tetramethyl-1-bora-3,6,10,13-tetraaza-2,14-dioxo-cyclotetradeca-3,5,10,12-tetraenato]copper(I), $Cu(LBF_2)$, reacts with monodentate ligands including CO to give five-coordinate Cu(I) adducts; e.g., $Cu(LBF_2)CO$, 1. The crystal and molecular structure of the four-coordinate complex, $Cu(LBF_2)$, 2, was determined in order to help elucidate the nature of the adduct formation reaction. Complex 2 crystallized in the space group $P2_1/n$ (14 N) with a = 11.800(2) Å, b = 9.005(1) Å, c = 13.704(1) Å, β = 96.40(1)° and Z = 4. An R(F) of 0.054 was obtained using 2882 reflections to 2θ = 140°. The complex contains isolated mononuclear molecules with no significant intermolecular interactions. Each copper atom is bound by the four nitrogens of the macrocyclic ligand in a near square-planar array, resulting in a highly unusual structural environment for Cu(I). The four nitrogens are, however, tetrahedrally distorted from planarity, with dihedral angles of 23° and 27° for the two sets of planes defined by copper and two adjacent nitrogen atoms. Copper-nitrogen bond lengths average to 1.939(3) Å. The infrared spectrum of 2 exhibits no bands in the 1500-1700 cm^{-1} region expected for the ligand α-diimine moiety but does show two bands at 1320 and 1470 cm^{-1} which might be associated with α-diimine stretching modes. The

infrared spectra of 1 and 2, as well as crystallographic, electrochemical and magnetic data, are used to discuss a reasonable description for the oxidation state of copper in both 1 and 2.

Introduction

The most frequently encountered copper(I) geometry is tetrahedral (four-coordinate), though linear (two-coordinate) and trigonal planar (three-coordinate) structures are known.[1] Some Cu(I) cluster and polymeric complexes do exhibit higher coordination numbers, notably five, six, and seven, but only if unusual copper-copper interactions are included.[2] In contrast, we recently reported the preparation and molecular structure of the square-pyramidal macrocyclic ligand complex, $Cu(LBF_2)CO$, 1, (carbonyl[1,1-difluoro-4,5,11,12-tetramethyl-1-bora-3,6,10,13-tetraaza-2,14-dioxo-cyclotetradeca-3,5,10,12-tetraenato]copper(I)).[3] This complex apparently contains unprecedented, mononuclear five-coordinate Cu(I).

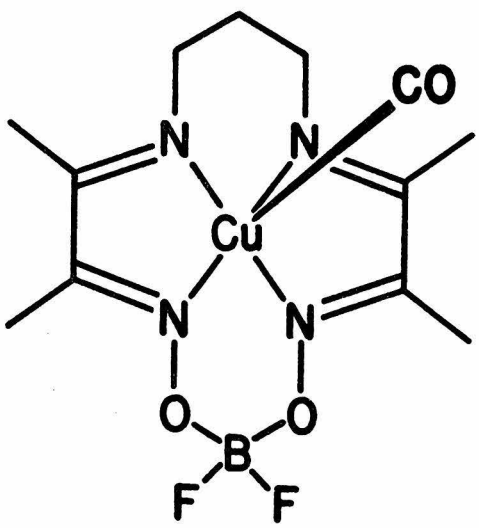

1

In the carbonyl complex, $Cu(LBF_2)CO$, 1, copper is bound to an axial carbon from CO (ν_{CO} = 2068 cm^{-1}) and four basal nitrogens. Copper is displaced an extraordinary 0.96 Å out of the mean plane of the four coordinated nitrogens. This displacement is especially notable when compared to metal-atom displacements in other square-pyramidal, metal macrocyclic ligand systems which are often in the range 0.3 - 0.6 Å. A few cases with extreme displacements are known, e.g., 0.73 Å for Mn(II) in $Mn(C_{22}H_{22}N_4)(N(C_2H_5)_3)$[4] ([7,16-dihydro-6,8,15,17-tetramethyldibenzo[b,i](1,4,8,11]tetraazacyclotetradecinato]triethylaminemanganese(II)), and 0.74 Å and 0.98 Å for Tl(III) in ClTlTPP[5] and CH_3TlTPP[5] (chloro- and methyl-5,10,15,20-tetraphenylporphinatothallium(III)), respectively. The large metal-atom displacement in $Cu(LBF_2)CO$, 1, results in an unusual square-pyramidal arrangement of ligands. The angles formed by the apical ligand (CO), copper, and the basal plane nitrogens, C-Cu-N, range from 114.8(1) to 120.3(1)°. The expected value would be 100°.[6] In addition the copper to carbon distance found (1.780(3) Å) might be regarded as being relatively short when the apparent presence of twenty electrons in the copper valence shell is considered. A similar Cu-C bond length (1.765(14) Å) is found in the only other crystallographically analyzed Cu-CO complex, carbonyl[hydro-

tris(1-pyrazolyl)borato]copper(I),[7] even though the central copper is four-coordinate and has an eighteen-electron valence shell.

In an attempt to better understand the formation and nature of the five-coordinate adduct, $Cu(LBF_2)CO$, 1, we have determined the molecular structure of its precursor, $Cu(LBF_2)$, 2. The ligand geometry observed in analogous metal complexes of the present ligand system,[8-13] might be predicted to force copper in $Cu(LBF_2)$, 2, into a square-planar configuration. The complex would thus contain Cu(I) in a highly unfavorable geometry or copper in a higher oxidation state, e.g., Cu(II) or Cu(III) complexed to a reduced macrocyclic ligand. Alternatively, the ligand configuration found in $Cu(LBF_2)CO$, 1, might imply the presence of a fifth ligand for $Cu(LBF_2)$, 2, either from a solvent molecule (analytical results did not suggest any solvent of crystallization) or via solid-state oligomerization. As reported herein, we believe that $Cu(LBF_2)$, 2, is best described presently as containing Cu(I) in a distorted square-planar geometry.

Results and Discussion

The Structure of $Cu(LBF_2)$, 2. Basic crystal data for $Cu(LBF_2)$, 2, are summarized in Table I; Tables II-IV

contain atomic parameters, bond lengths, and bond angles. Figure 1 is a schematic drawing of the molecule depicting the atom labelling scheme.

The complex crystallized in the space group $\underline{P2_1/n}$(14 $\underline{N}$) with four molecules in the unit cell, Figure 2. The two nearest neighbor molecules in the unit cell are related by an inversion center (Figure 2). The copper atoms of these two molecules are 4.55 Å apart. Calculated best planes through the four nitrogens of each of the two molecules shown in Figure 2 are separated by a distance of 3.62 Å. Several fluorine-hydrogen intermolecular distances less than 3.0 Å were found, which may indicate very long F-H interactions, contributing to crystal packing forces. No other intermolecular interactions appear to be important to the crystal structure.

Copper atoms in individual molecules of $Cu(LBF_2)$, 2, are bonded to the four macrocyclic ligand nitrogen atoms with essentially equal Cu-N bond lengths averaging to 1.939(3) Å.[14] No other atoms are within 3.6 Å of copper (Table V). As seen in the stereoview of a single molecule (Figure 3) the coordination geometry is best described as a distorted square plane. A perfect square would have 90° cis N-Cu-N bond angles; the observed values range from 82.3(1) to 103.3(1)°. Correspondingly, the trans N-Cu-N angles, theoretically 180°, are 161.5(1) and

Figure 1

Atomic numbering scheme used for $Cu(LBF_2)$, 2. Hydrogens are labelled in reference to the carbon to which they are bound (e.g., the hydrogens bound to C1 are H1a, H1b, and H1c).

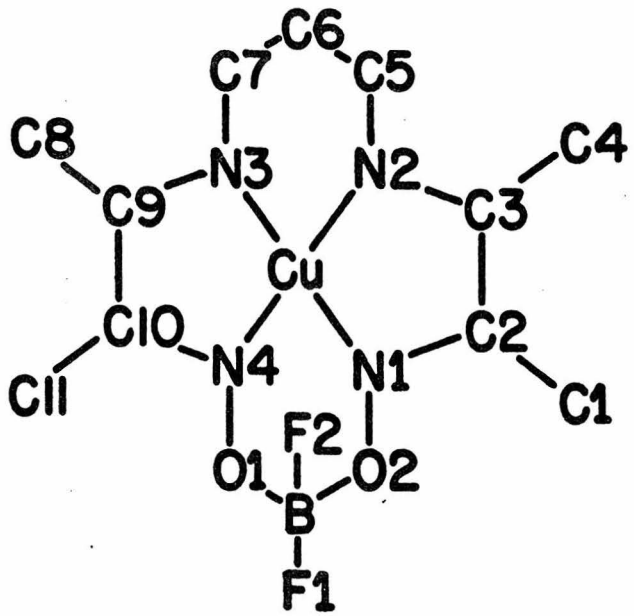
C6
C7
C5
C8
N3
N2
C4
C9
C3
Cu
C10
N4
N1
C2
C11
C1
F2
O1
O2
B
F1

Figure 2

The upper stereopair shows two parallel molecules of $Cu(LBF_2)$, 2, related in the crystal lattice by a center of symmetry. The molecules are viewed normal to the best planes determined by the four nitrogens of the ligands. An axial site of the copper atom is occupied by the non-coordinating C2-C3 bond (upper view). The other axial coordination site is vacant, as in the lower view which shows the contents of a unit cell. The origin of the unit cell is the upper front corner; a goes across, b down, and c back. Thermal ellipsoids are at 50% probability level. Hydrogen atoms are omitted.

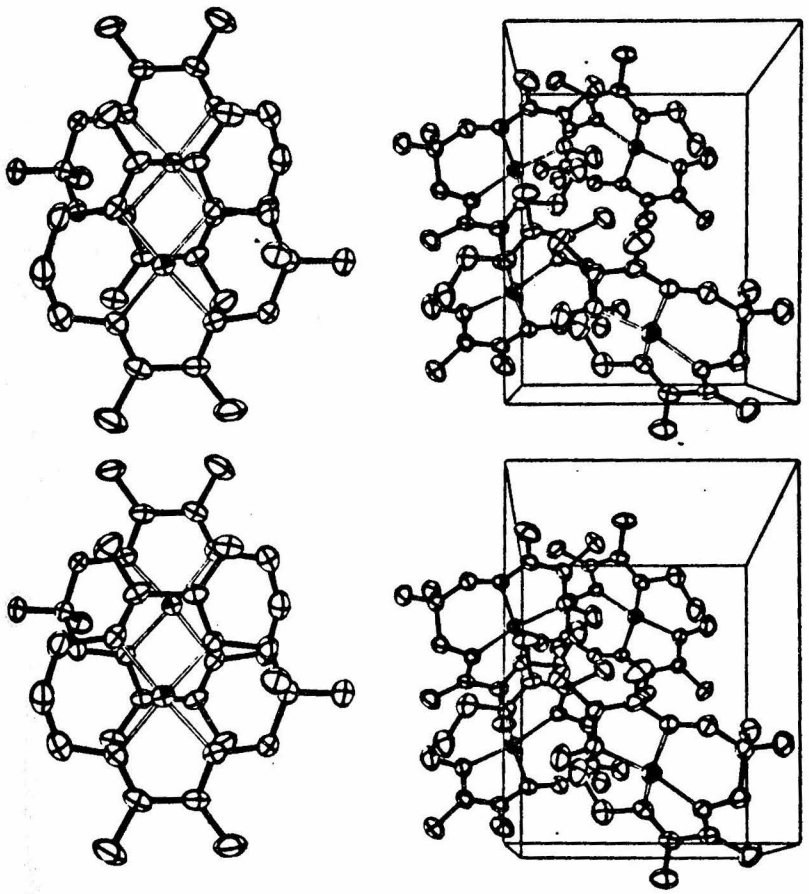

Figure 3

The upper stereopair shows the four-coordinate $Cu(LBF_2)$, 2,in a tetrahedrally distorted square-planar geometry. For comparison, a stereoview of $Cu(LBF_2)CO$, 1, is presented with the ligand in a similar orientation. Thermal ellipsoids are at the 50% probability level. Hydrogen atoms are omitted.

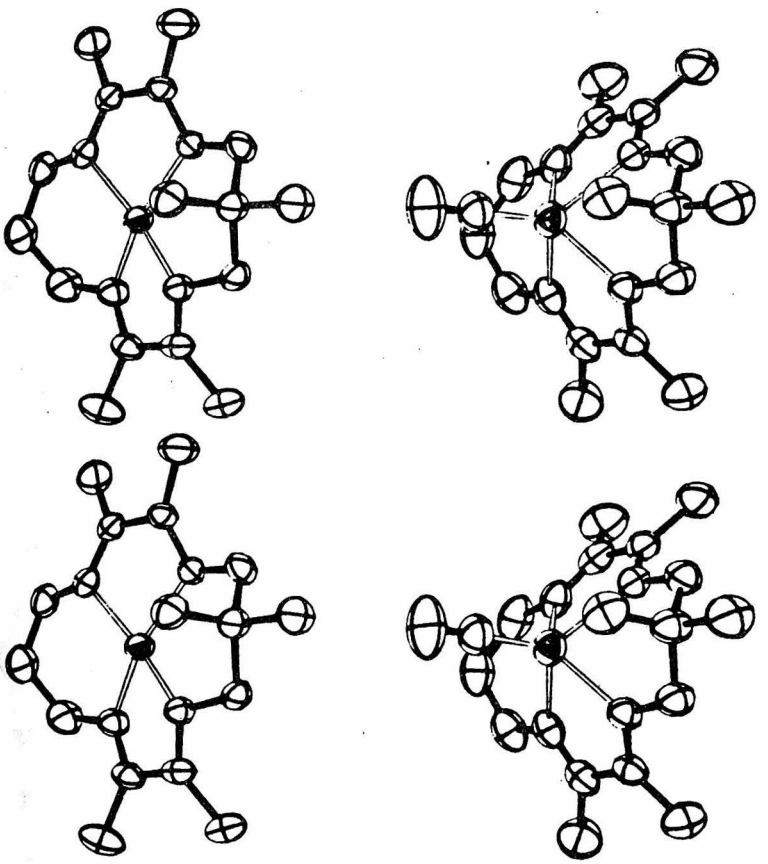

162.9(1)°. The four nitrogen-nitrogen non-bonding distances, Table V, range from 2.553(3) to 3.040(3) Å, distances which would be equal in a square-planar complex.

The macrocyclic ligand is in a boat conformation with boron of the BF_2 bridge and C6 of the propylene bridge both bent in the same direction away from the mean square plane of the copper and four nitrogens (Figure 4). Copper sits 0.01 Å out of this best plane and toward the same side as C6 and B. Table VI lists this and several other best plane calculations. Dihedral angles of 23° and 27° are found between the planes Cu, N1, N4 vs. Cu, N2, N3, and Cu, N1, N2 vs. Cu, N3, N4, respectively (Figure 4 and Table VI). These angles are closer to expected square-planar values, 0°, than to corresponding tetrahedral angles, 90°. The resulting distortion from planarity is reflected by substantial deviations from the best plane calculated for copper and the full ligand, even if the obvious out-of-plane atoms, C6, B, F1, and F2, are deleted (Table VI). Significant planar distortion is also indicated by ligand bond torsion angles listed in Table VII when compared with theoretical square-planar angles.

Comparisons to Related Structures. Structures have now been obtained for four-, five-, and six-coordinate

Figure 4

a). Deviations from best plane for copper and the four nitrogens (Table VI) are given in Å for the non-hydrogen atoms of $Cu(LBF_2)$, 2. Atomic positions correspond to those in Figure 1, i.e., with the BF_2 in the lower part of the figure. The positions of the four nitrogens indicate a tetrahedral distortion of the basic square plane about copper.

b),c). The angular distortion is illustrated by viewing the copper and the 4 nitrogens down A1(b) and A2(c). The angles given are those between the planes formed by two nitrogens and the copper: b). N1-Cu-N4 and N2-Cu-N3; c), N1-Cu-N2 and N3-Cu-N4. For a square planar complex these angles would be 0°, for a tetrahedral complex, 90°.

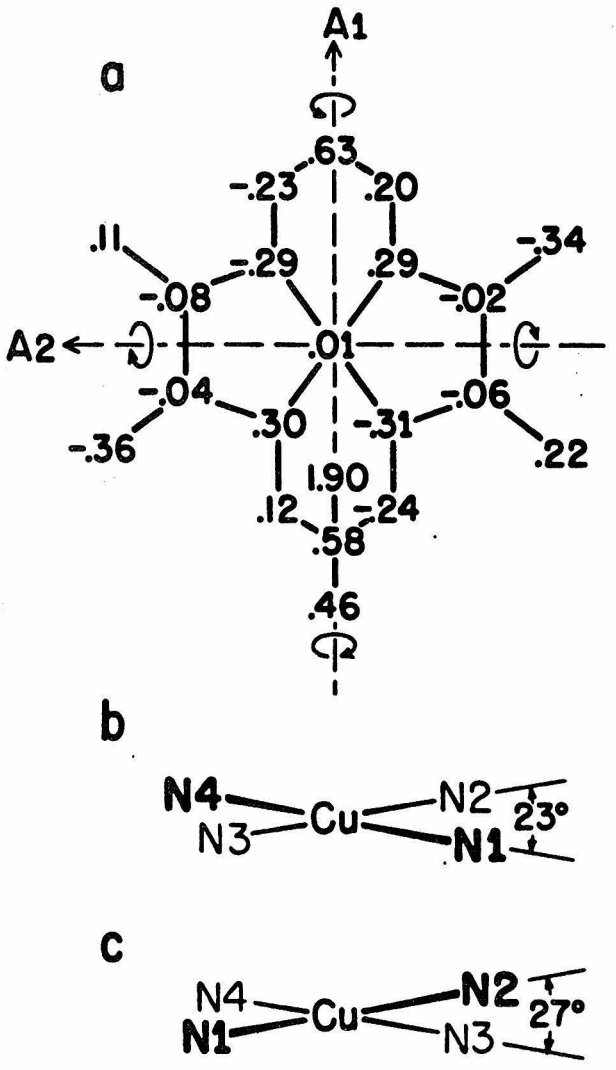
a
A1
.63
-.23
.20
.11
-.29
.29
-.34
-.08
-.02
A2
.01
-.04
.30
-.31
-.06
-.36
.22
1.90
.12
-.24
.58
.46
b
N4
Cu
N2
23°
N3
N1
c
N4
N2
27°
N1
Cu
N3

complexes containing LBF_2^- and LH^- (LH^- = the ligand in Figure 1 with a single hydrogen atom in place of the BF_2 group). Several distinctive ligand configurations are revealed in these structures. Boat conformations, in which B and C6 of LBF_2^- are bent in the same direction away from the mean macrocycle plane, have been found in $Cu(LBF_2)CO$, 1, $Cu(LBF_2)$, 2, and $Cu(LBF_2)NCO$, 3.[17] In contrast chair conformations with C6 and B on opposite sides of the mean macrocycle plane were found in the six-coordinate complexes $Rh(L'BF_2)(SeC_6H_5)_2$, 4,[8,15] and $Rh(L'BF_2)(CH_3)I$, 5.[9,15]

Whether a ligand is in a boat or a chair conformation may indicate overall distortion from planarity in the macrocycle. In turn the macrocyclic ligand configuration may be influenced by the preferred metal coordination geometry. Six-coordinate $Rh(L'BF_2)(CH_3)I$, 5, which has a chair conformation, is one example of a planar, unstrained system. The macrocyclic ligand itself is essentially square-planar; no special strain is indicated when its torsion angles are compared with theoretical planar angles (Table VII). In contrast when the macrocycle is distorted from planarity due to the influence of the preferred metal coordination geometry, the ligand assumes a boat conformation.

In both five-coordinate copper complexes, $Cu(LBF_2)CO$, 1, and $Cu(LBF_2)NCO$, 3, the metal is far above the mean plane of the four coordinated nitrogens. A distorted dome macrocyclic ligand configuration results. Projections of the two conjugated sections of the macrocycle, i.e., atoms N1-C2-C3-N2 and atoms N3-C9-C10-N4, point (from C to N) toward copper. The four methyl substituents are forced downward, away from copper. There is significant deviation from planar torsion angles, notably in the $(CH_2)_3$ and $O\text{-}BF_2\text{-}O$ bridges, for the dome configuration as shown for $Cu(LBF_2)CO$, 1, Table VII. Note that the molecule adopts a boat conformation which apparently serves to minimize macrocyclic ligand strain due to distortion from planarity.

No undistorted, four-coordinate, square-planar complexes of LBF_2^- have been structurally characterized. One might expect that the macrocyclic ligand in such complexes would not be strained by the metal coordination geometry but would be similar to that found in six-coordinate $Rh(L'BF_2)(CH_3)I$, 5, i.e., a strain-free, chair conformation. Four- and six-coordinate complexes of LH^-, $[Cu(LH)]_2(ClO_4)_2 \cdot CH_3OH$, 6,[10] $Co(LH)(CH_3)_2$, 7,[11] $Rh(LH)$, 8,[12] and $[Co(LH)(CH_3)H_2O]ClO$, 9,[13] have been structurally characterized. The LH^- ligands of these complexes do not exhibit either boat or chair conform-

ations due to the lack of the bridging BF_2 group found in LBF_2^-.

The macrocyclic ligand in $Cu(LBF_2)$, 2, exists in a boat conformation and is obviously strained. One can imagine twisting a perfectly square-planar molecule, about either A1 or A2 shown in Figure 4, to achieve the tetrahedral distortion of four nitrogens. Deviations from planarity in the rest of the ligand (Figure 4) are a reflection of the tetrahedral distortion. That the tetrahedral twist results in strain when compared to a theoretical planar molecule may be indicated by the torsion angles listed in Table VII. Significant distortions are found for the $(CH_2)_3$ and $O\text{-}BF_2\text{-}O$ bridges in $Cu(LBF_2)$, 2. As in the domed, five-coordinate molecule, $Cu(LBF_2)CO$, 1, these distortions do not suffice to indicate severe macrocyclic ligand strain. Unlike the dome configuration of $Cu(LBF_2)CO$, 1, the ligand of $Cu(LBF_2)$, 2, exhibits twisting about the C2-C3 and C9-C10 bonds (25 and 26°, respectively). This twisting evidences appreciable bonding strain if any π-delocalization is acknowledged for the N1-C2-C3-N2 and N3-C9-C10-N4 fragments.

The foregoing geometrical analysis of ligand strain raises the question of a proper bonding description for the macrocyclic ligand in $Cu(LBF_2)$, 2, as well as in the previously reported five-coordinate complex, $Cu(LBF_2)CO$, 1.

Is the LBF_2^- ligand in 1 and 2 adequately described by the line drawing for 1, which has carbon-nitrogen double bonds for C2-N1, C3-N2, C9-N3, and C10-N4? Or are both complexes better regarded as containing Cu(II) or even Cu(III) bound in a one- or two-electron reduced ligand system? Macrocyclic ligand structural parameters are helpful in addressing these questions. The structures obtained for $Cu(LBF_2)$, 2, and for $Cu(LBF_2)CO$, 1, permit a careful comparison of pertinent ligand bond lengths with those previously reported for several other complexes containing LBF_2^- or LH^- (Table VIII and Figure 5). In all structurally characterized complexes the ligands are essentially symmetric about a plane containing A1 and perpendicular to A2, Figure 4. Averaged bond lengths are presented in Table VIII and Figure 5, and the following discussion is restricted to pertinent bonds of only one half of the molecule.

Reduction of the macrocyclic ligand system might be expected to manifest itself by lengthening of either or both of the formally double, carbon-nitrogen bonds, C2-N1 and C3-N2. Additionally, partial reduction of the conjugated fragment, N1-C2-C3-N2, could lead to C2-C3 bond shortening. In fact, both of these parameters appear to be rather insensitive to changes in metal geometry and oxidation state. The C2-N1 and C3-N2 bonds range

Figure 5

Line graph of pertinent LBF_2^- and LH^- bond lengths for a variety of metal complexes.

C2-N1, C3-N2, C9-N3, C10-N4:
(Averaged)

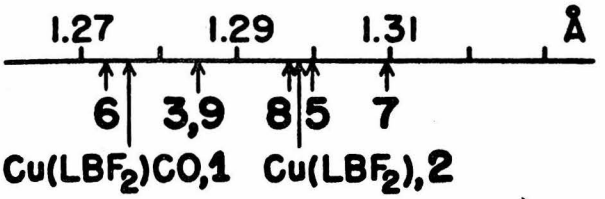

C2-C3, C9-C10 (Averaged):

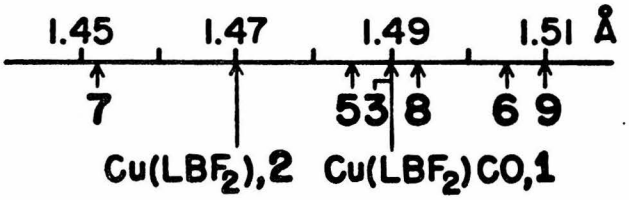

from 1.269(10) Å (C3-N2 in $[Cu(LH)]_2(ClO_4)_2 \cdot CH_3OH$, 6) to 1.312(13) Å (C2-N1 in $Co(LH)(CH_3)_2$, 7), a variation of 0.043 Å which is small when compared to typical bond differences in C-N single and double bonds (1.47 vs. 1.28 Å, a difference of 0.19 Å[18]). Similarly, the C2-C3 bond varies from 1.452(1) Å (in $Co(LH)(CH_3)_2$, 7) to 1.51(0) Å (in $[Co(LH)(CH_3)H_2O]ClO_4$, 9), a range of 0.058 Å, again small compared to the difference between typical C-C single and double bonds (1.54 Å vs. 1.34 Å, a difference of 0.20 Å[18]). Of greater significance, however, is a direct comparison of bond parameters in $Cu(LBF_2)CO$, 1, and in $Cu(LBF_2)$, 2, with related complexes.

The tetrahedrally distorted, square-planar complex, $Cu(LBF_2)$, 2, has no good structural analogue. The macrocyclic ligand exists in the boat conformation as in $Cu(LBF_2)CO$, 1, and in $Cu(LBF_2)NCO$, 3, but the latter are five-coordinate. Copper is essentially in the mean nitrogen plane in $Cu(LBF_2)$, 2, and the macrocyclic ligand is probably better compared to the ligands in square-planar or six-coordinate octahedral complexes. The only non-copper complex with a BF_2 bridge is $Rh(L^{\wedge}BF_2)(CH_3)I$, 5, which has a square-planar, chair macrocyclic conformation. The C2-C3 bond lengths in $Cu(LBF_2)$, 2, and in $Rh(L^{\wedge}BF_2)(CH_3)I$, 5, differ by only 0.015 Å and the C2-N1 and C3-N2 bonds by 0.003 and 0.006 Å, respectively. Similar results are

obtained on comparing $Cu(LBF_2)$, 2, with most other complexes in Table VIII. All comparisons reveal little ligand bond length variation. A better perspective for macrocyclic ligand parameters is obtained from Figure 5 which depicts a line graph for averaged C2-C3 and C2-N1 bond lengths for all structurally characterized LBF_2^- or LH^- complexes. Note the overall small variations and the relative location of $Cu(LBF_2)$, 2. All of the pertinent macrocycle bond lengths in $Cu(LBF_2)$, 2, are within the range observed for similar Co(III), Rh(I), Rh(III), and Cu(II) complexes and none of the latter contain LBF_2^- or LH^- which appear to be reduced. It does seem that in $Cu(LBF_2)$, 2, C2-C3 is slightly toward the short end and C2-N1 and C3-N2 are slightly toward the long end of the bond length ranges represented in Figure 5. In view of the very different macrocyclic ligand configurations involved in comparing $Cu(LBF_2)$, 2, (distorted square-planar, boat) with any of the other complexes in Table VIII (square-planar or dome, boat or chair) it is difficult to definitively attribute small bond length variations to any single factor. Nonetheless, the C2-C3, C2-N1, and C3-N2 bond lengths in $Cu(LBF_2)$, 2, might indicate π-delocalization of electron density from the copper into the π system of the ligand (Figure 6) with configuration a as the major contributing structure.

Figure 6

Proposed π-delocalization in $Cu(LBF_2)$, 2, which can also be regarded as metal to ligand back-bonding.

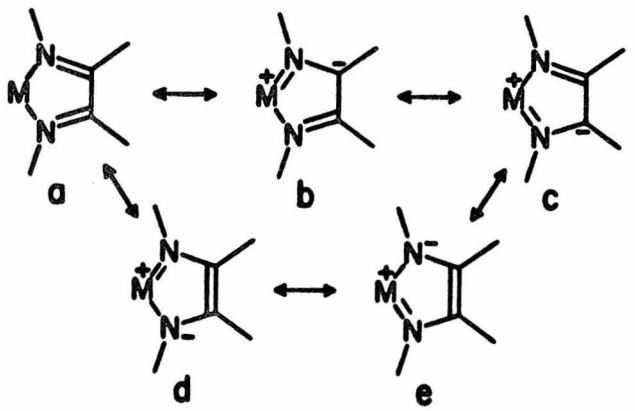
a
b
c
d
e

A π-delocalization scheme as represented in Figure 6 also helps to explain electronic and infrared spectral observations. The complex, $Cu(LBF_2)$, 2, is deep blue in color (677 nm, ε = 10,300 M^{-1} cm^{-1} at 25°)[3]. The visible band can be explained by a metal to ligand charge transfer transition, an assignment made more realistic by structural evidence of π-delocalization.

In the $Cu(LBF_2)$, 2, infrared spectrum, there are no bands in the 1500-1700 cm^{-1} region and, therefore, there are no bands which would normally be assigned to imine stretching modes, $\nu_{C=N}$. The absence of $\nu_{C=N}$ suggested the possibility of fully reduced C2-N1 and C3-N2 bonds, but that has been made unlikely on the basis of the structural data. When the infrared spectral data for several LBF_2^- metal complexes (Table IX) are examined, a strong similarity of all spectra is found. The sole exception is the spectrum of $Cu(LBF_2)$, 2, which has no bands from 1500 to 1700 cm^{-1} and has three additional bands from 1250 to 1500 cm^{-1}. The two bands at 1320 and 1470 cm^{-1} might be associated with the α-diimine stretching modes, although these values are unusually low.[24]

Because of metal back-bonding into macrocyclic ligand π* orbitals, alternatively regarded as the π-delocalization depicted in Figure 6, the imine bonds

in $Cu(LBF_2)$, 2, would be expected to be weaker than in the free ligand, or than in metals in higher oxidation states, and have α-diimine stretching modes shifted to lower energies. Note that $Cu(LBF_2)$, 2, which exhibits no usual α-diimine bands, reacts with CO to give the domed, five-coordinate $Cu(LBF_2)CO$, 1. The latter complex no longer absorbs at 677 nm and has bands in the infrared at 1640 and 1560 cm^{-1} (Table IX).

Delocalization of electron density into the macrocyclic ligand π system may best explain the ligand structural parameters and complex spectral properties discussed above. Structural parameters alone cannot serve to definitely preclude the possibility of a formal one- or two-electron reduction of the macrocyclic ligand in $Cu(LBF_2)$, 2. Even a one-electron reduction would affect at least three bonds in the ligand (C2-C3, C2-N1, and C3-N2), but delocalization through the copper or even crystallographic disorder could average the observed effect to six bonds, 2 C-C and 4 C-N bonds. No precedent in LBF_2^- or LH^- complex chemistry is available to adequately define the structural nature of a reduced ligand.

It would appear that the best structural description of $Cu(LBF_2)$, 2, is, at present, copper(I) in an uncommon, tetrahedrally distorted, square-planar coordination

geometry with substantial back-bonding into macrocyclic ligand π^* orbitals. Since $Cu(LBF_2)$, 2, yields comparable solution and solid-state electronic absorption spectra, it is likely that the solid-state structure is a good representation of the species in solution as well.

Structurally, the five-coordinate carbonyl, $Cu(LBF_2)CO$, 1, is probably most closely mirrored by the Cu(II) complex, $Cu(LBF_2)NCO$, 3. Both complexes are five-coordinate, square-pyramidal with LBF_2^- in a dome, boat conformation. Copper is displaced 0.96 Å out of the mean nitrogen plane in $Cu(LBF_2)CO$, 1, but only 0.58 Å in $Cu(LBF_2)NCO$, 3, leading to longer Cu-N bond lengths in the former (2.13(4) Å for 1, 2.00(1) Å for 3). There are no significant differences in pertinent macrocyclic ligand bond parameters (Table VIII). Figure 5 graphically illustrates that $Cu(LBF_2)CO$, 1, has C2-C3 and C2-N1, C3-N2 bond lengths which can be described as average for all known LBF_2^- and LH^- complexes. In addition, as noted earlier, $Cu(LBF_2)CO$, 1, has peaks in its infrared spectrum (Table IX) that can be assigned as normal imine stretching modes. There is no direct LBF_2^- structural evidence to support the suggested description of $Cu(LBF_2)CO$, 1, as containing Cu(II) or Cu(III) complexed to a reduced macrocyclic ligand system.

Oxidation State of Copper. An accurate oxidation state description for copper in both $Cu(LBF_2)$, 2, and $Cu(LBF_2)CO$, 1, is more than a mere formalism or question of semantics. These complexes represent new structural and reactivity types for copper and merit more precise description. Furthermore, the role of the macrocyclic ligand in promoting unusual complex structures and reactivities poses more general questions regarding other transition metal complexes.

While it is beyond the scope of this paper to present a detailed bonding description for $Cu(LBF_2)$, 2, or for $Cu(LBF_2)CO$, 1, it may be useful to summarize certain pertinent observations regarding their copper oxidation states. That these complexes are presently best described as containing Cu(I) is suggested by the following points. 1) $Cu(LBF_2)$, 2, was obtained from acetone by the one-electron electrochemical reduction, at -0.7 V vs. NHE, of the Cu(II) complex, $[Cu(LBF_2)]_2(ClO_4)_2 \cdot C_4H_8O_2$, 10.[3] In dimethylformamide the reversible wave of the Cu(II) complex, 10, is found at $E_{1/2}$ = -0.456 V vs. NHE, with further reduction occurring below -1.5 V. The corresponding Zn(II) complex, $[Zn(LBF_2)]_2(ClO_4)_2 \cdot CH_3OH$, 12, is electrochemically inactive in the region +0.20 to -0.95 V, but yields reduction waves below -0.95 V. The reduction processes in the zinc complex are presumably due to

LBF_2^- reduction. 2) $Cu(LBF_2)$, 2, and $Cu(LBF_2)CO$, 1, are diamagnetic by magnetic susceptibility, and give no EPR signals. 3) There is no obvious structural evidence of macrocyclic ligand reduction in either $Cu(LBF_2)$, 2, or $Cu(LBF_2)CO$, 1, as discussed earlier. 4) The four-coordinate complex, $Cu(LBF_2)$, 2, is not planar as would be expected for Cu(II) or Cu(III) and as has been demonstrated to be possible for $L'BF_2^-$ in $Rh(L'BF_2)(CH_3)I$, 5. Rather, the four-coordinated nitrogens exhibit a distortion toward tetrahedrality, suggestive of Cu(I). 5) $Cu(LBF_2)$, 2, binds both CO, a good π-acceptor, and 1-methylimidazole, a good σ-donor, but the former is bound more strongly ($K_c = 4.7 \times 10^4\ M^{-1}$, Eq. 1) than the latter ($K_c = 16\ M^{-1}$).[3]

$$Cu(LBF_2) + B \overset{K_c}{\rightleftharpoons} Cu(LBF_2)B \qquad (1)$$

These equilibrium constants and the charge transfer band (677 nm, $\varepsilon = 10{,}300\ M^{-1}\ cm^{-1}$) suggest an electron-rich copper atom. 6) The binding of CO to the four-coordinate, presumably Cu(I) species to give a five-coordinate carbonyl complex is not a unique reaction. The mixed-valence Cu(II)Cu(I) complex, 13, also binds CO to give what is probably a five-coordinate analogue of $Cu(LBF_2)CO$, 1. Complex 13 was obtained via one-electron reduction

of the corresponding Cu(II)Cu(II) species and has an intervalence transition in the near infrared which strongly implicates the Cu(I) assignment.[26] 7) From

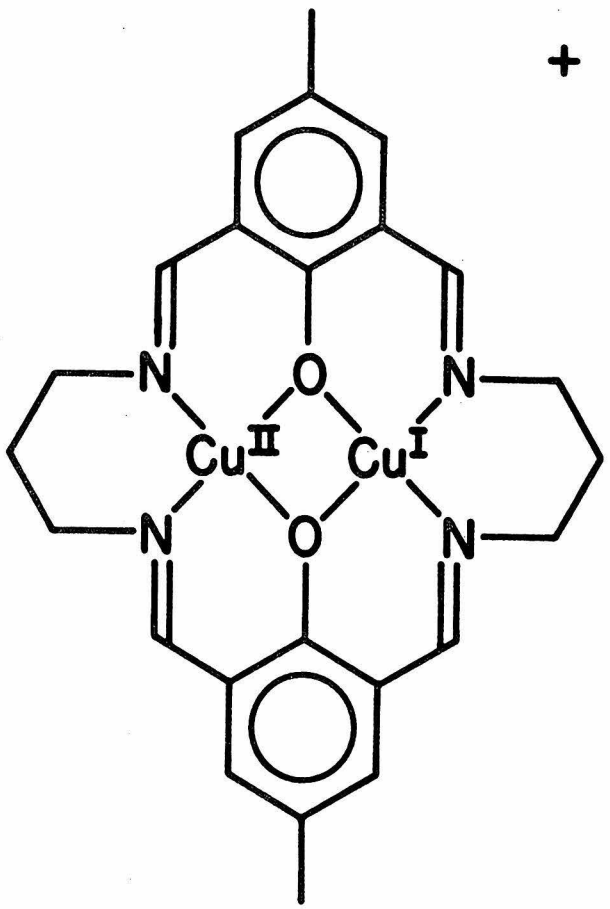

13

a reactivity viewpoint, the most important observation may be that Cu(LBF_2), 2, reacts like Cu(I). Certain Cu(II) complexes have recently been shown to be oxidized to Cu(III) by dioxygen.[27] However, no complexes characterized by

spectral or physical properties to be Cu(II) or Cu(III) have been reported to bind CO. In contrast $Cu(LBF_2)$, 2, reacts rapidly with both CO and O_2.

While it is presently convenient to regard both $Cu(LBF_2)$, 2, and $Cu(LBF_2)CO$, 1, as formally containing Cu(I), the nature of the bonding in both complexes is not apparent. We are presently engaged in ESCA studies of these and related complexes to better define the metal oxidation states. Further physical measurements will provide information on the factors conducive to the formation of five-coordinate complexes. These data along with theoretical bonding calculations may lead to acceptable bonding descriptions for these unusual copper complexes.

Conclusions

The macrocyclic ligand anion, LBF^-, is capable of producing unusual structural and reactivity types for copper, including square-planar and five-coordinate complexes apparently containing Cu(I). Most four-coordinate Cu(I) complexes enjoy a tetrahedral geometry in bonding. In contrast $Cu(LBF_2)$, 2, is a distorted square-planar structure and manifests its unusual structure by an unusual reactivity, the capacity to bind a fifth ligand such as CO. We are continuing our investigation of a wide variety of copper-macrocyclic ligand complexes

in order to delineate the structural and electronic factors which promote these new reactions.

Acknowledgment

We sincerely appreciate assistance from Charlotte Ma, Richard Marsh, and Sten Samson and helpful discussions with Harry Gray. This work was supported, in part , by the National Science Foundation, the National Institutes of Health, the International Copper Research Association, and the Biomedical Research Support Program (Grant No. RR07003).

Experimental

All operations requiring an inert atmosphere were performed in a Vacuum Atmospheres Dri-lab containing He. Electronic absorption spectroscopy (EAS) was performed on a Cary-14 automatic recording spectrometer, infrared spectra were obtained via KBr pellets on a Beckman IR-12 spectrometer, and nuclear magnetic resonance measurements were made using TMS as an internal standard on a Varian EM-390 90 MHz spectrometer.

Tetrabutylammonium perchlorate (TBAP) was dried exhaustively *in vacuo* before use. Spectroquality dimethylformamide (DMF) was dried and vacuum distilled before use as a solvent for polarographic measurements. All other solvents were reagent grade.

Electrochemistry. The apparatus used for sampled dc polarography and cyclic voltammetry was a Princeton Applied Research model 174A polarographic analyzer coupled with an X-Y recorder. A cell with two compartments separated by a medium porosity sintered glass frit was used for all measurements. The working compartment was filled with DMF, which was 0.1 M in TBAP, 0.5 mM in sample and 1 mM in ferrocene. The dropping mercury working and platinum auxiliary electrodes were placed in the

working half of the cell. The other compartment contained 0.1 M TBAP in DMF and the reference electrode, which was a silver wire in 0.01 M $AgNO_3$ and 0.1 M TBAP acetonitrile solution. The acetonitrile solution was separated from the DMF solution by a fine frit. The sampled dc polarographic measurements were done using a drop time of 5 sec and a scan rate of either 0.5 or 1 mV/sec. Cyclic voltammetric scan rates were 50 mV/sec. The polarographically determined half-wave potentials, $E_{1/2}$, of the samples were related to the normal hydrogen electrode (NHE) by the use of a solvent independent redox couple of ferrocene, its Fe(II)/Fe(III) couple.[28] The formal reduction potential, $E^f = (E_{p_a} + E_{p_c})/2$, of this couple was determined by cyclic voltammetry. The expression used was $E_{1/2}(Ag/Ag^+)$ - $E^f(Fe(II)/Fe(III)) + 0.400\ V = E_{1/2}$ (NHE).

X-Ray Data Collection and Reduction. Crystals of $Cu(LBF_2)$, 2, were grown from a slowly evaporating acetone solution under helium. Preliminary oscillation and Weissenberg photographs indicated space group Pn, P2/n or $P2_1/n$.

A purple crystal of dimensions 0.10 mm × 0.12 mm × 0.44 mm was mounted on a P_1-Syntex four-circle diffractometer.[29] Fifteen manually centered reflections were used to find the cell parameters for the data collection.

The final cell parameters given in Table I, and used in the crystal structure refinement, were found by a least squares fit to 46 reflections. Intensity data were collected out to $2\theta = 140°$, using θ-2θ scans from 1° below the $CuK\alpha_1$ value to 1° above the $CuK\alpha_2$ value (ranging from 2.02° to 2.78° in scan width) at a rate of 2°/min with an equal time spent counting background. Several check reflections measured after every 25 reflections to monitor crystal and instrument stability showed no significant changes.

The measured intensities were reduced to structure factor amplitudes by applying Lorentz and polarization corrections. The standard deviations of the intensities were calculated from the formula:

$$\underline{\sigma}^2(I) = \underline{S} + (\underline{B}1 + \underline{B}2) + (\underline{d}\underline{S})^2$$

where $\underline{S}$, $\underline{B}1$, and $\underline{B}2$ are the scan and two background counts and $\underline{d}$ was taken[30] as 0.02. Because of a small absorption coefficient, 24.9 cm^{-1}, no absorption correction was made. After deleting systematic absences and averaging equivalent reflections, the number of unique data was 2882 (2652 > 0). Examination of the intensity statistics showed a centrosymmetric structure, thus eliminating the possibility of $\underline{Pn}$ as a space group. The

more common of the two remaining possible space groups, $P2_1/n$, was chosen and later verified by the successful completion of the structure.

Solution and Refinement of the Structure. Scattering factors for C, B, F, N and O were taken from reference 31; the H scattering factors were from reference 32; and the neutral atom Cu scattering factors and the real part of the anomalous dispersion correction were taken from references 33 and 34, respectively. The function minimized in the least squares refinement was $\Sigma w(k^2F_o^2 - F_c^2)^2$ where the weight $w = 1/\sigma^2(F_o^2)$, F_o and F_c are the observed and calculated structure factors, and k is the scale factor for F_o.

The positions of the copper and four nitrogen atoms were located from a three-dimensional Patterson map.[35] These positions were used to phase a Fourier map which revealed the positions of all but two non-hydrogen atoms. Use of full matrix least squares and difference map techniques brought $R(F) = \Sigma||kF_o| - |F_c||/\Sigma|kF_o| = 0.125$, with isotropic temperature factors on all non-hydrogen atoms. Since several of the large intensity reflections seemed to suffer from extinction, a secondary extinction parameter, g, of the form $F_c = F_o\ (1 + gI)$, where I is the intensity after data reduction, was introduced. The

final refined value of g was 8.6×10^{-6}. With anisotropic temperature factors on all non-hydrogen atoms, this lowered $R(F)$ to 0.072. The 18 hydrogen atoms were then located by difference Fourier methods and their positional parameters refined in a second matrix. In the two final cycles of least squares refinement, the isotropic temperature factors of the hydrogen atoms were also allowed to vary. Most of the hydrogen temperature factors converged, although that of H8c shifted on the order of the estimated deviation during the last cycle. The final $R(F)$ equalled 0.054 for the 2652 reflections with magnitudes greater than zero, and the final goodness of fit $\Sigma w(k^2F_o^2 - F_c^2)^2/(n-p)k^4$ equalled 1.43, n = 2882 is the number of observations and p = 263 is the number of parameters. The highest peak in the final difference Fourier map was 0.7e A^{-3} and was not located in a chemically significant position (approximately equidistant from C5, C6, and C7). Final parameters are given in Table II. Bond lengths and angles are found in Tables III and IV.

Preparation and Further Characterization of Complexes. The infrared spectra of the first four of the complexes are reported in Table IX.

Cu(LBF_2), 2,[1,1-difluoro-4,5,11,12-tetramethyl-1-bora-3,6,10,13-tetraaza-2,14-dioxo-cyclotetradeca-3,5,10,12-tetraenato]copper(I), was prepared as described elsewhere.[3] The solid state visible spectrum was determined from a mineral oil suspension supported on filter paper. The observed peak at 695 nm corresponds to the peak at 677 nm reported previously in acetone solution.[3] The proton nuclear magnetic resonance spectrum in fully deuterated dimethyl sulfoxide shows singlets at 1.95 and 2.00 δ accounting for twelve hydrogen atoms, a multiplet at 2.27 δ which integrates as two hydrogen atoms and a triplet at 3.63 δ integrating as four hydrogen atoms.

Cu(LBF_2)CO, 1, carbonyl[1,1-difluoro-4,5,11,12-tetramethyl-1-bora-3,6,10,13-tetraaza-2,14-dioxo-cyclo-tetradeca-3,5,10,12-tetraenato]copper(I), was prepared as described elsewhere.[3] The proton nmr was determined on a sample of Cu(LBF_2), 2, in deuterated dimethyl sulfoxide solution which had been saturated with CO. Although the color did change from a very dark blue-brown to a pale greenish yellow, indicating formation of Cu(LBF_2)CO, 1, the nmr spectrum was identical to that of Cu(LBF_2), 2, in dimethyl sulfoxide.

[Cu(LBF$_2$)]$_2$(ClO$_4$)$_2$·C$_4$H$_8$O$_2$,10,bis[(1,1-difluoro-4,5,11,12-tetramethyl-1-bora-3,6,10,13-tetraaza-2,13-dioxo-cyclotetradeca-3,5,10,12-tetraenato)copper(II)] diperchlorate·dioxane was prepared as previously reported.[3] The electrochemical behavior of this complex was measured in DMF. Reduction waves (vs. NHE) occur at $E_{1/2}$ = -.456 V (n = 1) and at $E_{1/2}$ ≃ -1.65 V (irreversible).

Cu(LBF$_2$)I$_3$, 11, [1,1-difluoro-4,5,11,12-tetramethyl-1-bora-3,6,10,13-tetraaza-2,13-dioxo-cyclotetradeca-3,5,10,12-tetraenato]copper(II) triiodide·[Cu(LBF$_2$)]$_2$(ClO$_4$)$_2$·C$_4$H$_8$O$_2$, 10, and excess KI were stirred in pyridine. After filtering off a black solid, evaporation of the filtrate yielded a brown powder which was dissolved in a minimum of boiling acetone, filtered while hot, recovered by filtration after the solution had cooled. Anal. Calcd. for $C_{11}H_{18}B_1Cu_1F_2I_3N_4O_2$: C, 18.07; H, 2.48; Cu, 8.69; and N, 7.66. Found: C, 18.75; H, 2.55; Cu, 8.7; and N, 7.10.

[Zn(LBF$_2$)]$_2$(ClO$_4$)$_2$·CH$_3$OH, 12, bis[(1,1-difluoro-4,5,11,12-tetramethyl-1-bora-3,6,10,13-tetraaza-2,13-dioxo-cyclotetradeca-3,5,10,12-tetraenato)zinc(II)] diperchlorate·methanol·[Cu(LBF$_2$)]$_2$(ClO$_4$)$_2$·C$_4$H$_8$O$_2$, 10, and zinc amalgam were stirred in acetone in the absence

of oxygen. The solution turns from purple to clear, forming a copper mirror on the walls of the flask. The amalgam and a small amount of dark brown precipitate is filtered off and discarded. The white product is recovered by solution evaporation and can be recrystallized in small yield by dissolving in a minimum of boiling methanol, filtering hot, and recovering by filtration after the solution has cooled. Anal. Calcd. for $C_{23}H_{40}B_2Cl_2F_4N_8O_{11}Zn_2$: C, 29.52; H, 4.31; N, 11.97; and Zn, 13.97. Found: C, 29.55; H, 4.50; N, 12.10; and Zn, 13.9. The complex is diamagnetic (25°, Faraday method). Its infrared spectrum is similar to that of the copper(II) complex, 10, with additional bands due to the methanol. Electrochemical behavior of the zinc complex was measured in DMF. Reduction waves (vs. NHE) occur at $E_{1/2}$ = -1.015 V (n = 2) and at approximately -1.26 and -1.51 V (irreversible).

References and Notes

(1) F. H. Jardine in "Advances in Inorganic and Radiochemistry," Vol. 17, H. J. Emeleus and A. G. Sharpe, Eds., Academic Press, New York, N.Y., 1975, p. 115; W. S. McDonald in "Molecular Structure by Diffraction Methods," Vol. 4, G. A. Sim and L. E. Sutton, Senior Reporters, The Chemical Society, London, 1976, p. 319; and D. M. Johns and C. A. McAuliffe in "Inorganic Chemistry of the Transition Elements," Vol. 5, B. F. G. Johnson, Senior Reporter, The Chemical Society, London, 1977, p. 275.

(2) See, for example: D. T. Cromer, A. C. Larson, and R. B. Roof, Jr., Acta Cryst. 19, 192 (1965); S. L. Lawton, W. J. Rohrbaugh, and G. T. Kokotailo, Inorg. Chem., 11, 612 (1972); M. R. Churchill, S. A. Bezman, J. A. Osborn, and J. Wormald, Inorg. Chem., 11, 1818 (1972); G. Van Koten and J. G. Noltes, J. Organomet. Chem., 102, 551 (1975); and F. J. Hollander and D. Coucouvanis, J. Am. Chem. Soc., 99, 6268 (1977).

(3) R. R. Gagné, J. L. Allison, R. S. Gall, and C. A. Koval, J. Am. Chem. Soc., 99, 7170 (1977).

(4) M. C. Weiss, B. Bursten, S. -M. Peng, and V. L. Goedken, J. Am. Chem. Soc., 98, 8021 (1976).

(5) K. Henrick, R. W. Matthews, and P. A. Tasker, Inorg. Chem., 16, 3293 (1977).

(6) L. Sacconi, Coord. Chem. Rev., 8, 351 (1972).

(7) M. R. Churchill, B. G. DeBoer, F. J. Rotella, O. M. Abu Salah and M. I. Bruce, Inorg. Chem., 14, 2051 (1975).

(8) J. P. Collman, R. K. Rothrock, J. P. Sen, T. D. Tullius, and K. O. Hodgson, Inorg. Chem., 15, 2947 (1976).

(9) J. P. Collman, P. A. Christian, S. Current, P. Denisevich, T. R. Halbert, E. R. Schmittou, and K. O. Hodgson, Inorg. Chem., 15, 223 (1976).

(10) J. A. Bertrand, J. H. Smith, and D. G. Van Derveer, Inorg. Chem., 16, 1484 (1977).

(11) M. Calligaris, J. C. S. Dalton, 1628 (1974).

(12) D. W. Murphy, Ph.D. Dissertation, Stanford University, 1972.

(13) S. Brückner, M. Calligaris, G. Nardin, and L. Randaccio, Inorg. Chim. Acta, 13, 278 (1969).

(14) The standard deviation of the mean value, $\bar{X}$, is calculated by the formula $[\sum_{i=1}^{N} (X_i-\bar{X})^2/(N-1)]^{\frac{1}{2}}$.

(15) The macrocyclic ligand, $L'BF_2^-$, is 1,1-difluoro-4,12-diethyl-5,11-dimethyl-1-bora-3,6,10,13-tetraaza-2,14-dioxo-cyclotetradeca-3,5,10,12-tetraenato.

(16) The torsion angles for $Rh(L'BF_2)(CH_3)I$ were calculated using atomic parameters from ref. 8.

(17) O. P. Anderson and J. C. Marshall, private communication.

(18) J. March, "Advanced Organic Chemistry: Reactions, Mechanisms, and Structure," McGraw-Hill, New York, N.Y., 1968, p. 22.

(19) S. C. Jackels, K. Farmery, E. K. Barefield, N. J. Rose, and D. H. Busch, Inorg. Chem., 11, 2893 (1972); J. C. Dabrowiak and D. H. Busch, Inorg. Chem., 14, 1881 (1975); A. M. Tait, F. V. Lovecchio, and D. H. Busch, Inorg. Chem., 16, 2206 (1977).

(20) N. Yamazaki and Y. Hohokabe, Bull. Chem. Soc. Jap., 44, 63 (1971); Y. Yamano, I. Masuda, and K. Shinra, Bull. Chem. Soc. Jap., 44, 1581 (1971).

(21) A. Bigotto, G. Costa, V. Galasso, and G. DeAlti, Spect. Acta, 26A, 1939 (1970).

(22) G. N. Schrauzer, Chem. Ber., 95, 1438 (1962); D. R. Boston and N. J. Rose, J. Am. Chem. Soc., 90, 6859 (1968).

(23) B. J. Hathaway and A. E. Underhill, J. Chem. Soc., 3091 (1961).

(24) In the case of tris(biacetyl-bis-methylimine)iron(II) iodide,[25a] there is no infrared band, even at very low energy, which can be reasonably assigned to $\nu_{C=N}$. In this case, it was suggested that the metal-diimine five-membered ring might have predominant configurations like (d) and (e) of Figure 6. The Co(III) and Ni(II) complexes of the macrocyclic ligand 2,3,9,10-tetramethyl-1,4,8,11-tetraazacyclotetradeca-1,3,8,10-tetraene (TIM) exhibit the expected α-diimine stretching modes while the Fe(II) complexes show

only very weak bands in the 1600 cm^{-1} region.[25b] Clearly α-diimine stretching modes in some complexes, including these Fe(II) species, are not well behaved and may warrant further study.

(25) (a) P. E. Figgins and D. H. Busch, J. Phys. Chem., 65, 2236 (1961); (b) S. C. Jackels, K. Farmery, E. K. Barefield, N. J. Rose, and D. H. Busch, Inorg. Chem., 11, 2893 (1972); and D. A. Baldwin, R. M. Pfeiffer, D. W. Reichgott, and N. J. Rose, J. Am. Chem. Soc., 95, 5152 (1973).

(26) R. R. Gagné, C. A. Koval, and T. J. Smith, J. Am. Chem. Soc., 99, 8367 (1977).

(27) G. L. Burce, E. B. Paniago, and D. W. Magerum, Chem. Comm., 261 (1975); and G. L. Burce, Ph.D. Thesis, Purdue University, 1975.

(28) D. Baner and M. Breant, in "Electroanalytical Chemistry," Vol. VIII, A. J. Bard, Ed., Marcel Dekker, New York, N.Y. 1975, p. 300.

(29) The X-ray diffractometer was modernized with funds from NSF Instrument Grant No. CHE 76-05471.

(30) S. W. Peterson and H. A. Levy, Acta Cryst., 10, 70 (1957).

(31) "International Tables for X-Ray Crystallography," Vol. III, Kynoch Press, Birmingham, England, 1962.

(32) R. F. Stewart, E. R. Davidson, and W. T. Simpson, J. Chem. Phys., 42, 3175 (1965).

(33) D. T. Cromer and J. T. Waber, Acta Cryst., 18, 104 (1965).

(34) D. T. Cromer, Acta Cryst., 18, 17 (1965).

(35) Except for C. K. Johnson's ORTEP program, all computer programs used were from the CRYM system of crystallographic computer programs.

Table I. Crystal Data for $Cu(LBF_2)$, 2

$C_{11}H_{18}BCuF_2N_4O_2$, FW = 350.6 g $mole^{-1}$	
Space Group $P2_1/n$ (14 N)	
a = 11.800(2) Å	Z = 4
b = 9.005(1) Å	ρ_{calcd} = 1.61 g cm^{-3}
c = 13.704(1) Å	ρ_{exptl} = 1.62 g cm^{-3}
β = 96.40(1)°	μ = 24.9 cm^{-1}
V = 1447.2(4) $Å^3$	$\lambda(CuK_\alpha)$ = 1.54178 Å

Table II. Atomic Parameters for $Cu(LBF_2)$, 2.[a]

	x	y	z	U_{11}	U_{22}	U_{33}	U_{12}	U_{13}	U_{23}
Cu	0.18822(3)	0.50011(5)	0.05758(3)	0.0394(3)	0.0338(3)	0.0374(2)	0.0046(2)	0.0125(2)	0.0031(2)
N1	0.0905(2)	0.6720(3)	0.0294(2)	0.030(1)	0.035(2)	0.035(1)	0.002(1)	0.006(1)	0.005(1)
N2	0.1009(2)	0.4824(3)	0.1686(2)	0.037(1)	0.040(2)	0.028(1)	-.006(1)	0.008(1)	0.001(1)
N3	0.2553(2)	0.3047(3)	0.0488(2)	0.044(2)	0.031(2)	0.046(2)	0.004(1)	0.008(1)	0.000(1)
N4	0.3036(2)	0.5548(3)	-.0261(2)	0.033(1)	0.035(1)	0.037(1)	0.001(1)	0.010(1)	0.001(1)
O1	0.2912(2)	0.6762(2)	-.0876(1)	0.044(1)	0.037(1)	0.034(1)	0.004(1)	0.016(1)	0.007(1)
O2	0.1147(2)	0.7886(2)	-.0317(2)	0.037(1)	0.042(1)	0.047(1)	0.008(1)	0.012(1)	0.017(1)
B	0.2381(3)	0.8048(4)	-.0431(3)	0.040(2)	0.032(2)	0.042(2)	0.001(2)	0.013(2)	0.006(2)
F1	0.2431(2)	0.9196(2)	-.1094(1)	0.059(1)	0.042(1)	0.058(1)	0.006(1)	0.024(1)	0.020(1)
F2	0.2973(2)	0.8385(2)	0.0475(1)	0.051(1)	0.043(1)	0.045(1)	0.000(1)	0.004(1)	-.008(1)
C1	-.0256(3)	0.8481(4)	0.1129(3)	0.058(2)	0.053(2)	0.063(2)	0.017(2)	0.020(2)	0.000(2)
C2	0.0268(2)	0.7019(3)	0.0981(2)	0.025(2)	0.042(2)	0.037(2)	0.003(1)	0.005(1)	-.002(1)
C3	0.0167(2)	0.5745(4)	0.1638(2)	0.030(2)	0.048(2)	0.029(2)	-.004(2)	0.006(1)	-.006(2)
C4	-.0856(3)	0.5575(4)	0.2179(2)	0.042(2)	0.080(3)	0.051(2)	-.002(2)	0.018(2)	0.007(2)
C5	0.0976(3)	0.3396(4)	0.2202(2)	0.062(2)	0.051(2)	0.036(2)	-.003(2)	0.012(2)	0.010(2)
C6	0.2062(3)	0.2542(4)	0.2176(3)	0.082(3)	0.053(2)	0.056(2)	0.007(2)	0.013(2)	0.019(2)
C7	0.2349(3)	0.1891(4)	0.1210(3)	0.075(3)	0.039(2)	0.065(2)	0.010(2)	0.017(2)	0.010(2)
C8	0.4301(3)	0.1847(4)	0.0021(3)	0.052(2)	0.045(2)	0.101(3)	0.017(2)	0.013(2)	-.008(2)
C9	0.3433(3)	0.3060(3)	0.0007(2)	0.037(2)	0.033(2)	0.048(2)	0.007(2)	0.002(2)	-.010(2)
C10	0.3549(3)	0.4388(4)	-.0594(2)	0.032(2)	0.043(2)	0.045(2)	0.005(2)	0.010(1)	-.008(2)
C11	0.4166(3)	0.4437(4)	-.1489(3)	0.057(2)	0.074(3)	0.056(2)	0.016(2)	0.028(2)	-.005(2)

	x	y	z	B(Å²)		x	y	z	B(Å²)
H1a	0.001(3)	0.898(4)	0.166(3)	8.5(1.1)	H11a	0.493(3)	0.428(4)	-.141(3)	7.7(1.0)
H1b	0.000(3)	0.903(4)	0.076(3)	8.6(1.1)	H11b	0.397(4)	0.521(4)	-.189(3)	9.0(1.2)
H1c	-.093(4)	0.841(4)	0.120(3)	9.5(1.2)	H11c	0.380(3)	0.391(4)	-.195(3)	7.7(1.1)
H4a	-.134(3)	0.622(4)	0.203(3)	7.6(1.0)	H5a	0.084(2)	0.359(3)	0.282(2)	3.8(0.7)
H4b	-.069(3)	0.534(4)	0.285(3)	7.3(1.0)	H5b	0.038(3)	0.267(4)	0.176(2)	6.5(0.9)
H4c	-.122(3)	0.475(4)	0.198(3)	7.6(1.0)	H6a	0.205(2)	0.171(3)	0.266(2)	4.9(0.8)
H8a	0.489(4)	0.212(5)	-.020(3)	10.0(1.3)	H6b	0.273(3)	0.321(4)	0.239(2)	6.3(0.9)
H8b	0.467(4)	0.195(5)	0.059(3)	11.0(1.3)	H7a	0.149(3)	0.149(4)	0.105(2)	7.8(1.0)
H8c	0.402(4)	0.102(5)	-.007(3)	11.2(1.3)	H7b	0.298(3)	0.126(4)	0.127(2)	6.8(0.9)

[a]The form of the thermal ellipsoid is $\exp[-2\pi^2(U_{11}h^2a^{*2} + \ldots\ldots + 2U_{23}klb^*c^*)]$ for the anisotropic thermal parameters.

Table III. Bond Distances (Å) for $Cu(LBF_2)$, 2.

Cu-N1	1.943(2)	C1-H1a	0.88(4)
Cu-N2	1.937(2)	C1-H1b	0.79(4)
Cu-N3	1.938(2)	C1-H1c	0.82(4)
Cu-N4	1.939(2)	C4-H4a	0.82(3)
N1-C2	1.297(3)	C4-H4b	0.94(3)
N2-C3	1.290(3)	C4-H4c	0.89(3)
N3-C9	1.291(3)	C8-H8a	0.82(4)
N4-C10	1.315(3)	C8-H8b	0.85(4)
N2-C5	1.470(3)	C8-H8c	0.82(4)
N3-C7	1.474(4)	C11-H11a	0.91(3)
N1-O2	1.392(2)	C11-H11b	0.90(4)
N4-O1	1.378(3)	C11-H11c	0.87(4)
C1-C2	1.478(4)	C5-H5a	0.90(3)
C2-C3	1.472(3)	C5-H5b	1.09(3)
C3-C4	1.493(4)	C6-H6a	1.00(3)
C5-C6	1.499(4)	C6-H6b	1.00(3)
C6-C7	1.520(5)	C7-H7a	1.07(3)
C8-C9	1.496(4)	C7-H7b	0.94(3)
C9-C10	1.467(4)		
C10-C11	1.495(4)		
B-O1	1.480(3)		
B-O2	1.489(3)		
B-F1	1.381(3)		
B-F2	1.389(3)		

Table IV. Bond Angles (degrees) for $Cu(LBF_2)$, 2.

N1-Cu-N2	82.3(1)	C2-C3-C4	120.6(3)
N2-Cu-N3	103.3(1)	C2-C3-N2	114.7(2)
N3-Cu-N4	82.9(1)	N2-C3-C4	124.8(3)
N4-Cu-N1	96.9(1)	N2-C5-C6	111.7(3)
N1-Cu-N3	161.5(1)	C5-C6-C7	119.5(3)
N2-Cu-N4	162.9(1)	C6-C7-N3	112.4(3)
Cu-N1-O2	124.3(2)	C8-C9-C10	119.7(3)
Cu-N1-C2	113.6(2)	C8-C9-N3	125.2(3)
O2-N1-C2	117.0(2)	N3-C9-C10	115.1(3)
Cu-N2-C3	112.5(2)	C9-C10-C11	124.7(3)
Cu-N2-C5	119.7(2)	C9-C10-N4	112.2(3)
C3-N2-C5	121.6(2)	N4-C10-C11	123.1(3)
Cu-N3-C7	120.1(2)	N4-O1-B	113.0(2)
Cu-N3-C9	112.4(2)	N1-O2-B	113.9(2)
C7-N3-C9	123.3(3)	O1-B-O2	115.5(2)
Cu-N4-O1	122.0(2)	F1-B-O1	105.3(2)
Cu-N4-C10	112.6(2)	F2-B-O1	110.2(2)
O1-N4-C10	116.1(2)	F1-B-O2	104.8(2)
C1-C2-C3	123.1(3)	F2-B-O2	109.2(2)
C1-C2-N1	124.7(3)	F1-B-F2	111.7(3)
N1-C2-C3	112.1(2)		

Table V. Nonbonding Distances for $Cu(LBF_2)$, 2.

A. Intramolecular Distances (Å)

N1-N2	2.553(3)	N3-N4	2.565(3)
N2-N3	3.040(3)	N1-N4	2.905(3)

B. Intermolecular Distances Between Atom 1 and Atom 2 (Å)

Distance < 4.2 Å		Symmetry	
Atom 1 - Atom 2		Atom 1	Atom 2
Cu-C2	3.619	x,y,z	$\bar{x}$, 1-y, $\bar{z}$
Cu-N1	3.710	x,y,z	$\bar{x}$, 1-y, $\bar{z}$
Cu-C3	3.724	x,y,z	$\bar{x}$, 1-y, $\bar{z}$
Cu-C4	3.869	x,y,z	$\bar{x}$, 1-y, $\bar{z}$
Cu-C6	3.927	x,y,z	½-x, ½+y, ½-z

Table VI. Best Plane Calculations for $Cu(LBF_2)$, 2

Plane	Atoms in Plane (> dihedral angle° between planes)	Equation of Plane[a] A	B	C	D
1	Cu, N1, N2, N3, N4	0.5967	0.3965	0.6977	3.595
2	Cu, 20 non-hydrogen atoms	0.5939	0.3363	0.7309	3.453
3	Cu, N1-4, C1-5, C7-11, O1, O2	0.6023	0.3961	0.6931	3.560
4	Cu, N1, N4 (> 23°)	0.4212	0.4912	0.7624	3.708
5	Cu, N2, N3	0.7334	0.2939	0.6130	3.368
6	Cu, N1, N2 (> 27°)	0.6112	0.5735	0.5455	4.314
7	Cu, N3, N4	0.5535	0.1983	0.8089	2.708

Plane	Deviations from Plane (Å) Cu	N1	N2	N3	N4	C1	C2	C3	C4	C5	C6	C7	C8	C9	C10	C11	B	O1	O2	F1	F2
1	.01	-.31	.29	-.29	.30	.22	-.06	-.02	-.34	.20	.63	-.23	.11	-.08	-.04	-.36	.58	.12	-.24	.46	1.90
2	-.10	-.52	.24	-.30	.12	-.04	-.25	-.11	-.39	.25	.73	-.14	.14	-.11	-.17	-.54	.26	-.16	-.55	.05	1.60
3	.05	-.27	.31	-.24	.35	.25	-.03	.00	-.32	.22	.67	-.19	.17	-.02	.02	-.28	.64	.18	-.20	.52	1.95

[a]Equation of plane in the form $Ax + By + Cz = D$

Table VII. Torsion Angles (degrees).[a]

A-B-C-D	"Planar" Values[b]	$Rh(L'BF_2)(CH_3)I$[15,16]	$Cu(LBF_2)$	$Cu(LBF_2)CO$
O2-N1-C2-C3	180	-177	-174	175
N1-C2-C3-N2	0	3	26	-1
C2-C3-N2-C5	180	-177	-172	-174
C3-N2-C5-C6	-150	-155	-179	174
N2-C5-C6-C7	-60	-69	-69	-63
C5-C6-C7-N3	60	71	66	63
C6-C7-N3-C9	150	151	131	180
C7-N3-C9-C10	180	176	-173	174
N3-C9-C10-N4	0	-4	25	7
C9-C10-N4-O1	180	176	-168	-175
C10-N4-O1-B	±150[c]	157	-177	173
N4-O1-B-O2	±60[c]	62	-71	-64
O1-B-O2-N1	∓60[d]	-60	62	65
B-O2-N1-C2	∓150[d]	-156	130	-179

[a]The torsion angle is the angle defined by A-BC and BC-D when viewing the atoms A-B-C-D down the B-C axis from B to C. Clockwise rotation from A to D is regarded as positive.

[b]"Planar" values are based on a theoretical planar ligand; planar except for C6 and B.[c,d]

[c]Sign of angle is positive for B on the opposite side of the mean molecular plane from C6 and negative for B and C6 on the same side.

[d]Sign of angle is negative for B on the opposite side of the mean molecular plane from C6 and positive for B and C6 on the same side.

Table VIII. Comparisons of $M(LBF_2)$ and M(LH) Structural Parameters.

Complex	Complex Geometry	Ligand Geometry	Averaged Bond Lengths (Å)[a]			
			C2-N1[b]	C3-N2[c]	C2-C3[d]	R[e]
$Cu(LBF_2)CO$, 1[3]	square-pyramidal	dome, boat	1.279(6)	1.273(6)	1.490(6)	0.055
$Cu(LBF_2)$, 2[f]	square-planar	square-planar, boat	1.306(13)	1.291(1)	1.470(4)	0.054
$Cu(LBF_2)NCO$, 3[17]	square-pyramidal	dome, boat	1.293(9)	1.277(2)	1.490(12)	0.045
$Rh(L^{-}BF_2)(CH_3)I$, 5[9,15]	octahedral	square-planar, chair	1.303(3)	1.297(21)	1.485(16)	0.031
$[Cu(LH)]_2(ClO_4)_2 \cdot CH_3OH$, 6[10]	tetragonal	square-planar	1.278(7)	1.269(10)	1.505(8)	0.060
$Co(LH)(CH_3)_2$, 7[11]	octahedral	square-planar	1.312(13)	1.307(8)	1.452(1)	0.034
Rh(LH), 8[12]	square-planar	square-planar	1.303(4)	1.293[g]	1.493(5)	Not reported
$[Co(LH)(CH_3)H_2O]ClO_4$, 9[13]	octahedral	square-planar	1.29(4)	1.28(3)	1.51(0)	0.112

[a]All atom designations refer to a ligand numbered as in Figure 1; standard deviations of the mean bond length values, as defined in reference 14, are given in parentheses.

[b]The C2-N1 bond length values are averages of C2-N1 and C10-N4.

[c]The C3-N2 bond length values are averages of C3-N2 and C9-N3.

[d]The C2-C3 bond length values are averages of C2-C3 and C9-C10.

[e]$R = \Sigma||F_o| - |F_c||/\Sigma|F_o|$.

[f]This work.

[g]Only one value available, therefore no mean standard deviation is given.

Table IX. Infrared Spectra of LBF_2^- Complexes[a]

Possible Assignment	$Cu(LBF_2)$, 2	$[Cu(LBF_2)]_2(ClO_4)_2 \cdot C_4H_8O_2$, 10	$Cu(LBF_2)I_3$, 11	$Cu(LBF_2)CO$, 1
$\nu_{C=N\ asym}$ [12,19]		1660w	1645w	1640w
$\nu_{C=N\ sym}$ [12,19]		1590w	1580m	1560m
$\delta_{CH_3\ asym}$ [20,21]	(1430)w	1440w	1440w	1430w
$\delta_{CH_3\ sym}$ [20,21]	1380w	1390w	1390w	1380w
CH_3	1365w	(1370)w	1370w	1360w
ν_{B-O} [12,22]	1190m	1180m	1180m	1185m
ν_{N-O} [12,20-22]	1150s	(1150)[b]s	1130s	1135s
or				
ν_{B-F} [12]	1075m	(1060)[b]m	1100m, 1065m	1090m, 1075m, 1045m
ν_{B-F} [12,22]	995s	1030s	1030s	1015s
HCC [21]	(945)m	940s	950s	960s
ν_{B-O} [12,22]	795w	810m	805m	790m
ClO_4^- [23]		630m, 1115vs, 1130vs		
Other	1470m 1320s 1280w 910w 870w	880m (dioxane)	690w	2070vs (CO) 680w

[a] KBr pellet in region 600 to 2500 cm^{-1}. Shoulders given in parentheses. w = weak, m = medium, s = strong, vs = very strong.

[b] Obscured by perchlorate bands.

SECTION I

Summary and Conclusions

The complex, $Cu(LBF_2)$, 1, is best described as having a copper in the +I oxidation state and a monoanionic macrocycle. The copper in $Cu(LBF_2)$, 1, binds to the four nitrogens of the LBF_2 ligand in a distorted square plane.

In solution $Cu(LBF_2)$, 1, reacts rapidly with oxygen and with carbon monoxide. The product of the carbon monoxide reaction is $Cu(LBF_2)CO$, 2. The copper of $Cu(LBF_2)CO$, 2, is in the +I oxidation state. The square-pyramidal geometry of CO adduct is unusual. The apical angle, α, is larger than expected for a usual square pyramid. The metal is displaced 0.96 Å out of the four-nitrogen plane and the copper-nitrogen bond lengths are long. The copper-carbon bond is normal.

The geometry of $Cu(LBF_2)CO$, 2, cannot be adequately described by invoking the repulsions of the five electron pairs. The system is best viewed as providing linear electron density for copper(I) with the copper-π-acceptor interaction opposing the copper-macrocycle interactions. Copper(I) in $Cu(LBF_2)$, 1, acquires its desired symmetrical electron density by binding a fifth ligand.

Quantitative binding studies of $Cu(LBF_2)$, 1, and potential ligands B, have been done. Ligands which are π-acceptors bind more strongly to $Cu(LBF_2)$, 1, than σ-base ligands. The values of $K^I(B)$,

the binding constant of $Cu(LBF_2)$, 1, with ligands, B, decrease:

$$p\text{-}NC(C_6H_4)NC \sim p\text{-}NO_2(C_6H_4)NC >$$
$$P(O\text{-}C_6H_{11})_3 > P(O\text{-}Bu)_3 >$$
$$P(O\text{-}p\text{-}C_6H_4Cl)_3 > CO >$$
$$P(O\text{-}C_6H_5)_3 > P(O\text{-}p\text{-}C_6H_4CH_3)_3 >$$
$$P(p\text{-}C_6H_4Cl)_3 > P(p\text{-}C_6H_4CH_3)_3 \sim$$
$$P(C_6H_5)_3 > 1\text{-MeIm} > \text{pyridine}.$$

The binding constants of carbon monoxide to copper complexes with macrocycles that are closely related to the LBF_2 ligand have been measured. Carbon monoxide binds to varying degrees dependent on both the electronic and steric properties of the macrocycle. Electronic effects, as predicted by antisymbiosis, appear to be predominant.

Copper(I) macrocyclic complexes with ligands not related to LBF_2 bind fifth ligands also. Cu(trans-diene)ClO_4, 4, binds CO weakly and $p\text{-}NO_2(C_6H_4)NC$ well. On the other hand, $Cu(TAAB)NO_3$, 7, does not bind CO or $p\text{-}NO_2(C_6H_4)NC$ within experimental error. The binding of carbon monoxide and $p\text{-}NO_2(C_6H_4)NC$ to copper(I) macrocycles can be restricted by the choice of the tetraaza macrocycle.

Metal macrocyclic complexes have novel properties and reactivities in many cases. The macrocycle, LBF_2, stabilizes copper(I) in an unusual square-planar environment. The resulting four-coordinate complex, $Cu(LBF_2)$, 1, reacts with neutral molecules to form five-

coordinate complexes, $Cu(LBF_2)B$. These complexes are also unusual for copper(I). The use of macrocycles as ligands imparts interesting and unpredicted properties to copper(I).

SECTION J

Experimental Section

Operations requiring an inert atmosphere were performed in a Vacuum Atmospheres Dri-lab containing nitrogen or helium. Infrared spectra were obtained on a Beckman IR-12 spectrometer with samples in CH_2Cl_2 solution or in KBr pellets. Nuclear magnetic resonance spectroscopy utilized a Varian EM 390 instrument. Samples were referenced against internal tetramethylsilane. Electronic absorption spectra (EAS) were measured on a Cary-14 automatic recording spectrometer. Solid state visible spectra were run using a mineral oil suspension of sample spread evenly on filter paper. A Cahn Electrobalance Model 7500 was used for Faraday magnetic measurements. The Analytical Laboratory, California Institute of Technology, analyzed samples for carbon, hydrogen, nitrogen and metal content.

Starting materials which were commercially available were used without further purification. Tetraethylammonium perchlorate, TEAP, and tetrabutylammonium perchlorate, TBAP (Southwestern Analytical Chemicals), were dried in vacuo before use. Ferrocene was supplied by C. A. Koval. The isocyanides, p-$NC(C_6H_4)NC$ and p-$NO_2(C_6H_4)NC$, were provided by R. Williams and C. A. Ma, respectively. Solvents used for synthesis were reagent grade. For polarography N,N-dimethylformamide, DMF, was prepared by drying over $MgSO_4/CuSO_4$ and 4 Å

molecular sieves and vacuum distilling. Acetone used for electrochemistry was spectroquality.

Electrochemistry. A Princeton Applied Research Model 173 potentiostat-galvanostat coupled with a Model 179 digital coulometer was used for constant potential electrolysis (CPE). The cell used for synthetic CPE was a three compartment H-cell. The working and auxiliary compartments of the cell (25 ml volumes) are separated by a small center compartment. All compartments are separated by sintered glass frits of medium porosity. A 0.1 M solution of TEAP in acetone or DMF was used. The Ag/Ag^{+} reference electrode (Figure 18A) consists of a silver wire in an acetonitrile solution containing $AgNO_3$ (0.01 M) and TBAP (0.1 M). The solution and wire are contained in an 8-mm glass tube fitted on the bottom with a fine porosity sintered glass frit. The wire is threaded through a serum cap which fits over the end of the 8-mm tube. The tube was placed in the working solution with the platinum mesh working electrode. The counter electrode was a platinum wire. All potentials are versus the normal hydrogen electrode (NHE) unless indicated otherwise.

For sampled dc polarography a Princeton Applied Research dropping mercury electrode, model 9346 was used in conjunction with the PAR polarographic analyzer, Model 174. The mercury electrode has a drop knocker coupled with a capillary, Hg column, and Hg reservoir. The polarographic analyzer, capable of drop times, t, up to 5 seconds, was used with a Hewlett-Packard Model 7004B, x-y recorder.

Figure 18

A. The Ag/Ag^+ reference electrode is a silver wire in a 0.01 M $AgNO_3$ - 0.1 M TBAP solution contained in a glass tube with a fine frit on the bottom. B. Platinum disc electrode used for cyclic voltammetry. C. Support for platinum disc electrode with gas outlet and with platinum wire coiled for a counter electrode. The platinum disc electrode is placed in the coil of the counter platinum wire for cyclic voltammetry.

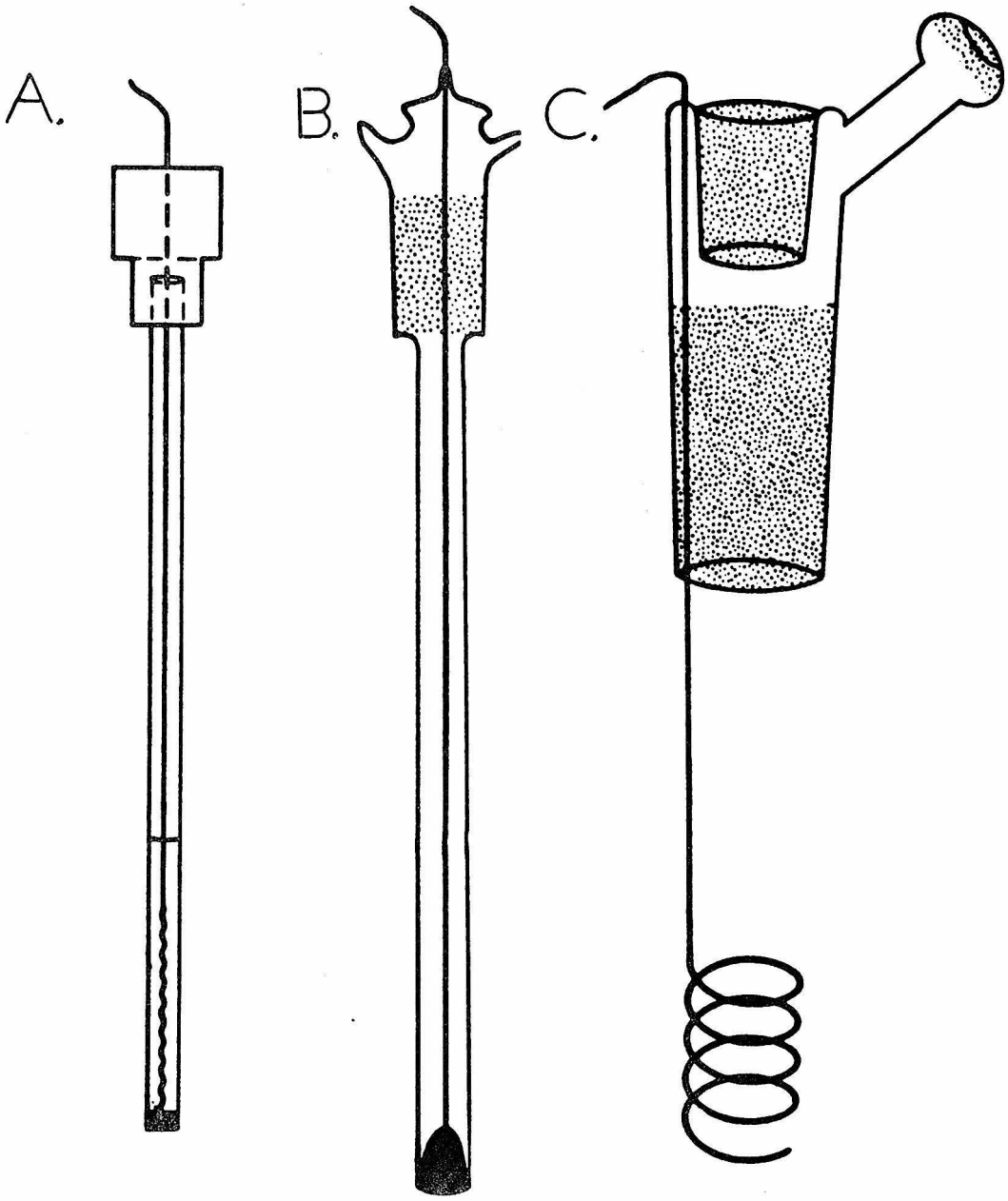

Figure 18

The cell (Figure 19) is a two compartment cell with a gas inlet to the working compartment for solution degassing. Acetone or DMF with 0.1 M TBAP, as a supporting electrolyte, was used. The working compartment also had 0.5 mM copper(II) sample, 1.0 mM ferrocene, and zero to x mM ligand B. The working solutions were prepared using volumetric amounts of stock copper(II) and ferrocene solutions stored in the dri-lab. Volumetric additions of ligand were then made. The working electrode was the dropping mercury electrode; the counter electrode was a platinum wire coiled around the mercury capillary. A reference electrode identical to that used for CPE is placed in the second compartment. The three-way stopcock on the gas inlet line was used to degas the solution or to have gas flow above the working solution. The stopcock at the base of the working compartment allowed the working solution to be easily changed. Purification of argon was accomplished by a copper furnace and 4 Å molecular sieves. Carbon monoxide was forced through molecular sieves (4 Å) and Ridox for purification.

The procedure for obtaining sampled dc polarograms began and ended with a mercury flow rate measurement. Mercury flowing from the capillary into a solvent was collected with the drop knocker set at a drop time of 5 seconds. (All polarograms were run with t = 5 s.) The time over which mercury was collected is recorded. The flow rate, m, is calculated in mg s^{-1}. The copper(II) sample was then purged with argon for twenty minutes. The cyclic voltammogram of ferrocene was measured with a platinum disc electrode with a platinum

Figure 19

Two compartment polarography cell with a gas inlet tube and a stopcock connected to the working compartment. The second compartment is separated from the main one by a medium frit and is used for the reference electrode (Figure 18A).

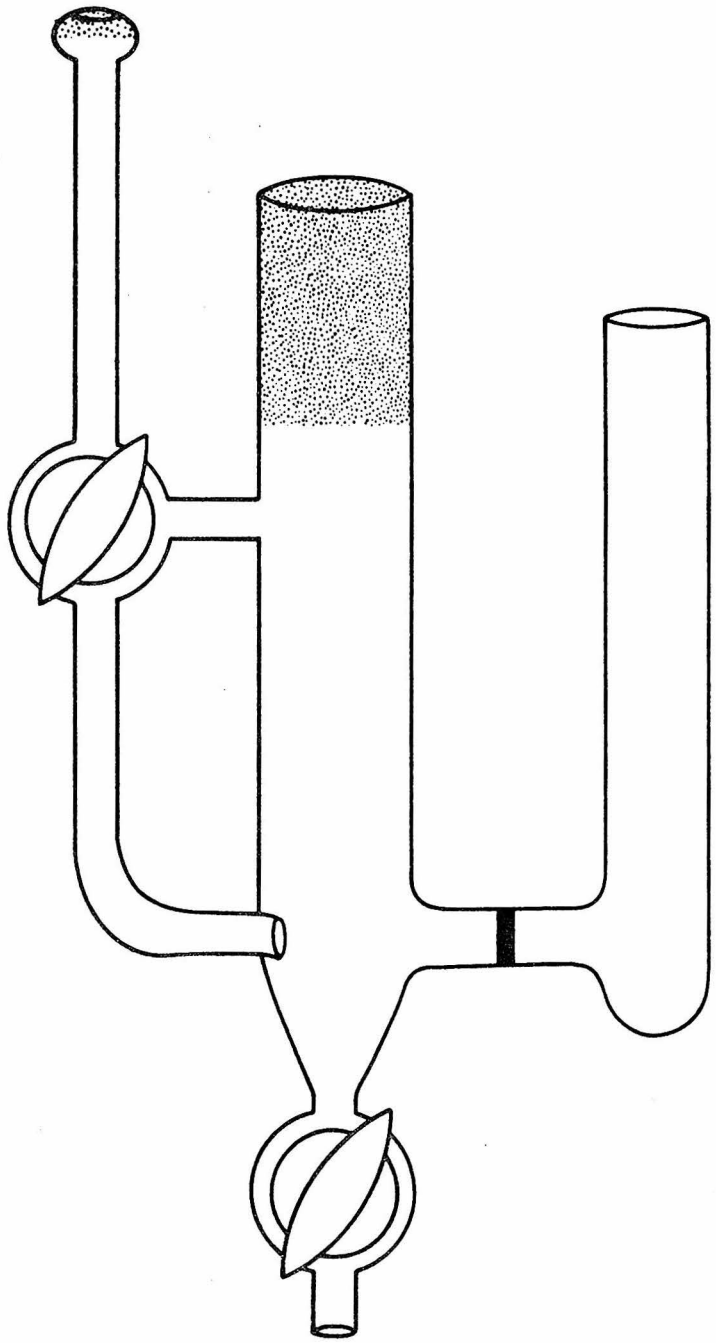

Figure 19

counter electrode coiled around it (Figure 18B,C). The sampled dc polarogram was run at 0.5 mV s^{-1} and the ambient temperature recorded.

The half-wave potential of the sample, $E_{1/2}$, was determined from an E vs. $\ln[i/(i_d-i)]$ plot. The linear regression of the plot was calculated by use of a program written for a Hewlett-Packard Model 25 programmable calculator. The intercept of the plot is $E_{1/2}$, Ag/Ag^+ and the slope is theoretically equal to -RT/nF. This $E_{1/2}$, Ag/Ag^+ was converted to a potential versus the normal hydrogen electrode, NHE, by use of the formal potential of ferrocene, $E^f(FeCp_2)$ (Figure 20).

$$E^f = \frac{E_{p_a} + E_{p_c}}{2} \qquad (15)$$

E_{p_a} = anodic peak potential
E_{p_c} = cathodic peak potential

The ferrocene couple is 0.400 V positive of NHE, independent of solvent. The half-wave potential vs. NHE is:

$$E_{1/2},NHE = E_{1/2},Ag/Ag^+ - E^f(FeCp_2) + .400\ V \qquad (16)$$

The average temperature of the polarographic runs was 22° C. An initial binding constant was calculated as described in the text. An iterative calculation using a program written for a Hewlett-Packward Model 25 calculator determined the final B concentration. The final binding constant was then calculated.

For the runs with B = carbon monoxide in DMF, the solubility of CO in DMF was needed. The weight of CO per weight of DMF is

Figure 20

Cyclic voltammogram of ferrocene (1 mM) in DMF, recorded at 100 mV/s. The anodic peak potential, E_{p_a}, and the cathodic peak potential, E_{p_c}, are 0.111 V and 0.020 V, vs. Ag/Ag^+. The formal potential of the ferrocene-ferrocenium couple is 0.0655 V, vs. Ag/Ag^+. (X is the starting point of the cyclic voltammogram.)

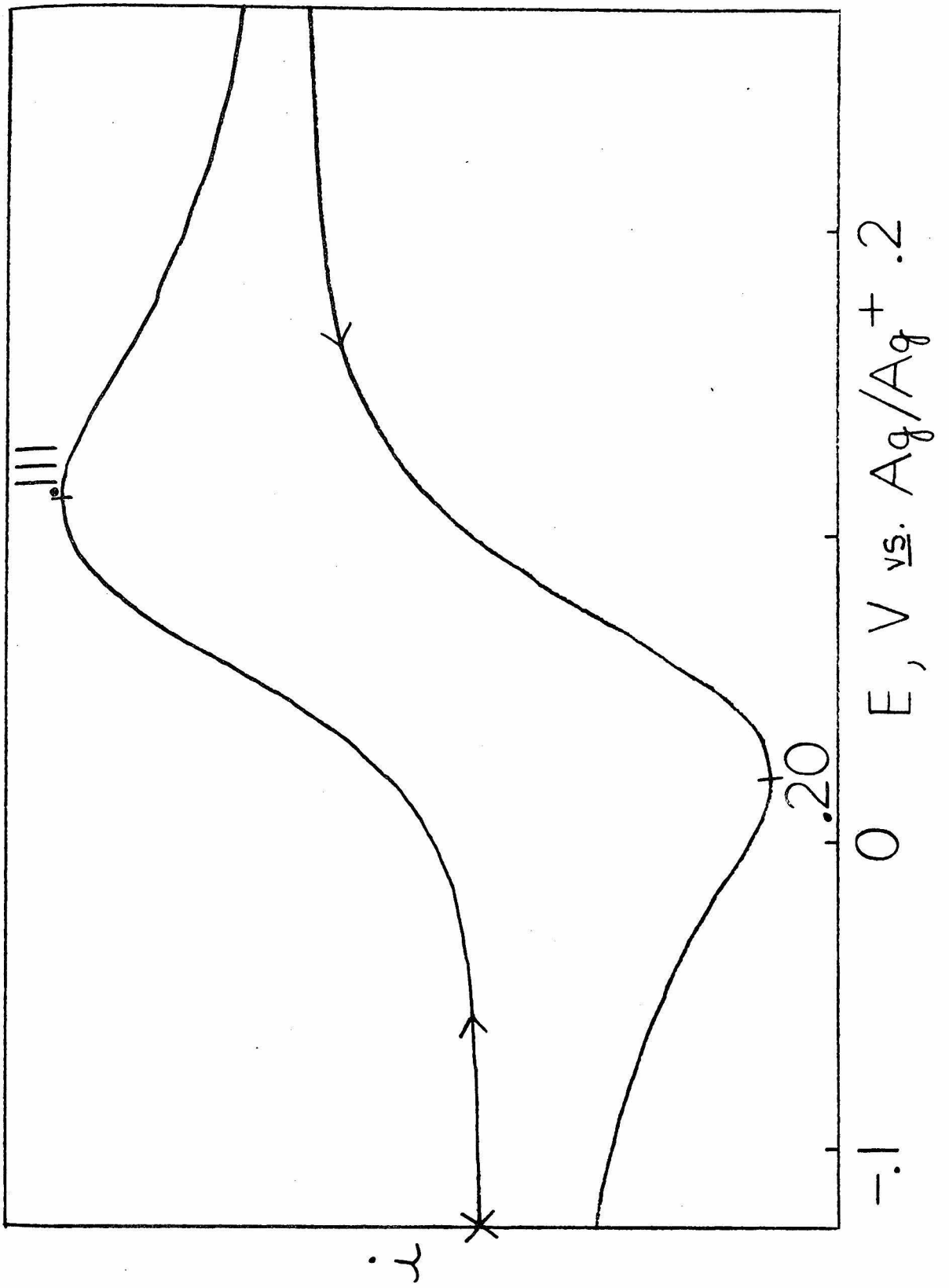

Figure 20

13.7×10^{-5} at 20° C (84). The concentration calculated from this weight per weight value was 4.64 mM.

Oxygen Uptake Measurement. Known amounts of complex and dry solvent were placed on a high vacuum line. The system was evacuated with the solvent frozen by liquid nitrogen. The solvent was thawed and added to the complex by vacuum transfer. The complex and solvent were kept frozen to preclude a reaction in the absence of oxygen. The system was flushed with O_2 and an appropriate pressure was introduced to the manometer and the calibrated gas bulb (cgb) above the sample. The pressure from the manometer, the cgb volume, and the ambient temperature were recorded. The oxygen from the cgb was introduced to the sample which was thawed and stirred. When the reaction was judged to be complete, the O_2 which had not reacted was measured using a Toepler pump. The O_2 dissolved in the solution was removed by the freeze-pump-thaw method. The amount of unreacted oxygen was found by determination of the volume into which the gas had been collected (a series of calibrated gas bulbs), the pressure of the O_2, and the ambient temperature. The oxygen which reacted with the complex is simply the moles of O_2 added initially minus the moles of O_2 which did not react.

Determination of Binding Constants by Electronic Absorption Spectroscopy. The equilibrium of $Cu(LBF_2)$, 1, with ligands, B, forms the five-coordinate species, $Cu(LBF_2)B$. As a first approximation for the binding constant of this equilibrium, the equilibrium concentration was defined:

$$K_c = \frac{[Cu(LBF_2)B]}{[Cu(LBF_2)][B]} \qquad (2)$$

The equilibrium concentrations of the copper complexes were determined by use of the Beer's law dependence of the $Cu(LBF_2)$ 1, band at 677 nm ($\varepsilon = 1.03 \times 10^4\ M^{-1}\ cm^{-1}$, 25° C). The assumption was made that $Cu(LBF_2)B$ does not absorb appreciably at 677 nm. Therefore, when $Cu(LBF_2)$ 1, reacted with B, ΔA (A initial - A equilibrium) was taken as a measure of the $Cu(LBF_2)B$ formed.

With B = 1-methylimidazole, the cells used have measured pathlengths of about 1 mm. The short pathlengths permitted relatively high concentrations of $Cu(LBF_2)$, 1, to be used, thus minimizing decomposition due to residual dissolved oxygen. Preparation of solutions of $Cu(LBF_2)$, 1, ($[Cu(LBF_2)]$ initial $\cong 8 \times 10^{-4}$ M), and addition of 1-MeIm ([1-MeIm] initial = 2×10^{-3} to 1 M) were done in the inert atmosphere dri-lab. The cells were closed with greased, glass stoppers and taped. Spectra were recorded to determine ΔA (677 nm). Measurements were made at 30±2° C. Only approximate isosbestic behavior was observed, most probably owing to the slight variation in pathlengths of the several cells employed. If a 1:1 stoichiometry for adduct formation is assumed, the constant K_c is 16±3 M^{-1}.

For carbon monoxide measurements, the cells each have approximately 1-mm pathlengths, a 10-mL side-arm reservoir, a Teflon high-vacuum stopper, and a standard taper joint for attachment to a vacuum line. The $Cu(LBF_2)$, 1 ($[Cu(LBF_2)]$ initial $\cong 1.6 \times 10^{-3}$ M), solutions were

prepared in the dri-lab and closed to the atmosphere. The solutions were then degassed by the freeze-pump-thaw technique (3 cycles) on the vacuum line. The spectra were measured before CO addition.

The $Cu(LBF_2)$, 1, solution was opened to a system with a mercury manometer and an acetone reservoir. The acetone vapor pressure was measured when the system was equilibrated. Addition of CO (10-88 mm Hg) was monitored by use of the manometer. The solution of $Cu(LBF_2)$, 1, was stirred under CO for twenty minutes and the pressure and temperature were then recorded. The spectra were run in order to find ΔA (677 nm). A plot of $[Cu(LBF_2)CO]/[Cu(LBF_2)]$ vs. P(CO) was extrapolated to give $P_{\frac{1}{2}}(CO) = 1.5$ mm when $[Cu(LBF_2)CO] = [Cu(LBF_2)]$. The equilibrium pressure constant, K_p, was calculated to be 500±15 atm^{-1}.

Conversion of K_p to K_c for the purpose of comparison to K_c (1-MeIm) used data for the solubility of CO in acetone. Use of a value of 0.2358 mL of CO per mL of acetone at 20° C (85) and of Henry's law allowed conversion of P(CO) to [CO]. Calculation of K_c gave a value of $4.7(2) \times 10^4$ M^{-1}.

X-Ray Photoelectron Spectroscopy. X-ray photoelectron spectra were recorded using a Hewlett-Packard Model 5950A ESCA spectrometer by Professor R. A. Walton's research group at Purdue University. Monochromatic aluminum $K\alpha_{1,2}$ radiation (1486.6 eV) was used as the x-ray excitation source and the powdered samples were dispersed on a gold-plated copper surface. An electron "floodgun" was used in conjunction with this instrument to eliminate, or at least reduce

to a minimum, surface charging effects. A Vacuum Atmospheres dri-lab filled with nitrogen was used in conjunction with the spectrometer to decrease the surface oxidation of air-sensitive samples. Further experimental details are described in a paper originating from the Walton group (86).

Different references are used in x-ray photoelectron spectroscopy. To adjust all binding energies to one scale (i.e., that of R. A. Walton), some measured values were compared. The graphite C 1s standard of Walton is 284.0 eV (36). Dillard and Taylor (55) used the same standard at 283.8 eV. Their values need an added 0.2 eV to be on the RAW scale. The copper metal binding energy they measure is 932.0 eV; it is adjusted to 932.2 eV. Keyes , et al. (87), measured spectra against the C 1s of the cellophane tape at 285.0 eV. Their Cu $2p_{3/2}$ binding energy for Cu(0) is 932.6 eV. To place these values on the RAW scale, 0.4 V must be subtracted. The resulting binding energies are 932.2 eV for copper(0) and 284.6 eV for cellophane tape's C 1s band. If various cellophane tape C 1s binding energies are adjusted to 284.6 eV, three values of the Cu $2p_{3/2}$ binding energy of bis(acetylacetonato)copper(II) are equal to 934.5 eV (37,41,88). This equivalence indicates a sound approach to binding energy scale adjustment.

Crystallography. The experimental details of the crystallographic analysis of $Cu(LBF_2)$, 1, have been given in the experimental part of Section II. They are not repeated here.

Synthesis and Characterization. Cu(trans-diene)$(ClO_4)_2$, 3, [5,7,7,12,14,14-hexamethyl-1,4,8,11-tetraazacyclotetradeca-4,11-diene]copper(II) perchlorate (16). To a solution of 20.00 g $Cu(ClO_4)_2 \cdot 6H_2O$ (54 mmol) in 200 mL of isobutyl alcohol were added slowly 20 mL of concentrated NH_4OH. The solution was stirred for 1.5 hours, filtered, and then the solid was washed with isobutyl alcohol. The bluish-violet precipitate is $Cu(NH_3)_6(ClO_4)_2$. Into 300 mL of acetone were dissolved 17.32 g of dry $Cu(NH_3)_6(ClO_4)_2$ (48 mmol). The solution was refluxed for one hour, then was cooled in ice. Ethylenediamine (15.5 mL, 242 mmol) was added over two minutes. The solution was refluxed for 24 hours and cooled to ambient temperature. The excess acetone was removed by reduced pressure. The remaining viscous solution was dissolved in 300 mL of absolute ethanol with heating on a steam bath. The solution was cooled in a refrigerator. The precipitate was filtered from the solution and was recrystallized from a hot acetone:water mixture (10:1 by volume) by the addition of ethanol with scratching. Crystals are red-orange. Anal. Calcd. for $C_{16}H_{32}Cl_2CuN_4O_8$: C, 35.40; H, 5.94; N, 10.32; Cu, 11.70. Found: C, 35.57; H, 5.82; N, 10.04; Cu, 12.22. Infrared spectrum (KBr pellet): b = broad, sh = sharp, s = strong, m = medium, w = weak 3495(s), 3450(s), 3210(m), 3095(m), 2930(m), 2980(m), 1670(s), 1635(m), 1380(m), 1100 region-ClO_4^- bands, 630(s).

Cu(trans-diene)ClO_4, 4, [5,7,7,12,14,14-hexamethyl-1,4,8,11-tetraazacyclotetradeca-4,11-diene]copper(I) perchlorate (16). A constant potential electrolysis of 1.51 g Cu(trans-diene)$(ClO_4)_2$, 3, in CH_3CN with TEAP as a supporting electrolyte was done at -1.3 V vs. Ag/Ag^+. The purple copper(II) solution changed to a yellow copper(I) solution. An n value of 1.00±.03 resulted. With a decrease in the solution volume a dark brown solid precipitated. The solution was filtered, the solid was discarded, and the solution volume was further reduced. A yellow solid precipitated. Recrystallization from warm CH_3CN yielded a very air-sensitive solid. Anal. Calcd. for $C_{16}H_{32}ClCuN_4O_4$: C, 43.34; H, 7.27; N, 12.64. Found: C, 43.97; H, 7.33; N, 12.76. An acetonitrile solution of Cu(trans-diene)ClO_4, 4, consumed 1.88 moles oxygen per mole of copper(I), as measured by the procedure described earlier.

Cu(TAAB)$(NO_3)_2$, 6, [Tetrabenzo[b,f,j,n][1,5,9,13]tetraaza-cyclohexadecine]copper(II) nitrate (18). The starting material, o-aminobenzaldehyde, was prepared by the literature method (89). NMR ($CHCl_3$-d_1): singlet at 10.3 ppm (1.0 H), aldehyde proton; multiplets at 7.8 and 7.13 ppm (2.5 and 2.2 H, respectively), benzene protons; broad peak at 6.5 ppm (2.0 H), amine protons. Wet o-aminobenzaldehyde (5g, 41 mmol), prepared no more than 24 hours earlier, was added to 200 mL of absolute ethanol. The solution was filtered to remove insoluble impurities; the filtrate was a clear yellow solution. This solution was heated to reflux as 1.61 g of $Cu(NO_3)_2 \cdot H_2O$ (11 mmol) were added. The solution was refluxed for 12

hours. Upon cooling, a dark green solid was collected and washed with absolute ethanol and ether. Recrystallization was attempted from various solvents with no success. Anal. Calcd. for $C_{28}H_{20}CuN_6O_6$: C, 56.05; H, 3.36; N, 14.01; Cu, 10.59. Found: C, 55.75; H, 3.68; N, 14.00; Cu, 11.27. Infrared spectrum (KBr pellet): 3450(b), 1625(s), 1615(s), 1595(s), 1570(s), 1495(m), 1450(m), 1410(s), 1400(s), 1365(s), 1345(s), 1305(s), 1290(m), 1250(m), 1200(m), weak, but sharp bands at 1170, 1120, 1035, 980, and 930, 790(m), 770(s), 760(m).

$Cu(TAAB)NO_3$, 7, [Tetrabenzo[b,f,j,n][1,5,9,13]tetraazacyclohexadecine]copper(I) nitrate (19). In the dri-lab 0.21 g of $Cu(TAAB)(NO_3)_2$, 6, was added to a stirred and heated solution of copper(0) in CH_3CN. The solution turned blue and a blue solid was collected after 24 hours. Anal. Calcd. for $C_{28}H_{20}CuN_5O_3$: C, 62.51; H, 3.75; N, 13.02; Cu, 11.81. Found: C, 61.18; H, 3.80; N, 12.56; Cu, 12.50. Infrared spectrum (KBr pellet): 1595(m), 1585(m), 1580(m), 1560(m), 1540(s), 1485(s), 1435(s), 1385(s), 1360(s,b), 1325(m), 1285(m), 1190(s), 1165(m), 965(m), 920(s), 825(m), 770(m), 760(s).

H_2L, 4,8-diaza-3,9-dimethylundeca-3,8-diene-2,10-dione dioxime (90). 1,3-Propanediamine (37.06 g, 0.5 mol) and 2,3-butanedione monoxime (101.0 g, 1.0 mol) were mixed together in hot diethyl ether to give a yellow solution of approximately 250 mL. The solution was allowed to cool to ambient temperature. The resulting white precipitate

was isolated immediately by vacuum filtration, washed well with diethyl ether, and dried in air. The precipitate was shown to be a mixture of starting material and product by nmr. Attempts to separate the two compounds failed and the white solid was used without purification.

$Cu(LH)ClO_4 \cdot H_2O$, 8, [4,8-diaza-3,9-dimethylundeca-3,8-diene-2,10-dione dioximato]copper(II) perchlorate monohydrate. A hot acetone solution (20 mL) of $Cu(ClO_4)_2 \cdot 6H_2O$ (dried in vacuo at 25° C, 3.7 g, 10 mmol) was added to a hot solution (20 mL) of the ligand, H_2L (4.8 g, 20 mmol). The solution turned deep red. The solution was refluxed for 15 minutes and then cooled. A dark red-brown crystalline solid precipitated. The solid was isolated by vacuum filtration, washed with diethyl ether, and dried in air. Anal. Calcd. for $C_{11}H_{21}ClCuN_4O_7$: C, 31.44; H, 5.04; N, 13.3; Cu, 15.1. Found: C, 30.71; H, 4.80; N, 13.1; Cu, 16.0.

$[Cu(LBF_2)]_2(ClO_4)_2 \cdot C_4H_8O_2$, 9, bis[(1,1-difluoro-4,5,11,12-tetramethyl-1-bora-3,6,10,13-tetraaza-2,14-dioxo-cyclotetradeca-3,5,10,12-tetraenato)copper(II)] diperchlorate monodioxane. Boron trifluoride etherate, $BF_3 \cdot Et_2O$ (6 mL, 50 mmol), was added slowly, with stirring, to a mixture of $Cu(LH)ClO_4 \cdot H_2O$, 8 (7.0 g, 17 mmol) in warm dioxane (150 mL, 70° C). The mixture was refluxed for 1 hour. The red-violet solid was isolated by vacuum filtration, washed well with dioxane and diethyl ether, and dried in air. The product was dissolved in a minimum amount of boiling acetone (150 mL). The hot solution was filtered and treated with 5 mL of dioxane. Crystalline product,

obtained upon cooling, was isolated and treated as before. A yield of 5.3 g (64%) was obtained. Anal. Calcd.for $C_{26}H_{44}B_2Cl_2Cu_2F_4N_8O_{14}$: C, 31.6; H, 4.49; N, 11.34; Cu, 12.86. Found: C, 31.7; H, 4.46; N, 11.51; Cu, 12.6. Magnetic susceptibility, μ(effective) = 1.85 B.M. (25° C). Infrared spectrum (KBr pellet): 2990(b,w), 1655(m), 1590(m), 1440(m), 1390(m), 1180(s), 1100 (ClO_4^- bands, s), 1020(s), 940(s), 880(s), 805(s), 750(w), 740(w).

$Cu(LBF_2)$, 1, [1,1-difluoro-4,5,11,12-tetramethyl-1-bora-3,6,10,13-tetraaza-2,14-dioxo-cyclotetradeca-3,5,10,12-tetraenato]copper(I). The copper(II) complex, $Cu(LBF_2)ClO_4$, 9 (0.8 g, 15 mmol), was reduced by CPE in a helium dri-lab. The electrolysis was carried out at -1.0 V vs. Ag/Ag^+ (-0.68 V vs. NHE) until the current was 1% of the initial value. During the reduction, $Cu(LBF_2)$, 1, crystallized from solution. The product was isolated by vacuum filtration, washed with ethanol, and dried under helium. Anal. Calcd.for $C_{11}H_{18}BCuF_2N_4O_2$: C, 37.68; H, 5.17; N, 15.98; Cu, 18.12. Found: C, 37.87; H, 5.12; N, 15.80; Cu, 18.2. The molar absorptivity, ε, is 1.03(2) x 10^4 M^{-1} cm^{-1} (acetone, 25° C, 677 nm). In the solid state λ_{max} is 695 nm. A magnetic susceptibility measurement showed the compound to be diamagnetic at 25° C. Infrared spectrum (KBr pellet): 2940(w), 1480(m), 1420(w), 1375(w), 1360(w), 1315(s), 1275(w), 1190(m), 1150(s), 1070(m), 1020(m), 990(s), 935(m), 900(b,m), 865(w), 790(w).

$Cu(LBF_2)CO$, 2, carbonyl[1,1-difluoro-4,5,11,12-tetramethyl-1-bora-3,6,10,13-tetraaza-2,14-dioxo-cyclotetradeca-3,5,10,12-tetraenato] copper(I). A blue solution of $Cu(LBF_2)$, 1 (0.35 g, 10 mmol), in

acetone (25 mL) under nitrogen was treated with carbon monoxide (1 atm) yielding a yellow solution. The solution was treated by slow addition of heptane. The resulting orange product was isolated by filtration and dried under a stream of CO. Anal. Calcd. for $C_{12}H_{18}BCuF_2N_4O_3$: C, 38.07; H,,4.79; N, 14.80; Cu, 16.78. Found: C, 38.03; H, 4.76; N, 14.86; Cu, 17.1. Infrared spectrum, ν_{CO} = 2068 cm^{-1} (KBr pellet), 2080 cm^{-1} (CH_2Cl_2 solution).

$CuEt_2(LBF_2)ClO_4$, 19, [1,1-difluoro-4,12-diethyl-5,11-dimethyl-1-bora-3,6,10,13-tetraaza-2,14-dioxo-cyclotetradeca-3,5,10,12-tetraenato] copper(II) perchlorate. The complex, $CuEt_2(LBF_2)ClO_4$, 19, was synthesized in a manner analogous to that used for $[Cu(LBF_2)]_2(ClO_4)_2 \cdot C_4H_8O_2$, 9, by R. R. Gagné. The starting dione monoxime, 2,3-pentanedione monoxime, was prepared as in the literature (91). The impure $CuEt_2(LBF_2)ClO_4$, 19, was recrystallized by the author by dissolving the complex in a minimum amount of hot acetone, filtering, and then adding a small amount of dioxane. Dark purple solid precipitated. The product was washed with diethyl ether and air dried. Anal. Calcd. for $C_{13}H_{22}BClCuF_2N_4O_6$: C, 32.66; H, 4.64; N, 11.72. Found: C, 32.57; H, 4.87; N, 10.83.

$BuLH_2$, 4,9-diaza-3,10-dimethyldodeca-3,9-diene-2,11-dione dioxime. To a refluxing solution of 20.2 g 2,3-butanedione monoxime (0.20 mol) in 75 mL ethanol were added to 8.82 g 1,4-diaminobutane (0.10 mol). The reaction mixture was refluxed for 2 hours and the solution volume was reduced to 50 mL. When the solution was allowed to cool to ambient temperature, a solid precipitated. The impure orange solid

was isolated by vacuum filtration, washed with ethanol and diethyl ether to remove impurities, and air dried. Yield of white product: 6.72 g, 26%. NMR [$(CH_3)_2SO$-d_6]: singlet at 11.28 ppm (1.0 H), oxime protons; multiplet at 3.35 ppm (2.7 H), methylene protons; singlets at 1.97 and 1.90 ppm (6.8 H), methyl protons; multiplet at 1.67 ppm (2.8 H), methylene protons.

$Cu(BuLH)ClO_4$, 28, [4,9-diaza-3,10-dimethyldodeca-3,9-diene-2,11-dione dioximato]copper(II) perchlorate. To a hot solution of $BuLH_2$ (5.1 g, 0.02 mol) in 50 mL ethanol was slowly added a hot solution of $Cu(ClO_4)_2 \cdot 6H_2O$ (3.7 g, 0.01 mol, dried in vacuo) in 20 mL ethanol. The solution turned red-brown and was refluxed for 5 minutes. The solution was cooled to ambient temperature and filtered. The dark solid was washed with ethanol and diethyl ether. Recrystallization from a minimum volume of acetone was done. Infrared spectrum (KBr pellet): 2950(m), 2870(b,w), 1665(b,w), 1630(m), 1530(m), 1440(m), 1385(m), 1330(m), 1315(m), 1215(m), 1200(m), 1190(m), 1100(s), 1030(m), 910(m), 840(w), 805(m), 760(w), 680(m).

$[Cu(BuLBF_2)]_2(ClO_4)_2 \cdot C_4H_8O_2$, 20, bis[(1,1-difluoro-4,5,12,13-tetramethyl-1-bora-3,6,11,14-tetraaza-2,15-dioxo-cyclopentadeca-3,5,11,13-tetraenato)copper(II)] diperchlorate monodioxane. Five mL of $BF_3 \cdot OEt_2$ (0.04 mol) were added to a refluxing solution of $Cu(BuLH)ClO_4$, 28, (1.5 g, 3.6 mmol) in 50 mL dioxane. Reflux was continued for 1 hour. A light-purple solid was isolated from the cool solution and washed with dioxane and diethyl ether. Recrystallization was done by the slow addition of dioxane to a saturated acetone

solution. Anal. Calcd. for $C_{14}H_{24}BClCuF_2N_4O_5$: C, 33.09; H, 4.76; N, 11.03. Found: C, 32.59; H, 4.59; N, 10.81. Infrared spectrum (KBr pellet): 2940(m), 2870(w), 1650(m), 1585(m), 1450(b,m), 1380(b,m), 1255(m), 1230(m), 1175(s), 1100(s), 1030(s), 945(s), 890(w), 870(s), 800(s), 760(w), 745(w), 680(w).

$Cu(dmgH)_2$, 29, bis[2,3-butanedione dioximato]copper(II). To a hot solution of 2,3-butanedione dioxime, $dmgH_2$ (dimethyl glyoxime, 3.25 g, 0.028 mol), were added 2.5 g $Cu(O_2CCH_3)_2 \cdot H_2O$ (0.013 mol). The solution was refluxed for 15 minutes and filtered hot. A dark solid was collected and washed with diethyl ether. Infrared spectrum (KBr pellet): 1585(m), 1540(s), 1425(b,m), 1375(m), 1330(b,m), 1210(s), 1070(b,s), 960(s), 860(b,m), 820(w), 725(s).

$[Cu(dmgBF_2)_2]_3 \cdot 2C_4H_8O_2$, 18, tris[(1,1,8,8-tetrafluoro-4,5,11,12-tetramethyl-1,8-dibora-3,6,10,13-tetraaza-2,7,9,14-tetraoxo-cyclotetradeca-3,5,10,12-tetraenato)copper(II)] bisdioxane. A solution of 2.0 g $Cu(dmgH_2)_2$, 29 (6.8 mmol), and 5 mL $BF_3 \cdot OEt_2$ (40 mmol) in 300 mL dioxane was refluxed for 1 hour. A brown solid was collected, washed with diethyl ether, and air dried. The solid was dissolved in a minimum amount of hot acetone. The acetone solution was filtered and dioxane added. Crystals precipitated over a two-day period. Anal. Calcd. for $C_{14}H_{24}B_2CuF_4N_4O_7$: C, 32.24; H, 4.64; N, 10.74. Found: C, 31.70; H, 4.54; N, 10.44. Infrared spectrum (KBr pellet): 2980(w), 2930(w), 2870(w), 1635(m), 1450(b,w), 1380(m), 1260(m), 1210(m), 1180(s), 1120(s), 1095(s), 1040(m), 1005(s), 935(s), 890(w), 875(s), 815(s).

APPENDIX 1

The Use of a Solvent Independent Redox Couple and the Derivation of the Electrochemical Binding Constant Expression

A solvent independent redox couple, SIRC, has been used in this work to standardize all potentials to the normal hydrogen electrode, NHE. The couple which has been used is the ferrocene, ferrocenium ion couple. Half-wave potentials of electroactive species, X, are measured vs. Ag/0.01 M Ag^+ (CH_3CN) by sampled dc polarography. Measurement of the formal potential, $E^f(FeCp_2)$, of the ferrocene couple (E^f is the average of the anodic and cathodic peak potentials) in the same solution as the electroactive species is performed by cyclic voltammetry. The half-wave potential of X is standardized to the normal hydrogen electrode by the expression: $E_{1/2}(X)$, NHE = $E_{1/2}(X)$, Ag/Ag^+ - $E^f(FeCp_2)$, Ag/Ag^+ + $E_{1/2}(FeCp_2)$, NHE. The value of $E_{1/2}(FeCp_2)$, NHE is +0.400 V and is independent of the solvent used for the electrochemical study (92). The values for $E_{1/2}(X)$ and $E^f(FeCp_2)$ vs. Ag/Ag^+ do vary as a function of the solvent and are measured in pairs.

The binding constant expression based on half-wave potentials and ligand concentrations can be derived in two manners. The first derivation is based on successive equilibrium constants for M^{ox} and M^{red} with B (93). The second depends on the Ilkovic equation applied to bulk vs. surface concentrations (63). The expression to be derived is

$$E_{\frac{1}{2}} = E^{o} + \frac{RT}{nF} \ln \frac{(1+K^{red}[B])}{(1+K^{ox}[B])}$$

where $E_{\frac{1}{2}} = E_{\frac{1}{2}}(B)$ and $E^{o} = E_{\frac{1}{2}}(Ar)$.

1. Begin with the general reduction

$$M^{ox} + ne^{-} \rightleftharpoons M^{red} \qquad (1)$$

and the Nernst equation

$$E = E^{o} + \frac{RT}{nF} \ln \frac{[M^{ox}]}{[M^{red}]} \qquad (2)$$

M^{ox} = oxidized species

M^{red} = reduced species.

On addition of ligand, B, the total concentrations of reduced and oxidized species, C^{red} and C^{ox}, respectively, are

$$C^{red} = [M^{red}] + [M^{red}B] + [M^{red}B_2] + \ldots + [M^{red}B_n] \qquad (3)$$

$$C^{ox} = [M^{ox}] + [M^{ox}B] + [M^{ox}B_2] + \ldots + [M^{ox}B_n] \qquad (4)$$

Equilibrium constants are expressed as

$$K_1^{red} = \frac{[M^{red}B]}{[M^{red}][B]} , \ldots, K_n^{red} = \frac{[M^{red}B_n]}{[M^{red}][B]^n}$$

$$K_1^{ox} = \frac{[M^{ox}B]}{[M^{ox}][B]} , \ldots, K_n^{ox} = \frac{[M^{ox}B_n]}{[M^{ox}][B]^n}$$

The total concentrations, C^{red} amd C^{ox} become

$$C^{red} = [M^{red}] + K_1^{red}[M^{red}][B] + \ldots$$

$$= [M^{red}] + \sum_{j=1}^{n} K_j^{red}[M^{red}][B]^j \quad (5)$$

$$C^{ox} = [M^{ox}] + K_1^{ox}[M^{ox}][B] + \ldots$$

$$= [M^{ox}] + \sum_{j=1}^{n} K_j^{ox}[M^{ox}][B] \quad (6)$$

Equations 5 and 6 are solved for $[M^{red}]$ and $[M^{ox}]$

$$[M^{red}] = \frac{C^{red}}{(1+ \sum_{j=1}^{n} K_j^{red}[B]^j)} \quad (7)$$

$$[M^{ox}] = \frac{C^{ox}}{(1+ \sum_{j=1}^{n} K_j^{ox}[B]^j)} \quad (8)$$

Substitution of equations 7 and 8 into the Nernst equation (2) gives

$$E = E^{o} + \frac{RT}{nF} \ln \frac{(C^{ox})(1+ \sum_{j=1}^{n} K_j^{red}[B]^j)}{(C^{red})(1+ \sum_{j=1}^{n} K_j^{ox}[B]^j)} \qquad (9)$$

Equation 9 is simplifed at $E_{1/2} = E$, when $C^{red} = C^{ox}$.

$$E_{1/2} = E^{o} + \frac{RT}{nF} \ln \frac{(1 + \sum_{j=1}^{n} K_j^{red}[B]^j)}{(1+ \sum_{j=1}^{n} K_j^{ox}[B]^j)} \qquad (10)$$

If only the following equilibria occur in solution

$$M^{ox} + B \rightleftharpoons M^{ox}B$$

$$M^{red} + B \rightleftharpoons M^{red}B$$

equation 10 is further simplified to

$$E_{1/2} = E^{o} + \frac{RT}{nF} \ln \frac{(1+K^{red}[B])}{(1+K^{ox}[B])} \qquad (11)$$

Equation 11 is the expression used for electrochemical binding constant studies. The equation is useful in this form when $K^{red} > K^{ox}$. The useful form of equation 11 for the case of $K^{ox} > K^{red}$ is

$$E_{\frac{1}{2}} = E^{o} - \frac{RT}{nF} \ln \frac{(1+K^{ox}[B])}{(1+K^{red}[B])} \qquad (12)$$

2. The same general reduction expression (equation 1) and the Nernst equation (equation 2) are the starting equations for the second derivation. It is necessary to remember that the Nernst equation refers to the surface concentrations of M^{ox} and M^{red}, i.e., $[M^{ox}]_s$ and $[M^{red}]_s$.

The equilibria to be considered are

$$M^{ox} + B \rightleftharpoons M^{ox}B$$

$$M^{red} + B \rightleftharpoons M^{red}B$$

for which

$$K_1^{ox} = \frac{[M^{ox}B]_s}{[M^{ox}]_s [B]_s}$$

$$K_1^{red} = \frac{[M^{red}B]_s}{[M^{red}]_s [B]_s}$$

If [B] in bulk is equal to $[B]_s$, substitution in the Nernst equation for $[M^{ox}]_s$ and $[M^{red}]_s$ gives

$$E = E^{o} + \frac{RT}{nF} \ln \left(\frac{[M^{ox}B]_s}{K_1^{ox}[B]} \right) \left(\frac{K_1^{red}[B]}{[M^{red}B]_s} \right) \qquad (13)$$

Equation 13 simplifies to

$$E = E^{o} + \frac{RT}{nF} \ln \frac{[M^{ox}B]_s K_1^{red}}{[M^{red}B]_s K_1^{ox}} \tag{14}$$

The mean current, i, for a cathodic reaction is expressed in terms of the Ilkovic equation

$$i = ([M^{ox}] - [M^{ox}]_s)\kappa \tag{15}$$

κ = Ilkovic constant, $0.627\ nFD^{1/2}m^{2/3}t^{1/6}$

D = diffusion coefficient

When there are two oxidized species in solution, M^{ox} and $M^{ox}B$, the mean current expression has two terms

$$i = ([M^{ox}] - [M^{ox}]_s)\kappa_1 + ([M^{ox}B] - [M^{ox}B]_s)\kappa_2 \tag{16}$$

The diffusion limited current, i_d, is dependent on bulk concentrations only:

$$i_d = [M^{ox}]\kappa_1 + [M^{ox}B]\kappa_2 \tag{17}$$

The difference between i_d and i can be simplified to

$$i_d - i = \frac{[M^{ox}B]_s}{[B]K_1^{ox}}\kappa_1 + [M^{ox}B]_s\kappa_2 \tag{18}$$

Equation 18 is solved for $[M^{ox}B]_s$

$$[M^{ox}B]_s = \frac{(i_d - i)}{\left(\frac{K_1}{[B]K_1^{ox}} + K_2\right)} \tag{19}$$

The mean current, i, expressed in terms of the reduced species in solution is simple because bulk concentrations equal zero.

$$i = [M^{red}]_s K_3 + [M^{red}B]_s K_4 \tag{20}$$

Substitution for $[M^{red}]_s$ gives

$$i = \frac{[M^{red}B]_s}{[B]K_1^{red}} K_3 + [M^{red}B]_s K_4 \tag{21}$$

Equation 21 is solved for $[M^{red}B]_s$

$$[M^{red}B]_s = \frac{i}{\frac{K_3}{[B]K_1^{red}} + K_4} \tag{22}$$

Substitution of equations 19 and 22 into equation 14 produces

$$E = E^o + \frac{RT}{nF} \ln \frac{(i_d - i)}{(i)} \left(\frac{\frac{K_3}{[B]K_1^{red}} + K_4}{\frac{K_1}{[B]K_1^{ox}} + K_2} \right) \left(\frac{K_1^{red}}{K_1^{ox}} \right) \tag{23}$$

Equation 23 is simplified to

$$E = E^{o} + \frac{RT}{nF} \ln\left(\frac{i_d - i}{i}\right)\left(\frac{\kappa_3 + \kappa_4 [B] K_1^{red}}{\kappa_1 + \kappa_2 [B] K_1^{ox}}\right) \tag{24}$$

Assuming the diffusion coefficients of the species M^{ox}, $M^{ox}B$, M^{red} and $M^{red}B$ are equal, then $\kappa_1 = \kappa_2 = \kappa_3 = \kappa_4$ and equation 24 becomes

$$E = E^{o} + \frac{RT}{nF} \ln\left(\frac{i_d - i}{i}\right)\left(\frac{1 + [B] K_1^{red}}{1 + [B] K_1^{ox}}\right) \tag{25}$$

At $E = E_{\frac{1}{2}}$, $i = \frac{1}{2} i_d$

$$E_{\frac{1}{2}} = E^{o} + \frac{RT}{nF} \ln\left(\frac{1 + [B] K_1^{red}}{1 + [B] K_1^{ox}}\right) \tag{26}$$

Equation 26 is equivalent to equation 11, the binding constant expression desired.

Equation 26 can be changed into linear form for use with data pairs. In terms of measured quantities, equation 26 is

$$E_{\frac{1}{2}}(B) = E_{\frac{1}{2}}(Ar) + \frac{RT}{nF} \ln\left(\frac{1 + [B] K_1^{red}}{1 + [B] K_1^{ox}}\right) \tag{27}$$

$$\Delta E \equiv E_{\frac{1}{2}}(B) - E_{\frac{1}{2}}(Ar).$$

The equality in equation 27 can be expressed in the linear form (68)

$$\frac{1}{e^{\Delta E(nF/RT)}-1} = \frac{1}{(K_1^{red}-K_1^{ox})}\left(\frac{1}{[B]}\right) + \frac{K_1^{ox}}{(K_1^{red}-K_1^{ox})} \qquad (28)$$

The reciprocal of $e^{\Delta E(nF/RT)}-1$ is plotted against 1/[B]. The least squares slope, a, and intercept, b, are solved simultaneously for K_1^{red} and K_1^{ox}. For $K_1^{red} > K_1^{ox}$,

$$K_1^{red} = b/a$$

$$K_1^{ox} = (1+b)/a.$$

APPENDIX 2

Models for Copper-Containing Proteins: Structure and Properties of Novel Five-Coordinate Copper(I) Complexes

[Reprinted from the Journal of the American Chemical Society, 99, 7170 (1977).]
Copyright 1977 by the American Chemical Society and reprinted by permission of the copyright owner

Models for Copper-Containing Proteins: Structure and Properties of Novel Five-Coordinate Copper(I) Complexes

Robert R. Gagné,* Judith L. Allison, Robert S. Gall, and Carl A. Koval

Contribution No. 5554 from the Division of Chemistry and Chemical Engineering, California Institute of Technology, Pasadena, California 91125. *Received March 31, 1977*

Abstract: The four-coordinate Cu(I) complex [difluoro-3,3′-(trimethylenedinitrilo)bis(2-butanone oximato)borate]copper(I), $Cu(LBF_2)$, can be produced by electrochemical reduction of the corresponding Cu(II) complex. The Cu(I) complex reacts with monodentate ligands (e.g., CO, 1-methylimidazole, acetonitrile) yielding five-coordinate adducts. The structure of the carbonyl derivative has a square-pyramidal copper displaced 0.96 Å out of the basal nitrogen plane. The Cu–CO distance is 1.780 (3) Å, with a Cu–C–O angle of 177.5 (3)°. The C–O bond length is 1.112 (4) Å. The space group is *Pbca* with a = 13.926 (1) Å, b = 14.209 (1) Å, c = 16.297 (1) Å, Z = 8, and R = 5.5%. Preliminary equilibrium constants were determined by cyclic voltammetry and by absorption spectroscopy. Carbon monoxide ($K_c = 4.7 \times 10^4\ M^{-1}$) binds significantly better than 1-MeIm ($K_c = 16\ m^{-1}$). The possible biochemical significance of five-coordinate Cu(I) is discussed.

Introduction

Numerous copper-containing proteins utilize molecular oxygen in respiratory and biosynthetic functions.[1-3] The best studied copper proteins, hemocyanin and tyrosinase, serve, respectively, in O_2 transport and in activating O_2 for the oxidation of tyrosine.[4] Both tyrosinase and hemocyanin apparently contain a pair of contiguous Cu atoms, commonly designated type III copper, at the active site. The structural nature of the type III copper site is not known for any protein. Stoichiometry,[13,14] EPR,[15-19] and magnetic susceptibility measurements[18-20] on various derivatives of hemocyanin and tyrosinase, however, suggest a strongly antiferromagnetically coupled pair of copper atoms separated by some 3–5 Å.[5-7] The number and identity of ligands bound to either copper are not known. Nonetheless, titration[21,22] and spectroscopic[23,24] studies tend to preclude sulfur and favor nitrogen ligands, probably imidazole nitrogen.

The paucity of structural and mechanistic information for these copper proteins is paralleled by an equally sparse literature on the reactions of Cu(I) complexes, particularly with nitrogen ligands.[25] Extreme lability, facile disproportionation, and air sensitivity have frustrated attempts to explore reactions of copper–nitrogen ligand complexes. For example, there are no well-characterized dioxygen complexes derived from Cu(I)[26] despite the large number of O_2 complexes known for several other metals.[27-30]

To help elucidate possible active site structures and mechanisms of copper protein activity, we are exploring the basic relationships between structure and chemical reactivity in a variety of Cu(I) complexes of predominantly nitrogen ligands. Both mononuclear and binuclear complexes are under investigation, in the hopes of eventually explaining the apparent necessity for a binuclear copper site (type III) for O_2 binding in the proteins.[4] Herein we report the synthesis and properties of novel *five*-coordinate Cu(I) complexes which have been communicated previously.[31]

Results and Discussion

Deducing structure–reactivity relationships for Cu(II) complexes is complicated by a number of factors which can be controlled, as follows.

(1) Both Cu(I) and Cu(II) are rather substitution labile.[25-33] Thus, complexes of monodentate and even bidentate ligands often lead to solutions containing several species including two-, three- and four-coordinate monomers as well as dimers, etc. Use of polydentate ligands, including macrocycles, inhibits both dissociation and dimer formation (via bridging atoms of the polydentate ligand) especially if the chelate is somewhat rigid structurally, as macrocycles are. Explaining solution behavior, especially in reference to solid-state structures, is thus simplified appreciably.

(2) Many Cu(I) complexes disproportionate rapidly at the ambient temperature to Cu(II) and Cu(0).[33] Ligand environments having saturated amines and/or an enforced rigid, square-planar structure destabilize Cu(I) with respect to Cu(II), as shown by electrochemical studies.[34,35] Conversely, employing flexible yet unsaturated nitrogen ligands should preclude disproportionation.

(3) Reducing Cu(II) to Cu(I) without undesirable further reduction to Cu(0) is difficult with most common chemical reducing agents. Likewise, complexing Cu(I) directly by reaction between some appropriate Cu(I) salt and a polydentate ligand most often leads to disproportionation, possibly owing to unstable intermediates.[36-39] Electrochemical reduction at constant potential has, however, been shown[35] to be both specific and practical.

(4) Finally, it must be recognized that most Cu(I) complexes are very air-sensitive. Schlenk, vacuum-line, and modern inert-atmosphere chamber techniques render this a relatively trivial problem.

After examining several other polydentate and macrocyclic ligand systems, the results of which are reported in part elsewhere,[39] we have found the tetradentate ligand **1** to adequately fulfill the requirements above and to yield novel Cu(I) chemistry.[31] The free ligand, 3,3′-(trimethylenedinitrilo)bis(2-butanone dioxime) (**1**, H_2L), has been prepared previously,[40] using boiling diisopropyl ether as solvent, although this procedure is difficult. Large quantities of ligand can be obtained far more simply, however, by combining 2,3-butanedione monoxime with 1,3-diaminopropane in ethanol at 25 °C (eq 1).

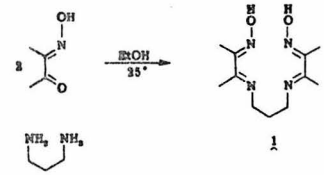

(1)

1

Treating warm acetone or ethanol solutions of the macrocycle **1** with Cu(II) salts gives red to green mixtures depending on the ligand to Cu(II) ratio. With a twofold excess of ligand,

Table I. Cyclic Voltammetric Data for $[Cu(LBF_2)ClO_4]_2{\cdot}C_4H_8O_2$ (5)[a]

Solvent	E_{p_c},[b] V	E_{p_a},[b] V	E^f,[b,c] V	i_{p_c}, μA	i_{p_a}, μA
CH_3CN	−0.432	−0.330	−0.381	18	19
$(CH_3)_2CO$	−0.459	−0.345	−0.402	18	17

[a] Conditions: [Cu] = 2×10^{-3} M under inert atmosphere; sweep rate = 100 mV/s; hanging mercury drop electrode. [b] Potentials are given vs. SHE as calculated in Table X. [c] $E^f = (E_{p_c} + E_{p_a})/2$.

dark red-brown, crystalline $Cu(HL)ClO_4{\cdot}H_2O$ (2) can be isolated. The product is contaminated with excess copper, possibly because of small amounts of a binuclear species such as 3. This species may be similar to the Cu(II) complex obtained[41] with salicylaldehydeethylenediamine, 4.

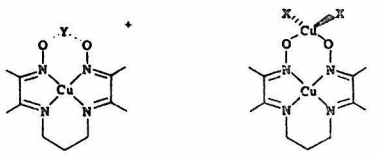

2, Y = H
5, Y = BF_2

3

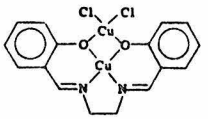

4

To inhibit binding of a second copper atom and to prevent possible hydrogen atom transfer reactions (as to dioxygen coordinated to copper), the bridging oxime hydrogen in 2 was replaced with BF_2 via treatment with boron trifluoride etherate in dioxane. The resulting complex has an analysis consistent with the formulation $[Cu(LBF_2)ClO_4]_2{\cdot}C_4H_8O_2$ (5). It has not been determined whether dioxane is acting as a μ-bidentate bridge between two coppers or is present simply as solvent of crystallization.

The reduction of complex 5 was attempted by several chemical reducing agents, including Na, Zn, Mg, and their amalgams, and hydrazine. In all cases some Cu(0) was produced, by direct reduction of Cu(II) or by disproportionation of intermediate Cu(I) species. For this reason, the electrochemical behavior of the complex was examined.

Cyclic voltammograms of 5 have been obtained both in acetonitrile and in acetone. A scan, representative of the first reduction process in either solvent, is given in Figure 1.[42] While the anodic and cathodic peak currents are nearly equal, the peak potential separation is much larger than the 58 mV expected for a reversible, one-electron process. That this reduction does involve only a single electron is confirmed by constant potential electrolysis at potentials slightly negative of the wave (~ −0.7 V) yielding n values of 1.0 ± 0.05.

The potential of the Cu(II)/Cu(I) couple for 5 (E^f = −0.381; see Table I) is more positive than that for complex 2 (E^f = −0.560; see Experimental Section) indicating a possible stabilization of Cu(I) in the former. Indeed, gram quantities of $Cu(LBF_2)$ (6) can be synthesized by CPE at −0.7 V. During the electrolysis, the original purple solution (Cu(II)) becomes deep blue (Cu(I), λ_{max} 677 nm) with subsequent precipitation of a microcrystalline, red solid. The product, which is blue upon being ground to a powder (an optical phenomenon since there is no other indication of chemical decomposition), is apparently not air-sensitive in the solid state.

In a formal sense the blue Cu(I) complex, $Cu(LBF_2)$, 6, is

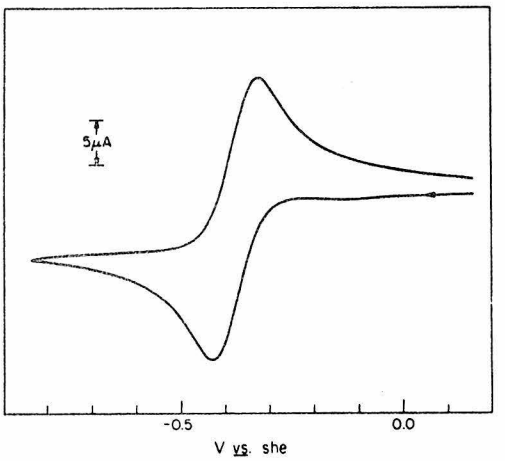

Figure 1. Cyclic voltammetry of $[Cu(LBF_2)(ClO_4)]_2{\cdot}C_4H_8O_2$ (5) in CH_3CN. Scan rate = 100 mV/s. [Cu] = 2×10^{-3} M.

a four-coordinate 18-electron system and as such is coordinatively saturated. Nonetheless, 6 reacts with a number of monodentate ligands to give presumably five-coordinate Cu(I) complexes. For example, addition of 1-methylimidazole, (1-MeIm) to the blue complex 6 in acetone gives a green solution (λ_{max} 420 nm) from which the imidazole adduct, $Cu(LBF_2)$(1-MeIm) (7) can be isolated. Even acetonitrile, usually considered a weak ligand, binds to $Cu(LBF_2)$ (6), giving aquamarine solutions at 25 °C. Green acetonitrile solutions result upon cooling to −40 °C, presumably indicating a greater degree of complex formation at the lower temperature.

Most surprisingly, carbon monoxide reacts rapidly with blue $Cu(LBF_2)$ (6) solutions at 25 °C, yielding light yellow solutions. The reaction is readily reversed upon purging with nitrogen. A stable carbonyl adduct can be isolated from CO treated solutions as a bright yellow microcrystalline material (ν_{CO} 2068 cm^{-1}), $Cu(LBF_2)(CO)$ (8). The solution infrared spectrum of $Cu(LBF_2)(CO)$ (8), (CH_2Cl_2, 1 atm CO) shows only a single peak attributable to coordinated CO (ν_{CO} 2080 cm^{-1}). This is consistent with the presence of a single carbonyl species in solution. Finally, the similarity between ν_{CO} in solution (2080 cm^{-1}) and in the solid state (2068 cm^{-1}) suggests that the solution species is most probably a five-coordinate, monocarbonyl adduct (vide infra).

Crystal Structure

The carbonyl adduct $Cu(LBF_2)(CO)$ (8) was easily crystallized by evaporation of an acetone solution, permitting a structural determination. Figure 2 shows the structure and labeling scheme of the novel copper(I) carbonyl complex while Table II details the crystal data. The structure's uniqueness lies in five-coordination for copper(I) which gives rise to a 20-electron count for the metal atom coordinated to five two-electron donors. Although five-coordination is known for other d^{10} metals,[43] it is not common for copper(I). In addition,

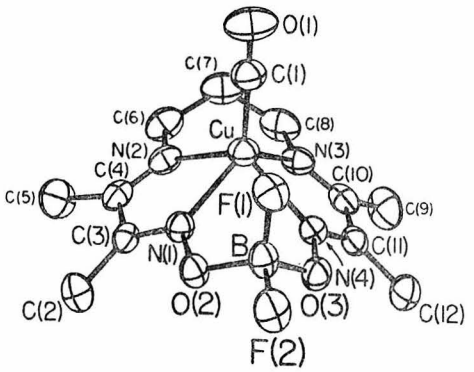

Figure 2. An ORTEP drawing of the structure and numbering scheme of $Cu(LBF_2)(CO)$ (8) with thermal ellipsoids at the 40% probability level. Hydrogen atoms are omitted.

Table II. Crystal Data for $Cu(LBF_2)(CO)$ (8)

Formula	$Cu(BF_2C_{11}H_{18}N_4O_2)CO$
FW	378.64
Space group	D_{2h}^{15}-*Pbca* (no. 61)
a	13.926 (1) Å
b	14.209 (1) Å
c	16.297 (1) Å
V	3224.8 Å^3
Z	8
ρ_{calcd}	1.56 g cm^{-3}
ρ_{obsd}	1.55 (3) g cm^{-3}
λ(Cu K$\bar{\alpha}$)	1.5418 Å
μ(Cu K$\bar{\alpha}$)	23.293 cm^{-1}

Table III. Bond Distances (Å)

Cu-N1	2.165 (2)	N1-C3	1.275 (3)
Cu-N4	2.163 (2)	N2-C4	1.277 (4)
Cu-N2	2.100 (2)	N2-C6	1.459 (4)
Cu-N3	2.108 (2)	C2-C3	1.488 (4)
		C3-C4	1.485 (4)
Cu-C1	1.780 (3)	C4-C5	1.484 (5)
O1-C1	1.112 (4)	C7-C8	1.500 (5)
F1-B	1.386 (4)		
F2-B	1.379 (4)	C2-H1	0.86 (3)
O3-B	1.478 (4)	C2-H2	0.93 (3)
O2-B	1.475 (4)	C2-H3	0.93 (3)
		C5-H4	0.82 (3)
O2-N1	1.374 (3)	C5-H5	1.05 (3)
O3-N4	1.371 (3)	C5-H6	0.89 (3)
		C6-H7	0.85 (3)
N4-C11	1.283 (3)	C6-H8	1.02 (3)
N3-C10	1.269 (4)	C7-H9	0.92 (3)
N3-C8	1.471 (4)	C7-H10	0.91 (3)
C11-C12	1.480 (4)	C8-H11	1.01 (3)
C10-C11	1.494 (4)	C8-H12	0.97 (3)
C9-C10	1.497 (5)	C9-H13	0.98 (3)
C6-C7	1.502 (5)	C9-H14	0.97 (3)
		C9-H15	0.89 (3)
		C12-H16	0.90 (3)
		C12-H17	0.94 (3)
		C12-18	0.87 (3)

$Cu(LBF_2)(CO)$ (8) is one of the few structurally characterized copper(I) carbonyl complexes and is apparently the only known 20-electron complex containing coordinated carbon monoxide.

Tables III and IV give bond lengths and angles for $Cu(LBF_2)(CO)$ (8). All nonhydrogen intermolecular separations are greater than 3.39 Å. There is no evidence for intermolecular or intramolecular hydrogen bonding.

Table IV. Bond Angles (Deg)

N2-Cu-N4	124.7 (1)	F1-B-F2	110.7 (3)
N1-Cu-N3	127.6 (1)	F1-B-O2	110.7 (3)
N1-Cu-N4	79.1 (1)	F1-B-O3	110.8 (3)
N2-Cu-N3	85.9 (1)	F2-B-O2	105.1 (3)
N3-Cu-N4	73.8 (1)	F2-B-O3	105.8 (3)
N1-Cu-N2	73.9 (1)	O2-B-O3	113.4 (3)
Cu-N1-O2	126.4 (2)	O3-N4-C11	116.0 (2)
Cu-N4-O3	126.2 (2)	O2-N1-C3	115.7 (2)
Cu-N1-C3	117.5 (2)	N1-O2-B	112.5 (2)
Cu-N2-C4	118.0 (2)	N4-O3-B	112.9 (2)
Cu-N2-C6	120.2 (2)		
Cu-N3-C8	119.4 (2)	N1-C3-C2	123.9 (3)
Cu-N3-C10	118.5 (2)	N1-C3-C4	113.6 (3)
Cu-N4-C11	117.8 (2)	N2-C4-C5	124.3 (3)
		N2-C4-C3	116.3 (3)
N1-Cu-C1	114.9 (1)	N3-C10-C9	125.6 (3)
N2-Cu-C1	114.8 (1)	N3-C8-C7	112.4 (3)
N3-Cu-C1	117.4 (1)	N4-C11-C10	113.3 (3)
N4-Cu-C1	120.3 (1)	N4-C11-C12	124.4 (3)
		C4-N2-C6	121.8 (3)
Cu-C1-O1	177.5 (3)	N2-C6-C7	112.2 (3)
		C8-N3-C10	122.0 (3)
		N_3-C10-C11	116.3 (3)
		C_2-C_3-C_4	122.3 (3)
		C_3-C_4-C5	119.3 (3)
		C9-C10-C11	118.0 (3)
		C10-C11-C12	122.1 (3)
		C6-C7-C8	117.1 (3)

Table V. Root-Mean Square Amplitudes of Vibration along the Principal Axes (Å)

Cu	0.21	0.23	0.24
F1	0.22	0.26	0.28
F2	0.19	0.26	0.34
O1	0.20	0.39	0.40
O2	0.19	0.21	0.27
O3	0.21	0.22	0.26
N1	0.20	0.22	0.23
N2	0.19	0.22	0.27
N3	0.19	0.23	0.27
N4	0.20	0.22	0.23
C1	0.22	0.25	0.28
C2	0.22	0.26	0.29
C3	0.19	0.20	0.24
C4	0.19	0.21	0.27
C5	0.22	0.30	0.35
C6	0.21	0.27	0.32
C7	0.20	0.29	0.34
C8	0.20	0.28	0.34
C9	0.22	0.30	0.35
C10	0.19	0.21	0.29
C11	0.19	0.20	0.27
C12	0.22	0.26	0.32
B	0.20	0.22	0.27

The carbonyl complex $Cu(LBF_2)(CO)$ (8) exhibits idealized C_s-*m* geometry with no crystallographically imposed symmetry. The copper atom sits in an asymmetrical square-pyramidal environment and is displaced 0.96 Å from the basal plane of the four nitrogen atoms. Two significantly different sets of Cu-N bond lengths which average 2.164 and 2.104 Å characterize the equatorial asymmetry. The trans N-Cu-N angles are 124.7 (1) and 127.6 (1)°; the cis N-Cu-N angles range from 73.8 (1) to 85.9 (1)°.

The carbonyl ligand coordinates at the apex of the square-pyramid with a Cu-CO distance of 1.780 (3) Å and a Cu-C-O angle of 177.5 (3)°. The C-O bond length, which has not been corrected for possible vibrational shortening (Table V), is 1.112

Table VI. Atomic Coordinates[a] for $Cu(LBF_2)(CO)$ (8)

Atom	X	Y	Z
Cu	23458 (3)	10234 (3)	41603 (3)
F1	3529 (1)	1537 (1)	5685 (1)
F2	2753 (1)	1957 (1)	6857 (1)
O1	4321 (2)	962 (2)	3617 (2)
O2	2120 (1)	2451 (1)	5651 (1)
O3	2092 (2)	787 (2)	6083 (1)
N1	1940 (2)	2274 (2)	4836 (2)
N2	1434 (2)	1791 (2)	3383 (2)
N3	1478 (2)	−147 (2)	3874 (2)
N4	1919 (2)	416 (2)	5321 (2)
C1	3568 (2)	986 (3)	3843 (2)
C2	1004 (3)	3726 (2)	4873 (2)
C3	1408 (2)	2873 (2)	4472 (2)
C4	1168 (2)	2609 (2)	3614 (2)
C5	625 (3)	3281 (3)	3094 (2)
C6	1164 (3)	1411 (3)	2584 (2)
C7	1554 (3)	437 (3)	2449 (2)
C8	1206 (3)	−322 (3)	3015 (2)
C9	586 (3)	−1535 (2)	4363 (3)
C10	1182 (2)	−664 (2)	4457 (2)
C11	1425 (2)	−346 (2)	5305 (2)
C12	1071 (3)	−844 (2)	6043 (2)
B	2643 (3)	1675 (2)	6053 (2)

Atom	X	Y	Z	B
H1	135 (2)	422 (2)	479 (2)	5.20
H2	99 (2)	365 (2)	544 (2)	5.20
H3	40 (2)	389 (2)	468 (2)	5.20
H4	8 (2)	307 (2)	310 (2)	6.90
H5	79 (2)	325 (2)	246 (2)	6.90
H6	40 (2)	381 (2)	331 (2)	6.90
H7	136 (2)	178 (2)	220 (2)	6.30
H8	43 (2)	140 (2)	262 (2)	6.30
H9	222 (2)	46 (2)	249 (2)	6.80
H10	134 (2)	24 (2)	195 (2)	6.80
H11	50 (2)	−48 (2)	298 (2)	6.60
H12	146 (2)	−94 (2)	290 (2)	6.60
H13	75 (2)	−180 (2)	383 (2)	7.10
H14	82 (2)	−200 (2)	475 (2)	7.10
H15	1 (2)	−144 (2)	458 (2)	7.10
H16	110 (2)	−47 (2)	648 (2)	5.80
H17	40 (2)	−87 (2)	603 (2)	5.80
H18	136 (2)	−137 (2)	614 (2)	5.80

[a] The X, Y, and Z fractional coordinates are multiplied by 10^5 for the copper atom, 10^4 in the case of the nonhydrogen atoms, and by 10^3 otherwise.

(4) Å. To our knowledge the only other copper(I) carbonyl complex which has been structurally characterized is [hydrotris(1-pyrazolyl)borato]copper(I) carbonyl, $[HB(pz)_3]CuCO$.[44] The latter complex has a four-coordinate copper(I) atom with a closed-shell configuration. Carbon monoxide is bonded linearly; the Cu-CO distance averages 1.765 Å and the C-O bond length is 1.120 Å. Thus, while the average Cu-N distance in $Cu(LBF_2)(CO)$ (8) is 0.09 Å longer than that in $[(HB(pz)_3)]CuCO$, both the Cu-CO and CO distances agree closely in spite of the difference in coordination numbers of the copper atom. As we have previously noted,[31] the carbonyl infrared stretching frequencies also show only a small variation despite the different coordination geometries for copper(I).

Several structural determinations of various metals coordinated to H_2L (1, or its derivatives) have been reported. These include six-coordinate d^6 metals Rh(III)[45a] and Co(III).[45b] A closely related copper(II) complex,[46] which has a saturated Cu-N (amine) bond, is square pyramidal with a perrhenate anion occupying the axial coordination site. The Cu-N bond lengths in $Cu(LBF_2)(CO)$ (8) average 0.16 Å longer than

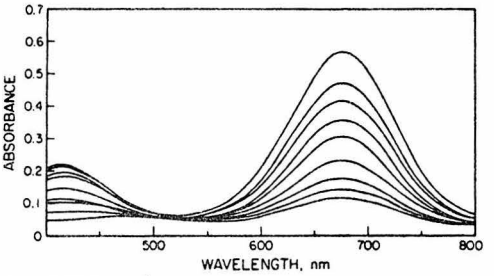

Figure 3. Visible spectral changes observed on addition of 1-methylimidazole to a solution of $Cu(LBF_2)$ (6) in acetone.

those in the copper(II)-amine complex. The copper(II) ion is displaced only 0.24 Å out of the plane of the equatorial nitrogen atoms.[46] Presumably, the larger size of the copper(I) ion accounts for the larger displacement of the metal atom from the plane of the four nitrogen atoms in $Cu(LBF_2)(CO)$ (8).

Rhodium(I) complexes of H_2L (1) have been found to be very reactive toward oxidative addition.[47] In some cases cis addition is indicated which would require distortion of the macrocycle from planarity. The macrocycle is nearly planar in the Rh(III), Rh(I), and Co(III) structures. In $Cu(LBF_2)(CO)$ (8), however, the macrocycle deviates considerably from planarity as evidenced by a dihedral angle of 60.0° between the Ni(1)-C(3)-C(4)-N(2) and N(3)-C(10)-C(11)-N(4) planes. This angle is less than 3° for the d^6 and d^8 complexes.

Other differences in the conformation of the macrocycle in the structures of the six-coordinate BF_2-bridged Rh(III) complex, $Rh[C_2(LBF_2)](CH_3)(I)$,[45a] and of $Cu(LBF_2)(CO)$ (8) are evident. In the latter complex, atom C(7) and the boron atom both lie above the plane of the four equatorial nitrogen atoms. A "boat" conformation is thus produced for the two six-membered rings which include the metal atom. In the Rh(III) complex, however, these atoms are located on opposite sides of the macrocycle plane leading to an overall "chair" conformation. This variation in conformation presumably results from the difference in steric requirements of both the metal atoms and the axial ligands in the Cu(I) and Rh(III) complexes.

The average values of the C=N, C—N, and C—C bond lengths in $Cu(LBF_2)(CO)$ (9) are 1.276 ± 0.006, 1.465 ±

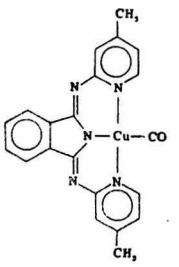

9

0.008, and 1.491 ± 0.008 Å, respectively.[48] For comparison, values of 1.300 ± 0.013, 1.476 ± 0.018, and 1.506 ± 0.025 Å are found for $Rh[C_2(LBF_2)](CH_3)I$.

The refined C-H bond lengths average 0.93 ± 0.06 Å. The H-C-H angles range from 89 to 129° with a mean value of 107 ± 10°.

Tables VI and VII give the atomic coordinates and the anisotropic thermal parameters for $Cu(LBF_2)(CO)$ (8).

Table VII. Anisotropic Thermal Parameters for $Cu(LBF_2)(CO)$ (8)

Atom	U_{11}	U_{22}	U_{33}	U_{12}	U_{13}	U_{23}
Cu	448 (2)	552 (3)	565 (3)	−10 (2)	59 (2)	−18 (2)
F1	51 (1)	68 (1)	74 (1)	2 (1)	−10 (1)	−2 (1)
F2	96 (2)	70 (1)	49 (1)	12 (1)	−28 (1)	−6 (1)
O1	61 (2)	155 (3)	132 (3)	−8 (2)	41 (2)	1 (2)
O2	64 (1)	45 (1)	43 (1)	7 (1)	−11 (1)	−2 (1)
O3	69 (2)	49 (1)	45 (1)	3 (1)	−3 (1)	3 (1)
N1	50 (2)	46 (2)	42 (2)	1 (1)	−4 (1)	3 (1)
N2	52 (2)	68 (2)	38 (2)	−9 (2)	−2 (1)	2 (1)
N3	54 (2)	53 (2)	57 (2)	−4 (1)	5 (1)	−18 (1)
N4	47 (1)	41 (1)	50 (2)	4 (1)	2 (1)	0 (1)
C1	56 (2)	64 (2)	69 (2)	−4 (2)	13 (2)	−2 (2)
C2	70 (2)	55 (2)	74 (2)	10 (2)	−11 (2)	2 (2)
C3	40 (2)	43 (2)	49 (2)	−4 (1)	−1 (1)	8 (1)
C4	45 (2)	64 (2)	46 (2)	−4 (2)	−1 (2)	16 (2)
C5	94 (3)	99 (3)	66 (2)	27 (2)	−13 (2)	15 (2)
C6	82 (3)	92 (2)	44 (2)	−14 (2)	−4 (2)	1 (2)
C7	84 (3)	108 (3)	48 (2)	−6 (3)	2 (2)	−26 (2)
C8	78 (2)	77 (3)	78 (3)	−8 (2)	3 (2)	−37 (2)
C9	85 (3)	54 (2)	125 (4)	−16 (2)	−6 (3)	−8 (2)
C10	41 (2)	40 (2)	83 (3)	2 (2)	3 (2)	−11 (2)
C11	41 (2)	40 (2)	71 (2)	4 (1)	9 (2)	6 (2)
C12	73 (2)	56 (2)	92 (3)	−1 (2)	16 (2)	15 (2)
B	64 (2)	47 (2)	49 (2)	4 (2)	−14 (2)	0 (2)

[a] The form of the thermal ellipsoid is $\exp[-2\pi^2(U_{11}h^2a^{*2} + \ldots + 2U_{23}klb^*c^*)]$. The U_{ij} elements are multiplied by 10^4 for the copper atom and by 10^3 otherwise.

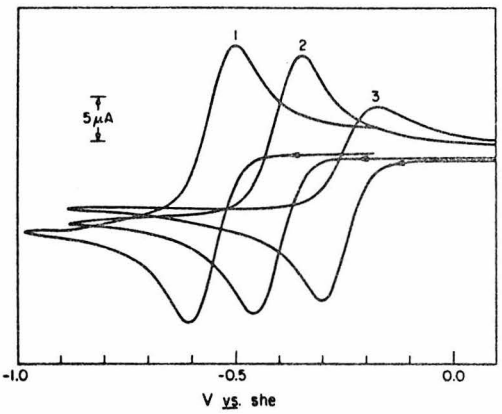

Figure 4. Cyclic voltammetry of $[Cu(LBF_2)(ClO_4)]_2$-$C_4H_8O_2$ (5) in acetone: (1) with 100 equiv 1-MeIm; (2) under N_2; and (3) with 1 atm CO. Scan rate = 100 mV/s. Concentrations of Cu(II) were not held precisely equal, $\simeq 2 \times 10^{-3}$ M.

Equilibrium Constants. Preliminary equilibrium (concentration) constants for the formation of five-coordinate complexes, $Cu(LBF_2)L'$ (eq 2)

$$Cu(LBF_2) + L' \overset{K_c}{\rightleftharpoons} Cu(LBF_2)L' \qquad (2)$$

have been determined via spectroscopic studies and by monitoring changes in electrochemical redox behavior upon addition of ligands, L', as follows.

The blue four-coordinate Cu(I) complex $Cu(LBF_2)$ (6) has a strong absorption at 677 nm (acetone, ϵ 1.03×10^4 M^{-1} cm^{-1}, 25 °C) which disappears upon addition of a large excess of CO or 1-MeIm. Monitoring the absorption at 677 nm as ligand was added was used to determine the extent of formation of the five-coordinate complex (eq 2). Figure 3 depicts the series of spectra obtained upon adding various amounts of 1-MeIm to an acetone solution of the four-coordinate complex, $Cu(LBF_2)$ (6). Only approximate isosbestic behavior was observed due to slight variations in the pathlengths of the sample cells utilized (see Experimental Section). For these preliminary measurements we assume therefore that there are only two principal species in solution, four-coordinate $Cu(LBF_2)$ and five-coordinate $Cu(LBF_2)L'$ (eq 2). Similar measurements with various partial pressures of CO permitted binding constant determinations but, again, no true isosbestic behavior was observed. Table VIII lists the values for the equilibrium constants determined.

Table VIII. Equilibrium Constants for the Formation of Five-Coordinate Complexes $Cu(LBF_2)L'$ in Acetone

$$Cu(LBF_2) + L' \overset{K}{\rightleftharpoons} Cu(LBF_2)L'$$

L'	K	Method
1-MeIm	$K_c = 16\ M^{-1}$	EAS
CO	$K_p = 500\ atm^{-1}$ ($P_{1/2} = 1.5$ mm)	EAS
CO	$K_c \simeq 4.7 \times 10^4\ M^{-1}$	EAS
CO	$K_c \simeq 6.7 \times 10^4\ M^{-1}$	ΔE^f

Changes in electrochemical redox behavior were also employed to determine equilibrium constants. As shown in Figure 4 and in Table IX the cyclic voltammograms obtained using the Cu(II) complex 5 as starting material depend on both the solvent and on other coordinating ligands in solution. A large excess of 1-MeIm causes a significant negative shift in E^f while excess CO results in a positive shift relative to the cyclic voltammogram obtained for 5 under nitrogen (Figure 4). These shifts are attributable to the formation of Cu(I) and Cu(II) adducts of the ligand added. In Figure 4, curves 1 and 3 have approximately the same wave shape as does curve 2. This suggests that the equilibria between Cu(I), Cu(II), and the added ligands are established rapidly compared to the cyclic voltammetry timescale. In the special case where adducts are formed very rapidly and with only one oxidation state of the metal, the shift in E^f can be correlated simply to the degree of

Table IX. Cyclic Voltammetric Data for $[Cu(LBF_2)ClO_4]_2$-$C_4H_8O_2$ (5) with Added Ligands[a]

Indicating electrode	Solution atm	L, eq[b]	E_{p_c}, V[c]	E_{p_a}, V[d]	E^f, V[e]
		In CH_3CN			
Hg	He	None	−0.432	−0.330	−0.381
Pt[f]	N_2	1-MeIm, 5	−0.517	−0.389	−0.453
Pt	N_2	20	−0.548	−0.423	−0.486
Pt	N_2	100	−0.567	−0.437	−0.502
Hg	He	1-MeIm, 100	−0.559	−0.457	−0.508
Hg	CO	CO, satd	−0.274	−0.169	−0.221
		In $(CH_3)_2CO$			
Hg	N_2	None	−0.459	−0.345	−0.402
Pt[f]	He	1-MeIm, 5	−0.561	−0.462	−0.512
Pt	He	20	−0.599	−0.492	−0.546
Pt	He	100	−0.614	−0.502	−0.558
Hg	He	1-MeIm, 100	−0.606	−0.496	−0.551
Hg	CO	CO, satd	−0.298	−0.169	−0.234

[a] Conditions: [Cu] = 2×10^{-3} M; sweep rate = 100 mV/s. [b] L = ligand added, eq = equivalents of L added. [c] Vs. SHE. [d] $E^f \simeq E_{p_c} + E_{p_a}/2$. [e] A Pt indicating electrode was used because with Hg, at approximately +0.035 V, a large reduction wave occurred swamping the Cu(II) + $1e^- \rightarrow$ Cu(I) peak. If the sweep was begun at −0.14 V (CH_3CN) or 0.18 V ($(CH_3)_2CO$) in Hg, the interference was avoided and the cyclical data given were measured. Pt and Hg results agree closely in cases where both were used.

adduct formation.[49] Carbon monoxide as a ligand appears to satisfy these conditions. Addition of CO to the Cu(II) complex 5 causes no observable spectral changes, nor are there any other indications of a Cu(II)–CO adduct. As a first approximation, therefore, the observed shifts in E^f can be totally attributed to formation of the five-coordinate Cu(I) carbonyl $Cu(LBF_2)(CO)$ (8). That this is a reasonable assumption is supported by the close approximation between the equilibrium constant obtained (see Experimental and Table VIII) and that found by spectral measurements (Table VIII). Unfortunately, nitrogen bases, including 1-MeIm, bind to both the Cu(I) and the Cu(II) complexes precluding the use of this electrochemical approach to determine equilibrium constants.

The value of K_c for CO ($\sim 4.7 \times 10^4$ M^{-1}) is significantly greater than that for 1-MeIm (16 M^{-1}). Moreover, the shift in E^f for CO is positive, implying stabilization of Cu(I), while that for 1-MeIm is negative, indicative of either stabilization of Cu(II) or destabilization of Cu(I). It can be argued that this may be attributed to the greater π acidity of CO, which serves to drain the 20-electron system of electron density. Such an explanation is not sufficient to account for a number of observations which are discussed below.

Several Cu(I) complexes of polydentate ligands form carbonyl adducts with very similar ν_{CO}'s despite dissimilar structures. In the tetrahedral [hydrotris(pyrazolyl)borato]copper(I) carbonyl and its dimethyl analogue, [hydrotris(3,5-dimethyl-1-pyrazolyl)borato]copper(I) carbonyl, ν_{CO}'s are 2083 and 2066 cm^{-1}, respectively.[38] The presumably four-coordinate (probably distorted square-planar) isoindoline complex 9 has ν_{CO} 2072 cm^{-1}.[39] As reported here, the five-coordinate complex $Cu(LBF_2)(CO)$ (8) has ν_{CO} 2068 cm^{-1}. The similarity of ν_{CO} for 8 relative to ν_{CO} in the four-coordinate complexes does not suggest a peculiar bonding situation in the five-coordinate complex which might be expected of a 20-electron species.

The formation of five-coordinate adducts from four-coordinate Cu(I)–macrocyclic ligand complexes is apparently not a general phenomenon. For example, the Cu(I) complex 10[35] does not change color when exposed to CO, nor is there any shift in E^f as determined by cyclic voltammetry.[50] In contrast, the binuclear mixed-valence Cu(II)Cu(I) carbonyl complex 11 (ν_{CO} 2067 cm^{-1}), which probably contains a five-coordinate Cu(I), has been isolated.[50]

The very formation of five-coordinate Cu(I) is somewhat enigmatic. The $Cu(LBF_2)(CO)$ (8) structure (Figure 3) may indicate, however, at least one factor helpful in explaining

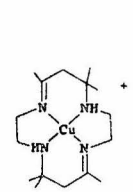

10

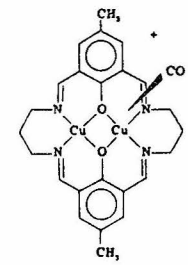

11

five-coordination. The Cu atom is seen to be a full 0.96 Å out of the mean plane of the four coordinating nitrogens of the macrocycle. Such a large displacement of a transition metal atom from a macrocycle is unusual and may be due in part to the large radius of Cu(I). In fact it is not unreasonable to expect that the structure of the four-coordinate species, when determined, will reveal Cu(I) to be significantly displaced from the basal plane of the relatively rigid macrocycle by perhaps as much as 0.4 to 0.5 Å. Poor metal–macrocyclic ligand orbital overlap would undoubtedly result. Though bound to four nitrogen atoms and thus formally an 18-electron system, the Cu(I) atom might be better described as coordinatively unsaturated, sterically if not electronically. In contrast, more flexible ligands, as in 10, may better accommodate Cu(I), by producing a more tetrahedral environment.

Oxygen Reactivity

Four-coordinate $Cu(LBF_2)$ (6) is very oxygen sensitive; royal blue acetone solutions rapidly turn yellow brown. The reaction is irreversible and is dependent on temperature, solvent, and electrolyte concentration. Oxidation products have thus far proven intractable but further work is in progress.

Conclusion

The four-coordinate Cu(I)–macrocyclic ligand complex reacts with certain monodentate ligands to give five-coordinate complexes. The available data are insufficient, but this unusual coordination number for Cu(I) may be partly explained by a rigid ligand environment imposed by the macrocycle. Certainly five-coordination for Cu(I) appears viable and worthy of further study. The complexes described herein are not purported to be accurate mimics of the active sites in any copper proteins.

Table X. Reference Electrode Data for Ferrocene Couple in Water, Acetonitrile, and Acetone

Solvent	$E°$, V	Correction, E', V[c]
Water	+0.400[a]	0.000
Acetonitrile	+0.043[b]	−0.043 + 0.400 = +0.357
Acetone	+0.078[b]	−0.078 + 0.400 = +0.322

[a] Vs. SHE. [b] Vs. Ag|$AgNO_3$ (0.1 M) with 0.1 M tetrabutylammonium perchlorate in acetonitrile. [c] Correction needed to bring measured potentials in acetonitrile, acetone originally vs. $Ag|Ag^+$ (0.1 M) in acetonitrile, to potentials vs. SHE.

Rather they suggest that consideration of Cu(I) active site structures must include the possibility of five-coordination. For example, the binuclear copper site in hemocyanin binds one CO. The carbonyl stretching frequency, $^{51}\nu_{CO}$ 2040–2060 cm^{-1}, indicates CO bound to only one Cu; however, that Cu atom could conceivably have as many as five ligands, including CO. Similarly, the resonance Raman spectra of Cu(II) "blue" copper proteins (type I) are interpretable in terms of five-coordination.[52] Since the "blue" copper proteins apparently serve primarily in electron transfer, it seems unlikely that drastic changes occur in the coordination sphere upon reduction of Cu(II) to Cu(I). In any case the present work would be consistent with five-coordination in the reduced, Cu(I), state as well.

Experimental Section

All operations requiring an inert atmosphere were performed in a Vacuum Atmospheres Dri-lab containing either N_2 or He. Electronic absorption spectroscopy (EAS) was performed on a Cary-14 automatic recording spectrometer while infrared spectra were obtained via KBr pellets or in CH_2Cl_2 solution on a Beckman IR-12 spectrometer.

Tetrabutylammonium perchlorate (Southwestern Analytical Chemicals) was dried exhaustively in vacuo before use. Spectroquality acetonitrile and acetone, dried over 4A molecular sieves, were used for cyclic voltammetry. All other solvents were reagent grade.

Electrochemistry. The apparatus used for constant potential electrolysis (CPE) and cyclic voltammetry consisted of Princeton Applied Research's Model 173 potentiostat-galvanostat coupled with Model 179 Digital coulometer, plus a ramp generator of our own design. For display purposes, both a storage oscilloscope and an X-Y recorder were available.

Constant potential electrolyses and cyclic voltammetry were done in a three compartment H-cell. The cell consisted of 25-mL sample and auxiliary compartments separated by a small center compartment, all separated by medium porosity sintered glass frits. In either CH_3CN or $(CH_3)_2CO$, the supporting electrolyte used was 0.1 M TBAP (tetrabutylammonium perchlorate). The $Ag|Ag^+$ reference electrode consisted of a silver wire immersed in an acetonitrile solution containing $AgNO_3$ (0.1 M) and TBAP (0.1 M), all contained in an 8-mm glass tube fitted on the bottom with a fine porosity sintered glass frit. To provide a more general reference, ferrocene's Fe(II)|Fe(III) couple[53] was examined in CH_3CN and $(CH_3)_2CO$. Table X gives measured data and the corrections which were used throughout this paper to adjust the potentials measured against $Ag|Ag^+$ to potentials vs. SHE.

Formal reduction potentials, E^f, were measured by cyclic voltammetry using the formula $E^f = (E_{p_a} + E_{p_c})/2$. The potentials so determined are approximate in that the systems examined did not display strict reversibility, nor were corrections made for diffusion coefficients.

Determination of Binding Constants. Equation 2 gives the equilibrium expression for the reaction of $Cu(LBF_2)$ (6) with ligands, L'. As a first approximation to the equilibrium constant for the formation of five-coordinate species, the equilibrium concentration constant is defined:

$$K_c = [Cu(LBF_2)L']/[Cu(LBF_2)][L'] \quad (3)$$

The equilibrium concentrations of the Cu complexes were determined by use of the Beer's law dependence of the $Cu(LBF_2)$ 677-nm band. It was assumed that $Cu(LBF_2)L'$ did not absorb appreciably at 677 nm. Therefore, when $Cu(LBF_2)$ reacted with L', ΔA ($A_{initial} - A_{equilibrium}$) was taken as a measure of $Cu(LBF_2)L'$ formed.

With L' = 1-MeIm, the cells used had measured pathlengths of about 1 mm. The short pathlength permitted relatively high concentrations of $Cu(LBF_2)$ to be used, thus minimizing decomposition due to residual dissolved oxygen. Preparation of solutions of $Cu(LBF_2)$ ($[Cu(LBF_2)]_{initial} \cong 8 \times 10^{-4}$ M) and addition of 1-MeIm ($[1\text{-MeIm}]_{initial} = 2 \times 10^{-3}$ to 1 M) was effected in the inert atmosphere chamber. The cells were closed with greased, glass stoppers and taped. Spectra were recorded to determine ΔA (677 nm). Measurements were made at 30 ± 2 °C. Only approximate isosbestic behavior was observed, most probably owing to the slight variation in pathlengths of the several cells employed (e.g., see Figure 3). If a 1:1 stoichiometry for adduct formation is assumed (eq 2), the constant K_c is found to be 16 ± 3 M^{-1}.

For CO measurements, the cells used each had approximately 1-mm pathlengths, a 10-mL side-arm reservoir, a Teflon high-vacuum stopper, and a standard taper joint for attachment to a vacuum line. The $Cu(LBF_2)$ ($[Cu(LBF_2)]_{initial} \cong 1.6 \times 10^{-3}$ M) solutions were prepared in the inert atmosphere chamber and closed to the atmosphere. The solutions were then degassed by the freeze-pump-thaw technique (3 cycles) on the vacuum line. The spectra were measured before addition of CO.

The $Cu(LBF_2)$ solution was opened to a system with a mercury manometer and an acetone reservoir. The acetone vapor pressure was measured when the system had equilibrated. Addition of CO (10–80 mmHg) was monitored by use of the manometer. The $Cu(LBF_2)$ solution was stirred under CO for 20 min and the pressure and temperature were then recorded. The spectra were recorded in order to find ΔA (677 nm). A plot of $[Cu(LBF_2)(CO)]/[Cu(LBF_2)]$ vs. P(CO) was extrapolated to give $P_{1/2}(CO) = 1.5$ mm when the $[Cu(LBF_2)(CO)] = [Cu(LBF_2)]$. The equilibrium (pressure) constant, K_p, was calculated as 500 ± 15 atm^{-1}.

Conversion of K_p to K_c for the purpose of comparison to K_c (1-MeIm) utilized data for CO solubility in acetone. Use of a value of 0.2358 mL of CO per mL of acetone at 20 °C[54] and of Henry's law allowed conversion of P(CO) to [CO]. Calculation of K_c resulted in a value of $4.7 \pm 0.2 \times 10^4$ M^{-1}.

The CO binding constant $K_c(CO)$ was also estimated via the shift in E^f. Cyclic voltammograms of the Cu(II) complex **5** (acetone/Hg) under 1 atm of CO showed a shift of E^f of 0.168 V vs. that found under N_2 (Table IX). Such shifts can be related to the binding of ligand to metal in both the oxidized and the reduced state.[49] A simplified relationship can be derived for the case in which ligand binds, effectively, to only one oxidation state, e.g., eq 4.

$$[Cu(LBF_2)]^+ + CO + e^- \rightleftharpoons [Cu(LBF_2)(CO)] \quad (4)$$

In this equation

$$E°_{(CO)} = E° + (RT/F) \ln (1 + K_c[CO])$$

$E°$ and $E°_{(CO)}$ are the standard potentials for the reduction in the absence and presence of CO, respectively. The equilibrium constant K_c was calculated using the appropriate formal potentials E^f in place of the standard potentials $E°$.

X-Ray Data Collection. Crystals of the carbonyl adduct were grown by quick evaporation of an acetone solution under carbon monoxide. Weissenberg photographs revealed orthorhombic symmetry and systematic absences: $h = 2n + 1$, $hk0$ data; $k = 2n + 1$, $0kl$ data; $l = 2n + 1$, $h0l$ data. These extinctions are consistent only with the space group *Pbca*.

A multifaceted crystal of dimensions 0.15 mm × 0.15 mm × 0.30 mm was positioned on a Datex-automated General Electric quarter-circle diffractometer with the [001] direction nearly coincident with the ϕ axis of the diffractometer. The lattice parameters (Table I) were determined by a least-squares fit of 14 manually centered reflections. Data were collected out to $2\theta_{max} = 130°$ above which only a small number of the reflections had measurable intensity. The scan widths were varied linearly from 1.80° at $2\theta = 3°$ to 3.50° at $2\theta = 130°$. The scan speed was 2° min^{-1}. Intensities of 2738 reflections were measured by the moving-crystal, moving-counter techniques using a takeoff angle of 3°. The total background time was 40 s. Three reflections measured every 25 reflections served to monitor crystal and instrumental stability. No significant falloff in the intensities of these reflections was observed.

The measured intensities were reduced to structure factor amplitudes by applying Lorentz and polarization corrections. The standard deviations in the intensities were calculated from the formula: $\sigma^2(I) = S + (B1 + B2)T^2 + (dS)^2$, where S, $B1$, and $B2$ are the scan counts and two background counts, T is a factor which corrects for the difference in time spent on the scan and background counts, and d is the Peterson-Levy[55] factor taken to be 0.02. For the purpose of an absorption correction, the shape of the crystal was approximated by a rectangular prism.

Solution and Refinement of the Structure. The position of the copper atom was determined from a three-dimensional Patterson map. Difference-Fourier syntheses revealed the positions of all the other nonhydrogen atoms. Full-matrix isotropic refinement[56] with data out to 100° in 2θ lowered the R factor to 10%. At this point hydrogen atoms were included. After additional least-squares, a systematically negative disparity between the observed and calculated structure factors was noted. A secondary extinction parameter was included in the refinement as a correction.[61] Least-squares refinement was continued to convergence with two matrices; one matrix contained all nonhydrogen atom coordinates and anisotropic temperature factors, the other contained coordinates of the hydrogen atoms. Isotropic thermal parameters of the hydrogen atoms were fixed at the value of the carbon atom to which they were bonded plus 1.0 Å^2. The R factor[62] at the end of the refinement was 5.5% for 2511 data ($F_o^2 > 0$). No observations other than systematically absent reflections were omitted from the refinement. The goodness of fit was 1.39. A final difference-Fourier synthesis showed no residual electron density greater than 0.34 e Å^{-3}.

Final positional parameters are given in Table VI. Table VII lists the anisotropic thermal parameters.

Preparation of Complexes. 3,3'-(Trimethylenedinitrilo)bis(2-butanone oxime), H_2L (1). 1,3-Propanediamine (37.06 g, 0.5 mol) and 2,3-butanedione monoxime (101.0 g, 1.0 mol) were mixed together in hot ethanol to give a yellow solution approximately 250 mL volume. The solution was allowed to cool to ambient temperature. The resulting white precipitate was isolated immediately by vacuum filtration, washed well with diethyl ether, and dried in air. The ligand was used without further purification.

[3,3'-(Trimethylenedinitrilo)bis(2-butanone oximato)]copper(II) Perchlorate Monohydrate, $(Cu(LH)ClO_4 \cdot H_2O$ (2). A hot acetone solution (20 mL) of $Cu(ClO_4)_2 \cdot xH_2O$ (dried in vacuo at 25 °C, 3.7 g, 10 mmol) was added to a hot acetone solution of the ligand, H_2L, **1** (4.8 g, 20 mmol, in 20 mL), giving a deep red solution. As the solution cooled, a dark red-brown crystalline product precipitated. The solid was isolated by vacuum filtration, washed with diethyl ether, and dried in air. Anal. Calcd for $C_{11}H_{21}ClCuN_4O_7$: C, 31.45; H, 5.00; N, 13.3; Cu, 15.1. Found: C, 31.55; H, 4.75; N, 13.3; Cu, 16.0.

Millimolar solutions of this compound were examined by cyclic voltammetry. A quasireversible wave, complicated by a copper stripping wave, yielded an $E^f \approx 0.56$ V. Constant potential electrolysis at −0.8 V caused the purple solution to become blue with a small amount of copper being plated out on the platinum working electrode. The n values were slightly greater than 1.

Bis[difluoro-3,3'-(trimethylenedinitrilo)bis(2-butanone oximato)boratecopper(II) Perchlorate] Monodioxane, $(Cu(LBF_2)ClO_4)_2 \cdot C_4H_8O_2$ (5). Boron trifluoride etherate, $BF_3 \cdot Et_2O$ (6 mL, 50 mmol), was added slowly, with stirring, to a mixture of $Cu(LH)ClO_4 \cdot H_2O$ (2) (7.0 g, 17 mmol) in warm dioxane (150 mL, 70 °C). The mixture was heated, with stirring, at a boil for 1 h. The red-violet mixture was cooled slowly to ambient temperature. Dark red-violet solid was isolated by vacuum filtration, washed well with dioxane and diethyl ether, and dried in air. The product was dissolved in a minimum amount of boiling acetone (150 mL). The hot solution was filtered and treated with 5 mL of dioxane. Crystalline product, obtained upon cooling, was isolated and treated as before. A yield of 5.3 g (64%) was obtained. Anal. Calcd for $C_{26}H_{44}B_2Cl_2Cu_2F_4N_8O_{14}$: C, 31.6; H, 4.45; N, 11.35; Cu, 12.85. Found: C, 31.9; H, 4.5; N, 11.25; Cu, 12.6.

[Difluoro-3,3'-(trimethylenedinitrilo)bis(2-butanone oximato)borate]copper(I), $Cu(LBF_2)$ (6). This copper(I) complex was prepared by constant potential electrolysis in a He atmosphere chamber. A simple H-cell was employed with 0.1 M TBAP in acetone in all three chambers. The Cu(II) complex $[Cu(LBF_2)ClO_4]_2 \cdot C_4H_8O_2$, (5) (0.8 g, 15 mmol) was dissolved in the cathodic compartment which also contained a magnetic stir bar and a platinum gauze electrode. A self-contained $Ag|Ag^+$ reference electrode was placed in the middle chamber while a platinum wire was employed in the anodic chamber. Constant potential electrolysis was carried out at −1.0 V vs. $Ag|Ag^+$ (−0.678 V vs. SHE; see Table X) until the current was 1% of the initial value. During electrolysis, red $Cu(LBF_2)$ (6) crystallized from solution. The product was isolated by vacuum filtration, washed with ethanol, and dried under He. Anal. Calcd for $C_{11}H_{18}BCuF_2N_4O_2$: C, 37.65; H, 5.15; N, 16.0; Cu, 18.1. Found: C, 37.8; H, 5.1; N, 16.1; Cu, 18.2; ϵ(acetone, 25 °C, 677 nm) = 1.03 ± 0.02 × 10^4 M^{-1} cm^{-1}. A magnetic susceptibility measurement by the Faraday method showed the compound to be diamagnetic at 25 °C.

Carbonyl[difluoro-3,3'-(trimethylenedinitrilo)bis(2-butanone oximato)borate]copper(I), $Cu(LBF_2)(CO)$ (8). A blue solution of $Cu(LBF_2)$ (6) (0.35 g, 10 mmol) in acetone (25 mL) under N_2 was treated with CO (1 atm) yielding a greenish-yellow solution with some green solid. The green solid was removed by filtration and the resulting filtrate was treated with slow additions of heptane. The resulting orange crystalline product was isolated by filtration and dried under a stream of CO. Anal. Calcd for $C_{12}H_{18}BCuF_2N_4O_3$: C, 38.05; H, 4.75; N, 14.8; Cu, 16.8. Found: C, 38.1; H, 4.9; N, 14.7; Cu, 17.1.

[Difluoro-3,3'-(trimethylenedinitrilo)bis(2-butanone oximato)borate](1-methylimidazole)copper(I), $Cu(LBF_2)$(1-MeIm) (7). 1-Methylimidazole (0.1 g, 1.2 mmol) was added under nitrogen to a blue solution of $Cu(LBF_2)$ (6) (0.1 g, 0.2 mmol) in acetone (15 mL). A dark emerald-green solution resulted. Aliquots of heptane (5 mL) were added every 10 min until 30 mL total had been added. After 2 h, red crystalline product (red even when ground to a powder) was isolated by vacuum filtration, washed with 1:1 acetone:heptane, and dried under N_2. Anal. Calcd for $C_{15}H_{24}BCuF_2N_6O_2$: C, 41.6; H, 5.55; N, 19.4; Cu, 14.7. Found: C, 42.0; H, 5.55; N, 19.6; Cu, 14.4.

Note Added in Proof. Crystallographic analysis shows complex 6 to contain essentially square-planar Cu(I) with the four-coordinated nitrogen atoms distorted slightly toward tetrahedrality.[63]

Acknowledgment. We appreciate the assistance of F. Anson, G. Mauk, J. Fujitaki, and J. Koval. This work was supported by the National Institutes of Health and the National Science Foundation.

Supplementary Material Available: Listing of structure factor amplitudes (11 pp). Ordering information is given on current masthead page.

References and Notes

(1) J. Peisach, P. Aisen, and W. E. Blumberg, "The Biochemistry of Copper", Academic Press, New York, N.Y., 1966.
(2) W. H. Vanneste and A. Zuberbuhler in "Molecular Mechanisms of Oxygen Activation," O. Hayaishi, Ed., Academic Press, New York, N.Y., 1974, p 371
(3) R. Malkin in "Inorganic Biochemistry", G. L. Eichhorn, Ed., Elsevier, New York, N.Y., 1973, p 689.
(4) In certain copper-containing proteins the copper appears to serve principally in electron transport with no evidence of Cu–O_2 interaction, e.g., as in cytochrome oxidase.[5] In contrast hemocyanin[6–8] and tyrosinase[9] apparently rely on direct, covalent interaction between Cu(I) and O_2, both forming observable dioxygen adducts. The four-copper protein, laccase, may also rely on covalent interaction between O_2 and a binuclear, type III, Cu site.[10–12]
(5) W. S. Caughey, W. J. Wallace, J. A. Volpe, and S. Yoshikawa, *Enzymes*, **12**, 299 (1975).
(6) K. E. Van Holde and E. F. J. Van Bruggen in "Biological Macromolecules Series", Vol. 5, S. M. Timasheff and G. D. Fasman, Ed., Marcel Dekker, New York, N.Y., 1971.
(7) R. Lontie and R. Witters in ref 3, p 344.
(8) J. Bonaventura, C. Bonaventura, and B. Sullivan, *J. Exp. Zool.*, **194**, 155 (1975).
(9) (a) R. L. Jolley, Jr., L. H. Evans, and H. S. Mason, *Biochem. Biophys. Res. Commun.*, **46**, 878 (1972); (b) R. L. Jolley, Jr., L. H. Evans, N. Makino, and H. S. Mason, *J. Biol. Chem.*, **249**, 335 (1974).
(10) R. Aasa, R. Branden, J. Deinum, B. G. Malmstrom, B. Reinhammar, and T. Vanngard, *FEBS Lett.*, **61**, 115 (1976).
(11) R. Branden and J. Deinum, *FEBS Lett.*, **73**, 144 (1977).
(12) O. Farver, M. Goldberg, D. Lancet, and I. Pecht, *Biochem. Biophys. Res. Commun.*, **73**, 494 (1976).
(13) B. Reinhammar, *Biochim. Biophys. Acta*, **205**, 35 (1970).
(14) K. Lerch, *FEBS Lett.*, **69**, 157 (1976).
(15) A. J. M. Schoot Uiterkamp, H. VanDerDeen, H. C. J. Berendsen, and J. F. Boss, *Biochim. Biophys. Acta*, **372**, 407 (1974).
(16) A. J. M. Schoot Uiterkamp, *FEBS Lett.*, **20**, 93 (1972).
(17) A. J. M. Schoot Uiterkamp and H. S. Mason, *Proc. Natl. Acad. Sci. U.S.A.*, **70**, 993 (1973).
(18) N. Makino, P. McMahill, H. S. Mason, and T. H. Moss, *J. Biol. Chem.*, **249**, 6662 (1974).

(19) E. I. Solomon, D. M. Dooley, R.-H. Wang, H. B. Gray, M. Cerdonio, F. Mogno, and G. L. Romani, *J. Am. Chem. Soc.*, **98**, 1029 (1976).
(20) T. H. Moss, D. C. Gould, A. Ehrenberg, J. S. Loehr, and H. S. Mason, *Biochemistry*, **12**, 2444 (1973).
(21) Y. Engelborghs, S. H. DeBruin, and R. Lontie, *Biophys. Chem.*, **4**, 343 (1976).
(22) B. Salvato, A. Ghiretti-Magaldi, and F. Ghiretti, *Biochemistry*, **13**, 4778 (1974).
(23) J. S. Loehr, T. B. Freedman, and T. M. Loehr, *Biochem. Biophys. Res. Commun.*, **56**, 510 (1974).
(24) T. B. Freedman, J. S. Loehr, and T. M. Loehr, *J. Am. Chem. Soc.*, **98**, 2809 (1976).
(25) R. H. Jardine, *Adv. Inorg. Biochem.*, **17**, 115 (1975).
(26) There are several reports of reversible oxygenation in solution or complexes whose stoichiometry implies possible dioxygen complexation, but these are poorly characterized. See (a) T. Graf and S. Fallab, *Experientia*, **20**, 46 (1964); (b) E. Ochiai, *Inorg. Nucl. Chem. Lett.*, **9**, 987 (1973); (c) C. E. Kramer, G. Davies, R. B. Davis, and R. W. Slaven, *J. Chem. Soc., Chem. Commun.*, 606 (1975); (d) C. S. Arcus, J. L. Wilkinson, C. Mealli, T. J. Marks, and J. A. Ibers, *J. Am. Chem. Soc.*, **96**, 7564 ([974(/
(27) R. W. Erskine and B. O. Field in "Structure and Bonding", Vol. 28, Springer-Verlag, New York, N.Y., 1976, p 1.
(28) A. V. Savitskii and V. I. Nelyubin, *Russ. Chem. Rev.*, **44**, 110 (1975).
(29) J. S. Valentine, *Chem. Rev.*, **73**, 235 (1973).
(30) V. J. Choy and C. J. O'Connor, *Coord. Chem. Rev.*, **9**, 145 (1972–73).
(31) R. R. Gagné, *J. Am. Chem. Soc.*, **98**, 6709 (1976).
(32) For an excellent review see: W. E. Hatfield and R. Whyman, *Trans. Metal Chem.*, **5**, 47 (1969).
(33) F. A. Cotton and G. Wilkinson in "Advanced Inorganic Chemistry", 3rd ed, Interscience, New York, N.Y., 1972, p 905.
(34) G. S. Patterson and R. H. Holm, *Bioinorg. Chem.*, **4**, 257 (1975).
(35) D. C. Olson and J. Vasilevskis, *Inorg. Chem.*, **10**, 463 (1971).
(36) There are notable exceptions; see ref 37–39.
(37) M. I. Bruce and A. P. P. Ostazewski, *J. Chem. Soc., Dalton Trans.*, 2433 (1973).
(38) C. Mealli, C. S. Arcus, J. L. Wilkinson, T. J. Marks, and J. A. Ibers, *J. Am. Chem. Soc.*, **98**, 711 (1976).
(39) R. R. Gagné, L. Speltz, and R. Gall, manuscript in preparation.
(40) E. Uhlig and M. Friedrich, *Z. Anorg. Allg. Chem.*, **343**, 299 (1966).
(41) R. M. Countryman, W. T. Robinson, and E. Sinn, *Inorg. Chem.*, **13**, 2013 (1974).
(42) Another quasireversible wave, which is comparable in size to the wave depicted in Figure 1, appears at far more negative potentials, $E^{1} \simeq -1.2$ V. This process may be attributable to reduction of the ligand.
(43) F. Bigoli, A. Braibanti, A. Tiripicchio, and M. Tiripicchio Camellini, *Chem. Commun.*, 120 (1970), for example.
(44) M. R. Churchill, B. G. DeBoer, F. J. Rotella, O. M. Abu Salah, and M. I. Bruce, *Inorg. Chem.*, **14**, 2051 (1975).
(45) (a) J. P. Collman, P. A. Christian, S. Current, P. Denisevich, T. R. Halbert, E. R. Schmittou, and K. O. Hodgson, *Inorg. Chem.*, **15**, 223 (1976); (b) S. Bruckner, M. Calligaris, G. Nardin, and L. Randaccio, *Inorg. Chim. Acta*, **3**, 278 (1969).
(46) I. B. Liss and E. O. Schlemper, *Inorg. Chem.*, **14**, 3035 (1975).
(47) (a) J. P. Collman and M. R. MacLaury, *J. Am. Chem. Soc.*, **96**, 3019 (1974); (b) J. P. Collman, D. W. Murphy, and G. Dolcetti, *Ibid.*, **95**, 2687 (1973).
(48) The standard deviation of the mean is calculated by the formula $[\sum^{N}_{i=1}(X_i - \bar{X})^2/N-1)]^{1/2}$.
(49) J. Heyrovski and J. Kuta, "Principles of Polarography", Academic Press, New York, N.Y., 1966, p 157.
(50) R. R. Gagné, C. Koval, T. Smith, and M. Cimolino, manuscript in preparation.
(51) (a) L. Y. Fager and J. O. Alben, *Biochemistry*, **11**, 4786 (1972); (b) J. O. Alben, L. Yen, and N. J. Farrier, *J. Am. Chem. Soc.*, **92**, 4475 (1970).
(52) V. Miskowski, S.-P. W. Wang, T. G. Spiro, E. Shapiro, and T. H. Moss, *Biochemistry*, **14**, 1244 (1975).
(53) D. Baner and M. Breant, in "Electroanalytical Chemistry", Vol. VIII, A. J. Bard, Ed., Marcel Dekker, New York, N.Y., 1975, p 306.
(54) J. Horiuti, *Sci. Pap. Inst. Phys. Chem. Res. (Jpn.)*, **17**, 125 (1931).
(55) S. W. Peterson and H. A. Levy, *Acta Crystallogr.*, **10**, 70 (1957).
(56) Except for C. K. Johnson's ORTEP program, the computer programs used were from the CRYM system of crystallographic computer programs. The function minimized in the least-squares refinement was $\sum w(F_o^2 - F_c^2)^2$ where F_o and F_c are the observed and calculated structure factors and the weights, w, are $1/\sigma^2(F_o^2)$. Neutral atom scattering factors for Cu were taken from the compilation of Cromer and Waber;[57] those for the other nonhydrogen atoms were from ref 58. Hydrogen atom scattering factors are those of Stewart et al.[59] The real component of the anomalous dispersion correction[60] was included for Cu.
(57) D. T. Cromer and J. T. Waber, *Acta Crystallogr.*, **18**, 104 (1965).
(58) "International Tables for X-Ray Crystallography", Vol. III, Kynoch Press, Birmingham, England, 1962.
(59) R. F. Stewart, E. R. Davidson, and W. T. Simpson, *J. Chem. Phys.*, **42**, 3175 (1965).
(60) D. T. Cromer, *Acta Crystallogr.*, **18**, 17 (1965).
(61) The form of the correction for secondary extinction is $F_c = F_o(1 + cI_c)$. The value from the refinement is $2.00\ (9) \times 10^{-8}\ e^{-2}$.
(62) The R index is $\sum||F_o| - |F_c||/\sum|F_o|$. The goodness of fit is $\sum w(F_o^2 - F_c^2)^2/(n - p)$, where n is the number of observations and p is the number of parameters.
(63) R. R. Gagné, J. L. Allison, and G. Lisensky, manuscript in preparation.

References

(1) F. H. Jardine in "Advances in Inorganic and Radiochemistry," Vol. 17, H. J. Emeleus and A. G. Sharpe, Eds., Academic Press, New York, N.Y., 1975, p. 115.

(2) P. Murray-Rust in "Molecular Structure by Diffraction Methods," Vol. 5, L. E. Sutton and M. R. Truter, Senior Reporters, The Chemical Society, London, 1977, p. 352.

(3) D. M. Johns and C. A. McAuliffe in "Inorganic Chemistry of the Transition Elements," Vol. 5, B. F. G. Johnson, Senior Reporter, The Chemical Society, London, 1977, p. 275.

(4) A. Camus, N. Marsich, G. Nardin, and L. Randaccio, Inorg. Chim. Acta, 23, 131 (1977).

(5) A. H. Lewin, R. J. Michl, P. Ganis, and U. Lepore, J. Chem. Soc., Chem. Commun., 661 (1972).

(6) I. Csöregh, P. Kierkegaard, and R. Norrestam, Acta Crystallogr., Sect. B, 31, 314 (1975).

(7) R. R. Gagné, J. Am. Chem. Soc., 98, 6709 (1976).

(8) R. R. Gagné, J. L. Allison, R. S. Gall, and C. A. Koval, J. Am. Chem. Soc., 99, 7170 (1977).

(9) See, for example, a) V. Schramm, Inorg. Chem., 17, 714 (1978); b) G. vanKoten and J. G. Noltes, J. Organomet. Chem., 102, 551 (1975); c) M. R. Churchill, S. A. Bezman, J. A. Osborn, and J. Wormald, Inorg. Chem., 11, 1818 (1972); d) S. L. Lawton, W. J. Rohrbaugh, and G. T. Kokotailo, Inorg. Chem., 11, 612 (1972); and e) J. M. Guss, R. Mason, I. Sotofte, G. vanKoten, and J. G. Noltes, J. Chem. Soc., Chem. Commun., 446 (1972).

(10) P. K. Mehrotra and R. Hoffmann, Inorg. Chem., 17, 2187 (1978).

(11) F. J. Hollander and D. Coucouvanis, J. Am. Chem. Soc., 99, 6268 (1977).

(12) A. Avdeef and J. P. Fackler, Jr., Inorg. Chem., 17, 2182 (1978).

(13) G. Struckmeier, U. Thewalt, and J.-H. Fuhrhop, J. Am. Chem. Soc., 98, 278 (1976).

(14) D. P. Freyberg, G. M. Mockler, and E. Sinn, J. Chem. Soc., Dalton Trans., 447 (1976).

(15) D. H. Busch, K. Farmery, V. Goedken, V. Katovic, A. C. Melnyk, C. R. Sperati, and N. Tokel in "Bioinorganic Chemistry," Advances in Chemistry Series, Vol. 100, R. F. Gould, Ed., American Chemical Society, Washington, D.C., 1971, p. 52.

(16) D. C. Olson and J. Vasilevskis, Inorg. Chem., 10, 463 (1971).

(17) V. L. Goedken and D. H. Busch, J. Am. Chem. Soc., 94, 7355 (1972).

(18) G. A. Melson and D. H. Busch, J. Am. Chem. Soc., 86, 4834 (1964).

(19) V. Katovic, L. T. Taylor, F. L. Urbach, W. H. White, and D. H. Busch, Inorg. Chem., 11, 479 (1972).

(20) N. Takvoryan, K. Farmery, V. Katovic, F. V. Lovecchio, E. S. Gore, L. B. Anderson, and D. H. Busch, J. Am. Chem. Soc., 96, 731 (1974).

(21) E. Uhlig and M. Friedrich, Z. Anorg. Allg. Chem., 343, 299 (1966).

(22) G. Costa and G. Mestroni, Tetrahedron Lett., 41, 4005 (1967).

(23) D. W. Murphy, Ph.D. Dissertation, Stanford University, 1972.

(24) M. R. Churchill, B. G. DeBoer, F. J. Rotella, O. M. Abu Salah, and M. I. Bruce, Inorg. Chem., 14, 2051 (1975).

(25) M. Pasquali, F. Marchetti, and C. Floriani, Inorg. Chem., 17, 1684 (1978).

(26) M. Pasquali, C. Floriani, A. Gaetani-Manfredotti, and C. Guastini, submitted for publication.

(27) L. Sacconi, Coord. Chem. Rev., 8, 351 (1972).

(28) K. Henrick, R. W. Matthews, and P. A. Tasker, Inorg. Chem., 16, 3293 (1977).

(29) O. P. Anderson and J. C. Marshall, Inorg. Chem., 17, 1258 (1978).

(30) See,for example, a) R. J. Dudley and B. J. Hathaway, J. Chem. Soc., A, 1442 (1971) and b) O. P. Anderson, A. B. Packard, and M. Wicholas, Inorg. Chem., 15, 1613 (1976).

(31) D. T. Cromer and A. C. Larson, Acta Crystallogr., 15, 397 (1962).

(32) C. Kappenstein and R. P. Hugel, Inorg. Chem., 16, 250 (1977).

(33) D. T. Cromer and A. C. Larson, Acta Crystallogr., Sect. B, 28, 1052 (1972).

(34) D. T. Cromer, A. C. Larson, and R. B. Roof, Acta Crystallogr,, 20, 279 (1966).

(35) C. Kappenstein and R. P. Hugel, Inorg. Chem., 17, 1945 (1978).

(36) R. B. Roof, A. C. Larson, and D. T. Cromer, Acta Crystallogr., Sect. B., 24, 269 (1968).

(37) J. A. J. Jarvis, R. Pearce, and M. F. Lappert, J. Chem. Soc., Dalton Trans., 999 (1977).

(38) I. D. Brown and J. D. Dunitz, Acta Crystallogr., 14, 480 (1961).

(39) C. Mealli, C. S. Arcus, J. L. Wilkinson, T. J. Marks, and J. A. Ibers, J. Am. Chem. Soc., 98, 711 (1976).

(40) J. F. Blount, H. C. Freeman, P. Hemmerich, and C. Sigwart, Acta Crystallogr., Sect. B, 25, 1518 (1969).

(41) A. H. Lewin, R. J. Michl, P. Ganis, U. Lepore, and G. Avitabile, J. Chem. Soc., Chem. Commun., 1400 (1971).

(42) S. R. Hall, D. L. Kepert, C. L. Raston, and A. H. White, Aust. J. Chem., 30, 1955 (1977).

(43) R. Graziani, G. Bombieri, and E. Forsellini, J. Chem. Soc., A, 2331 (1971).

(44) M. I. Bruce and A. P. P. Ostazewski, J. Chem. Soc., Dalton Trans., 2433 (1973).

(45) M. I. Bruce, J. Organomet. Chem., 44, 209 (1972).

(46) W. England, L. S. Salmon, and K. Ruedenberg, in "Topics in Current Chemistry: Molecular Orbitals," Vol. 23, Springer-Verlag, New York, N.Y., 1971, p. 54f.

(47) R. D. Cowan, J. Chem. Phys., 18, 1101 (1950).

(48) R. D. Mounts, T. Ogura, and Q. Fernando, Inorg. Chem., 13, 802 (1974).

(49) M. G. B. Drew, D. A. Edwards, and R. Richards, J. Chem. Soc., Chem. Commun., 124 (1973).

(50) E. R. Dockal, L. L. Diaddario, M. D. Glick, and D. R. Rorabacher, J. Am. Chem. Soc., 99, 4530 (1977).

(51) J. P. Collman, P. A. Christian, S. Current, P. Denisevich, T. R. Halbert, E. R. Schmittou, and K. O. Hodgson, Inorg. Chem., 15, 223 (1976).

(52) S. A. Best and R. A. Walton, Isr. J. Chem., 15, 160 (1976/77).

(53) D. C. Frost, C. A. McDowell, and R. L. Tapping, J. Electron Spectrosc. Relat. Phenom., 6, 347 (1975).

(54) W. Mialki and R. A. Walton, private communication.

(55) J. G. Dillard and L. T. Taylor, J. Electron Spectrosc. Relat. Phenom., 3, 455 (1974).

(56) K. S. Kim, J. Electron Spectrosc. Relat. Phenom., 3, 217 (1974).

(57) D. C. Frost, A. Ishitani, and C. A. McDowell, Mol. Phys., 24, 861 (1972).

(58) D. A. Edwards, Inorg. Chim. Acta, 18, 65 (1976).

(59) G. L. Burce. E. B. Paniago, and D. W. Margerum, J. Chem. Soc., Chem. Commun., 261 (1975).

(60) D. R. Crow, "Polarography of Metal Complexes," Academic Press, New York, N.Y., 1969.

(61) Y. M. Kargin, E. V. Nikitin, G. V. Romanov, O. V. Parakin, B. S. Mironov, and A. N. Pudovik, Dokl. Acad. Nauk SSSR, 226, 1101 (1976).

(62) G. Schiavon, S. Zecchin, G. Cogoni, and G. Bontempelli, J. Electroanal. Chem. Interfacial Electrochem., 48, 425 (1973).

(63) J. Heyrovsky and J. Kuta, "Principles of Polarography," Academic Press, New York, N.Y., 1966.

(64) J. E. Huheey, "Inorganic Chemistry, Principles of Structure and Reactivity," Harper and Row, New York, N.Y., 1972, p. 353.

(65) C. A. Tolman, J. Am. Chem. Soc., 92, 2956 (1970).

(66) C. A. Tolman, J. Am. Chem. Soc., 92, 2953 (1970).

(67) A. J. Gordon and R. A. Ford, "The Chemist's Companion," John Wiley, New York, N.Y., pp. 144-155.

(68) A. W. Addison, M. Carpenter, L. K. -M. Lau, and M. Wicholas, Inorg. Chem., 17, 1545 (1978).

(69) R. R. Gagné, C. A. Koval, and T. J. Smith, J. Am. Chem. Soc., 99, 8367 (1977).

(70) G. S. Patterson and R. H. Holm. Bioinorg. Chem., 4, 257 (1975).

(71) D. H. Busch, D. G. Pillsbury, F. V. Lovecchio, A. M. Tait, Y. Hung, S. Jackels, M. C. Rakowski, W. P. Schammel, and L. Y. Martin, in "American Chemical Society Symposium Series," Vol. 38, American Chemical Society, Washington, D.C., 1976, p. 32.

(72) I. W. Pang and D. V. Stynes, Inorg. Chem., 16, 2192 (1977).

(73) R. G. Pearson, Inorg. Chem., 12, 712 (1973).

(74) S. Ahrland, J. Chatt, and N. R. Davies, Quart. Rev., 12, 265 (1958).

(75) R. G. Pearson, J. Am. Chem. Soc., 85, 3533 (1963).

(76) S. Ahrland in "Structure and Bonding," Vol. 5, C. K. Jørgensen, J. B. Neilands, R. S. Nyholm, D. Reinen, and R. J. P. Williams, Eds., Springer-Verlag, New York, N.Y., 1968, p. 118.

(77) A. Pidcock, R. E. Richards, and L. M. Venanzi, J. Chem. Soc., A, 1707 (1966).

(78) C. K. Jørgensen, Inorg. Chem., 3, 1201 (1964).

(79) J. L. Burmeister and J. B. Melpolder, J. Chem. Soc., Chem. Commun., 613 (1973).

(80) F. A. Cotton and T. J. Marks, J. Am. Chem. Soc., 92, 5114 (1970).

(81) F. A. Cotton and G. Wilkinson, "Advanced Inorganic Chemistry," Interscience, New York, N.Y., 1972, p. 738.

(82) D. L. Cullen and E. F. Meyer, Acta Crystallogr., Sect. B, 32, 2259 (1976).

(83) M. Pasquali, C. Floriani, A. Gaetani-Manfredotti, and A. Chiesi-Villa, J. Am. Chem. Soc., 100, 4918 (1978).

(84) "Properties and Uses of Dimethylformamide," duPont, Industrial Chemicals Dept., Wilmington, DE., 1976.

(85) J. Horiuti, Sci. Pap. Inst. Phys. Chem. Res. (Jpn.), 17, 125 (1931).

(86) A. D. Hamer and R. A. Walton, Inorg. Chem., 13, 1446 (1974).

(87) W. E. Keyes, W. E. Swartz, and T. M. Loehr, Inorg. Chem., 17, 3316 (1978).

(88) H. Rupp and U. Weser, Bioinorg. Chem., 6, 45 (1976).

(89) L. I. Smith and J. W. Opie, Org. Syn., 28, 11 (1948).

(90) E. Uhlig and M. Friedrich, Z. Anorg. Allg. Chem., 343, 299 (1966).

(91) A. F. Ferris, J. Org. Chem., 24, 1726 (1959).

(92) D. Bauer and M. Breant in "Electroanalytical Chemistry," Vol. 8, A. J. Bard, Ed., Marcel Dekker, Inc., New York, N.Y., 1975, p. 300.

(93) H. A. Laitinen, "Chemical Analysis," McGraw-Hill, New York, N.Y., 1960, p. 286.

PROPOSITIONS

PROPOSITION 1

A New Type of Chemically Modified Electrode - The Attachment of Tertiary Phosphines to a Graphite Electrode

There is a great deal of research being done in the area of chemically modified electrodes (CME). Electrodes of graphite,(1-6), silicon (7), metal oxides (ruthenium, tin, titanium and indium) (8-11), and platinum (12,13) have been modified. The study of these modified electrodes has centered on surface analysis of the electrode and electrochemical analysis of the attached species. Far reaching goals of the research include the synthesis of electrodes which have specialized electron-transfer properties and which can catalytically or selectively react with a compound in solution. Success in reaching these goals is more likely if there exists a variety of compounds that can be successfully attached to an electrode surface. On graphite organic compounds (1,3,6) have been attached as well as nitrogenous bases which directly bind redox centers (2,4,5,14). Attachment of different redox centers to an electrode surface will result in different electrode properties. The ability to vary electrode properties will provide a path to electrodes which catalytically or selectively react with solution species. As a small step toward the long range goals, this proposition introduces synthetic procedures for the attachment of a new type of base, phosphines.

Phosphine ligands are very important in transition metal coordination chemistry (15). One of the most widely used phosphines is triphenylphosphine. Because the body of synthetic literature on phosphine ligands is huge (an introduction to general synthetic methods is given by I. Maier (16)), the synthesis of derivatized triphenylphosphine and related phosphines for electrode attachment is predictable. Graphite is to be used as an electrode material because of its known and previously utilized surface functionalities. Attachment to graphite's carboxylic acid functions (or to the derived acyl chlorides) will be accomplished using primary amines. The overall approach will be to attach a phosphine to the electrode and then introduce a metal complex that will bind to the phosphine and undergo an electrochemical change. Experimental details are not given, because the general approach is found in the literature (1-6).

As a first step, a simple triphenylphosphine-like compound will be attached to the electrode. The requirements of the phosphine include an amine function to react with the graphite surface and a stereochemistry which allows the phosphine lone pair to be accessible to the bulk solution. There are two phosphines in the literature which fulfill these requirements. Both the meta- and para-nitrophenylbiphenylphosphines have been synthesized (17,18). Reduction to the p-amine has been carried out (19). The meta isomer has a conformation in which the phosphorus lone pair is perpendicular to the electrode surface. The para isomer has many conformations in which the lone pair is about 30° from perpendicular. The attachment

to the graphite surface will be done in two ways. The amine ligands will be reacted both with air oxidized surface and with the thionyl chloride treated surface (1). There is precedent that the activity of these two surfaces will be identical (4). The phosphine modified surfaces (two different preparations with two amine ligands) will be compared by x-ray photoelectron spectroscopy (XPS) to the air oxidized and thionyl chloride treated controls. (All surfaces in this study will be examined by XPS.)

When the presence of phosphine which is not adsorbed is confirmed, a metal complex is introduced. The redox couple chosen is $[Fe(II/III)(CN)_5]^{3-/2-}$. The ferrous complex, $Na_3[Fe(CN)_5P(C_6H_5)_3]$, was synthesized from the amminepentakiscyano complex (20). The ferrous complex was oxidized to the ferric complex by bromine (20). Reaction of the modified electrode with $Na_2[Fe(CN)_5NH_3]$ will yield the ferrous complex attached to the electrode by phosphine.

Electrochemical studies are needed next to analyze the redox behavior of the system before more complicated surface modifications are proposed. Control experiments are needed. The redox behavior of the solution species $[Fe(CN)_5P(C_6H_5)_3]^{3-}$, and a complex more closely related to the attached iron complex, $[Fe(CN)_5P(C_6H_5)_2(C_6H_4NHCOC_6H_5)]^{3-}$, is determined by cyclic voltammetry. (The necessary phosphine, $P(C_6H_5)_2(C_6H_4NHCOC_6H_5)$, is synthesized by reaction of $MP(C_6H_5)_2$ (M = Li, Na, K) (16) and p-$BrC_6H_4NHCOC_6H_5$ (21).) The formal potentials of these solution complexes will be compared to the potentials of the modified electrodes.

Cyclic voltammetric measurements of the modified electrodes must include further controls to rule out adsorption of the ferrous complex. Treating an air-oxidized or $SOCl_2$-treated electrode with $Na_2[Fe(CN)_5NH_3]$ and then rinsing provides an electrode that should have no more electrochemical activity other than that of the electrode not treated with $Na_2[Fe(CN)_5NH_3]$. Therefore, cyclic voltammograms of the basic electrodes treated stepwise up to, but not including, iron treatment are needed for controls.

Finally, the redox behavior of the phosphine-iron chemically modified electrodes is determined. The electrochemical properties of the electrodes from the two different approaches (-COOH vs.-COCl) to the amide linkage are predicted to be the same (6). The stereochemically different electrodes from the para- and meta-substituted phenylphosphines will probably have similar behavior, but if one has greater ability to pass current, that isomer will be used for future modifications.

At this point, it should be clear that the surface of a graphite electrode (in -COOH and -COCl forms) reacts with amine-derivatized phenylphosphines. To make the attachment of phosphines more general a second approach to attaching $NH_2(C_6H_4)P(C_6H_5)_2$ to graphite is presented. The end product can be compared electrochemically to the other iron-phosphine electrode for an evaluation of the method.

To simplify, only the air-oxidized, not $SOCl_2$-treated, electrode will be used along with only one isomer of the phosphine. The second approach initially attaches the commercially available

$NH_2(C_6H_4)Br$ to the air-oxidized electrode. Then, addition of the alkali metal diphenylphosphine, $MP(C_6H_5)_2$ (M = Li, Na, or K, from $P(C_6H_5)_3$ and M(0) (16)), results in the earlier phosphine electrode surface by the reaction:

$$R - Br + MP(C_6H_5)_2 \longrightarrow RP(C_6H_5)_2 + MBr$$

When it has been established that the phosphine electrodes from (1) $NH_2(C_6H_4)P(C_6H_5)_2$ and electrode and (2) $NH_2(C_6H_4)Br$ and electrode, and $MP(C_6H_5)_2$ are the same, the general route to phosphine electrodes using MPR_1R_2 compounds is available.

A literature preparation of the alkali derivative, $LiP(C_6H_5)CH_2CH_3$ is known (22). The electrode with $R^{\phi}P(C_6H_5)CH_2CH_3$ (R^{ϕ} = phenyl group with amide linkage to surface) is of interest because it is a monodentate model for an attached bidentate phosphine compound. A bidentate surface modification can readily be made. The compound, $(C_6H_5)HPCH_2CH_2P(C_6H_5)_2$, has been synthesized (23). The metal phosphide is available by reaction with an alkali metal. The reaction of the electrode surface, E-$CONH(C_6H_4)Br$, and the metal phosphide, $(C_6H_5)MPCH_2CH_2P(C_6H_5)_2$, proceeds as outlined earlier.

A possible complex to be attached to the bidentate phosphine is a ruthenium(II) complex, $[Ru(CH_3CN)_4(C_8H_{12})](PF_6)_2$ (C_8H_{12} = 1,5-cyclooctadiene) (24). Reaction of this complex with $P(C_6H_5)_3$ or $P(C_6H_5)_2CH_3$ results in the formation of complexes of the formula $[Ru(CH_3CN)_4L_2](PF_6)_2$ (L = tertiary phosphine). Reaction of the

cyclooctadiene cation with a bidentate phosphine CME should give a ruthenium(II)-bidentate phosphine complex. The electrochemical behavior of this attached species can be investigated as before.

Solutions species to be electrochemically analyzed for comparative purposes are the known complexes $[Ru(CH_3CN)_4L_2](PF_6)_2$ ($L = P(C_6H_5)_3$ and $P(C_6H_5)_2CH_3$) and the complex with $L_2 = (C_6H_5)_2PCH_2CH_2P(C_6H_5)_2$ (25) which should form in a manner analogous to the monodentate phosphine complexes.

The following goals are to be met:

1. Finding a general pattern for the attachment of phosphine compounds to graphite;
2. Binding transition metals to the phosphines ligands on the electrode surface; and,
3. Predicting the electrochemical behavior of the attached metals with knowledge of solution species redox behavior.

A long range use of phosphine modified electrodes is for electrocatalytic hydrogenations. A report on electrocatalysis of hydrogenations using the heterogeneous catalysts platinum black and rhodium(III) chloride supported on carbon has appeared (26). Use of a homogeneous catalyst, e.g., $Rh(P(C_6H_5)_3)_3Cl$, attached to a graphite electrode has the advantages of providing an electrode with reproducible activity and a catalyst that is now heterogeneous. Such potential for phosphine modified electrodes will be difficult to realize, but the potential for synthesis of these electrodes is real.

References

(1) B. F. Watkins, J. R. Behling, E. Kariv, and L. L. Miller, J. Am. Chem. Soc., 97, 3549 (1975).

(2) C. M. Elliott and R. W. Murray, Anal. Chem., 48, 1247 (1976).

(3) M. Fujihira, A. Tamura, and T. Osa, Chem. Letters, 361 (1977).

(4) C. A. Koval and F. C. Anson, Anal. Chem., 50, 223 (1978).

(5) N. Oyama, A. P. Brown, and F. C. Anson, J. Electroanal. Chem., 87, 435 (1978), and 88, 289 (1978).

(6) A. M. Yacynych and T. Kuwana, Anal. Chem., 50, 640 (1978).

(7) M. S. Wrighton, R. G. Austin, A. B. Bocarsly, J. M. Bolts, O. Haas, K. D. Legg, L. Nadjo, and M. C. Palazzotto, J. Am. Chem. Soc., 100, 1602 (1978).

(8) P. R. Moses and R. W. Murray, J. Electroanal. Chem., 77, 393 (1977).

(9) P. R. Moses, L. Wier, and R. W. Murray, Anal. Chem., 47, 1882 (1975).

(10) B. E. Firth and L. L. Miller, J. Am. Chem. Soc., 98, 8272 (1976).

(11) P. R. Moses and R. W. Murray, J. Am. Chem. Soc., 98, 7435 (1976).

(12) J. R. Lenhard and R. W. Murray, J. Electroanal. Chem., 78, 195 (1977).

(13) M. S. Wrighton, R. G. Austin, A. B. Bocarsly, J. M. Bolts, O. Haas, K. D. Legg, L. Nadjo, and M. C. Palazzotto, J. Electroanal. Chem., 87, 429 (1978).

(14) J. C. Lennox and R. W. Murray, J. Electroanal. Chem., 78, 395 (1977).

(15) See, for example: O. Stelzer in "Topics in Phosphorus Chemistry," Vol. 9, E. J. Griffith and M. Grayson, Eds., Interscience, New York, N.Y., 1977, p. 1, and "Transition Metal Complexes of Phosphorus, Arsenic, and Antimony Ligands," C. A. McAuliffe, Ed., John Wiley, New York, N.Y., 1973.

(16) I. Maier in "Progress in Inorganic Chemistry," Vol. 5, F. A. Cotton, Ed., Interscience, New York, N.Y., 1963, p. 27.

(17) G. P. Schiemenz and K. Rohlk, Chem. Ber., 104, 1219 (1971).

(18) G. P. Schiemenz, Chem. Ber., 99, 514 (1966).

(19) G. P. Schiemenz and K. Rohlk, Chem. Ber., 104, 1722 (1971).

(20) R. Nast and K. W. Krüger, Z. Anorg. Allg. Chem., 341, 189 (1965).

(21) V. Knoppova, E. Komanova, K. Kada, A. Jurasek, and J. Kovac, Collect. Czech. Chem. Commun., 39, 3728 (1974).

(22) T. E. Snider, D. L. Morris, W. R. Purdum, G. A. Dildeck, and K. D. Berlin, Org. Prep. Proced. Int., 6, 221 (1974).

(23) J. C. Cloyd and R. B. King in "Inorganic Syntheses," Vol. 16, F. Basolo, Ed., McGraw-Hill, New York, N.Y., 1976, p. 202.

(24) T. V. Ashworth and E. Singleton, J. Organomet. Chem., 77, C31 (1974).

(25) J. Chatt and F. A. Hart, J. Chem. Soc., 1378 (1960).

(26) L. L. Miller and L. Christensen, J. Org. Chem., 43, 2059 (1978).

PROPOSITION 2

A Mechanistic Investigation into the Synthesis of Asymmetric Epoxides by Phase Transfer Catalysis

The synthesis of optically active compounds can be approached by several routes. Asymmetric reagents can react one-to-one with prochiral compounds to produce optically active products. Asymmetric centers already present in a starting compound can induce further reactions to occur asymmetrically. Chiral catalysts can promote the formation of one enantiomer over another. The last route is the preferable pathway because it requires the smallest amount of optically active reagent, which can be recovered at the end of a reaction.

All three routes have been used for the synthesis of optically active epoxides. The one-to-one reaction of prochiral alkenes and chiral peroxyacids produces low yields of optically active epoxides (1,2). The reaction of hydrogen peroxide and an asymmetric α,β unsaturated ketone forms one epoxide enantiomer preferentially (3). The phase transfer catalyzed reaction of α,β unsaturated ketones and hydrogen peroxide also promotes formation of one epoxide enantiomer over the other when a chiral quaternary ammonium salt catalyzes the reaction (4). Figure 1 summarizes this asymmetric synthesis.

The investigation of the mechanism of this catalytic asymmetric reaction is the subject of this proposition. If the mechanism of

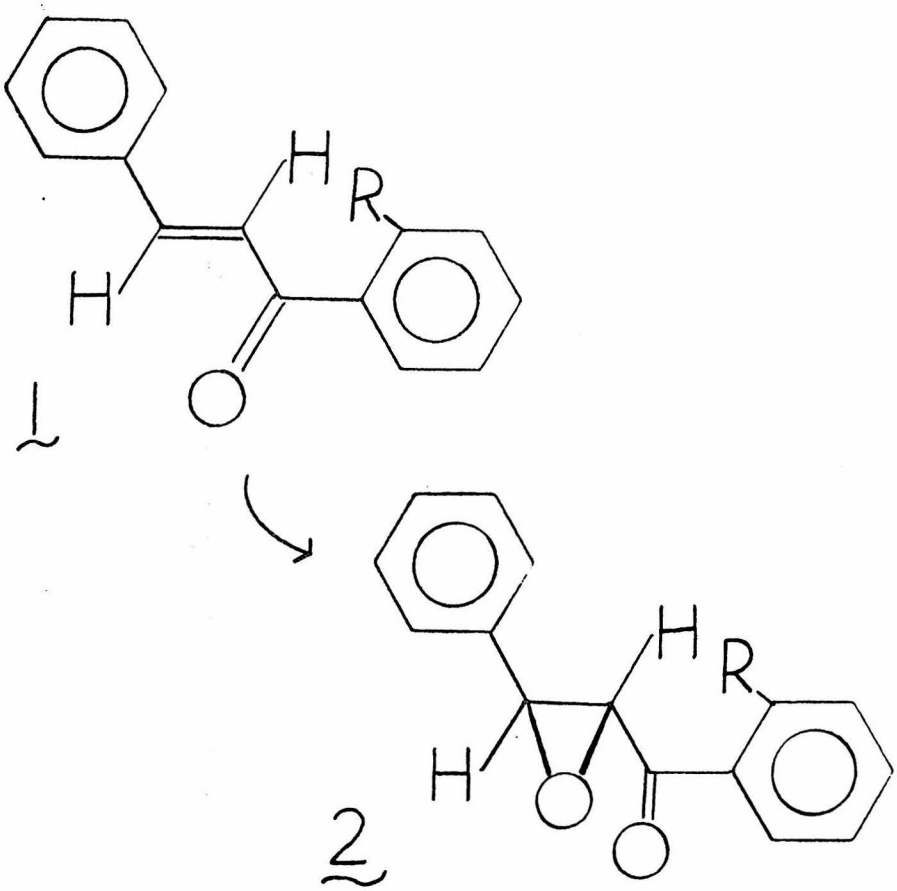

Figure 1

The reaction of the E-chalcone, 1, to give the optically active E-epoxide, 2, occurred with a 25% enantiomeric excess with the $ClCH_2(C_6H_5)$ salt of quinine, 3. Conditions for the phase transfer catalyzed reaction were: 30% aqueous H_2O_2, NaOH, and toluene with substrate 1.

the reaction is understood, optimization of the asymmetric selectivity is easier.

The formation of epoxides by the base-catalyzed reaction of electron-deficient alkenes and hydrogen peroxides is the Weitz-Scheffer reaction (5). The mechanism of the reaction has been investigated. The rate limiting step involves an attack on the β-position of an α,β unsaturated ketone by the nucleophile, O_2H^-, to form an enolate anion.

For a phase transfer catalyzed reaction the nucleophile will be the ion pair of the quaternary ammonium cation and O_2H^- (6). Evidence for an ion pair nucleophile for the reaction of Figure 1 comes from two sources. A change in absolute configuration of C1 and C2 (quinine, 3, to quinidine, 4, Figure 2) changes the optical rotation of the epoxide product (4). Also, the enantiomeric excess of the reaction increases with decreasing solvent dielectric constant (8). Since the force between two charged species varies with the reciprocal of the dielectric constant, the stronger ion pair produces an increased enantiomeric selectivity.

The predominant nucleophile in the epoxidation reaction is the ion pair, $\{Q^+O_2H^-\}$ (Q^+ = quaternary ammonium cation). A change in chirality at both C1 and C2 changes the product enantiomer. A hydrogen-bonding interaction between the anion O_2H^- and the alcohol function of carbon 1 is indicated. Whether or not the optical activity of the product epoxide is dependent on a -C-OH $\cdots$ O_2H^- hydrogen bond can be tested. A catalyst that varies from quinine

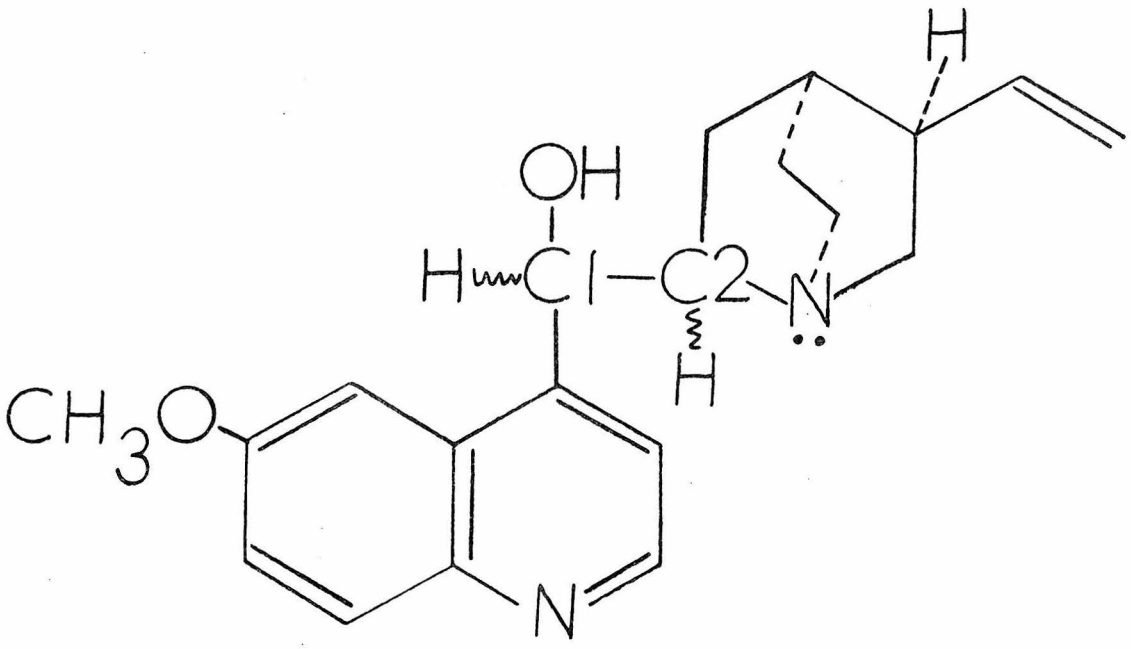

Figure 2

Alkaloids and their absolute configuration at C1 and C2.

Alkaloid	C1	C2
Quinine, 3 (7)	R	S
Quinidine, 4 (7)	S	R
Epiquinine, 5 (7)	S	S
Epiquinidine, 6 (7)	R	R
Chloroquinine, 7	R	S

solely at carbon 1, i.e., does not have an alcohol function on C1, should form epoxides that are not optically active. The optically similar chloro-derivative, chloroquinine, 7, can be synthesized from epiquinine, 5 (Figure 2) by the method of Klayman, et al. (9). This alkaloid will form a quaternary ammonium cation, which is incapable of forming a hydrogen bonded ion pair. The ion pair which the chloroquinine cation forms with O_2H^- is not stereospecifically formed and will not show the preference for one-sided attack of the alkene that is shown by the quinine cation-O_2H^- ion pair.

With the establishment of the necessity of a chiral alcoholic carbon, further mechanistic studies can be done. The forces directing the approach of a chiral ion pair, $\{Q^+O_2H^-\}$, specifically to one side of the alkene can be based on steric or charge effects. The approach of the ion pair to the β-end of the alkene can be visualized as in Figure 3A. The emphasis is on carbon 1 because of the known importance of its configuration to the optical activity of the product. An enolate intermediate for the specific alkene, E-1,3-diphenylpropen-3-one, is shown in Figure 4A. The arrangement of the three substituents, H, R, and +C2, with respect to the alkene substituents will determine the enantiomeric selectivity. By the steric requirements of the three substituents (decreasing bulkiness: +C2 > R > H) the arrangement of Figure 4B is least strained. The approach to the face shown is preferred by quinidine on steric considerations. On the other hand, if there is stabilization by a (-)/(+) interaction as in Figure 4C, quinine will preferably attack

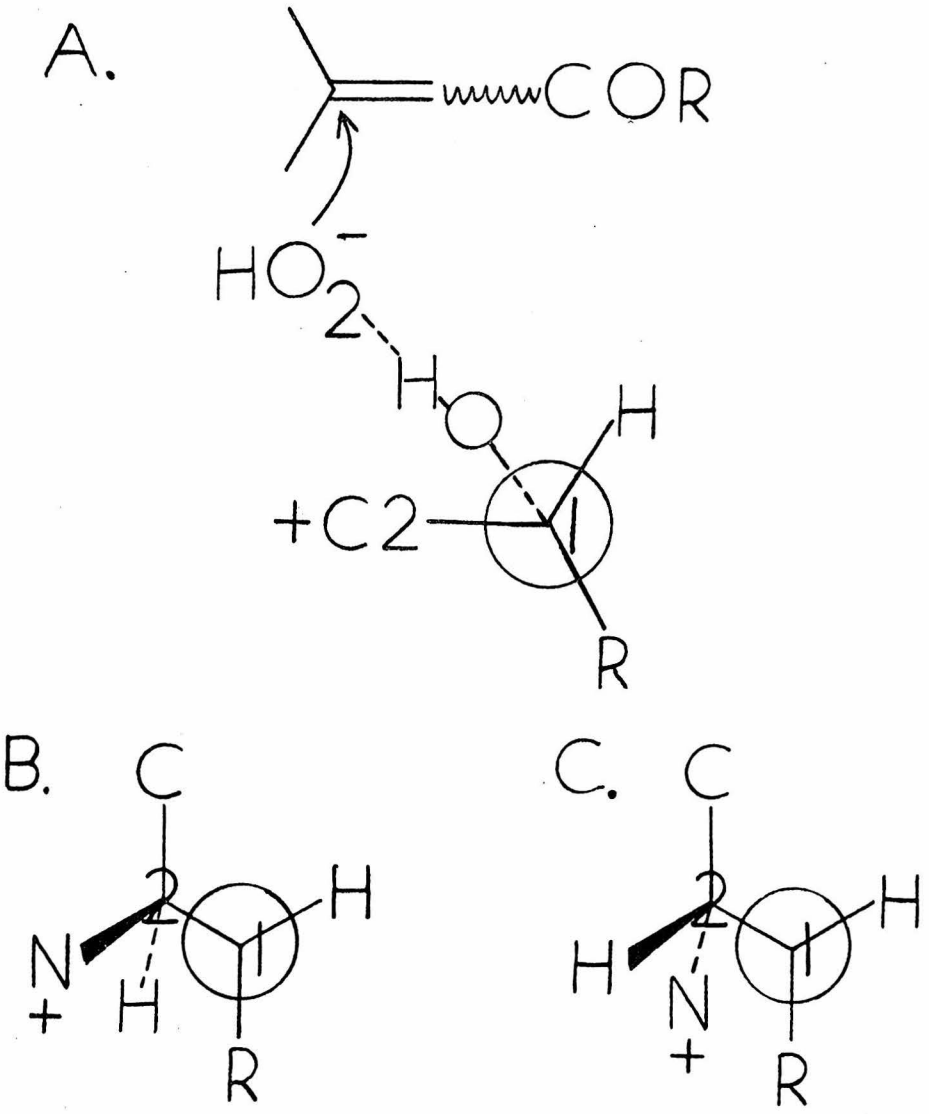

Figure 3

R = $-C_9NH_5OCH_3$, +C2 = carbon 2 substituent with ammonium salt. A. The ion pair approaches the β-end of the alkene (-OH of C1 points toward the alkene). The configurations at C1 and C2 are given, with -OH into the paper, for B. quinine salt and C. epiquinidine salt.

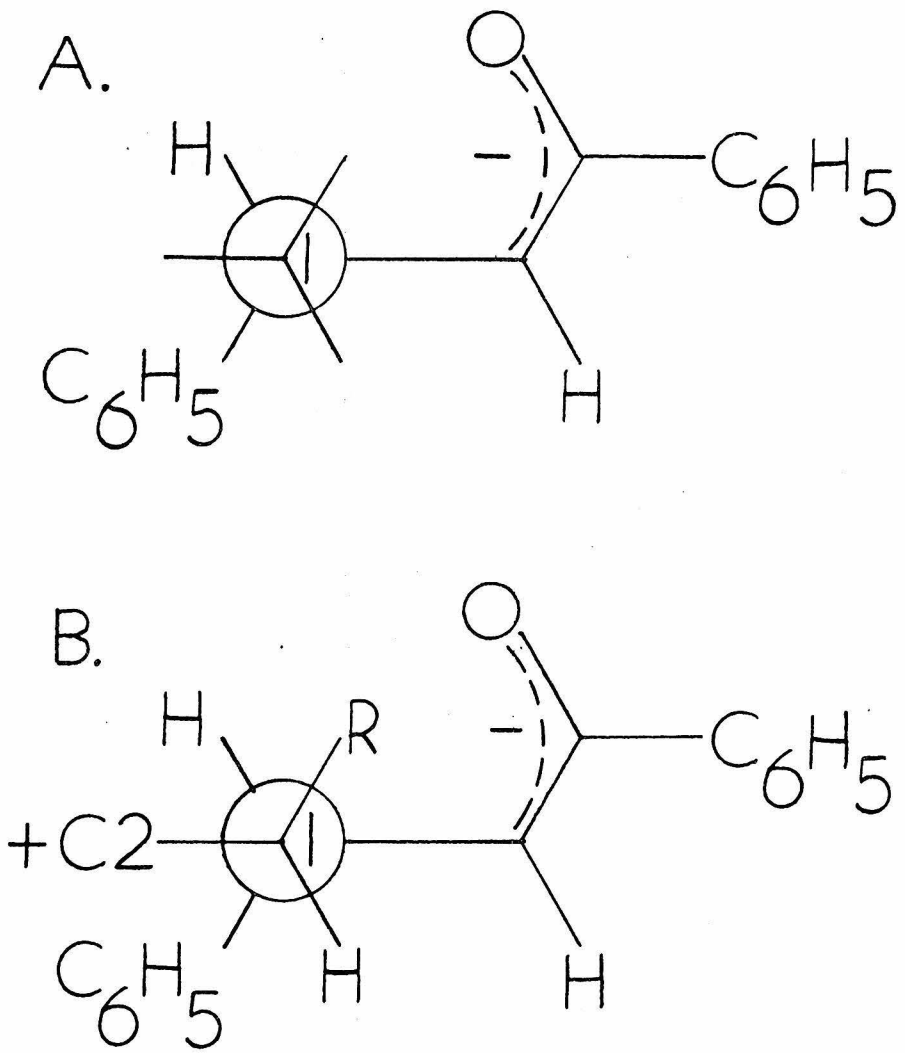

FIGURE 4

this alkene face. The positively charged nitrogen may interact weakly with the enolate anion.

The first experiment to be done to differentiate these two possibilities is the determination of the absolute configurations of the product epoxides. The optically pure epoxide, 2, has been isolated as a crystalline solid (4). Crystals that are large enough for structure analysis should be obtained by slow growth. The crystal structure will indicate the side of the alkene approached by the quinine-salt catalyst.

To test whether the nitrogen(+)-enolate(-) interaction controls the stereochemistry, two diastereomeric isomers of quinine and quinidine can be used as catalysts. For the quinine salt (Figure 3B) the positively charged nitrogen points away from the alcohol due to rotational restrictions along the C1-C2 bond. The isomer, epiquinidine, 6 (Figure 3C), has the same configuration as C1, but the opposite at C2. Therefore, the nitrogen is closer to the alcohol. With the same approach of the ion pair to the alkene, the (+)-(-) interaction is stronger and the enantiomeric excess should be greater. Use of epiquinine, 5, and epiquinidine, 6, should increase the enantiomeric selectivity of the epoxidations if the arrangement, Figure 4C, is important. If steric interactions are solely responsible, no change in selectivity is predicted.

Investigation of the possible steric control of the asymmetric epoxidation is more difficult. The R group on C1 can easily be made smaller by synthesis of compounds using the approach of Taylor

and Martin and ylid starting materials (10). However, optical activity might decrease by either pathway. Formulation of a complex with R larger than +C2 is difficult. A reasonable approach to the study of steric effects is the use of a similar, but more easily modified, optically active amine. The complex, ephedrine, can be methylated to form N-methylephedrine, 8, (Figure 5). This compound can react with alkyl halides, RX, to form quaternary ammonium salts, 9 (Figure 5)(11).The last substituent on the nitrogen can be progressively enlarged from methyl to n-butyl. Because even the group, $-C(CH_3)HN(CH_3)_3^+$, is bulkier than the phenyl substituent on the alcohol carbon, the enantiomeric direction will be the same as with the quinine salt. If steric effects are important in determining the direction of attack, increasing the bulkiness of N^+ will increase the enantiomeric selectivity. If the (+)-(-) interaction predominates, no changes will occur.

By these experiments, the driving force for the asymmetric oxidation of electron-poor olefins has been investigated. Design of catalysts to optimize the selectivity of the reaction will be vastly simplified with this mechanistic information.

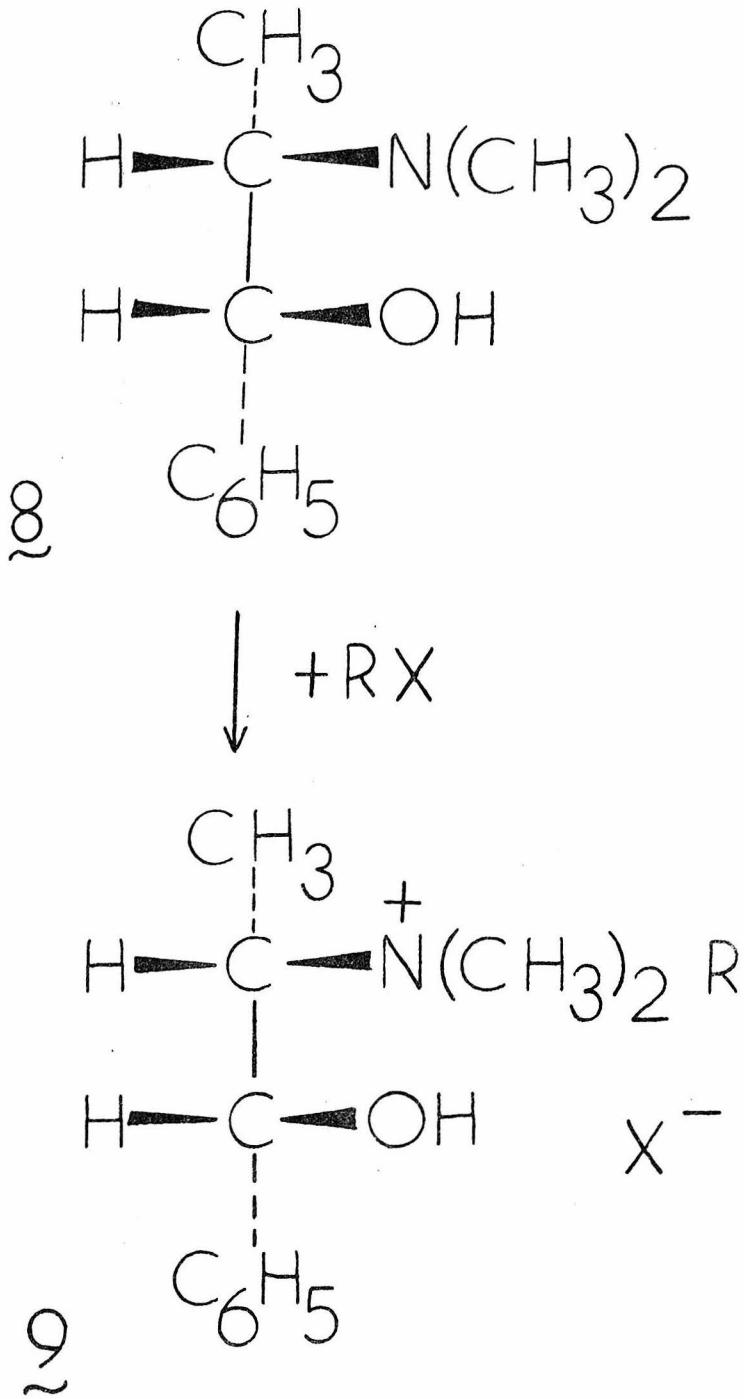

FIGURE 5

References

(1) F. Montanari, I. Moretti, and G. Torre, J. Chem. Soc., Chem. Commun., 135 (1969).

(2) D. R. Boyd and M. A. McKerry, Quart. Rev., London, 22, 111 (1968).

(3) M. Igarashi and H. Midorikawa, Bull. Chem. Soc., Japan, 40, 2624 (1967).

(4) R. Helder, J. C. Hummelen, R. W. P. M. Laane, J. S. Wiering, and H. Wynberg, Tetrahedron Lett., 1831 (1976).

(5) G. Berti in "Topics in Stereochemistry," Vol. 7, N. L. Allinger and E. L. Eliel, Eds., Interscience, New York, N.Y., 1973, p. 111.

(6) E. V. Dehmlov, Angew. Chem., Intl. Ed. Eng., 16, 493 (1977).

(7) For the synthesis of the four alkaloids, 3 - 6, see: G. Grethe, H. L. Lee, T. Mitt, and M. R. Uskokovic, Helv. Chim. Acta, 56 1485 (1973), and J. Gutzwiller and M. R. Uskokovic, Helv. Chim. Acta, 56, 1494 (1973).

(8) H. Wynberg and B. Greijdanus, J. Chem. Soc., Chem. Commun., 427 (1978).

(9) D. L. Klayman, T. S. Griffin, J. D. Bower, and S. W. Page, J. Med. Chem., 16, 1042 (1973).

(10) E. C. Taylor and S. F. Martin, J. Am. Chem. Soc., 96, 8095 (1974)

(11) T. Hiyama, T. Mishima, H. Sawada, and H. Nozaki, J. Am. Chem. Soc., 97, 1626 (1975).

PROPOSITION 3

The Binding of Carbon Monoxide to Sterically Similar Copper(I) Macrocycles

The discovery of the binding of carbon monoxide to $Cu(LBF_2)$, [1,1-difluoro-4,5,11,12-tetramethyl-1-bora-3,6,10,13-tetraaza-2,14-dioxo-cyclotetradeca-3,5,10,12-tetraenato]copper(I), to form $Cu(LBF_2)CO$ (1,2) led to an investigation of the bonding forces in five-coordinate copper(I) complexes, $Cu(LBF_2)B$ (3). It was originally predicted that the strength of the copper-carbon monoxide bond and, therefore, the binding constant, would be proportional to the electron density on the copper.

An electron-rich copper(I) center has a more electron-donating macrocycle. The copper(II) complex of this macrocycle would have a more negative reduction potential and the copper(I) would bind CO better. This prediction has not been upheld. The discrepancies can be explained by a complex mixture of steric and electronic effects. Alternatively, the ordering of binding constants can be predicted by antisymbiosis (4). Softer, more electron-rich nitrogens cause the reduction potential and the binding constant to decrease. Determination of which prediction is more accurate is difficult because of steric changes of the macrocycles. To investigate the influence of isolated electronic effects on CO binding constants,

the synthesis of four structurally similar but electronically different complexes is proposed.

Careful choice of macrocyclic ligands to bind copper can provide electronically, but not sterically, variable complexes. Two sets of complexes which fulfill these requirements are shown in the Figure. The substituent interactions to be evaluated are between the two α-diimine substituents (R1 and R2) and between an α-diimine substituent, R1, and the methylene of the $-CH_2CH_2CH_2-$ bridge or between R2 and the oxygen of the $-OBF_2O-$ bridge. The steric requirements of a trifluoromethyl group (C-F ≃ 1.3 Å (5)) and a methyl group (C-H ≃ 1.0-1.1 Å (6)) are similar, but CPK molecular models (7) permit a better appraisal to be made of steric interactions.

There is no steric hindrance between the α-diimine substituents, R1 and R2, for either $-CH_3$ or $-CF_3$. The macrocyclic ligand is not forced to twist from a square plane, when one substituent is the small hydrogen atom.

The interaction of the trifluoromethyl group (R1) with the $-CH_2CH_2CH_2-$ bridge is slightly greater than that of the methyl group in all macrocycle configurations (planar, tetrahedrally twisted, and domed). However, free rotation can still occur. When R2 is $-CH_3$, the interaction with the $-OBF_2O-$ bridge is slight. The concern in this case is not one of size but of electron repulsions. In both cases in which $-CF_3$ is used, the size of the group does not force a tetrahedral twist of the macrocycle, nor does it preclude either a planar or domed configuration.

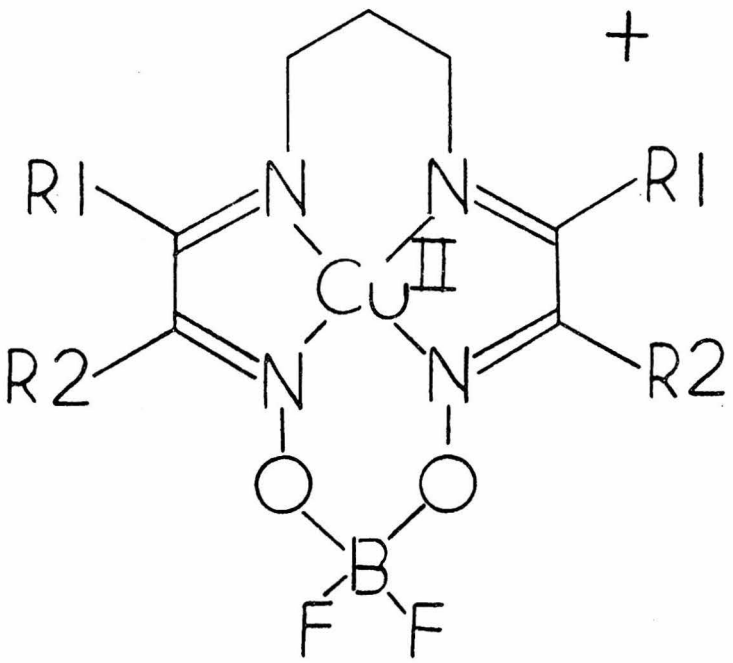

	R1	R2
1	CH_3	H
2	CF_3	H
3	H	CH_3
4	H	CF_3

Synthesis of the four copper(II) complexes begins with the synthesis of the dione monoxime macrocycle precursor. The oxime, $CH_3COCH(NOH)$ (starting material for complex 1), has been previously synthesized from acetone and methyl nitrite (8). The starting oxime for complex 3, $CH_3C(NOH)CHO$, has been synthesized also (9). The preparation of the $-CF_3$ derivatives should be possible by similar routes beginning with the commercially available ketone, CF_3COCH_3. The preparation of $CF_3COCH(NOH)$ is straightforward; a one-step reaction between CF_3COCH_3 and methyl nitrite will form the desired monoxime. The starting material for complex 4 should be prepared by the route:

$$CF_3COCH_3 \xrightarrow{a} CF_3COCHO \xrightarrow{b}$$

$$CF_3COCH(OCH_2CH_3)_3 \xrightarrow{c}$$

$$CF_3C(NOH)CH(OCH_2CH_3)_3 \xrightarrow{d}$$

$$CF_3C(NOH)CHO.$$

Step a should occur on addition of selenium dioxide to the trifluoromethyl ketone (10). (Steps a-d occur with acetone as a starting material.) The diethyl acetal reaction (b) is done with acid and ethanol (11). The oxime forms on addition of hydroxylamine to the acetal (c) and the acetal is easily converted back to the aldehyde with acetic acid (d) (9).

The four dione monoximes are reacted with 1,3-diaminopropane to form the polydentate ligand, (HON)C(R2)C(R1)N(CH_2)$_3$NC(R1)C(R2)(NOH) (1,2). Copper(II) perchlorate and then $BF_3 \cdot O(CH_2CH_3)_2$ are introduced (1,2) and the products are the copper(II) complexes, 1 - 4.

The determination of the reduction potentials of the copper(II) complexes will be done by sampled dc polarography (3). It is predicted that the -CF_3 complexes will have more positive half-wave potentials than the -CH_3 complexes. Also, complexes 1 and 3 and 2 and 4 will have similar potentials. The binding constants of the complexes with carbon monoxide will be determined by the shift in the half-wave potential (3). With an antisymbiotic trend, the -CF_3 complexes will bind CO more strongly. By simple electron-wealth of the copper(I), the -CH_3 complexes will bind more strongly to CO. With the preliminary evidence from reference 3, it is predicted that an antisymbiotic trend will be observed.

References

(1) R. R. Gagné, J. Am. Chem. Soc., 98, 6709 (1976).

(2) R. R. Gagné, J. L. Allison, R. S. Gall, and C. A. Koval, J. Am. Chem. Soc., 99, 7170 (1977).

(3) J. L. Allison, Ph.D. Dissertation, California Institute of Technology, Pasadena, California, 1979.

(4) R. G. Pearson, Inorg. Chem., 12, 712 (1973).

(5) See, for example: P. G. Jones, O. Kennard, and A. S. Horn, Acta Crystallogr., Sect. B, 33, 3744 (1977) and N. Van Opdenbosch, F. Durant, S. A. Chawdhury, and M. H. J. Koch, Acta Crystallogr., Sect. B, 33, 3233 (1977).

(6) See, for example: E. O. Schlemper and C. K. Fair, Acta Crystallogr., Sect. B, 33, 2482 (1977).

(7) CPK Atomic Models are space filling models which simulate positional and steric interactions of molecules; from Schwarz BioResearch.

(8) W. K. Slater, J. Chem. Soc., 117, 587 (1920).

(9) G. T. Newbold, W. Sharp, and F. S. Spring, J. Chem. Soc., 2679 (1951).

(10) M. Henze and R. Muller, Z. Physiol. Chem., 214, 281 (1933).

(11) E. A. Braude and E. A. Evans, J. Chem. Soc., 3324 (1955).

PROPOSITION 4

An X-ray Photoelectron Spectroscopy Study of Electron-transfer Pairs of Transition Metal Chelate Complexes

An XPS (x-ray photoelectron spectroscopy, also known as esca, electron spectroscopy for chemical analysis (1)) study is proposed to determine the site of electron density in transition metal chelate complexes. The binding energies of core electrons of the metal and donor atoms are to be found for the complexes in Table I. The tabulated complexes exist in pairs related by an electron-transfer process:

$$Cu(mnt)_2^{2-} \longrightarrow Cu(mnt)_2^{1-} + 1e^- \qquad (1)$$

(mnt = maleonitriledithiolate dianion)

The chemical shifts of the metals and donor atoms will be compared pairwise in a qualitative manner. A shift to higher binding energies indicates a higher oxidation state, because removal of electron density from the valence shell of an atom increases the binding of the core electrons. Therefore, the observed binding energies will be indicative of whether the metal or ligand atoms lose electron density.

Molecular orbital calculations (2) predict ligand oxidation in the case of reaction 2.

Table I. Formulae and Predicted Metal Oxidation States for Complexes to be Investigated by XPS.

	Complex[a]	Oxidation State	Ref.
1	$(n\text{-}Bu)_4N[Cu(mnt)_2]$	III	2
	$[(n\text{-}Bu)_4N]_2[Cu(mnt)_2]$	II	3
2	$(Ph_3AsCH_3)[Ni(tdt)_2]$	II	4
	$(Ph_3AsCH_3)_2[Ni(tdt)_2]$	II	5
3	$(Ph_3AsCH_3)[Cu(tdt)_2]$	III	4
	$(Ph_3AsCH_3)_2[Cu(tdt)_2]$	II	5
4	$Ni(C_6H_4O_2)_2$	II	6
	$[(n\text{-}Pr)_4N]_2Ni(C_6H_4O_2)_2$	II	6
5	$[Ni(C_6H_4(NH)_2)_2]I$	II	7
	$Ni(C_6H_4(NH)_2)_2$	II	7
6	$KCu(oxam)_2$	III	8
	$K_2Cu(oxam)_2$	II	9
7	$KCu(DED)_2$	III	10
	$K_2Cu(DED)_2$	II	10
8	$KCu(bi)_2$	III	11
9	$KNi(bi)_2$	III	11

[a]Ligand abbreviations: n-Bu = n-C_4H_9; mnt = maleonitrilethiolate dianion; Ph = C_6H_5; tdt = toluene-3,4-dithiolate dianion; n-Pr = n-C_3H_7; oxam = oxamidate dianion; DED = 1,1-dicarboethoxy-2,2-ethylenedithiolate dianion; bi = biuretate dianion.

$$Ni(mnt)_2^{2-} \longrightarrow Ni(mnt)_2^{1-} + 1e^- \qquad (2)$$

Metal oxidation is predicted for reaction 1. The XPS study of the species $Ni(mnt)_2^{-n}$ with n = 1 and 2 provides equivalent binding energies for the nickel in both cases (12). Table II gives the results for the $Ni(mnt)_2^{-n}$ and related complexes. The $Cu(mnt)_2^{-n}$ complexes have not been examined by XPS nor have the other complexes in Table I. Further support for the MO calculation could be gained from an increase in the Cu E_b's when one compares $Cu(mnt)_2^{1-}$ to $Cu(mnt)_2^{2-}$. Further clarification of the metal oxidation states in the other complexes would be important in determining the existence of high oxidation states of Cu and Ni. The technique would also be applicable to other metal electron-transfer complexes.

It is proposed that the complexes be studied in electron-transfer pairs instead of studying related complexes of a given charge. In the case of studying pairs, shifts in binding energies will be indicative only of changing atomic charge (15). For the study of related complexes one must be aware that for different geometries of the same ligand the 2p binding energies of Ni increase (planar < tetrahedral < octahedral) (16). Minimization of variables is possible by the use of pairs. Enough of the abilities of various bidentate ligands to change oxidation state may be learned in this study to promote the prediction of electron environments of future complexes which can not be synthesized in stable pairs.

Table II. Complexes and Metal $2p_{3/2}$ Binding Energies

Complex[a]	E_b, M $2p_{3/2}$ (eV)	Ref.
$(Et_4N)[Ni(mnt)_2]$	853.1	12
$(Et_4N)_2[Ni(mnt)_2]$	853.1	12
$Ni(S_2C_2Ph_2)_2$	852.9	12
$(Et_4N)[Ni(S_2C_2Ph_2)_2]$	852.5	12
$(N_2H_5)_2[Ni(S_2C_2Ph_2)_2]$	852.8	12
$K_2Cu(bi)_2$	934.7	13,14
$K_2Ni(bi)_2$	855.0	9,14

[a] Et = CH_2CH_3.

It will be questioned as to whether the knowledge of the site of electron density is important and necessary. As the chemistry of catalytic systems can often depend on charge transfer and variable coordination, factors which affect binding energies, the author feels sufficient import can be attached to the study of chemical shifts to warrant this work. Determining whether the metal or certain ligands give up electron density more easily is important in the design of high oxidation state complexes. These complexes are gaining significance as postulated reaction intermediates and as catalytically active species. Synthesis and study of such species as models will provide insight into possible mechanistic routes.

The use of XPS has advantages over the other techniques used to determine charge density. Electron spin resonance is helpful, although not definitive, in determining the location of unpaired spins. It gives no information in the case of paired spins. Detailed analyses of electronic spectra coupled with MO calculations can add insight to the positions of electrons. This procedure is quite involved, though, and an error in peak assignment may invalidate an argument. Also Mössbauer spectroscopy can be used as a means of evaluating electronic changes, but is limited to samples which can absorb γ-rays. Definite assignment of peaks in XPS is relatively straightforward as binding energies are atom specific. XPS does have its disadvantages, though. The oxidation or reduction of samples may occur as a result of x-ray bombardment. For instance, under the Al Kα x-ray band $Cu(OAc)_2 \cdot H_2O$ rapidly becomes the cuprous complex (17). Also some samples will decompose in the x-ray beam.

The complexes will be examined with Al Kα (1487 eV) or Mg Kα (1254 eV) x-rays. Gold will be vacuum deposited on the powder samples both as a reference (Au:$4f_{7/2}$, E_b = 83.0 eV) and as a means to maintain electrical equilibrium with insulating compounds. The Ni and Cu $2p_{1/2}$ and $2p_{3/2}$ peaks will be monitored along with the donor atoms' major peaks. The atomic binding energies of these atoms and other atoms in the complexes to be studied are given in Table III. It can be seen that the peaks of the metal and donor atoms will not be interfered with by the other elements present.

In the case of electron-transfer pairs 1-3 (with sulfur donor atoms, Table I), it is expected that the predicted metallic oxidation states will be upheld, because of the MO calculations and the $Ni(mnt)_2^{-n}$ XPS work previously done. For pair 4 with oxygen donor atoms and pair 5 with nitrogen donor atoms, it is predicted that the metal binding energies will vary more than in the $Ni(mnt)_2^{-n}$ case, as the N and O ligands will not be able to vary electron density as well as the sulfur ligands. For pairs 6 and 7 the Cu(III) state will be evidenced as long as the ligands are capable of stabilizing a mono-anionic species. Changes in the metal binding energies for complexes 8 and 9, when compared to the corresponding M(II) values, Table II, are not expected to be similar, even though the oxidation states of the complexes are predicted to be the same. Nickel(II) and copper(II) usually evidence different reactivities dependent on their different d electronic structure.

Table III. Atomic Binding Energies (1).

Element	Peak	E_b (eV)
Metals		
Cu	$2p_{1/2}$	951
	$2p_{3/2}$	931
Ni	$2p_{1/2}$	872
	$2p_{3/2}$	855
Donor Atoms		
S	$2s_{1/2}$	229
	$2p_{1/2,3/2}$	165,164
N	$1s_{1/2}$	399
O	$1s_{1/2}$	532
Other Elements		
C	$1s_{1/2}$	284
As	$3s_{1/2}$	204
	$3p_{1/2}$	147
	$3p_{3/2}$	141
K	$2s_{1/2}$	377
	$2p_{1/2}$	297
	$2p_{3/2}$	294
Reference		
Au	$4f_{7/2}$	83.0

An experimentally significant change between the binding energies of a M(II) and M(III) species will be evidenced. The first XPS measurement on a copper(III) complex has been reported (18), but no analogous copper(II) complex has been studied. However, complexes with different metal oxidation states have been studied by XPS (nickel compounds (12,16,19,20) and copper compounds (17,21-25)) and the difference in the metal binding constants is real. A monoanionic change may not be discernible in the donor atom binding energies if an electron is delocalized over the chelating ligands. In the case of lack of chemical shifts for both the metal and donor atoms, the electronic change should be assigned to the ligand, because of its ability to stabilize the extra charge by delocalization.

In general the results of this study will be important as a guide to the synthesis of high oxidation state complexes and the method of determining electron density will find much wider applicability after metallic oxidation states of electron pairs are shown to be easily distinguished.

References

(1) K. Siegbahn, C. Nordling, A. Fahlman, R. Nordberg, K. Hamrin, J. Hedman, G. Johansson, T. Bergmark, S. -E. Karlson, I. Lindgren, and B. Lindberg, "ESCA; Atomic, Molecular, and Solid State Structure Studied by Means of Electron Spectroscopy," Almqvist and Wiksell, Uppsala, 1967.

(2) S. I. Shupack, E. Billig, R. J. H. Clark, R. Williams, and H. B. Gray, J. Am. Chem. Soc., 86, 4594 (1964).

(3) H. B. Gray, R. Williams, I. Bernal, and E. Billig, J. Am. Chem. Soc., 84, 3596 (1962).

(4) H. B. Gray and E. Billig, J. Am. Chem. Soc., 85, 2019 (1963).

(5) R. Williams, E. Billig, J. H. Waters, and H. B. Gray, J. Am. Chem. Soc., 88, 43 (1966).

(6) F. Rohrscheid, A. L. Balch, and R. H. Holm, Inorg. Chem., 5, 1542 (1966).

(7) A. L. Balch and R. H. Holm, J. Am. Chem. Soc., 88, 5201 (1966).

(8) J. J. Bour, P. J. M. W. L. Birker, and J. J. Steggerda, Inorg. Chem., 10, 1202 (1971).

(9) M. M. Rising, J. S. Hicks, and G. A. Moerke, J. Biol. Chem., 1, 1 (1930).

(10) F. J. Hollander, M. L. Caffery, and D. Coucouvanis, J. Am. Chem. Soc., 96, 4682 (1974).

(11) J. J. Bour and J. J. Steggerda, J. Chem. Soc., Chem. Commun., 85 (1967).

(12) S. O. Grim, L. J. Matienzo, and W. E. Swartz, J. Am. Chem. Soc., 94, 5116 (1972).

(13) H. C. Freeman, J. E. W. L. Smith, and J. C. Taylor, Acta Crystallogr., 14, 407 (1961).

(14) T. Yoshida, K. Yamasaki, and S. Sawada, Bull. Chem. Soc., Jap., 51, 1561 (1978).

(15) G. J. Leigh, Inorg. Chim. Acta, 14, L35 (1975).

(16) L. J. Matienzo, L. I. Yin, S. O. Grim, and W. E. Swartz, Inorg. Chem., 12, 2762 (1973).

(17) D. C. Frost, A. Ishitani, and C. A. McDowell, Mol. Phys., 24, 861 (1972).

(18) W. E. Keyes, W. E. Swartz, and T. M. Loehr, Inorg. Chem., 17, 3316 (1978).

(19) C. A. Tolman, W. M. Riggs, W. J. Linn, C. M. King, and R. C. Wendt, Inorg. Chem., 12, 2770 (1973).

(20) L. O. Pont, A. R. Siedle, M. S. Lazarus, and W. L. Jolly, Inorg. Chem., 13, 483 (1974).

(21) K. S. Kim, J. Electron Spectrosc. Relat. Phenom., 3, 217 (1974).

(22) H. Rupp and U. Weser, Bioinorg. Chem., 6, 45 (1976).

(23) D. W. Edwards, Inorg. Chim. Acta, 18, 65 (1976).

(24) P. Brant and W. Fernando, J. Inorg. Nucl. Chem., 40, 235 (1978).

(25) J. L. Allison, Ph.D. Dissertation, California Institute of Technology, Pasadena, California, 1979.

PROPOSITION 5

Elucidation of the Components of Asphaltene by Photoacoustic Spectroscopy

An understanding of the structure of coal is important to facilitate its efficient conversion to oil products, which can be used as fuels. The structure of coal has been investigated through two major routes. Degradation of coal with oxidants or by liquefaction into recognizable units, that must be pieced back together for a structural hypothesis to be made, is the first (1). Direct techniques have also been employed (2). However, because of coal's opaqueness and insolubility, usual techniques do not yield much information and do little to elucidate coal's structure.

In the conversion of coal to oil products, an intermediate class of compounds formed are the asphaltenes (3), which have been meagerly studied (4). Asphaltenes can also be isolated by low temperature extraction of coal (5). Simple, low temperature extraction of coal can remove compounds that are components of the original coal. Elucidation of the structures of these compounds will provide information on the building blocks of coal.

The asphaltene compounds isolated by low temperature extraction have been separated by thin-layer chromatography and studied by spray reagent tests and mass spectrometry (5). The functional

groups, aromatic alcohols,pyrrol N-H's, pyridine nitrogens, and aromatic amines, were found. Also, formulae for nitrogen and oxygen-containing compounds were determined and possible structural types hypothesized. However, differentiation between the possible compounds, e.g., dibenzofuranes and hydroxyfluorenes, could not be made. Many of the hypothesized structures could be studied by examination of their ultraviolet spectra. However, separation of sufficient quantitites of compound for a solution spectrum is tedious and time consuming. In a much simpler manner, the structural types can be elucidated by means of photoacoustic spectroscopy (PAS) (6) on the samples separated by thin-layer chromatography (TLC).

Photoacoustic spectroscopy is a way of measuring the interaction of photons and amorphous compounds. Light scattering is avoided and spectra are obtained that are similar to optical spectra in the UV and near-IR regions. Surface studies can be done using PAS if the bulk material is nonabsorbing. The resulting optical spectrum is that of the adsorbed species. The technique has been used for the identification of compounds, separated by TLC, still on the TLC plates (7).

Measurement of the photoacoustic spectra of the TLC separated asphaltene compounds is proposed. The ultraviolet spectra of the compounds, predicted to be present by mass spectrometry, can be compared to the photoacoustic spectra measured for compound identification.

The question which must be addressed is whether or not the spectra of the predicted compounds are different enough for identification. The ultraviolet region shows absorptions due to conjugated systems. The extracted asphaltene compounds are highly conjugated and will have extensive UV absorptions. The ultraviolet spectral band maxima, λ_{max}, and the base 10 logarithm of the extinction coefficient, log ε, are given in the Table for some of the oxo-compounds proposed to be components of asphaltene (5). Considerable differences are found in the ultraviolet spectra of these compounds. A figure illustrating the actual spectra of dibenzofuran and 2-hydroxy-fluorene is also given (9). To further substantiate that significant differences exist among proposed oxo-compounds' UV spectra, the spectra of the precursors to hydroxy-compounds can be examined. The presence of a hydroxy group on an aromatic ring causes a bathochromic shift of 7 nm or 25 nm for ortho- and meta- or para-substituted compounds, respectively (10). Therefore, examination of non-hydroxylated compounds will provide relative information. The compounds, phenylnaphthalene, pyrene, and chrysene, have spectra different than those in the Table, and different from each other (8).

The conclusion is reached that the components of asphaltene can be differentiated on the basis of their ultraviolet spectra. The UV spectra can be easily measured by photoacoustic spectroscopy on the TLC separated compounds. The actual use of PAS with condensed samples has been described (11). Solid samples may have spectra that are less intense, but sharper than the corresponding spectra

Table. Band Maxima, λ_{max}, and Logarithmic Extinction Coefficients, log ε, for Possible Components of Asphaltene (8).

Compound	λ_{max}(log ε)
1-hydroxynaphthalene	292(3.7), 308(3.5), 322(3.3)
dibenzofuran	217(4.5), 245(4.0), 250(4.3), 280(4.2), 285(4.2), 295(4.0), 300(4.2)
2-hydroxyfluorene	271(4.3), 304(3.7), 315(3.8)
1-hydroxyanthracene	395(3.6)
1-hydroxyphenanthrene	245(4.1), 308(4.1), 335(3.5)
2,5-diphenylfuran	324(4.5)

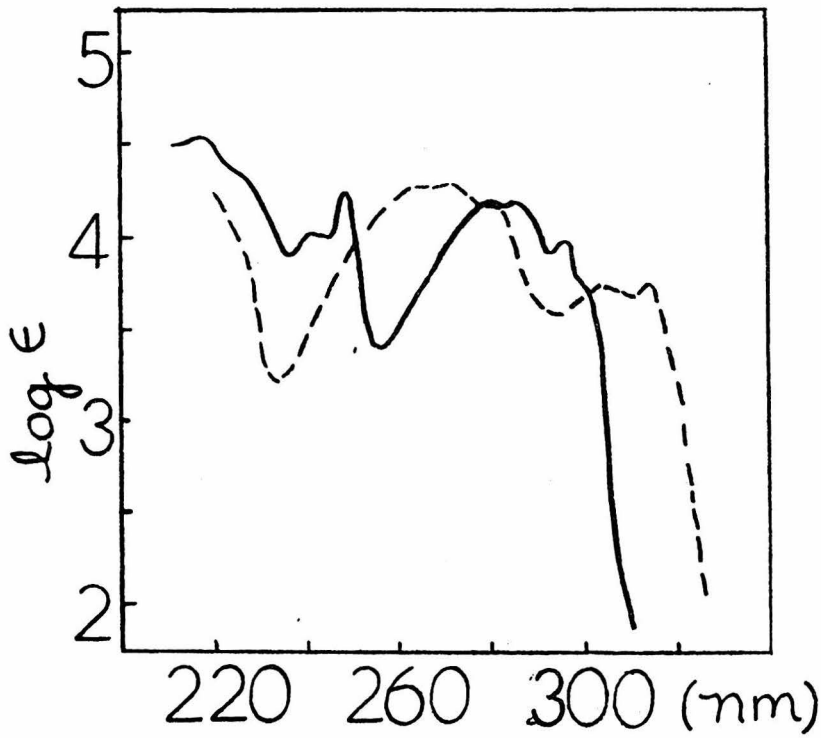

Figure

Ultraviolet spectra of dibenzofuran, ——, and 2-hydroxy-fluorene, ----.

from solution samples. Therefore, the photoacoustic spectra of the asphaltene compounds will provide sufficient information to elucidate the component structures.

References

(1) See,for example: N. C. Deno, B. A. Greigger, and S. G. Stroud, Fuel, 57, 455 (1978); A. Farcasiu, Fuel, 56, 9 (1977); R. Hayatsu, R. E. Winans, R. G. Scott, L. P. Moore, and M. H. Studier in "Organic Chemistry of Coal," J. W. Larson, Ed., American Chemical Society, Washington, D.C., 1978, p. 108; and S. K. Chakrabartty and R. Hayatsu, Fuel, 53, 240 (1974).

(2) See, for example: P. H. Given and M. E. Peover, Fuel, 39, 463 (1960); R. A. Friedel and J. A. Queiser, Fuel, 38, 369 (1959); and S. Ergun and V. H. Tiensuu, Acta Crystallogr., 12, 1050 (1959).

(3) H. W. Sternberg, ACS Div. Fuel Chem., Preprints, 21 (7), 1 (1976); R. Yoshida, Y. Maekawa, T. Ishii, and G. Takeya, Fuel, 55, 337 (1976); H. W. Sternberg, R. Raymond, and F. K. Schweighardt, ACS Div. Petroleum Chem., 20,(4), 763 (1975); B. J. Liebenberg and H. G. J. Potgieter, Fuel, 52, 130 (1973); and S. Weller, M. G. Pelipetz, and S. Friedman, Ind. Eng. Chem., 41, 1572 (1951).

(4) L. J. Darlage, H. N. Finkbone, S. J. King, J. Ghosal and M. E. Bailey, Fuel, 57, 479 (1978).

(5) A. Marzec, D. Dodzek, and T. Krzyzanowska, in "Organic Chemistry of Coal," J. W. Larson, Ed., American Chemical Society, Washington, D.C., 1978, p. 71.

(6) A. Rosencwaig, Anal. Chem., 47, 592A (1975).

(7) A. Rosencwaig and S. S. Hall, Anal. Chem., 47, 548 (1975).

(8) R. C. Weast, Ed., "Handbook of Chemistry and Physics," 54th Ed., CRC Press, Cleveland, OH, 1973, p. C-75.

(9) R. A. Friedel and M. Orchin, "Ultraviolet Spectra of Aromatic Compounds," John Wiley, New York, N.Y., 1951.

(10) R. M. Silverstein, G. C. Bassler, and T. C. Morrill, "Spectrometric Identification of Organic Compounds," 3rd Ed., John Wiley, New York, N.Y., p. 251.

(11) J. E. McClelland and R. N. Kniseley, Appl. Optics, 15, 2658 (1976).